PolyPublie
Polytechnique Montréal

POLYTECHNIQUE MONTRÉAL
UNIVERSITÉ D'INGÉNIERIE

Titre: Title:	Development of a Thermal Conductivity Model for Molten Salt Solutions
Auteur: Author:	Huiqiang Yang
Date:	2025
Type:	Mémoire ou thèse / Dissertation or Thesis
Référence: Citation:	Yang, H. (2025). Development of a Thermal Conductivity Model for Molten Salt Solutions [Thèse de doctorat, Polytechnique Montréal]. PolyPublie. https://publications.polymtl.ca/70096/

Document en libre accès dans PolyPublie
Open Access document in PolyPublie

URL de PolyPublie: PolyPublie URL:	https://publications.polymtl.ca/70096/
Directeurs de recherche: Advisors:	Patrice Chartrand
Programme: Program:	Génie des matériaux

Ce fichier a été téléchargé à partir de PolyPublie, le dépôt institutionnel de Polytechnique Montréal
This file has been downloaded from PolyPublie, the institutional repository of Polytechnique Montréal

https://publications.polymtl.ca

POLYTECHNIQUE MONTRÉAL
affiliée à l'Université de Montréal

Development of a thermal conductivity model for molten salt solutions

HUIQIANG YANG
Département de génie chimique

Thèse présentée en vue de l'obtention du diplôme de *Philosophiæ Doctor*
Génie des matériaux

Novembre 2025

© Huiqiang Yang, 2025.

POLYTECHNIQUE MONTRÉAL
affiliée à l'Université de Montréal

Cette thèse intitulée :

Development of a thermal conductivity model for molten salt solutions

présentée par **Huiqiang YANG**
en vue de l'obtention du diplôme de *Philosophiæ Doctor*
a été dûment acceptée par le jury d'examen constitué de :

Jean-Philippe HARVEY, président
Patrice CHARTRAND, membre et directeur de recherche
Julian SELF, membre
Didier HAILLOT, membre externe

DEDICATION

To my family.

ACKNOWLEDGEMENTS

I would like to express my deepest gratitude to my research supervisor, Patrice Chartrand, for his invaluable guidance, patience, and scientific expertise, which were essential to the success of this work. His insightful recommendations and comments greatly enhanced my understanding of the discipline and provided me with a clearer perspective on the industrial challenges associated with it.

I am also sincerely thankful to Dr. Aïmen E. Gheribi for his outstanding supervision, thoughtful suggestions, and valuable discussions during the first two years of the project. His support was crucial in the progress of my research and the completion of this work.

My appreciation extends to Anh-Thu Phan for her contribution and collaboration, which played a significant role in advancing this project.

I would also like to thank Ryan C. Gallagher for his insightful discussions and comments on molten salts in nuclear reactors.

I am grateful to all my colleagues and friends at CRCT for creating a stimulating work environment and for their constant support. Their fruitful exchanges and positive spirit were a continuous source of motivation throughout this journey.

Finally, I am profoundly thankful to my wife for her unwavering support, love, and encouragement, which helped me overcome challenging moments and maintain my motivation.

RÉSUMÉ

Les sels fondus sont l'un des meilleurs matériaux pour les technologies d'énergie avancées et dans les applications industrielles, comme les réacteurs nucléaires à sels fondus, le stockage d'énergie, les matériaux à changement de phase, ainsi que la production et le recyclage des métaux. Dans ces applications d'ingénierie, la conductivité thermique est l'un des facteurs les plus importants qui impactent le design, l'efficacité et la sûreté du système. Malheureusement, les données expérimentales sur la conductivité thermique des sels fondus sont souvent limitées, en particulier dans le cas des mélanges de sels fondus. Les données expérimentales ne sont souvent pas en accord, les valeurs obtenues expérimentalement étant assez dispersées, en raison des difficultés liées aux conditions de mesure, comme les hautes températures, les environnements corrosifs et les mécanismes de transfert de chaleur pendant l'expérience. De plus, il existe encore des sels fondus dont la conductivité thermique est totalement inconnue. Par conséquent, le développement d'un modèle théorique capable de prédire avec précision la conductivité thermique des sels fondus est essentiel pour faire avancer le développement de la technologie des sels fondus, établir une base de données solide sur ces matériaux, comparer expérimentalement les techniques de mesure pour les nouvelles données, et enfin améliorer la connaissance globale de la conductivité thermique des sels fondus.

Pour répondre à ce besoin, un modèle théorique basé sur la théorie cinétique est proposé dans un premier temps. Ce modèle a démontré sa précision pour prédire la conductivité thermique des sels fondus en fonction de la température à partir du point de fusion pour les sels fondus purs monoatomiques et polyatomiques. Ce modèle n'a besoin d'aucune constante d'ajustement empirique, mais dépend principalement du nombre de cations et d'anions des sels fondus, et des propriétés physiques connnues des sels. Les prédictions de la conductivité thermique des sels fondus sont en accord avec les données expérimentales communememt admises, à la fois aux points de fusion et en termes de leur dépendance à la température. La méthode de Bland-Altman est appliquée pour vérifier la fiabilité du modèle, qui présente une erreur inférieure à $\pm$ 10%. En outre, le modèle a démontré une précision de prédiction comparable aux données expérimentales à travers les différentes familles de sels fondus, y compris les halogénures, les halogénures divalents, les carbonates, les nitrates/nitrites, les sulfates et les hydroxydes. Pour faciliter son utilisation, le modèle est ensuite paramétrisé comme une fonction linéaire de la température pour chacun des sels fondus purs.

Ensuite, le modèle a été étendu pour tenir compte de la dépendance à la composition pour les mélanges de sels fondus en ion commun, en considérant l'effet des fluctuations de masse entre

différents ions dans la solution de mélange. Le modèle est applicable aux sels fondus simples en anion commun et cation commun, où on néglige les interactions interatomiques entre les ions. Le modèle est validé par les résultats des simulations de dynamique moléculaire à l'équilibre et les données expérimentales de plusieurs mélanges simples de sels fondus binaires de fluorures, chlorures, bromures et iodures. Les résultats ont montré une amélioration significative de la précision par rapport aux modèles les plus utilisés du mélange idéal. De plus, le modèle a également démontré sa capacité à prédire les mélanges à anion commun pour les systèmes ternaires, quaternaires et de plus haut ordre dans l'intervalle d'erreur des données expérimentales. Notamment, la masse molaire et la conductivité thermique des sels purs constituant les mélanges sont identifiées comme des facteurs clés influençant la diminution de la conductivité thermique dans les mélanges de sels fondus. Notons que la disponibilité des données expérimentales sur la conductivité thermique des mélanges de sels fondus est beaucoup plus limitée que pour les sels fondus purs. Par conséquent, nous avons réalisé des centaines de simulations de dynamique moléculaire à l'équilibre avec le modèle d'ion polarisé afin de combler le manque de données concernant la conductivité thermique des mélanges de sels fondus à ions communs et réciproques. Le modèle d'ion polarisé utilise des potentiels ajustés obtenus par la théorie de la fonctionnelle de la densité plutôt que des potentiels empiriques et est considéré comme l'un des modèles les plus performants et précis pour la simulation des chlorures, fluorures et autres sels fondus.

Dernièrement, les interactions interatomiques impliquant plus de deux cations et plus de deux anions des mélanges de sels fondus réciproques ont été intégrées dans le modèle en appliquant le Modèle Quasichimique Modifié dans l'Approximation des Quadruplets (MQMQA), où les fractions des paires sont considérées pour chaque composant du mélange. Ce modèle est le premier qui inclut les effets des interactions entre les premiers plus proches voisins et l'ordre à courte distance entre les cations et les anions qui en résulte, ainsi que l'énergie de Gibbs d'échange ($AY + BX \rightleftharpoons AX + BY,\ \Delta g^{exchange}_{AB/XY}$) pour la solution des sels fondus réciproques. Les prédictions sont en accord avec les résultats de la simulation de dynamique moléculaire pour trois mélanges de sels réciproques : Li^+, Na^+ / F^-, Cl^- ; Li^+, K^+ / F^-, Cl^- ; et Na^+, K^+ / F^-, Cl^-. De plus, le modèle décrit bien les données expérimentales disponibles pour deux sels fondus réciproques, avec une erreur de prédiction estimée à $\pm 20\%$. Le modèle permet également d'estimer la conductivité thermique de plusieurs sels fondus utilisés comme matériaux à changement de phase, dont les donées ne sont pas encore présentes dans la littérature. Pour résumer, ce projet de recherche fait avancer de manière significative l'évaluation de la conductivité thermique des sels fondus avec précision en termes de dépendance à la température et à la composition, offrant ainsi une nette amelioration dans l'évaluation de la conductivité thermique des mélanges de sels fondus pour les applications d'ingénierie.

Comme information complémentaire sur les solutions complexes des mélanges de sels fondus, le modèle des mélanges simples de sels fondus a été étendu afin de considérer les effets de la structure locale, lorsque les ions complexes se forment en faisant varier la composition du mélange. La formation des ions complexes peut encore plus diminuer la conductivité thermique par rapport aux mélanges simples où les ions sont dissociés. La structure locale est représentée par la concentration des ions libres et complexes, qui peut être déterminée par des méthodes expérimentales (comme la spectroscopie RMN), des simulations atomistiques à l'équilibre ou d'autres modèles. Les prédictions étaient bien alignées avec les données expérimentales et les résultats de la dynamique moléculaire pour les mélanges de KCl-$MgCl_2$ et NaF-AlF_3. Le modèle a démontré une amélioration importante en comparaison, à la fois avec la méthode du mélange idéal, et avec le modèle de mélange simple qui supposait que les ions étaient dissociés sans effet sur la structure locale. De plus, des différences plus importantes de masse molaire et de conductivité thermique des composants ont entraîné des écarts plus significatifs, ce qui peut être observé dans le cas de NaF-AlF_3. Il est important de noter que la précision de la représentation de la structure locale est essentielle pour obtenir une prédiction fiable des solutions complexes de sels fondus.

ABSTRACT

Molten salts are some of the most promising materials for advanced energy technologies and industrial applications, such as nuclear reactors, thermal energy storage, phase change materials, and metal production. In these engineering applications, thermal conductivity is an important factor impacting analyses related to the design, efficiency, and safety of the system. Unfortunately, experimental datasets on the thermal conductivity of molten salts are often limited, especially molten salt mixtures. The reported experimental data tends to be inconsistent, likely due to challenging experimental conditions such as high temperatures, corrosive environments, and competing heat transfer mechanisms that can bias measurements. Indeed, many molten salts lack comprehensive knowledge regarding their thermal conductivity. Therefore, a theoretical model to accurately predict the thermal conductivity of molten salts is essential for developing molten salt technologies, advancing molten salt property databases, verifying experimental measurements, and improving the overall understanding of molten salt thermal conductivity.

To address this need, a theoretical model based on kinetic theory was proposed as the initial step. This model succeeded in predicting the temperature-dependent thermal conductivity of both simple and complex pure molten salts without requiring any empirical fitting constants. The predicted thermal conductivity values showed good agreement with reliable experimental datasets, both at melting points and in terms of their temperature dependence, with an average deviation of $\pm 10\%$ or less, as verified by the Bland-Altman method. Furthermore, the model exhibited predictive accuracy comparable to reliable experimental measurements across various salt families, including halides, divalent halides, carbonates, nitrates/nitrites, sulfates, and hydroxides. To facilitate practical use, the model was parameterized as a linear function of temperature.

Building on the model for pure molten salts, it was extended to account for the composition dependent thermal conductivity of simple molten salt mixtures, incorporating mass fluctuation effects due to the distinct characteristics of different ions within the melt. This model proved applicable for common-anion or common-cation mixtures, where no interatomic interactions occur between the ions. Predictions were validated against numerous common-ion binary mixtures of fluorides, chlorides, bromides, and iodides, utilizing equilibrium molecular dynamics simulations and available experimental data. The results showed a significant improvement in accuracy over the commonly used ideal mixing rule. Additionally, the model also demonstrated predictive accuracy for common-ion ternary, quaternary and higher-order

salt mixtures within the experimental error interval. Notably, the molecular weight and thermal conductivity of the end-members were identified as key influencing factors in the molten salt mixtures. It is worth to mention that the availability of experimental datasets for the thermal conductivity of molten salt solutions is much more limited than for pure molten salts. Thus, we have performed hundreds of simulations using equilibrium molecular dynamics simulations with the polarized ion model to fill the gaps in the thermal conductivity of common-ion and reciprocal molten salt mixtures. The polarized ion model employs fitting potentials obtained from DFT as input rather than empirical potentials, and is considered one of the most successful models for simulating chlorides, fluorides, and other molten salts with strong performance and accuracy.

Lastly, interatomic interactions involving more than two cations and more than two anions of reciprocal molten salt mixtures were integrated into the model using the Modified Quasi-chemical Model in the Quadruplet Approximation approach, where the pair fractions of the components were considered for each species. This represents the first model of thermal conductivity that includes interaction effects through first-nearest neighbor short-range ordering between cations and anions and the Gibbs energy of exchange ($AY + BX \rightleftharpoons AX + BY,\ \Delta g^{exchange}_{AB/XY}$) for reciprocal molten salt solutions. The predictions showed good agreement with equilibrium molecular dynamics simulations for three reciprocal mixtures of Li^+, Na^+ / F^-, Cl^-; Li^+, K^+ / F^-, Cl^-; and Na^+, K^+ / F^-, Cl^-. Additionally, the model aligned well with two experimental reciprocal molten salt mixtures found in the literature, with an estimated error of less than $\pm 20\%$. The model demonstrated its predictive capability for estimating the thermal conductivity of several reciprocal molten salt phase change materials, whose thermal conductivities have not been previously reported. Overall, this research project significantly advances the assessment of thermal conductivity with precision in terms of temperature and composition dependence, providing valuable insights for evaluating the thermal conductivity of molten salt mixtures in engineering applications.

As complementary information on the complex molten salt solutions, the model was further refined to account for local structure effects arising from the formation of complex ions across the compositional range, which can further reduce thermal conductivity compared to fully dissociated ions in the simple molten salt mixtures. The local structure was represented by the concentration of free and complex ions, determined through either experimental methods (such as NMR spectroscopy), equilibrium atomistic simulations, or models. Predictions aligned well with both experimental and molecular dynamics data for mixtures of KCl-$MgCl_2$ and NaF-AlF_3, showing improved accuracy over the ideal mixing rule and the model of simple molten salt mixtures that assumed fully dissociated ions, which do not account for local structure effects. Additionally, larger differences in molecular weight and thermal conduc-

tivity resulted in more significant deviations, as seen in the case of NaF-AlF_3. Importantly, this underscores that accurate local structure representation is essential for reliable thermal conductivity predictions in complex molten salt mixtures.

TABLE OF CONTENTS

LIST OF TABLES

LIST OF FIGURES

LIST OF SYMBOLS AND ACRONYMS

Acronyms

AC	Alternating Current
AIMD	*Ab initio* Molecular Dynamics
CSP	Concentrating Solar Power
DFT	Density Functional Theory
EMD	Equilibrium Molecular Dynamics
FNN	First-Nearest Neighbors
GK	Green-Kubo
HTF	Heat Transfer Fluid
MS	Molten Salt
MSR	Molten Salt Reactor
MQMQA	Modified Quasi-chemical Model in the Quadruplet Approximation
ORNL	Oak Ridge National Laboratory
PCMs	Phase Change Materials
PIM	Polarized Ion Model
RIM	Rigid Ion Model
SNN	Second-Nearest Neighbors
SRO	Short-Range Ordering

Symbols

λ	Thermal conductivity [W.m^{-1}K^{-1}]
T	Temperature [K]
ρ	Density [kg.m^{-3}]
P	Pressure [Pa]
α	Thermal expansivity [K^{-1}]
α_{dif}	Thermal diffusivity [m^2.s^{-1}]
$< l_{pr.} >$	Phonon mean free path [m]
r_a	Anionic radius [m]
r_c	Cationic radius [m]
r	Cylinder radius [m]
K_{emp}	Empirical fitting constant (dimensionless)
k_B	Boltzmann constant [J.K^{-1}]

$\mathbf{N_A}$	Avogadro constant [mol^{-1}]
n_a	Number of atoms per molecule
n_d	Number density per atom [atom.m^{-3}]
V_m	Molar volume [$\text{m}^3\text{.mol}^{-1}$]
c_s	Sound velocity [m.s^{-1}]
M	Molecular weight [kg.mol^{-1}]
λ_{min}	Lower minimum thermal conductivity [$\text{W.m}^{-1}\text{K}^{-1}$]
$\boldsymbol{K}$	Complexity of local structure (dimensionless)
n_s^-	Total number of anionic atoms per molecule
n_s^+	Total number of cationic atoms per molecule
T_m	Melting temperature [K]
λ_m	Thermal conductivity at T_m [$\text{W.m}^{-1}\text{K}^{-1}$]
α_m	Thermal expansivity at T_m [K^{-1}]
γ_m	Grüneisen parameter at T_m (dimensionless)
U_m	Sound velocity at T_m [m.s^{-1}]
V_m	Molar volume at T_m [$\text{m}^3\text{.mol}^{-1}$]
Cp_m	Molar constant pressure heat capacity at T_m [$\text{J.mol}^{-1}\text{K}^{-1}$]
Cv_m	Molar constant volume heat capacity at T_m [$\text{J.mol}^{-1}\text{K}^{-1}$]
$\overline{Cv}_m$	Constant volume heat capacity per unit volume at T_m [$\text{J.m}^{-3}\text{K}^{-1}$]
$\rho^{'}$	Density temperature dependency [$\text{kg.m}^{-3}\text{K}^{-1}$]
$\lambda^{'}$	Thermal conductivity temperature dependency [$\text{W.m}^{-1}\text{K}^{-2}$]
$\hbar$	Reduced Planck constant [eV.s]
χ	Isothermal compressibility [Pa^{-1}]
h_{diff}	Damping factor
F	View factor
n	Number density of atoms
Φ	Thermal expansion with volume fraction
K	Dimensionless measure of local structure complexity
Θ_D	Debye temperature [K]
r_e	Interatomic distance [m]
N	Number of compounds in a mixture
Δg	Gibbs energy [kJ.mol^{-1}]
q	Absolute ionic charge
$\dot{q}$	Specific heat flux [W.m^{-2}]
X	Fraction (mole or weight depends in the text)
Y	Equivalent ionic site fraction

β_T	Isothermal bulk modulus [Pa]
h	Heat transfer coefficient [W.m^{-2}K^{-1}]
σ	Stefant-Boltzmann constant [W.m^{-2}K^{-4}]
ε	Surface emissivity of the material

Super/Subscripts

Exp	Experimental
id	Ideal
ms	Molten salt
i	Index of component
min	Minimum
m	Melting
M	Mass
k	Kinetic
d	Density
ph	Phonon
diff	Diffusons
C	Cation
A	Anion
cal	Calibrated
C/A	FNN pair
EX	Exchange
Quad	Quadruplet
Temkin	Temkin model
emp	Empirical
cv	Convection
s	Surface
suf	Surroundings
rad	Radiation

LIST OF APPENDICES

CHAPTER 1 INTRODUCTION

Commonly known as "table salt", sodium chloride (NaCl) is one of the simplest and most stable ionic compounds. Sodium, which has a positive charge as a cation, easily loses an electron, while chlorine, which has a negative charge as an anion, readily gains that electron to form a neutral, stable sodium chloride structure through a strong ionic bond.

At room temperature, salts exist in a solid crystalline form. They become liquid when heated to their melting point. In other words, solid salts have a long-range ordered structure, where atoms are arranged in a repeating, regular pattern. However, when sufficient energy is supplied to break this long-range ordering, the solid undergoes a phase transition, becoming a disordered, short-range ordered ionic liquid. These high temperature salts ($> 100°C$) in the liquid phase is referred to as molten salt, NaCl melts at 801°C. Molten salts are widely utilized in various industries for high-temperature applications. For example, NaF-AlF_3 molten salt mixture serves as the main electrolyte in aluminum production [1], while several other metal production processes, such as those for magnesium (Mg), titanium (Ti), copper (Cu), zirconium (Zr), and nickel (Ni) involve the use of molten sodium chloride (NaCl) and potassium chloride (KCl) as electrolytes to dissolve their corresponding chlorides [2]. The LiF-BeF_2 mixture has been proposed as both fuel and coolant in molten salt reactors, and the $NaNO_3$-KNO_3 mixture ("solar salt"- 40% wt potassium nitrate (KNO_3) and 60% sodium nitrate wt ($NaNO_3$)) is commonly employed as heat transfer fluids (HTF) and thermal energy storage (TES) media in solar thermal power plants.

Among these industrial applications, molten salt mixtures that consist of two or more salts, are often preferred over pure salts due to their improved properties. One significant advantage of using salt mixtures is their lower melting point compared to that of the individual salts. Figure 1.1 demonstrates the phase transition of "solar salt" from solid to liquid as it is heated in an atmospheric environment. The energy required to melt the salt is determined by its melting enthalpy; however, the rate at which the salt melts or solidifies depends on its thermal conductivity (λ), which reflects its ability to transfer heat within the material. "Solar salt" begins to melt at approximately 221°C [3], while KNO_3 and $NaNO_3$ have melting points of around 334°C and 308°C, respectively.

Since 19 century, molten salts have gained recognition and found several industrial applications. Early in that century, Sir Humphry Davy successfully isolated alkali metals from molten hydroxides. Building on this, Deville later used sodium as a powerful reducing agent to isolate and produce aluminum (Al) from $AlCl_3$. Furthermore, in 1834, Michael Faraday established his laws of electrolysis by utilizing materials such as molten lead halides.

Figure 1.1 Demonstration of heating "solar salt" from solid to liquid (screen capture from documentation [4]).

In 1886, Héroult and Hall independently developed the molten salt electrolytic process for aluminum production. This invention led to the establishment of large-scale extraction plants. Now known as the Hall-Héroult process, which remains fundamental in modern aluminum production and has played a key role in advancing technologies, especially in the aerospace industry [5].

At Oak Ridge National Laboratory (ORNL), molten salts were initially investigated for use in a nuclear-powered aircraft engine utilizing a molten salt reactor (MSR) in the 1950s. This MSR project initiated extensive research into nuclear reactors that utilize fuel dissolved in molten salts [6–9]. Since then, MSRs have become one of the most attractive and promising technologies for clean power generation and isotopes for medical applications.

Over the past decades, numerous molten salt mixtures have been investigated for their potential use as fuel and/or coolant salts, including LiF-KF, LiF-RbF, LiF-NaF-KF, LiF-NaF-RbF, LiF-BeF_2, among others [10]. Furthermore, molten salts have also been proposed for tritium breeding and as thermal blankets in nuclear fusion reactors [11]. The growing interest in molten salts extended to the concentrated solar power (CSP) industry in the 1980s. The first significant application of molten salts as both (heat transfer fluid (HTF) and thermal energy storage (TES) medium was implemented at the SOLAR TWO molten salt power tower plant, in which "solar salt" was employed [3].

More recently, CSP systems integrated with TES and hybridization with other renewable energy sources like photovoltaic and wind have been widely developed to deliver 24-hour dispatchable electricity generation. This development has also motivated researchers to look for

higher temperature molten salt mixtures [12–16], and larger thermal energy storage capacities through molten salt phase change materials (PCMs) [17–20].

As shown in Figure 1.1, the "solar salt" was melted under ambient conditions. It is highly stable when exposed to the environment, non-flammable, and the melted salt is very clear, resembling water in appearance.

In contrast to conventional HTFs, such as water, molten salts offer numerous advantages in high temperatures applications. For instance, consider the role of HTFs in nuclear reactors. Light water reactors are currently used in most nuclear power plants; however, advanced reactor designs have been developed over several decades due to safety concerns.

These new conceptual reactors employ liquid metals (such as sodium), high-temperature gases (like helium), and molten salts as HTFs. Among these advanced reactors, molten salt reactors (MSRs) are one of the most promising technologies. They operate at very low pressure to overcome the pressure losses in the molten salt loop (typically less than 0.5 MPa), which is much lower pressures compared to water (with supercritical water reaching approximately 22.1 MPa) and gas helium. Moreover, they feature better chemical stability than liquid sodium. In addition, their ability to operate at higher operating temperatures enhances the efficiency of the power generation cycle, which in turn lowers the cost of electricity generation.

An accurate design of thermal systems in industry relies directly on understanding the properties of molten salts. Given their significant roles across various industries, as shown in Figure 1.2, Well-characterized properties of molten salts are crucial for designing efficient processes, developing new molten salt mixtures, and selecting materials for the critical equipment, including molten salt heat exchangers, molten salt pumps, molten salt valves, and instrumentation.

Each industrial application relies on specific properties. For example, in aluminum production, the solubility and high electrical conductivity of molten salt mixtures are primary importance to drive the process. However, thermal conductivity also plays an indispensable role in heat transfer within the electrolysis cell, as well as in the formation and stability of the protective frozen ledge on the cell's walls.

In power generation—whether from nuclear reactors, solar energy, or heat recovery—rapid removal and transfer of heat to a Rankine cycle is required. In such cases, low viscosity is necessary for optimal fluid dynamics in the flow of molten salt loop, and a lower melting point helps prevent the molten salt from freezing (solidifying) in the pipes. Additionally, a high specific heat capacity allows for a large amount of energy to be removed or stored in the system. The thermal conductivity of the fluid (for example, molten salt) is particularly important to prevent overheating of the heat exchangers, in order to ensure the safe operation of the system.

The operation of a molten salt receiver in a CSP power tower illustrates the importance of thermal conductivity of molten salt. In the last panel of the receiver, the heat exchanger tubes may experience very high heat fluxes exceeding 1.5 $[MWth/m^2]$ with a small temperature difference between the inlet and outlet of the panel. In such a case, there is the potential to create hot spots that lead to the decomposition of solar salts. Gases like oxygen and nitrogen will be generated during the decomposition. These gases can act as a thermal barrier that reduces energy transfer. Ultimately, the molten salt receiver will be damaged.
In the current molten solar salt TES system, sensible heat is utilized, where the solar salt is typically heated from 290°C to 565°C, making specific heat capacity an important factor. In contrast, a molten salt PCM storage system uses latent heat, requiring a large amount of energy for the phase transition from solid to liquid, making the enthalpy of fusion the primary characteristic for PCMs. In such systems, the thermal conductivity of molten salts is also critical, as it determines the efficiency of heat transfer during the charging and discharging the system.

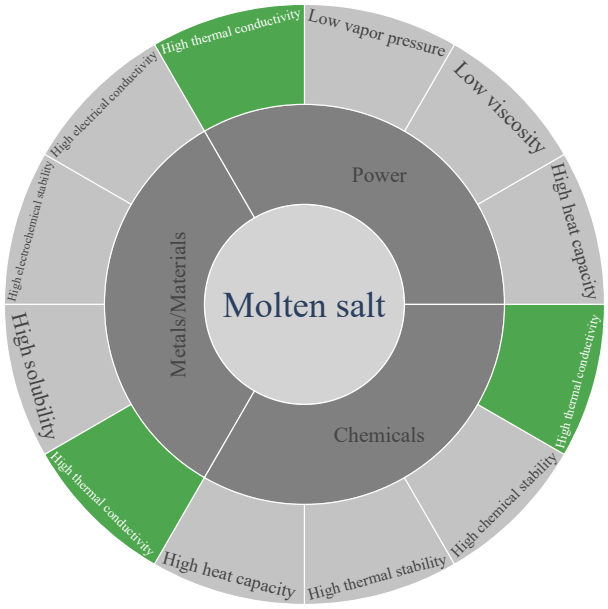

Figure 1.2 Molten salt industrial applications and their properties [5]

Among the various properties, thermal conductivity (λ) is one of the most important thermophysical parameters that determine the efficiency of heat transfer within thermal systems. It is commonly found in practical engineering design for fluid mechanics and heat transfer processes, numerous dimensionless numbers are used to analyze flow characteristics and facilitate comparisons across systems, such as the Reynolds number ($Re = \rho u D/\mu$), the Nusselt number ($Nu = hD/\lambda$), and the Prandtl number ($Pr = \mu Cp/\lambda$).

The Reynolds number is one of the most important dimensionless quantities in microfluidics, as it correlates the inertial forces to the viscous forces [21]. The Nusselt number provides critical insight into heat transfer performance through convection relative to conduction within a fluid. Accurate knowledge of the thermal conductivity of the fluid is essential to determining the Nu number, which in turn supports design improvement and system optimizations.

The Pr is defined as the ratio of momentum diffusivity to thermal diffusivity, describes the efficiency of heat transfer within a fluid. When $Pr \gg 1$ (typically when the fluid has low thermal conductivity), convection dominates heat transfer; conversely, when $Pr \ll 1$, conduction becomes more significant. Many of these dimensionless numbers can be formulated in equations to solve for unknown parameters, such as $Nu = f(Re, Pr, ...)$ such as the global heat transfer coefficient [22].

The concept of thermal conductivity was introduced by Joseph Fourier in 1822, where he described how heat is transferred through a medium via conduction from regions of higher temperature to lower temperature. The heat flow rate (or surface specific heat flux, $\dot{q}$ [W.m^{-2}]) through a material is proportional to the negative temperature gradient (∇T [m^{-1} K^{-1}]) and depends on the material's specific thermal conductivity (λ [W.m^{-1}K^{-1}]). This relationship is famously known as Fourier's law of heat conduction [23].

$$\dot{q} = -\lambda \, \nabla T, \tag{1.1}$$

This fundamental principle has been extensively applied to heat conduction problems in various engineering fields since then. In heat transfer phenomena, two additional modes—convection and radiation—are generally present at the same time in the system, particularly in high-temperature environments.

Convection heat transfer is defined as the heat exchanged between a surface and a moving fluid with different temperatures. The equation is given by [24]:

$$\dot{q}_{cv} = h_{cv}(T_s - T_\infty), \tag{1.2}$$

where $\dot{q}_{cv}$ [$W.m^{-2}$] is the convective heat flux, T_s and T_∞ represent the surface temperature and the fluid temperature, receptively. Convective heat transfer coefficient, h_{cv} [W.m^{-2}K^{-1}], is directly influenced by the thermal conductivity (λ) of the fluid. Higher thermal conductivity in the fluid leads to more efficient heat transfer by conduction within the fluid, thereby enhancing the overall convective heat transfer. Radiation heat transfer occurs through electromagnetic waves, and the rate of radiative heat transfer between a surface and its sur-

roundings is quantified by the Stefan-Boltzmann law:

$$\dot{q}_{rad} = F\varepsilon\sigma(T_s^4 - T_{sur}^4), \tag{1.3}$$

where $\dot{q}_{rad}$ [W.m^{-2}] is the radiative heat flux, $\sigma = 5.67 * 10^{-8}$ [W.m^{-2}K^{-4}] is the Stefan-Boltzmann constant, ε represents the surface emissivity of the material, with values ranging from 0 to 1, T_s [K] and T_{sur} [K] represent the absolute temperatures of the surface and surroundings, respectively. The geometric view factor (F) between the sample surface and the surroundings is assumed to correspond to the simplest configuration, in which the container faces a large surrounding surface, F≈1. At high temperatures, radiative heat transfer becomes significant due to the 4th power of the temperature, which often affects experimental techniques used to determine the thermal conductivity of molten salts, and provides larger values. For example, the thermal conductivity of molten salt obtained by using the coaxial-cylinder techniques often produced larger values, and a positive slope as increasing measurement temperature. This will be discussed in detail in Chapter 2.

Thermal conductivity (λ [W.m^{-1}K^{-1}]) is a transport property, an intrinsic material characteristic that quantifies a material's ability to conduct heat. From a microscopic perspective, it reflects the internal energy transport mechanisms within the material, which includes atomic bonding, lattice vibrations (phonons), and the dominant contribution of electrons in metals. These mechanisms are governed entirely by the material's internal structure and composition, which makes thermal conductivity independent of the material's shape, size, or external conditions.

In contrast to the heat transfer coefficient (h [W m^{-2}K^{-1}]) and radiative heat transfer, which are extrinsic quantities, they depend on external factors such as geometry, boundary conditions, and the surrounding environment. These dependencies make them system-specific and variable to the environment, unlike the intrinsic nature of thermal conductivity [24].

Interest in the thermal conductivity of molten salts has began to grow significantly since the mid-20th century due to their potential applications as fuel and HTFs in nuclear reactors and high-temperature energy systems. Many experimental studies have been conducted to determine the thermophysical properties of molten salts. Notably, ORNL extensively explored the thermal conductivity of molten fluoride salts as part of the Molten Salt Reactor Experiment in the 1960s.

Today, with the global push for carbon neutrality established by most countries before 2025 [25]. Molten salts garner significant attention as one of the most promising high-temperature HTF and TES materials in clean power generation. Efforts are increasingly focused on developing new salt mixtures for high-temperature applications and modeling

tools for their simulations. Many key properties have been extensively studied, including density, viscosity, specific heat capacity, thermal conductivity, melting point, vapor pressure and phase equilibria [26].

Thermal conductivity is one of the most important properties for molten salts, as it directly influences the performance, stability, safety, and economic aspect of energy systems. Nunes et al. [27] highlighted the importance of thermal conductivity of molten salts by studying molten nitrate salts in CSP plants and molten sodium carbonate for molten salt oxidation. Researchers have also investigated to add nano-particles to improve the apparent thermal conductivity of molten salts [28–30]. In addition, many studies have focused on determining the thermal conductivity, and establishing additional databases and thermal properties data for molten salts to support modeling efforts, particularly for the deployment of molten salt reactors [31]. For example, Janz [32–37] compiled one of the most comprehensive handbooks of properties of molten salts, including commonly used pure salts and mixtures. Unfortunately, they were limited on the specific composition of molten salt mixtures.

Despite the important role of thermal conductivity in molten salt system, large discrepancies and disagreements on the temperature dependence of thermal conductivity across datasets still remains from different researchers and different techniques today.

Molten salts in their liquid state can be categorized into three main groups as follows:

- Pure salts: also known as unary salts, which consist of a single chemical compound. They can include monoatomic anions, such as LiF, NaCl, and KBr; or polyatomic ions, such as $LiNO_3$, Na_2CO_3, K_2SO_4, and NH_4Cl.
- Common-ion mixtures: these mixtures consist of two or more compounds that share either the same anion (e.g., NaCl-KCl-$MgCl_2$) or the same cation (e.g., LiF-LiCl-$LiNO_3$).
- Reciprocal mixtures: these mixtures contain more than one cation and more than one anion, which forms a reciprocal mixture of a more complex mixture, for examples, LiF-KCl, LiF-KCl-$MgCl_2$ and NaCl-$CaCl_2$-$MgCl_2$-CaF_2.

Most properties of molten salts can be accurately determined using experimental techniques, numerical estimations, or physical models. Nevertheless, thermal conductivity remains one of the most difficult properties to ascertain experimentally due to challenges arising from several factors, including chemical reactions, corrosion, volatility, and electrical conductivity of molten salts at high temperatures. Furthermore, the treatment of contributions from convection, conduction, and radiation heat transfer in the apparatus further complicates experimental work [38–40]. Even when employing numerical simulation techniques, determining thermal conductivity remains challenging and time-consuming due to the lack of knowledge regarding relative force field data, particularly for high-order complex molten salt mixtures.

The objective of this thesis is to develop a theoretical model that accurately predicts the thermal conductivity of molten salts. It is designed to be applicable to pure salts, common-ion mixtures, and reciprocal mixtures as a function of both temperature and composition dependence. The focus will be on advanced energy applications such as MSRs, CSP, and TES. The studied salts will include alkali and alkaline earth metal halides, carbonates, nitrate/nitrites, sulfates, and hydroxides, which are the most commonly used in energy systems. A molten salt database will be established for engineering and academic research purposes. This framework aims to provide precise thermal conductivity predictions that are comparable to recommended experimental datasets for any molten salt mixtures, ensuring the proper design and safe operation of molten salt systems.

It is now important to review experimental techniques, reported results, numerical estimation methods, and existing models for predicting the thermal conductivity of molten salts to identify gaps in the current models and guide the theoretical approach of our development. This review will be the objective of the next chapter. Chapter 3 will define the specific objective and sub-objectives of the research. The research results will then be presented in the following chapters, organized by article: Chapter 4 will focus on the development of a model for pure molten salts; Chapter 5 will extend this pure molten salt model to simple common-ion molten salt mixtures; Chapter 6 will address the modeling reciprocal molten salt mixtures based on the model of molten salt mixtures. Chapter 7 will provide a comprehensive discussion of the findings. Finally, we will conclude with an assessment of the strengths and limitations of this work, along with future perspectives.

CHAPTER 2 LITERATURE REVIEW

The thermal conductivity of molten salts is crucial for the performance of heat transfer within molten salt systems and their safe operation in industrial processes, ultimately influencing their economic payback time. Designing these processes necessitates a thorough understanding of thermal conductivity and the ability to predict its values in response to changes in temperature and composition for various potential salt candidates.

In systems where a specific salt mixture has been preselected, the thermal conductivity can be determined through experimental techniques or numerical estimations. The reliability of the results obtained varies with each technique employed, and the accuracy of these results is often questioned. While numerical estimation can mitigate some hazardous measurement conditions, challenges remain in obtaining thermal conductivity due to certain unknown input parameters. For fuel salts in MSRs, regulatory safety concerns may further restrict experimental measurements.

In complex processes where the composition of molten salt mixtures may change according to operational conditions (binary mixtures solidification, impurity removal by electrolysis, etc...), experimental determination becomes laborious, and numerical estimation may also prove impractical. Therefore, robust modeling approaches are essential for accurately predicting the thermal conductivity of molten salts in relation to both temperature and composition.

This chapter provides a comprehensive review of three primary approaches used to determine the thermal conductivity of molten salts: experimental techniques, numerical simulations, and theoretical models. Given the significance of experimental data for model validation, we begin by reviewing various experimental methods, discussing their characteristics and results. Next, we introduce equilibrium molecular dynamics (EMD) techniques, which have been extensively employed to address gaps in the available data on thermal conductivity for molten salt mixtures. While EMD simulations are constrained by compositional variation and the computational intensity required for high-order mixtures, we then explore the Modified Quasi-chemical Model in the Quadruplet Approximation (MQMQA) [41], which we intend to use for modeling the internal structure of reciprocal salts from its thermodynamic properties. This approach estimates thermodynamic properties by accounting for interatomic interactions and short-range ordering, making it essential for modeling complex and reciprocal molten salt mixtures with temperature and composition dependence. Finally, we overview existing models that predict the thermal conductivity of molten salts, which have informed the development of our own model.

2.1 Experimental techniques

Accurate knowledge of thermal conductivity is essential not only for the proper dimensioning of engineering systems but also for ensuring the project's thermo-economic efficiency. Over several decades, various experimental techniques have been developed and employed to determine the thermal conductivity of materials, including gases, liquids (such as molten salts), and solid phases. These experimental techniques can be categorized into two main groups: steady-state methods and transient methods. Figure 2.1 illustrates the commonly used techniques within each category. Each technique possesses unique features, but the overarching goal remains the accurate determination of thermal conductivity or thermal diffusivity. However, heat losses through conduction, convection, and radiation pose critical concerns regarding the precision of the obtained data.

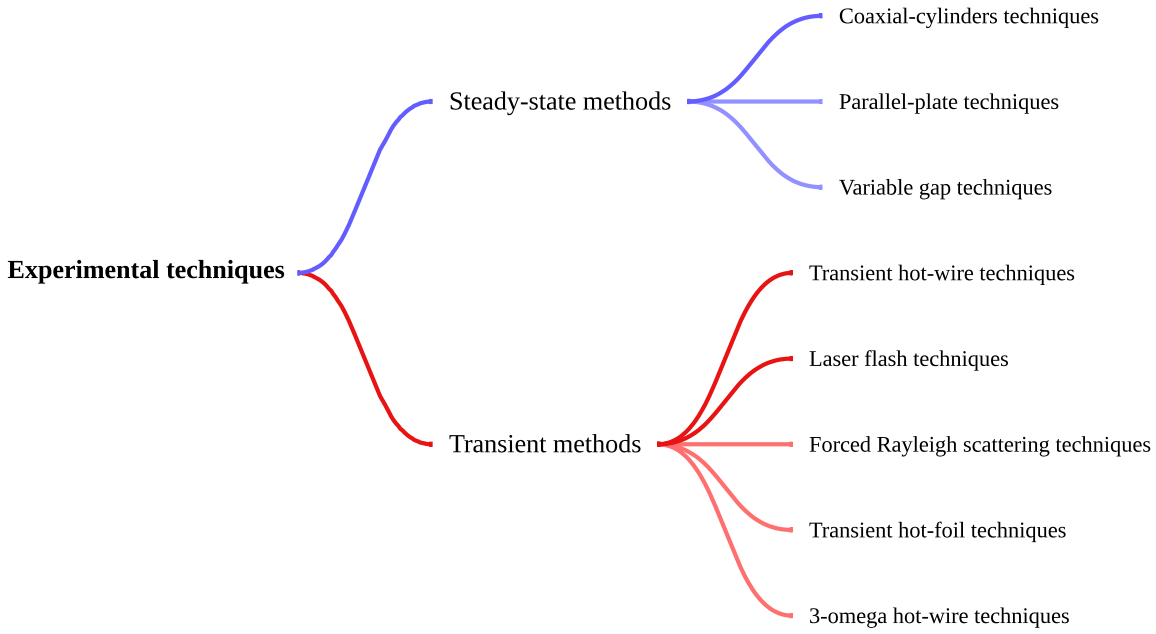

Figure 2.1 Two main categories of experimental techniques [42, 43]

Measurements at high temperatures involve various modes of heat transfer: convective, conductive, and radiative. All of these modes are present during experimental work and can significantly affect experimental accuracy. To obtain reliable values, it is essential to carefully assess and estimate each mode of heat transfer. The following points outline potential sources of error associated with each heat transfer mode:

- Convection is primarily influenced by the gap thickness in the measurement setup. A

larger gap holding the specimen can create convective flow in the liquid when temperature gradients are present, leading to increased uncertainty in the results.

- Heat conduction can occur through the cylinders and instrumentation, potentially resulting in greater-than-expected heat losses.
- Radiative heat transfer becomes significant at high temperatures; therefore, the cylinder material should possess low emissivity. Accurate correction for radiative heat transfer is necessary; otherwise, the temperature dependence of thermal conductivity may exhibit a positive trend, which is often indicative of unreliable experimental data.

2.1.1 Steady-state methods

The steady-state methods are based on Fourier's law of conduction, where thermal conductivity is determined by introducing a heat flux into a layer of salt of known thickness and measuring the resulting temperature difference across the layer. These techniques present challenges, as accurately determining the heat transfer due to convection, conduction, and radiation through the apparatus can be difficult. However, when carefully designed, these techniques can yield reasonably precise data [44]. Common measurement techniques within the steady-state method include coaxial-cylinder techniques, parallel-plate techniques, and variable gap techniques.

Coaxial-cylinders techniques

Coaxial-cylinder techniques consist of an inner cylinder and an outer cylinder, with the molten salt held in between. An isothermal temperature difference is maintained to achieve thermal equilibrium. By determining the heat flux from the inner cylinder across the known thickness of the molten salt to the outer cylinder, the thermal conductivity can be directly obtained using Fourier's law in cylindrical coordinates. The equation is given:

$$\lambda = \frac{\dot{q}\ ln(r_2/r_1)}{2\pi\ l\Delta T}, \tag{2.1}$$

where r_1 and r_2 represent the inner and outer radius of the liquid sample located, ΔT is the temperature difference between two radius. l is the length of the liquid sample, and $\dot{q}$ is the input heat flux. Figure 2.2 (a) schematically illustrates the principle of the technique.
This technique offers a direct measurement of thermal conductivity, in contrast to other indirect methods that determine thermal diffusivity. Once again, the accuracy of the measurement relies on the careful assessment of the effects of convection, conduction, and radiation heat transfer. Various experimental measurements have been conducted by employing

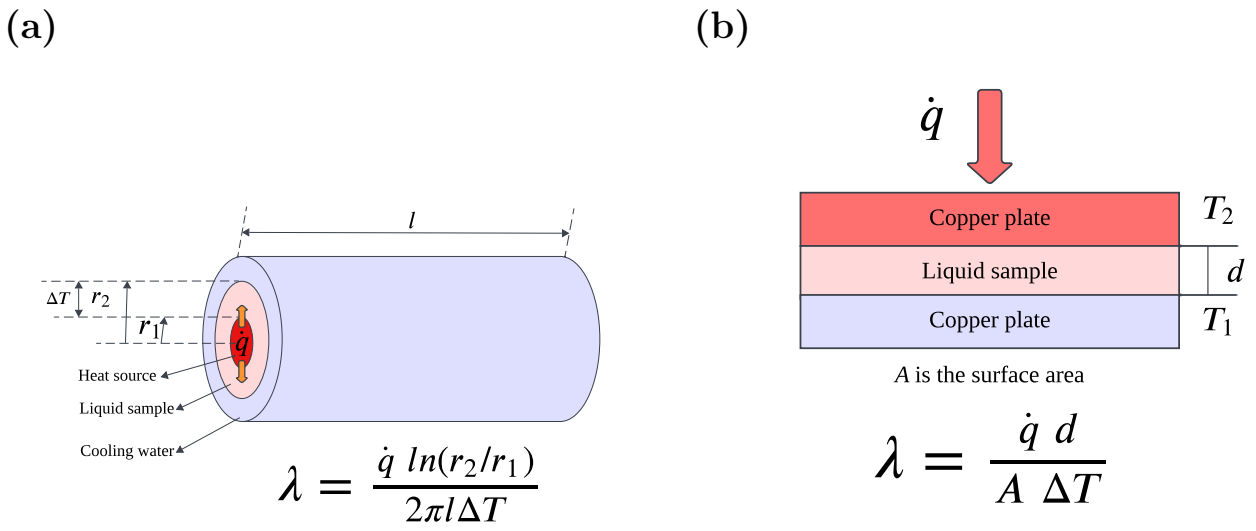

Figure 2.2 Schematic of different techniques: (a) Coaxial-cylinders techniques (adapted from Zhao's paper [45]), and (b) Parallel-plate technique (adapted from Zhao's paper [43]).

this technique. Table 2.1 summarizes the work of different investigators, includes the gap thickness, cylinder materials used, the sign of temperature dependence ($(\partial\lambda/\partial T)|_P$), and the reliability of their measurements. DiGuilio and Teja [57] emphasized that accurate thermal

Table 2.1 Summary of numerous investigators' measurements [40].

Investigator	**Gap [mm]**	**Cylinder material**	**Uncertainty [%]**	$(\partial\lambda/\partial T)\|_P$
Golyshev and Gonik [46]	1	Molybdenum	5–6	-
Tufeu et al. [47]	0.2	Silver	5	∼0
Veneraki et al. [48]	1.37-2.19	Graphite	8	-
White and Davis [49]	3.18	Silver	-	+
McDonald and Davis [50]	2.54	Silver	-	+
Fedorov and Machuev [51]	3	Graphite	8-10	+
Polyakov and Gildebrandt [52]	3	Graphite	10	+
Savintsev et al. [53]	2	Platinum	9-10	+
Egorev and Revyakina [54]	3	Stainless steel	10	+
Bloom et al. [55]	0.9	Silver	5	+
Smirnov et al. [56]	1.2	Platinum	4	+

conductivity data should exhibit a non-positive temperature dependence ($(\partial\lambda/\partial T)|_P \leq 0$). This observation aligns with the findings of Nagasaka and co-workers [58], Harada and co-workers [59], as well as several recent studies [40,60,61]. According to the signs of temperature dependence presented in Table 2.1, most studies have reported unreliable datasets. Although all investigators claimed measurement uncertainty within 10%, underestimated heat losses often lead to inflated results. For instance, a large gap between the inner and outer cylinders

can significantly enhance heat transfer due to convection and radiation. Additionally, while guard rings are used to minimize heat losses at the ends of apparatus, significant errors can arise from inaccurate measurement of the axial temperature gradient [47].

Parallel-plate techniques

These techniques consist of three layers, resembling a sandwiched structure, where heat transfer is considered solely through conduction. The top layer is made of a highly conductive metal (such as copper) to which the heat flux is applied. The second layer contains the liquid to be studied, while the bottom layer is also composed of a good conductive metal that receives heat from the top layer until thermal equilibrium is reached. Both the top and bottom layers should be coated to resist corrosion from high-temperature molten salts. Consequently, the thermal conductivity of the liquid can be estimated using Fourier's law, as given:

$$\lambda = \frac{\dot{q}\ d}{A\Delta T}, \tag{2.2}$$

where A and d are the surface area and thickness of the liquid sample. The schematic of these techniques is shown in Figure 2.2 (b).
Tye et al. [62], Kato et al. [63], Santini et al. [64], and Araki et al. [65] employed this technique to determine the thermal conductivity of molten salts. Unfortunately, their reported datasets all exhibited a strong positive temperature dependence. The primary concern regarding significant heat losses at high temperatures is the impact of radiative heat transfer.

Variable gap techniques

The variable gap techniques (Figure 2.3) were originally developed at ORNL for determiningthe thermal conductivity of molten fluoride salts for the purpose of MSRs [66]. These techniques are similar in principle to the parallel-plates method, which measures steady-state temperature differences across a gap containing the sample. In these techniques, the gap thickness is variable, typically less than 0.3mm, to minimize convective flow within the liquid. A small temperature difference of 10°C to 15°C is maintained across the sample [61]. Since the measurement only considers changes in the specimen's thickness and temperature, potential errors due to convection, radiation, and conduction heat losses can be estimated and minimized [66]. The thermal conductivity of liquid sample is considered as a linear function of the variable gap x, the expression is shown:

$$\frac{\Delta T}{\dot{q}} = \frac{x}{\lambda} + R_{th,fix}, \tag{2.3}$$

where $R_{th,fix}$ represents the upper and lower resistances, which are expected to remain nearly

constant or fixed during measurement [67]. Merritt et al. [68] noted that these techniques

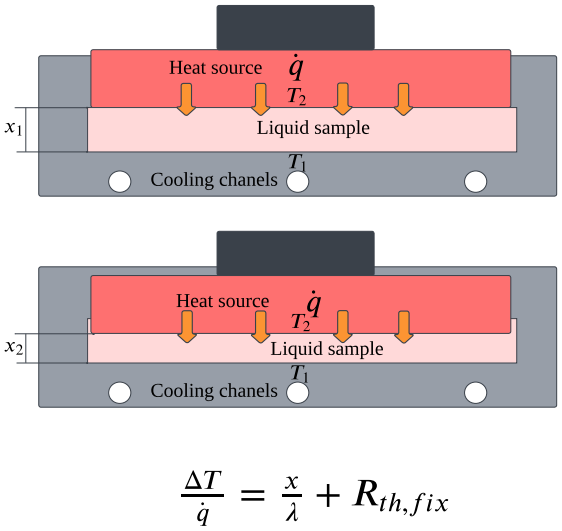

$$\frac{\Delta T}{\dot{q}} = \frac{x}{\lambda} + R_{th,fix}$$

Figure 2.3 Schematic of variable gap technique (adapted from Gallagher's paper [67])

could introduce considerable errors due to heat loss through pathways other than the sample liquid itself. Nevertheless, Cooke [66] successfully determined the thermal conductivity of HITEC salt, which was consistent with other reliable datasets and exhibited a negative temperature dependence. More recently, Gallagher et al. [44] employed the same technique with some improvement to determine the thermal conductivity of FLiNaK, finding a negative temperature dependence in their minimum obtained values. Both datasets were in good agreement with other reliable datasets.

2.1.2 Transient methods

Transient techniques offer short measurement times, require minimal sample quantities, and often involve indirect contact with the sample. These advantages make them highly recommended for obtaining data on the thermal conductivity of molten salts [58, 69, 70].
Common transient methods include (modified) transient hot-wire, transient hot strip, laser flash, and forced Rayleigh scattering, among others [59, 69, 71–75]. Some of these techniques measure thermal diffusivity, which requires the knowledge of additional properties such as salt density and heat capacity to determine thermal conductivity.
These techniques can be challenging to apply to certain molten salts due to high temperatures, corrosion of probes or containers, and possible errors arising from different modes of heat transfer. For instance, fluoride salts can react adversely with many types of glasses and dielectric materials used for optical windows or probe insulation [69, 71]. Furthermore, recent

findings using laser flash diffusivity techniques have sometimes indicated a positive temperature dependence $(\partial\lambda/\partial T)|_P > 0$ [76, 77], which can be attributed to the heat leakage.
While many experimental results obtained through transient techniques are considered reliable, careful evaluation is still necessary due to the lack of standardized measurement procedures [68, 78–80].

Transient hot-wire techniques

Transient hot-wire techniques provide reliable measurements of thermal conductivity for liquids, solids, gases, and powders, and have become widely employed methods for liquids. These techniques utilize a thin wire, typically made of platinum, which functions as both a heater and a thermocouple, suspended or embedded in the sample. The voltage of the platinum wire changes in incremental steps, creating a transient temperature that heats the measurement environment. This generates a line source with a uniform heat flux per unit length that remains constant over time [81]. The thermal conductivity can be determined by observing the time-dependent temperature change of the platinum wire. The schematic of the transient hot-wire techniques is illustrated in Figure 2.4 (a).
Given that molten salts are corrosive and electrically conductive at high temperatures, the platinum wire must be coated to prevent current leakage and corrosion. Various coatings have been developed to address these challenges [58, 69, 71]. The equation governing the transient hot-wire technique is expressed as follows [82]:

$$\lambda = \frac{\dot{q}/l}{4\pi\ \Delta T}\ ln(\frac{4\alpha_{dif}}{r^2 C}t), \tag{2.4}$$

where α is the thermal diffusivity of the fluid, normally taken at the temperature T_{ref} and is nearly constant. r is radius of the wire, $ln(C) = \gamma_{Euler}$, γ_{Euler} is Euler's constant. In earlier studies, Turnbull et al. [83] used this technique to determine the thermal conductivity of molten nitrate salts. However, the time increment of his experimental measurements was set to 1 minute, which seemed too long to achieve accurate thermal conductivity results [72]. In addition, the current leakage was occupied due to the lack of insulation on the wire, which greatly impacted the results because of the influence of electrical conductivity. Similar issues were present in McLaughlin et al. [84]'s work, where no insulation was used.
Omotani et al. [71] improved this technique by using liquid mercury in a quartz tube as the heat source rather than exposing the wire directly to the sample, effectively minimizing convection errors. Their results showed a negative temperature dependence, were consistent with other reliable datasets. Nakazawa et al. [85] and Kitade et al. [69] further modified the technique by using ceramic Al_2O_3 as an insulator, which was coated on the platinum

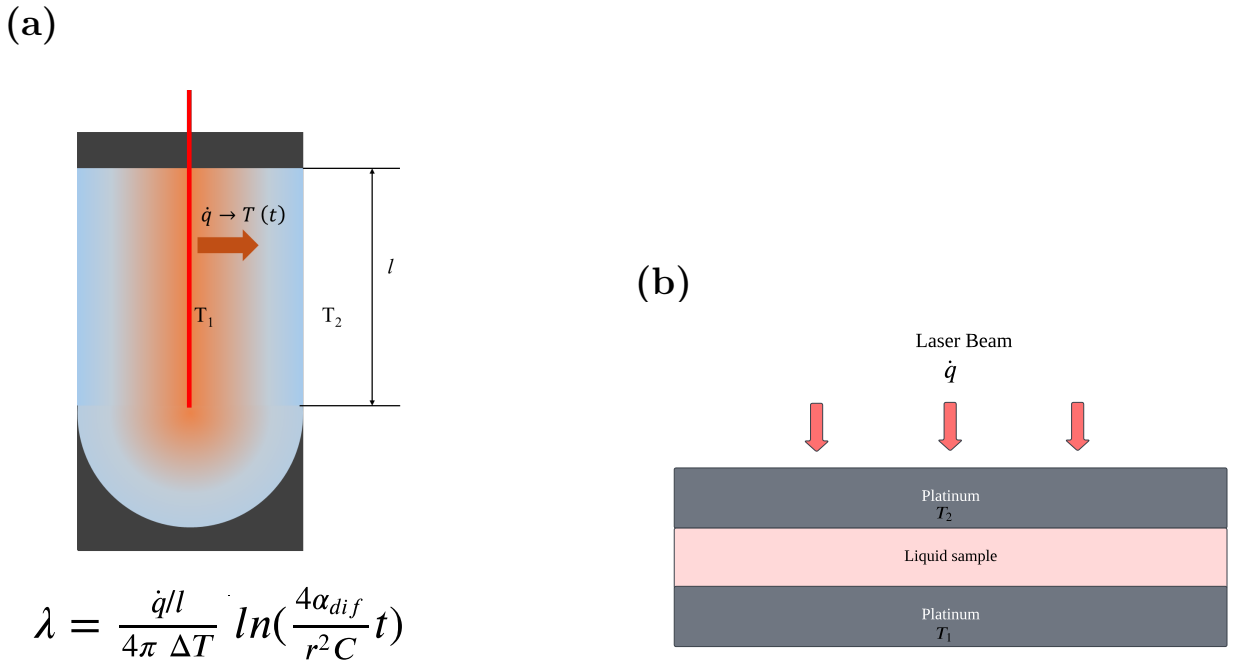

Figure 2.4 Schematic of different techniques: (a) Transient hot-wire technique, and (b) Laser flash technique (adapted from Zhao's paper [43]).

wire. Their reported results agreed well with those other researchers, and remained within acceptable accuracy.

More recently, Merritt et al. [68] developed a modified transient hot-wire needle probe by combining the advantages of the transient hot-wire technique and the concentric cylinder techniques, which shortened the measurement times and minimized convection and radiation heat losses. Their results also aligned well with other reliable experimental datasets for molten nitrate salts and FLiNaK.

Laser flash technique

The laser flash technique is one of the most widely used methods for indirectly determining thermal conductivity. It measures the thermal diffusivity (α_{dif} [$m^2.s^{-1}$]) of liquids at high temperatures, requiring additional knowledge of density (ρ) and heat capacity (Cp) to calculate the thermal conductivity of the sample. The formula is given by:

$$\alpha_{dif} = \frac{\lambda}{\rho Cp} \tag{2.5}$$

This technique consists of a sandwiched structure with three layers of well-defined geometry. The liquid sample is heated by a laser or flash lamp. The high-intensity laser beam strikes and heats the first layer, and heat is subsequently transferred through the liquid by conduction.

An infrared detector located on the third layer captures the transient temperature changes. Figure 2.4 (b) illustrates the concept the laser flash technique.
The thermal conductivity obtained using the laser flash technique often shows a positive temperature dependence. This is likely due to a lack of correction for radiative effects and conductive losses within the structure [61]. Furthermore, this sign of temperature dependence is also influenced by the precision of heat capacity and density. An et al. [76] used the laser flash technique to measure the thermal conductivity of FLiNaK. Their results, near the melting point aligned with other studies; however, an increase in thermal conductivity was observed with rising temperature. More recently, Rudenko et al. [86] employed the same technique to measure the thermal conductivity of FLiNaK in 2022. Their results were consistent with other reliable studies but demonstrated a negative temperature dependence.

Forced Rayleigh scattering techniques

Forced Rayleigh scattering (FRS) is another optical method used to measure the thermal diffusivity of liquids. In this technique, a laser beam is split into two beams of identical intensity, which cross the liquid sample to create an interference pattern. This pattern induces a sinusoidal temperature distribution that acts as an optical phase grating for the probing beam. The liquid sample is colored with a small amount of dye to absorb the energy from the heating laser beam. The transient decay of the temperature distribution induced by a short heat pulse follows the diffusion heat equation. By analyzing the diffracted probing laser, the thermal diffusivity of the liquid sample can be determined [58].
Nagasaka and his co-workers redesigned the FRS techniques to measure the thermal conductivity of molten alkali halides, claiming a measurement accuracy within a few percent [58, 72, 87]. However, it was not possible to measure molten fluoride salts due to their strong corrosiveness towards the sample containers. All of Nagasaka's work demonstrated a negative temperature dependence, which aligned with findings from other researchers. We have therefore used Nagasaka's work as the model development reference for our study.

Other experimental techniques

Various techniques have been developed to measure the thermal conductivity of liquids. Among the transient methods, the transient hot-foil (hot-disc) technique stands out, operating similarly to the transient hot-wire method. However, instead of a wire, this approach uses a plane-shaped foil to generate a plane heat source. While the method offers certain advantages, its application to molten salts is more complex due to the lower ionization within the salt. The reduced voltage along the heat source causes polarization at the interface between the heated foil and the molten salt, limiting current flow. Nonetheless, in practice,

other voltage potentials can exist within the cell, allowing some current to flow into the salt despite surface polarization [66].

Zhao et al. [43] utilized the 3-omega hot-wire technique to measure the thermal conductivity of nitrate salts. This method separates frequency domain measurements from steady-state and transient measurements. Similar to the transient hot-wire technique, it employs an alternating current with a fundamental angular frequency (ω) to heat the platinum wire sensor and surrounding liquid at 2ω, resulting in a voltage response at three times the input frequency, or 3ω. This frequency-domain approach minimizes errors due to corrosion and convection that can affect other measurement methods. Zhao et al. [78] successfully determined the thermal conductivity of molten nitrate salts, reporting an uncertainty of less than 3%. The results showed a negative temperature dependence, though both sodium nitrate and potassium nitrate datasets exhibited slightly higher values compared to other reliable measurements. Unfortunately, no additional studies on the thermal conductivity of other molten salts have been conducted.

Please refer to Chapter 4 (Article 1) for a comparative review of the characteristics of the most commonly used experimental techniques to measure the thermal conductivity and diffusivity of molten salts, along with their reported accuracy.

2.2 Current status of thermal conductivity measurements of molten salts using experimental techniques

In our work, most of the experimental data available in the literature have been collected for molten fluorides [56, 88–91] [92–94], chlorides [50–53, 56, 83, 95–99] [58, 59, 79, 92, 100], bromides [50, 56, 95] [59, 73, 94], iodides [50, 56] [59, 74], carbonates [54, 97, 101, 102] [75], nitrates/nitrites [49, 50, 55, 64, 83, 84, 102–111] [38, 47, 63, 69–71, 112], sulfates [113], and hydroxides [104, 114, 115]. To highlight the important experimental works, the corresponding references have been underlined to facilitate reading. These data points will be shown in chapter 4 and 5. These datasets can be categorized based on their sign of temperature dependence. Data exhibiting a positive temperature dependence ($(\partial\lambda/\partial \mathrm{T})|_{\mathrm{P}} > 0$) are generally obtained using steady-state methods, whereas those showing a negative temperature dependence ($(\partial\lambda/\partial \mathrm{T})|_{\mathrm{P}} < 0$) are typically acquired through transient techniques. This disagreement in the sign results in significant discrepancies among experimental datasets for both pure molten salts and mixtures. However, values close to the melting point are sometimes quite similar across studies. The thermal conductivity of molten unary salts reported by different researchers generally falls within the range of 0.1 to 3 [$\mathrm{W.m^{-1}K^{-1}}$]. Among these pure molten salt datasets, approximately 62% were obtained using coaxial-cylinder techniques, which was the most popular method before the 1980s. This is followed by tran-

sient hot-wire and laser flash techniques, each accounting for roughly 13% of the datasets. Some techniques were developed and used exclusively for that research group. For example, the variable gap method exclusively belonged to the ORNL group; while the FRS techniques were employed only by Nagasaka and his co-workers. Other techniques have contributed to the remaining datasets. For a detailed visual representation of the available datasets on pure molten salt thermal conductivity, please refer to the figures in Chapter 4.

Looking at two widely studied heat transfer fluids: FLiNaK, commonly studied in MSRs; and solar salt, the most used in CSP plants. Fig. 2.5 illustrates a simple common-anion ternary fluoride salt at the eutectic composition $(\mathrm{LiF})_{0.465} - (\mathrm{NaF})_{0.115} - (\mathrm{KF})_{0.42}$ (mole fraction) commonly referred to as FLiNaK, which has been proposed for implementation as a coolant in MSRs. Figure 2.5 depicts that the most recent experimental datasets mostly exhibited a negative temperature dependence, contrasting with earlier works that demonstrated a positive sign. Notably, Janz et al. [34] reported thermal conductivity values with a significantly positive sign, and approximately 300% higher than other studies near the melting temperature. Moreover, it is noteworthy that thermal conductivity values remained relatively consistent near the melting temperature in the works published after 1987. Yet, as the measurement temperature increased, the discrepancy became notably significant, mainly due to errors caused by the radiation effect. Hence, the analysis and selection of reliable experimental datasets is of prior importance for developing a reliable thermal conductivity model of molten salts. We believe that the negative temperature dependence observed is accurate.

Figure 2.6 presents available experimental datasets for molten nitrate salt mixtures found in the literature. These datasets exhibit consistency in both temperature dependence and the thermal conductivity values obtained from different experimental techniques. This consistency is likely attributed to the extensive research on $NaNO_3$ and KNO_3 (figures in Chapter 4), with many reported datasets aligning closely near the melting temperature. Consequently, there are fewer constraints in using solar salt compared to working with FLiNaK, as the experimental datasets for solar salt are more consistent.

As emphasized previously, experimental techniques often underestimate heat losses through convection, conduction, and radiation at high temperatures. Consequently, the thermal conductivity values obtained are generally overestimated. These losses become significant as the measurement temperature increases, making it challenging to accurately quantify the individual contributions. Moreover, the complexity of heat transfer in these cases is influenced by various factors, including device geometries, materials, sample container properties, and

[1]The abbreviations for different experimental techniques are as follows: VGT—variable gap techniques, LFT—Laser flash techniques, MTHW—Modified transient hot-wire techniques, CCT—Coaxial cylinder techniques, TGST—Transient grating spectroscopy techniques, and 3ω—3-Omega techniques.

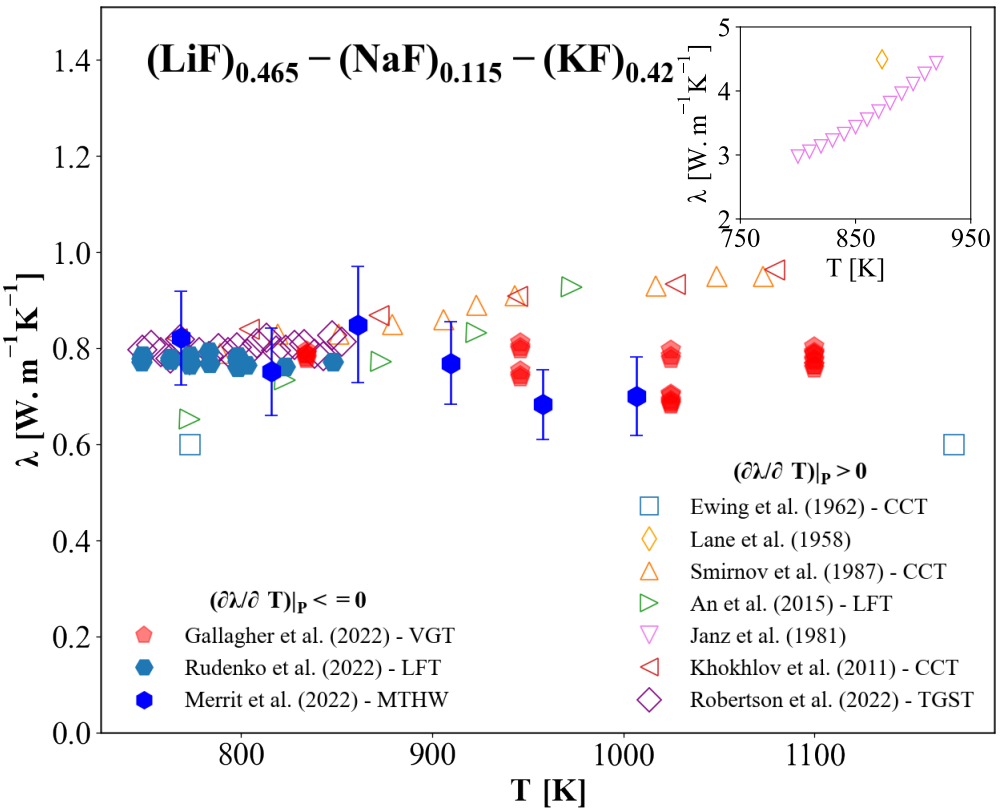

Figure 2.5 Thermal conductivity of a common-anion ternary fluoride salt - FLiNaK $(LiF)_{0.465} - (NaF)_{0.115} - (KF)_{0.42}$ as a function of temperature obtained via experimental techniques[1].

other technique-specific parameters, which are beyond the scope of this research.
Conversely, by considering these heat losses, results obtained from numerical simulations or modeling can be validated indirectly. Unlike experimental techniques, numerical simulations and modeling mitigate the impact of these heat losses, providing generally more reliable predictions of thermal conductivity. With this context in mind, let us now shift our focus to the technique of MD simulations.

2.3 Numerical simulations

In recent years, advancements in computational power have made numerical simulations an alternative approach for predicting the physical properties of materials. Numerical simulations include methods such as Monte Carlo and molecular dynamics (MD) simulations. The

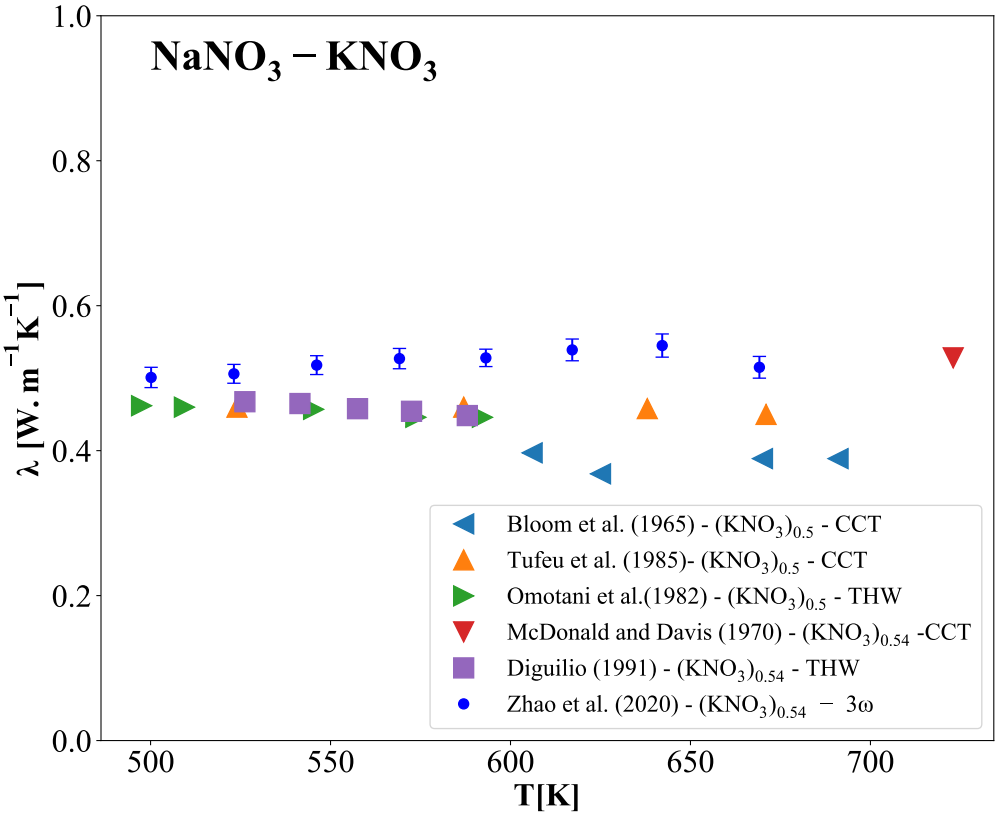

Figure 2.6 Thermal conductivity of a molten nitrate salt $NaNO_3 - (KNO_3)_x$(mol) as a function of temperature obtained via experimental techniques.

Monte Carlo method is faster and more suitable for determining thermodynamic properties, while MD simulations are more appropriate for studying transport properties [116].

In MD simulations, atoms are represented as particles, and their movements are driven by interactions with one another, which are determined by solving Newton's equations of motion. These interactions are described by a force field, which defines the potential forces acting on the particles. Consequently, the accuracy of the force field is crucial for ensuring the precision of the simulation.

Many studies have employed the MD method to investigate the properties and local structures of molten salts. However, these methods are limited by the accuracy of their underlying parameters (potentials) and assumptions, which can sometimes yield results that are larger than those obtained from experimental work [60]. Despite the larger uncertainty, MD simulations can provide a preliminary understanding of the behavior of salts, particularly for

molten salt mixtures in relation to their composition.

2.3.1 Classical MD

Classical MD employs predefined potentials and force fields derived from either empirical data or independent electronic structure calculations. This approach has become a well-established and powerful method for studying many-body condensed matter systems [117]. The two most common methods for calculating atomic interactions in salt systems during MD simulations are the "Rigid Ion Model (RIM)" and the "Polarized Ion Model (PIM)". RIM, a simpler and more commonly used method, assumes that each ion carries a point charge at its center of mass, completely ignoring electronic polarization. This simplification can reduce the accuracy of the results, especially when simulating dynamic properties [118]. On the other hand, the PIM accounts for ion polarizability, capturing the important polarizable effects in salt systems. It is considered one of the most successful models [119]. Rather than relying on predefined empirical input potentials, the PIM derives these parameters by fitting to Density Functional Theory (DFT) data. This approach enables the parametrization of complex force fields, leading to accurate energy estimates [120].

To address the lack of thermal conductivity for certain molten salt mixtures, we performed extensive EMD simulations using the Polarized Ion Model (PIM). The PIM, developed by Madden and colleagues [121, 122], has demonstrated strong performance and accuracy in simulating chloride and fluoride salts, and is expected to be well-suited for other salts as well. For a more detailed discussion of the model's development, refer to the work of Salanne et al. [123]. Here, we provide a brief overview of the PIM model.

The interionic potential accounts for interactions such as charge-charge, charge-dipole, dipole-charge, dipole-dipole, overlap repulsion, dispersion, and polarization, and is expressed as follows [122, 124, 125]:

$$
\begin{aligned}
U_{ij}(\boldsymbol{r_{ij}}) = & \underbrace{\frac{q_i q_j}{r_{ij}}}_{\text{Charge-charge}} + \underbrace{B_{ij} e^{-\alpha_{ij} r_{ij}}}_{\text{Overlap repulsion}} \underbrace{-\frac{C_6^{ij} f_6^{ij}(r_{ij})}{r_{ij}^6} - \frac{C_8^{ij} f_8^{ij}(r_{ij})}{r_{ij}^8}}_{\text{Dispersion}} \\
& \underbrace{+ \frac{q_i \boldsymbol{r}_{ij} \boldsymbol{\mu}_j}{r_{ij}^3} f_4^{ij}(r_{ij}) - \frac{\boldsymbol{\mu}_i \boldsymbol{r}_{ij} q_j}{r_{ij}^3} f_4^{ij}(r_{ij})}_{\text{Polarization}} \\
& \underbrace{+ \frac{\boldsymbol{\mu}_i \boldsymbol{\mu}_j}{r_{ij}^3} - \frac{3(\boldsymbol{r}_{ij} \cdot \boldsymbol{\mu}_i)(\boldsymbol{r}_{ij} \cdot \boldsymbol{\mu}_j)}{r_{ij}^5}}_{\text{Polarization}}
\end{aligned}
\tag{2.6}
$$

In the Eq. 2.6, q_i and μ_i are respectively the charge and the dipole moment of the i particle.

The Born-Mayer-Huggins short range potential term, $B_{ij}e^{-\alpha_i r_i}$, is used to describe the short-distance overlap repulsion of electronic clouds. C_6^{ij} and C_8^{ij} are the dispersion coefficients. The dispersion damping function, f_n^{ij}, for short-range correction of interactions between charge and dipole and dispersion interactions is expressed as follows [126]:

$$f_n^{ij} = 1 - c_n^{ij} e^{-b_n^{ij} r_{ij}} \sum_{i=0}^{n} \frac{(b_n^{ij}\ r^{ij})^k}{k!} \tag{2.7}$$

The long-range electrostatic interactions, $U^{Coul} = \frac{1}{2} \sum_{i \neq j}^{N} \frac{q_i q_j}{r_{ij}}$, are considered by employing a three-dimension Ewald summation method [127].

The parameter set $B_{ij}, \alpha_{ij}, C_6^{ij}, C_8^{ij}, b_n^{ij}, c_n^{ij}$ in the formalism is used to describe the total pair-wise potentials between ionic pairs. These parameters were calculated by Ishii et al. [128] via a procedure for determining potential parameters based on Madden's work [122], which relies solely on electronic structure calculations employing density functional theory (DFT). Subsequently, by matching the dipoles and forces on the ions calculated from DFT for condensed phase ionic configurations, the potential parameters are deduced using an objective minimization procedure. Since no experimental information was considered in the parametrization process, the generated potentials are classified as *ab initio* MD (AIMD) [124].

2.3.2 *Ab initio* MD

Instead of relying on pre-determined parameters used in classical MD, *ab initio* MD, also known as first-principles MD, using quantum mechanics to calculate the forces acting on the nuclei "on-the-fly" through electronic structure calculations as the simulation progresses [117]. AIMD is widely applied to novel or poorly characterized materials, including complex molten salts and reactions occurring under extreme conditions. AIMD requires only fundamental constants such as the fine-structure constant, electron mass and charge, atomic nucleus mass and charge, Planck's constant, and the speed of light [129]. Due to the high computational demand of quantum mechanical calculations at each time step, AIMD is typically limited to systems with only a few hundred atoms and short timescales.

Machine learning potential (MLP) has been paid much attention in recent years, thanks to its high speed and accuracy to simulate the complex interactions between molecules. The MLP applies deep neural networks to learn the potential energy function of the interatomic interactions [130]. MLP significantly reduces the computational demands of AIMD simulations by approximating quantum mechanical interactions without requiring electronic structure calculations at each time step. This enables the simulation of larger systems and longer timescales.

2.3.3 Derivation of thermal conductivity from EMD simulations

Thermal conductivity from molecular dynamics (MD) simulations can be determined using two primary approaches: the Green-Kubo (GK) formalism for equilibrium molecular dynamics (EMD) and direct methods for non-equilibrium MD, which are based on the known heat flux and temperature gradient of the system [43]. In this discussion, we will focus on the GK formalism for EMD.

According to the GK formalism [98], thermal conductivity can be calculated from EMD. The GK formalism is based on the fluctuation-dissipation theorem reported by Weber [131], allowing for the interpretation of thermal conductivity from the fluctuations in energy and charge currents obtained from EMD. The entropy of a molten mixture can be calculated using non-convective fluxes of heat, mass, and charge [132].

In line with our previous work, the macroscopic energy flux is calculated as a summation of heat and enthalpy contributions in the present study [133]. Following the GK method, the thermal conductivity induced by lattice vibrations for a given molten mixture of composition X, at a given temperature T is evaluated from the simulations as a function of the correlation time, τ:

$$\lambda(T,\tau,X) = \frac{1}{T^2}[L_{ee} - B^{-1}\sum_{i=0}^{2} L_{ez_i} A_{z_i z_j z_k}] \tag{2.8}$$

Where both A and B are the matrix determinants which calculated for pure compound (C), binary (B), or ternary (T) as follows:

$$A^C = L_{ez_0},\ B^C = L_{z_0 z_0} \tag{2.9a}$$

$$A^B_{\alpha\beta} = \begin{vmatrix} L_{e\alpha} & L_{\beta\alpha} \\ L_{e\beta} & L_{\beta\beta} \end{vmatrix},\ B^B = \begin{vmatrix} L_{z_0 z_0} & L_{z_1 z_0} \\ L_{z_0 z_1} & L_{z_1 z_1} \end{vmatrix} \tag{2.9b}$$

$$A^T_{\alpha\beta\gamma} = \begin{vmatrix} L_{e\alpha} & L_{\beta\alpha} & L_{\gamma\alpha} \\ L_{e\beta} & L_{\beta\beta} & L_{\gamma\beta} \\ L_{e\gamma} & L_{\beta\gamma} & L_{\gamma\gamma} \end{vmatrix},\ B^T = \begin{vmatrix} L_{z_0 z_0} & L_{z_1 z_0} & Lz_2 z_0 \\ L_{z_0 z_1} & L_{z_1 z_1} & L_{z_2 z_1} \\ L_{z_0 z_2} & L_{z_1 z_2} & L_{z_2 z_2} \end{vmatrix} \tag{2.9c}$$

The transport coefficients L in the above equations are determined through the GK formulation [98]:

$$L_{nm}(\tau,T,X) = \frac{1}{3k_B V}\int_0^\tau \langle \boldsymbol{J}_m(t)\ \boldsymbol{J}_n(0)\rangle\ dt \tag{2.10}$$

Where m and n can be e or z_i; J_e and J_z are correspondingly the energy (e) and charge (z) flux of the i ion; k_B and V are Boltzmann constant and equilibrium volume of the

system, respectively. Notice that in Eq. 2.8, the first term L_{ee}/T^2 is responsible for the thermal conductivity of an electrically neutral fluid. The second term of Eq. 2.8 describes the thermo-electrical effect on thermal conductivity.

In practice, the total canonical statistical ensemble (NVT) run is divided into 20 blocks of 0.5ns and the transport coefficients L were calculated independently in each block. The correlation time, τ, is set to 5ps which is large enough to ensure convergence of the thermal conductivity. Lastly, an average value over all the different blocks is considered as the thermal conductivity of a perfectly thermally equilibrated system:

$$\lambda(X,T) = \lim_{\tau\to\infty} \langle \lambda\ (\tau, T, X) \rangle_{all\ blocks} \tag{2.11}$$

In 2008, Salanne et al. [134] defined one of the most widely used interatomic potentials. Since then, the PIM has been employed to simulate various properties of molten salts, with most results validated by experiments [123, 134–161], demonstrating its accuracy in reproducing the thermal conductivity of molten salt mixtures [133, 138, 141, 147, 151, 152, 154].

The main advantages of MD simulations of molten salts are not only to avoid the costly and hazardous experiments, but also the insights to provide the complex fluid dynamics and chemical interactions, leading to stable complex structures. The radial distribution function reveals local structures and short-range ordering within molten salts, which provides a better understanding of the behavior of molten salt solutions. As discussed earlier, NaCl is the simplest ionic liquid, where Na^+ ions are surrounded by Cl^- ions, and vice versa, in the molten state. This structure has a high degree of short-range ordering, though ions remain free to move. In molten salt solutions, the behavior is different, since multiple ions are present in the melt. For example, in common-ion salt mixtures (for example, KCl-$MgCl_2$, LiF-BeF_2), interactions primarily occur at the second-nearest-neighbor level, and complex structures form due to polarization effects. These complex ions generally have lower mobility than simple ions, which impacts the transport properties of the melt. In the case of LiF-BeF_2 mixtures, for example, a dissociated melt (Li^+, BeF_4^{2-}, F^-) forms at low BeF_2 content, while species such as $Be_2F_7^{3-}$, $Be_3F_{10}^{4-}$, $Be_4F_{14}^{5-}$, and higher-order polymers appear with increasing BeF_2 content [162]. In some mixtures, more than one different cation and more than one anion are present within the melt, which is referred to as reciprocal mixtures, where interactions occur at both the first and second-nearest-neighbor short-range ordering. This results in significant deviations from ideal behavior, reducing the thermal conductivity of the melt, particularly when there are large differences in ionic masses and size, as in LiF-CsI mixtures. In industrial processes such as metal electrolysis, common-ion and reciprocal mixtures often form very complex solutions. Simulating these intricate systems using numerical techniques is highly challenging due to the need for numerous force field interactions, many of which are

frequently unavailable. Furthermore, molecular dynamics (MD) simulations are limited to performing only one specific molten salt composition and temperature per run. For context, each MD simulation typically requires at least 48 hours to complete, with additional hours needed for data analysis and calculations to obtain the results. Consequently, exploring a broad range of compositions and temperatures, as commonly occurs in industrial processes, significantly increases the required simulation time, computational complexity, and overall effort.

This limitation restricts the applicability of MD simulations in practical engineering scenarios, such as molten salt reactors (MSRs). In these reactors, numerous simulations are conducted to support development and optimization through finite element analysis (FEA) and fluid dynamics, which evaluate heat transfer, mechanical stresses, and flow characteristics. Accurate simulations must account for the variable thermal conductivity of molten salts across varying temperatures and compositions, as this critically influences reactor efficiency and safety. However, obtaining comprehensive compositional and temperature-dependent data as inputs for FEA becomes impractical for large-scale industrial process simulations using MD simulations.

In such cases, more efficient methods are necessary to estimate the properties of complex molten salt solutions. This need has driven efforts to develop robust thermophysical property databases for molten salt mixtures, including eutectic behaviors and temperature-composition dependencies [163]. Among various models, the Modified Quasi-chemical Model in the Quadruplet Approximation (MQMQA) [41] has shown great promise in modeling complex molten salt solutions, including reciprocal salt systems. We can further develop our model for reciprocal molten salt mixtures by leveraging the outcomes of the MQMQA model, which will help fill the gaps in thermal conductivity predictions for these mixtures. A review of the MQMQA model follows.

2.4 Thermodynamic modeling: modified quasi-chemical model in the quadruplet approximation

The Modified Quasi-chemical Model in the Quadruplet Approximation (MQMQA) evaluates the interactions of short-range ordering in molten salt solutions and was specifically developed for reciprocal molten salt mixtures. Reciprocal molten salt mixtures are characterized by the presence of more than one cation and more than one anion. The interactions within these solutions are notably intricate due to the significant influence of both first-nearest neighbors (FNN) and second-nearest neighbors (SNN) short-range orderings (SRO). In particular, the FNN interactions, primarily between cations and anions, are very strong, leading to considerable deviations from ideal mixing behavior. Additionally, the SNN interactions between

cation-cation further complicate the system. Together, these factors introduce substantial challenges in accurately modeling the thermodynamic properties of reciprocal molten salt solutions [41].

In the solution, cationic species (A, B, C, ...) and anionic species (X, Y, Z, ...) occupy two distinct sublattices. In a ternary reciprocal molten salt system denoted as (A^+, B^+ / X^-, Y^-), there are nine quadruplets. These include four unary quadruplets, which are the pure end-members: $[A_2X_2]_{quad}$, $[B_2X_2]_{quad}$, $[A_2Y_2]_{quad}$, and $[B_2Y_2]_{quad}$; and four binary quadruplets: $[ABX_2]_{quad}$, $[ABY_2]_{quad}$, $[A_2XY]_{quad}$, and $[B_2XY]_{quad}$; and one reciprocal quadruplet, $[ABXY]_{quad}$. The exchange reaction of formation of the unary quadruplets are following [41, 164, 165]:

$$\text{FNN SRO reciprocal: } [A_2X_2]_{\text{quad}}+[B_2Y_2]_{\text{quad}} = [A_2Y_2]_{\text{quad}}+[B_2X_2]_{\text{quad}}, \quad \Delta g^{exchange}_{AB/XY}, \tag{2.12}$$

Let's assume another reaction with $A = A^+$, $B = B^{3+}$, $X = X^-$, and $Y = Y^{2-}$, the reaction is given by $3A_2Y + 2BX_3 \rightleftharpoons 6AX + B_2Y_3$, $\quad \Delta g^{exchange}_{AB/XY}$, where $\Delta g^{exchange}_{AB/XY} = \Delta g^0_R/6$, Δg^0_R is determined by the Gibbs energy of four unary quadruplets, which corresponds to four unary components. The factor 6 is the number of equivalent ions.

If $\Delta g^{exchange}_{AB/XY} < 0$, SRO occurs predominantly in the form of $[A_2X_2]$ and $[B_2Y_2]$ pairs within the FNN interactions for (A^+, B^+ / X^-, Y^-). Consequently, the formation of $[ABX_2]$ pairs is less favored compared to random mixing, leading to a reduction in the contribution of the $[ABX_2]$ SNN energy ($\Delta g_{AB/X_2}$) to the total Gibbs energy. The binary quadruplets are expressed:

$$\text{SNN SRO Common-anion: } [A_2X_2]_{\text{quad}} + [B_2X_2]_{\text{quad}} = 2[ABX_2]_{\text{quad}}, \quad \Delta g_{AB/X_2} \tag{2.13}$$

$$\text{SNN SRO Common-cation: } [A_2X_2]_{\text{quad}} + [A_2Y_2]_{\text{quad}} = 2[A_2XY]_{\text{quad}}, \quad \Delta g_{A_2/XY} \tag{2.14}$$

$\Delta g_{AB/X_2}$ and $\Delta g_{A_2/XY}$ are the Gibbs free energy of formation of binary quadruplet that of the exchange reaction of FNN pairs of two unary quadruplets $[A_2X_2]_{\text{quad}} + [B_2X_2]_{\text{quad}}$ or $[A_2X_2]_{\text{quad}} + [A_2Y_2]_{\text{quad}}$. The parameters was optimized to reproduce the available experimental data. And eventually, the Gibbs energy of formation of the reciprocal quadruplet $[ABXY]_{\text{quad}}$ is given from the binary quadruplets [41]:

$$\begin{aligned}\frac{1}{2}\left([ABX_2]_{\text{quad}} + [ABY_2]_{\text{quad}} + [A_2XY]_{\text{quad}} + [B_2XY]_{\text{quad}}\right) \\ = 2[ABXY]_{\text{quad}}, \quad \Delta g_{AB/XY}\end{aligned} \tag{2.15}$$

Here, we would like to mention the FNN pair fraction is defined as:

$$X_{A/X} = \frac{n_{A/X}}{n_{A/X} + n_{B/X} + n_{A/Y} + ...} \tag{2.16}$$

$n_{A/X}$ is the number of moles of FNN [AX] pairs, similarly n_{A_2/X_2}, n_{AB/X_2} and $n_{AB/XY}$ etc., are the numbers of moles of $[A_2X_2]_{\text{quad}}$, $[ABX_2]_{\text{quad}}$, $[ABXY]_{\text{quad}}$, etc., quadruplets. The equation is further simplified by assuming that the ratio of SNN coordination number and FNN coordination number is identical for all species, therefore the pair fraction of the quadruplet is shown:

$$X_{A/X} = X_{A_2/X_2} + \frac{1}{2}X_{AB/X_2} + \frac{1}{2}X_{A_2/XY} + \frac{1}{4}X_{AB/XY} + ... \tag{2.17}$$

where $X_{AB/XY}$ are the quadruplet fractions, for a more detailed demonstration, please refer to the article of Pelton et al. [41].

Apart from the pair fractions defined in the MQMQA, the Temkin model also describes pair fractions. In the Temkin model, cations and anions are assumed to randomly occupy their respective sublattices, representing ideal mixing with no Gibbs energy exchange in the mixture ($\Delta g^{exchange}_{AB/XY} = 0$). This scenario typically applies to monoatomic common-ion mixtures, where the pair fractions in the Temkin model and in the MQMQA approach are identical to the nominal fractions. For a detailed discussion on the relationship between nominal fractions and pair fractions in both the Temkin model and the MQMQA approach within molten salt mixtures, refer to Chapter 6.

The MQMQA has proven to be a robust and effective method for modeling the complex thermodynamic behavior of numerous molten salt systems, including fluorides, chlorides, nitrates, carbonates, and sulfates, among others [166–178]. Over the years, it has enabled precise optimization of thermodynamic properties for a broad range of salt mixtures.

The MQMQA approach has been implemented in FactSage$^{\text{TM}}$ [179], and has become a reliable method for predicting the thermodynamic properties of complex molten salt systems in terms of temperature and compositional variations. This provides significant benefits for molten salt applications in energy systems and industrial processes. This well-established approach, along with the optimized database in FactSage$^{\text{TM}}$, greatly facilitates the development of molten salt thermal conductivity by accounting for interatomic interactions between diverse cations and anions within complex or reciprocal molten salt systems, while also allowing for the direct application of optimized thermodynamic data in model development..

2.5 Molten salt thermal conductivity models

Various theoretical and empirical models have been developed to estimate the thermal conductivity of molten salts. Gallagher [67] identified five categories of thermal conductivity models, introducing two additional categories beyond those summarized by DiGuilio and Teja [39]. In this chapter, we classify them based on models for pure molten salts, and models for molten salt mixtures.

2.5.1 Models for pure molten salt

Certain theoretical models have successfully estimated the thermal conductivity of pure molten salts as a function of temperature, exhibiting a negative temperature dependence and demonstrating good agreement with reliable experimental datasets for specific salt families. Nevertheless, the lack of required knowledge about other salt families poses challenges to their applicability across different salt families. While some theoretical models employ empirical fitting parameters to achieve accurate predictions for pure salts, extending these models to predict the thermal conductivity of multi-component salt mixtures remains very difficult.

Bridgman-type models

Bridgman's model was the first theoretical framework developed to describe the thermal conductivity of liquids. It was adapted from his earlier work on insulators, based on the assumption that the molecules in liquids behave similarly to those in a lattice, where energy is transmitted along the lattice in the direction of the gradient at the speed of sound. The equation for Bridgman's model [180] is as follows:

$$\lambda_{Bridgman} = \frac{3k_B c_s}{l^2} \tag{2.18}$$

$$l = \left(\frac{V}{n_a N_A}\right)^{\frac{1}{3}}, \tag{2.19}$$

where λ, k_B, c_s, V, n_a, and N_A are the thermal conductivity, Boltzmann constant, sound velocity, molar volume, number of ions per molecule, and Avogadro number, respectively. Kincaid and Eyring [181] advanced this model by incorporating the internal degrees of freedom associated with polyatomic molecules, and Powell et al. [91],

$$\lambda_{Kincaid-Eyring} = \frac{0.931}{\gamma} 3k_B \left(\frac{n_a N_A}{V}\right)^{\frac{2}{3}} c_s \tag{2.20}$$

$$\lambda_{Powell} = 2.8 k_B U \left(\frac{n_a N_A}{V}\right)^{\frac{2}{3}}, \tag{2.21}$$

where $\gamma = C_p/C_v$ is the ratio of the heat capacity at constant pressure to that at constant volume.

Using the Bridgman equations to calculate the thermal conductivity of molten alkali nitrates, Turnbull [83] and Gustafsson et al. [103] found that the model's predicted values were approximately 25% higher than expected. In contrast, the Kincaid & Eyring's model provided more accurate estimations for molten alkali nitrates, with errors limited to around 7%. Nagasaka et al. pointed out that the realistic accuracy of these models is likely between 20-40%, because of the use of erroneously large data in Turnbull's and Gustafsson's original comparisons. DiGuilio and Teja [39] pointed out that the lack of reliable data on sound velocity and heat capacity was the main limitation of this model. However, these properties are more readily available than thermal conductivity, and can often be determined with accuracy today through experimental techniques or modeling.

Mechanistic-type models

Mechanistic-type models, also known as quasi-crystalline models, assume that molecules are arranged similarly to a lattice structure in a liquid, much like in a solid [44]. In these models, the thermal conductivity is viewed as having two main contributions: a vibrational contribution, which involves heat transfer through molecular collisions (similar to solid materials); and a diffusive contribution, where high-energy molecules diffuse into regions of lower energy (similar to gases) [57]. The total thermal conductivity is expressed as the sum of these two mechanisms:

$$\lambda = \lambda_{vib} + \lambda_{dif} = \frac{avC_v}{l} + \frac{2DC_v}{l^2}, \tag{2.22}$$

where C_v is the specific heat capacity at constant volume, v is the mean vibrational frequency, D is the diffusion coefficient, and a is a constant, usually taken as 2. Turnbull [83] utilized this approach to predict the thermal conductivity of molten salts, noted that the diffusive contribution accounts for less than 5% compared to the vibrational contribution. The diffusive contribution was assumed to be negligible. More importantly, the model is primarily applicable near the melting point, where the molten salt can be treated as a quasi-crystalline structure. This validity is attributed to the high ratio of thermal diffusivity to mass diffusivity and a relatively large Lorenz number, as discussed by Cornwell [182]. Rao applied this approach by focusing only on the vibrational contribution, deriving the vibrational frequency using Lindmann's harmonic oscillator model [183]. The expression for Rao's

model is as follows [184]:

$$\lambda_{Rao} = A \left(\frac{R^{\frac{2}{3}}}{N_A^{\frac{1}{3}}} \right) \left(\frac{T_m}{M V^{\frac{4}{3}}} \right)^{\frac{1}{2}} \tag{2.23}$$

where $A = 23.44$ is a dimensionless empirical fitting constant when λ in [W. $m^{-1}K^{-1}$], and T_m, R, and M are the melting temperature, the universal gas constant, and the molar mass, respectively. Turnbull modified Rao's model to account for liquid dissociation by incorporating the number of ions per molecule of molten salt, denoted as n, resulting in the following expression [83]:

$$\lambda_{Rao-Turnbull} = B \left(\frac{R^{\frac{2}{3}}}{N_A^{\frac{1}{3}}} \right) \left(\frac{T_m}{\frac{M}{n} (\frac{V}{n})^{\frac{4}{3}}} \right)^{\frac{1}{2}} \tag{2.24}$$

where $B = 13.28$ is a dimensionless empirical fitting constant. The constants A and B were determined by fitting empirical thermal conductivity data for molten salts. As a result, these empirical fitting constants restrict the model's predictive capability, leading to significant errors when predicting the properties of certain salts [182]. Additionally, this model does not account for temperature effects. Horrocks and McLaughlin [185] developed a similar model that utilizes the rectangular cell potential instead of the vibrational frequency. This model is expressed as follows:

$$\lambda_{Horr-McLau} \simeq \lambda_{vib} \tag{2.25}$$

$$\lambda_{vib} = 2 \; P_{te} \; v \; n \; l \; C_v, \tag{2.26}$$

where P_{te} is the probability of transferring energy on each collision, v is the vibrational frequency, n the number of molecules per unit area of a lattice plane in the liquid, l the distance between nearest neighbor lattice planes and C_v is the specific heat capacity per molecule volume. This model successfully predicted the thermal conductivity of simple liquids, such as argon, nitrogen, benzene, and carbon tetrachloride, which are nonpolar molecules with zero dipole moments. Unfortunately, its applicability to a broader range of liquids is limited, due to improper assumptions about the liquid structure and the reliance on fitting parameters to determine P_{te} [78]. Gustafsson [103] evaluated Horrocks-McLaughlin's model and noted that the accuracy varies between 10-40%, depending on the selected molecular diameter. Mechanistic-type models are derived empirically, which restricts their predictive capability, and their applicability to multi-component molten salt mixtures.

Corresponding states principle models

Some successful theoretical models for molten salt thermal conductivity are based on the corresponding states principle. This principle was initially formulated to derive thermodynamic and transport properties of gases and liquids [186]. It assumes that relationships between thermodynamic properties can be established using reduced properties. For molten salts, it has been proposed that the reduced thermal conductivity can be expressed as a function of reduced volume or reduced temperature, utilizing the properties of a reference fluid.
White and Davis [49] plotted λ/λ_m against ρ/ρ_m and T/T_m, where m denotes properties at the melting point. They concluded that reduced density serves as a more effective parameter for correlating the reduced thermal conductivity of nitrates to a reference nitrate.
Employing the corresponding states principle requires a reference fluid from the same salt family. Subsequently, Young and O'Connell [187] selected a point on the liquid saturation curve as their reference for characteristic parameters. The reference thermal conductivity was determined empirically and is unique to each salt. Both the studies by White and Davis, as well as Young and O'Connell, face limitations in their predictive capabilities because they rely on existing reference thermal conductivity data from similar salts.
Nagasaka and Nagashima [94] applied Harada's corresponding state correlation [186] to thermal conductivity by comparing the model to experimental data of several molten salt families. This correlation demonstrated an appreciable precision for molten alkali halides. The model was also used to predict the thermal conductivity of molten alkali metal fluorides, which could not be measured experimentally due to the corrosion of quartz and sapphire cells required in the forced Rayleigh scattering measurement technique. The model provided reliable predictions for unary alkali halides with an accuracy of 15-20%. Unfortunately, specific parameters used in the model are not always available for each compound, which limits the application to other salts. For example, CsCl, CsBr, and CsI have different crystal structures than alkali halides, and their interatomic potentials remain unknown [44].

Rough hard-sphere models

DiGuilio and Teja [39] proposed a model based on the rough hard-sphere theory, which was developed earlier by Chandeler et al. [188], Li et al. [189], Assael et al. [190] and Ciotta et al. [191] to describe non-spherical liquids. Li et al. pointed out that real molecules are not hard spheres, therefore the reduced thermal conductivity of a system of rough hard spheres can be:

$$\lambda^*_{RHS} = \frac{64}{75}\left(\frac{M\pi}{k_B^3 T}\right)^{1/2} \frac{2^{1/3}}{N_A^{2/3}} \lambda V^{2/3}, \tag{2.27}$$

where M, k_B, and V are the molar mass, Boltzmann constant, and the molar volume. Moreover, λ^*_{RHS} is a function of only the molar volume:

$$\lambda^*_{RHS} = f(V/V_0), \tag{2.28}$$

where V_0 represents the molar volume at closest packing, given by the expression $V_0 = N_A r^3/2^{1/2}$ for spheres, r is the molecular diameter. DiGuilio and Teja suggested that the thermal conductivity of molten salts can be related to that of a smooth monatomic reference liquid, such as argon. This idea is inspired by the work of Chandler et al., which established a relationship between the viscosity of rough hard spheres and that of smooth hard spheres. They proposed the following equation:

$$\lambda^*_{MS} = C_\lambda \lambda^*_{Argon}, \tag{2.29}$$

where C_λ is a constant that is independent of temperature and density but varies with each specific salt, being empirically fitted based on data from one salt in the same salt families. This model effectively predicted the thermal conductivity of both the chloride and nitrate salt families, demonstrating strong agreement with reliable experimental data. However, the thermal conductivity values for sodium chloride and sodium nitrate were derived by fitting C_λ using experimental data from the common anion family of salts. Nevertheless, there is often insufficient reliable dataset available for each family of molten salts to perform accurate fitting, which limits the applicability of this model. Additionally, extending the model to multi-component molten salt mixtures is nearly impossible.

Kinetic theory models

Gheribi et al. [60] introduced a model based on classical kinetic theory derived from the Boltzmann transport equation. It assumes that conduction is driven by vibration-based energy transfer. In this model, the thermal conductivity of molten salts is not strongly temperature-dependent but instead correlates with the coefficient of thermal expansion (or density). The inter-molecular distance, or the mean free path $< l_{ph} >$ within atomic vibrations, is proportional to the combined radii of the anions and cations and inversely proportional to the number of atoms per molecule $< l > \propto (r_a + r_c)/n$. As the liquid expands with increasing temperature, the mean free path grows, leading to a decrease in energy transfer, expressed as a negative temperature dependence $(\partial\lambda/\partial T)|_P < 0$. The formulation of this model is given by:

$$\lambda_{m,Gheribi} = K_{emp}\left(\frac{C_{vm}\ c_{s,m}}{3nV_m}\right)\left(\frac{r_a + r_c}{n_a}\right) \tag{2.30}$$

The temperature dependence of the model is expressed:

$$\lambda_{Gheribi}(T) = \lambda_{m,Gheribi}\left[1 - \alpha_m(\gamma_m + \frac{1}{3})(T - T_m)\right], \tag{2.31}$$

where C_{vm}, $c_{s,m}$, n_a, V_m, α_m, λ_m, and γ_m represent respectively the heat capacity per unit volume, sound velocity, number of ions, molar volume, thermal expansion, the thermal conductivity, and the Grüneisen parameter, all taken at the melting temperature T_m. Here, m denotes the melting temperature.

The model's predictions for thermal conductivity, spanning from the melting temperature to the boiling temperature, showed strong agreement with experimental data for many molten alkali and alkaline earth metal halides, carbonates, nitrates/nitrites, sulfates, and hydroxides. However, the model introduced a dimensionless fitting constant K_{emp}, which was empirically determined to be approximately 4.33. This reliance on an empirical fitting constant limits the model's applicability when predicting the properties of multi-component mixtures, complex salts, or polymerizing salts. Therefore, developing a model that is less dependent on experimental data is desirable.

Free volume models

Zhao et al. [109] developed a theoretical model based on free volume, where an elementary particle in the liquid moves according to the ideal gas law. The model assumes that molten salt molecules are spherical particles with cubic packing, and considers molecular diameter instead of anionic or cationic radii. This allows for calculating the ratio of the total volume to the free volume. By applying the thermal conductivity model for monoatomic liquids proposed by Hirschfelder and Curtiss [192], the temperature dependence of the thermal conductivity for a monatomic liquid is expressed as follows:

$$\lambda_{Zhao} = (\frac{N_A}{D_{cell}})^{2/3} k_B (\frac{8k}{\pi m_1})^{1/2} (\frac{D_{cell} P}{R})^{1/3} \rho^{1/3} T^{1/6}, \tag{2.32}$$

where D_{cell} is the density of the cell, m_1 is the mass of one molecule, P is the pressure. The model is extendable to polyatomic liquids by applying a correction factor to account for the internal degrees of freedom of the polyatomic molecules. The predicted results were compared with several experimental datasets, including the work of Smirnov et al. [56], which was not recommended and made it difficult to assess the reliability of the model. Additionally, the model exhibited a slightly positive temperature dependence for thermal conductivity, which is inconsistent with other findings.

2.5.2 Models for molten salt mixtures

Molten salt mixtures are of greater interest than unary salts for industrial applications due to their enhanced properties, such as lower melting points, higher heat capacities, and improved thermal conductivity. These characteristics make them more efficient for processes such as heat transfer, energy storage, and high-temperature operations in systems like MSRs and the Hall-Héroult process.

To date, the most commonly used approach for estimating the thermal conductivity of multi-component molten salts is the ideal mixing rule (see the following). While this assumption can provide reasonable results for some mixtures, such as molten nitrate salts, it may not hold true for others. For instance, in LiF-BeF_2 mixtures, the ions within the melt may exhibit some degree of network polymerization, leading to significant deviations from ideal behavior. Unfortunately, validating these models is challenging due to the lack of data in the literature. In fact, because of the differences in intermolecular interactions, no model has been able to predict the thermal conductivity of any compositions of molten salt mixtures as of this research.

Ideal mixing rule

Diguilio et Teja [57] proposed that the thermal conductivity of molten salt mixtures can be calculated as a linear function of the mole fraction of each pure component. The expression for the ideal mixing rule is given by:

$$\lambda_{id} = \sum_{i=1}^{n} X_i \ \lambda_i, \tag{2.33}$$

where λ_{id} represents the linear solution of thermal conductivity of salt mixtures, X_i is the molar fraction of the unary component, and λ_i represents the thermal conductivity of each pure compound. The model is simple to apply and performs well for molten nitrate mixtures. However, since it is not based on thermodynamic theory, it is not suitable for other salt mixtures, especially those that form complex ions. Even though there is evidence questioning the reliability of the ideal linear model, some studies still choose to utilize this [39, 47, 71, 193].

Kinetic theory models

Gheribi and Chartrand [133] proposed a theoretical framework for predicting the thermal conductivity of molten salt mixtures as a function of temperature and composition. This framework builds upon their earlier work on the thermal conductivity model for pure molten salts [60]. In molten salt solutions, the mixing of ions leads to a significant decrease in the phonon mean free path, thereby reducing thermal conductivity. This reduction is attributed

to differences in atomic masses, cation sizes, and neighboring coupling forces. As a result, the phonon scattering relaxation time is influenced by the chemical disorder introduced by the mass variations in liquid solutions. The expression for the thermal conductivity of molten salt mixtures is given by:

$$\lambda(\underline{X}, T) = \lambda_\sigma(\underline{X}, T)\left[1 - \delta_M^\lambda(\underline{X}, T)\right] \tag{2.34}$$

$$\lambda_\sigma^{-3/2}(\underline{X}, T_0) = \left[\frac{V/V_{id}}{\Gamma^{3/2}}\right](\underline{X}, T_0)\sum_{i=0}^{N} X_i \left(\frac{\Gamma_i}{\lambda_i}\right)^{-3/2}(T_0) \tag{2.35}$$

$$\delta_M^\lambda \simeq \begin{cases} \epsilon \cdot \frac{l_{\text{ph}}}{r_e} \cdot g_{\text{mass}} & \text{if } l_{\text{ph}} \geq r_e \\ 0 & \text{if } l_{\text{ph}} < r_e \end{cases} \tag{2.36}$$

where the mass fluctuation term is $g_{mass} = \sum_{i=0}^{N} X_i \left[\frac{m_i}{m} - 1\right]^2$. l_{ph} is the phonon mean free path, r_e is the average interatomic length, V/V_{id} is the ratio of the excess molar volume. Γ is a parameter defined as $\Gamma = C_v c_s/n_a$, C_v is the specific heat capacity at constant volume, where c_s is the sound velocity, n_a is the number of atoms per chemical formula.
Their reported results aligned well with equilibrium molecular dynamics (EMD) results and experimental datasets, indicating that the thermal conductivity of molten salt mixtures does not adhere to the ideal mixing rule but rather reflects reductions in the solutions. However, a "universal" constant $\epsilon \simeq 0.4872$ was introduced into Equation 2.36, derived from solid solutions and assumed to be applicable to all ionic mixtures. This assumption limits the reliability of the model when predicting significant mass variations within the mixtures, as well as in the case of complex salts.

Unit cell models

Zhao et al. [194] developed a theoretical unit cell model to predict the thermal conductivity of binary molten salts, building on their previous model for pure molten salts. An important finding was that the thermal conductivity of binary molten salt mixtures exhibited a negative deviation from the ideal mixing rule. Their predictions aligned well with experimental data. Unfortunately, this model was only validated for binary molten salt mixtures. Additionally, their earlier model for pure molten salts was validated using non-recommended datasets, which complicates the assessment of the overall reliability of this model for binary molten salt mixtures.
Muhmood et al. [195] extended Zhao et al.'s unit cell concept to ternary salt mixtures, with predictions indicating a negative temperature dependence of thermal conductivity. Never-

theless, the predictive accuracy of the unit cell models for molten salt mixtures remains uncertain and requires further validation with other systems.

2.5.3 Empirical models

Empirical (or semi-empirical) models depend on correlations or fitting to experimental data. As previously mentioned, it's really challenging and costly to obtain reliable experimental measurements. Additionally, many of these models lack a solid theoretical basis, as they are often limited to adapt to specific mixtures, salts with common anions, or chemically similar systems. Consequently, their predictive capabilities to other mixtures are very limited [10, 44, 196, 197].

Smirnov et al. [56] proposed that the thermal conductivity of molten alkali halide mixtures is inversely proportional to molar volume, which is consistent with other models for pure salts [83, 103, 180, 181, 198]. The expression is given:

$$\lambda_{mix} = (x_1\lambda_1 + x_2\lambda_2)(1 - \frac{\Delta\beta}{\beta_{ad}}) \tag{2.37}$$

where $\Delta\beta/\beta_{ad}$, the adiabatic compressibility is related to the deviations in thermal conductivity within the mixture. This compressibility was obtained from experimental data. However, the experimental results reported by Smirnov et al. for pure molten salts were considered unreliable due to a significant positive temperature dependence of thermal conductivity [40, 44, 199, 200]. Since heat losses are less significant at lower temperatures, the results from Smirnov et al. occasionally align with reliable data near the melting point. Nevertheless, this model remains constrained by the available experimental datasets.

2.5.4 Chapter conclusion

This chapter reviewed commonly used methods for determining thermal conductivity, including experimental techniques, numerical simulations, and existing models. We collected and carefully analyzed the available experimental datasets of thermal conductivity for salts relevant to energy applications, including fluorides, chlorides, bromides, iodides, nitrates/nitrites, carbonates, sulfates, and hydroxides. Only experimental datasets exhibiting a negative temperature dependence or temperature independence were considered reliable. Inadequate treatment of convective and radiative heat transfer effects would otherwise significantly inflate the measured thermal conductivity of the liquid salts. Fortunately, hundreds of reliable datasets exist for many pure salts, as well as for some salt mixtures.

Salt mixtures are particularly interesting for industrial applications due to their improved properties. However, very limited experimental datasets of thermal conductivity for mixed

salts are available. Molecular dynamics (MD) simulations have demonstrated their reliability in simulating molten salt mixtures, including complex salt systems and reciprocal systems. These simulations provide insights into the interactions between different ions and the structures formed in the melt. In particular, the Polarized Ion Model (PIM) technique has shown strong performance and accuracy in simulating chloride and fluoride salts in numerous studies, and it will be used to simulate molten salt mixtures in the present study.

Both experimental and numerical techniques are suitable for determining the thermal conductivity of specific salt mixtures. However, when addressing variable or dynamically changing compositions during a process, experimental techniques become impractical, and numerical techniques face challenges related to computational intensity and unknown potentials.

Therefore, modeling becomes an effective method for rapidly estimating behaviors across temperature or composition variations. Among modeling approaches, the Modified Quasichemical Model in the Quadruplet Approximation (MQMQA), which considers both first-nearest-neighbor (FNN) and second-nearest-neighbor (SNN) interactions within molten salt solutions, has demonstrated high accuracy in predicting thermodynamic properties for various molten salts, especially for reciprocal mixtures. The MQMQA approach will be employed in the thermal conductivity modeling of reciprocal molten salt solutions in this study to estimate the FNN and SNN structure of the mixtures a computed homogeneous Gibbs energy minimization.

Numerous models have been developed to predict the thermal conductivity of pure molten salts and molten salt mixtures over the past several decades. However, most models have limitations in predictive capability, as many rely on empirical fitting constants specific to a particular salt or salt family, especially in models for pure molten salts. For mixtures, the ideal mixing rule is commonly used, yet this rule lacks a solid basis in thermodynamic theory. Moreover, none of the current models adequately address intermolecular interactions in the melt.

To address these gaps, including the need for models that can handle variable compositions without relying on empirical parameters or neglecting intermolecular interactions, the goal of this thesis is to develop a reliable thermal conductivity model for molten salt mixtures. This model will account for both temperature and compositional variations, taking into consideration the short-range ordering interactions between different ions. The model aims to demonstrate its predictive capability for salts of alkali and alkaline earth metal halides, carbonates, nitrates/nitrites, sulfates, and hydroxides. Additionally, the model should be independent of empirical fitting constants while accurately predicting thermal conductivity values comparable to reliable experimental data.

With this foundation, the next chapter outlines the specific objectives of the study, detailing

the approach to model development and validation across diverse molten salt systems, including unary, common-anion, common-cation, complex, and reciprocal salts. Additionally, the thesis outline will be presented.

CHAPTER 3 OBJECTIVE AND THESIS STRUCTURE

The previous chapter reviewed existing techniques for determining the thermal conductivity of molten salts. These techniques include experimental methods, numerical simulation techniques, and physical models. This review identified a significant gap in accurately simulating the thermal conductivity as a function of temperature and compositional dependence of molten salts.

Both experimental and numerical techniques require extensive work on data collection and analysis, often relying on extrapolation. Additionally, most existing thermal conductivity models are tailored to specific salt families through empirical fitting constants, which limits their applicability to other salt mixtures. Indeed, none of these models account for interatomic interactions and short-range ordering within mixtures that contain more than two cations and more than two anions in reciprocal molten salt mixtures.

This study aims to develop a molten salt thermal conductivity model that overcomes the mentioned limitations. Based on prior research [60], this model builds on classical kinetic theory and is theoretically grounded. It requires only a few input parameters, the majority of which are easily found in the literature or in molten salt databases.

The model is designed to predict thermal conductivity across a diverse range of molten salt mixtures as a function of both temperature and composition. To enhance predictive capability for the thermal conductivity of molten salt mixtures, four specific sub-objectives have been established. This research seeks to bridge the gap between current knowledge and practical applications through a series of modeling and validation steps. Ultimately, the goal is to ensure the reliability of thermal conductivity predictions for molten salt systems in both simulations and industrial processes.

The specific objectives of this thesis are presented below, followed by an outline of its general structure.

3.1 Research objective

Research question: How can a theoretical model be developed to accurately predict the thermal conductivity of molten salt mixtures that account for the interatomic interactions in solutions containing multiple cations and anions as a function of temperature and composition?

Main objective: To develop a thermal conductivity model for molten salt solutions that eliminates the reliance on empirical fitting constants, enabling accurate predictions of thermal conductivity for any molten salt mixture as a function of both temperature and composition.

To achieve this objective, several sub-objectives have been defined as follows:
Sub-objectives:

1. Develop a model for the thermal conductivity of pure molten salts as a function of temperature, without relying on empirical fitting parameters, and create a comprehensive database of pure molten salt properties.

2. Extend the model for pure molten salts to accommodate multi-component mixtures of common ions, including both monoatomic and polyatomic anions, while accounting for mass fluctuations among different ions.

3. Incorporate pair fractions into the MQMQA approach for the common-ion model, considering the short-range ordering interactions between cations and anions and the Gibbs energy exchange in reciprocal molten salt solutions.

Following the completion of the second sub-objective, the same methodology will be applied to another supplementary study that focuses on modeling complex solutions of molten salt mixtures, such as those involving molten cryolite (NaF-AlF_3).

3.2 Organization of the thesis

This thesis will consist of articles, with the outcomes presented within these works. Each of the sub-objectives defined in the previous section corresponds to a chapter. Specifically, there are three articles that represent Chapters 4, 5, and 6. Additionally, another sub-objective, as a supplementary work of this project related to the thermal conductivity model for complex molten salt solutions, will be included in the Appendix E. The overall structure of the thesis is outlined as follows:
Chapter 4 introduces a molten salt thermal conductivity model for unary molten salts based on the kinetic theory, and establishes a comprehensive database for further development of molten salt mixture models. In order to develop a reliable model, extensive collection and careful analysis of available experimental datasets were conducted. Among the numerous studies reviewed, the works reported by Nagasaka and colleagues, as well as those by Harada and colleagues, were identified as the most reliable experimental datasets and will be used to validate the thermal conductivity model for pure molten salts.
The classical kinetic theory, based on the concept of minimum thermal conductivity, was used to develop the thermal conductivity model for pure molten salts, which is commonly employed in characterizing thermal transport properties in amorphous solids and non-metallic glasses. This approach has been applied to accurately predict the thermal conductivity of 58 different pure molten salts, including halides, divalent halides, carbonates, nitrates/nitrites,

sulfates, and hydroxides. Furthermore, a database has been established to parameterize the temperature dependence of these unary salts, facilitating their application and extending the model for multi-component molten salt mixtures (Article 1 has been published in journal of «Solar Energy»).

Chapter 5 further develops the unary thermal conductivity model to address common-anion multi-component molten salt mixtures as a function of both composition and temperature. The model introduces a new parameter to quantify the decrease in thermal conductivity within the melt-the disorder scattering parameter.

In mixtures involving mixed ions, these ions serve as scattering centers for phonons. The mean free path of phonons reduces due to differences in atomic mass, cation size, and inter-ionic coupling forces. In molten salt solutions, a mass fluctuation term of the disorder scattering parameter contributes to the reduction in thermal conductivity.

Given the limited availability of experimental datasets on molten salt mixtures, over 100 EMD simulations were conducted for various common-anion binary mixtures, which include fluorides (LiF-NaF, LiF-KF, NaF-KF), chlorides (LiCl-NaCl, LiCl-KCl, NaCl-KCl), bromides (LiBr-NaBr, LiBr-KBr, NaBr-KBr, RbBr-CsBr), and iodides (LiI-NaI, LiI-KI, NaI-KI, RbI-CsI). The predicted results were validated against various EMD simulations and compared to available experimental datasets reported in the literature for common-anion molten salt mixtures. Therefore, we can confidently assert that the accuracy and reliability of the developed model are comparable to experimental findings (Article 2 has been published in journal of «Materials Today Energy»).

For common-anion molten salt mixtures that form complex structures and polymer chains, such as LiF-BeF_2), strong SNN short-range ordering leads to the creation of intricate coordination complexes and polymers, which significantly decrease thermal conductivity. To model these complex solutions, a new parameter, "complex rate"-τ, that represents the local structure of the solutions, was introduced to describe the mass-based evolution of these complexes and polymers. The model for complex solutions was validated using both numerical simulations and experimental datasets for the KCl-$MgCl_2$ and NaF-AlF_3 systems. As a supplementary study of this thesis will be included in the appendix E (This supplementary study has been published in journal of «Journal of Molecular Liquids»).

Chapter 6 extends the thermal conductivity model for multi-component common-ion molten salt mixtures to reciprocal molten salt mixtures by applying the MQMQA approach, while accounting for short-range ordering as a function of temperature and composition. Currently, there is no existing model to predict the thermal conductivity for reciprocal molten salt mixtures, and very few experimental datasets are available. To address this gap, we conducted EMD simulations on three reciprocal mixtures: $Li^+, Na^+/F^-, Cl^-$, $Li^+, K^+/F^-, Cl^-$, and

$Na^+, K^+/F^-, Cl^-$. A total of 25 EMD simulations were performed for each reciprocal mixture at 1300 [K].

Using EMD simulations can help prevent hazardous accidents associated with high-temperature experimental measurements. However, these simulations are time-consuming and computationally intensive, particularly when simulating high-order mixtures, some of which may involve unknown potentials. This change is particularly relevant in industrial processes where temperature and composition changes in molten salt mixtures occur frequently. Therefore, modeling becomes an efficient alternative approach for quickly estimating values under variable temperature and composition conditions, thereby ensuring system safety, such as in MSRs.

Fortunately, the Modified Quasi-chemical Model in the Quadruplet Approximation (MQMQA) has successfully modeled and optimized numerous high-order reciprocal molten salt systems with precision in thermodynamic simulations. The MQMQA accounts for the interactions of short-range ordering between first-nearest-neighbor ions (cation-anion) and second-nearest-neighbor ions (cation-cation and anion-anion), and exchanges of Gibbs energy. Consequently, we leverage the advantages of the pair fractions in the MQMQA model to further develop our latter model of thermal conductivity for reciprocal molten salt mixtures. The predictive values obtained from this model have been validated against EMD results and available experimental datasets. Furthermore, the model predicted the thermal conductivity of several reciprocal molten salt mixtures identified in the literature as potential PCMs for energy applications (Article 3 has been published in journal of « Solar Energy Materials and Solar Cells»).

CHAPTER 4 ARTICLE 1: DEVELOPMENT OF A MOLTEN SALT THERMAL CONDUCTIVITY MODEL AND DATABASE FOR ADVANCED ENERGY SYSTEMS

Huiqiang Yang, Ryan C. Gallagher, Patrice Chartrand, Aïmen E. Gheribi

Published in Solar Energy, April 14 2023, volume 256, pages 158-178

My contributions to this article are: Conceptualization, Methodology, Validation, Software, Formal analysis, Investigation, Data curation, Writing – original draft, Visualization.

Abstract: A theoretical model for predicting the temperature-dependent thermal conductivity of pure molten salts, both simple and complex, is presented. The model is based on kinetic theory and incorporates Einstein's concept of minimum thermal conductivity. The proposed formulation can consider the magnitude of thermal conductivity for separate salts, including complex and polymerizing salts. The model's thermal conductivity predictions were compared to reliable experimental data in the literature and a previously recommended thermal conductivity model using the Bland-Altman method. The comparison showed accurate thermal conductivity predictions relative to the reliable experimental data, with an average deviation of 10% or less. The model's predictions were also compared to the experimental data on an individual basis for halide, divalent halide, carbonate, nitrate, nitrite, sulfate, and hydroxide molten salts, demonstrating reliable predictions for the molten salts studied and improved accuracy over the previous model. Lastly, a database of simple and complex molten salts, with the necessary parameters for modeling their thermal conductivity, is recommended.

4.1 Introduction

As the global average atmospheric concentration of CO_2 reaches new levels each year, climate change mitigation is one of the highest priorities universally. One effective method to combat climate change is adopting renewable and clean energy production technologies as alternatives to existing fossil fuel energy sources. The development and deployment of renewable technologies, including high-temperature thermal energy storage (TES), thermal concentrating solar plants (CSP), and advanced nuclear reactors, are widely being pursued

as potential alternatives to fossil fuel energy sources [201,202]. One commonality for some of these developing technologies is their proposed use of high-temperature molten salts, which have favorable thermo-physical and thermo-chemical properties. Given their potential benefits in various advanced energy systems, molten salts are of interest to engineering and scientific communities. Yet, accurate knowledge of many properties of molten salts is not well established, hindering effective design, optimization, and deployment of these energy technologies. Therefore, establishing reliable data and predictive models for these properties is necessary to enable new molten salt energy technologies [79]. The thermal conductivity of molten salt features relatively significant uncertainties in experimental measurements and predictive simulations, gaps in existing experimental data, and scatter amongst different data sets. Given these issues, a theory-based model that is not empirically derived could provide predictions of the thermal conductivity for molten salts with significant experimental uncertainties or those without existing data. Such a model would circumvent the burden of performing intensive computational predictions and experimental measurements. A reliable model could be widely applied for developing high-temperature molten salt technologies.

Molten salts have many thermo-physical properties that are suitable and cost-effective for utilization in high-temperature energy technologies. These characteristics include a wide operational temperature range, low vapor pressure, high heat capacity, and high thermal stability [32]. For example, a high specific heat capacity is beneficial for integrating a high-temperature TES system with renewable energy sources allowing for dispatchable power production and flexibility from the primary heat/energy source. This capability is primarily demonstrated by modern CSP plants using nitrate-based "solar salts", which are low cost and have established implementation processes [203, 204]. In the case of CSP TES, classified as sensible TES, the liquid phase and thermal mass are utilized to transfer and store thermal energy. Another promising type of TES is latent TES technology, using the heat of material phase changes to transfer energy. Latent TES with molten salts acting as phase change materials (PCMs) is gaining interest due to their high melting point, high energy density, high thermal conductivity, and constant temperature during charging and discharging at the phase change temperature [205]. For TES, the thermal conductivity influences the rate of charging and discharging thermal energy. Therefore reliable information on the thermal conductivity of molten salts will be necessary to design and develop commercial molten salt TES systems adequately. Ultimately, the selection of molten salt for these TES applications will depend on the mixture's thermo-physical properties, which dictate the energy system's design, efficiency, and operational constraints.

The initial interest in molten salts is often associated with molten salt reactor (MSR) programs at Oak Ridge National Laboratory, namely the Aircraft Reactor Experiment and the

Molten salt Reactor Experiments. Under these programs expansive studies were initiated to develop nuclear reactors using fuel dissolved in a molten salt [6–9]. Since then, the interest in MSRs for energy production persists today due to several advantages over conventional reactors, including online refueling, low vapor pressures, high thermal capacity, and higher operating temperatures [206, 207]. Recently, nuclear reactors have been proposed to utilize molten salts as a TES fluid, leveraging the development of CSP technologies [208]. Using molten salt as a reactor coolant with solid fuel in place of water or gas coolants allows for low-pressure systems while providing superior heat transfer characteristics, potentially lowering capital costs and improving safety relative to existing reactors [206]. Nuclear fusion reactor concepts have also been proposed, utilizing molten salts as a thermal blanket and for tritium breeding [11]. Like TES and CSP, the design and deployment of nuclear systems will depend on reliable knowledge of the thermo-physical properties of molten salt mixtures, which will vary depending on the type of reactor concepts. Though, it is generally accepted that the knowledge thermal conductivity of molten salts for nuclear applications is the least mature relative to the other thermo-physical properties [10, 199].

While these aforementioned energy technologies are inherently different, they share similar technological and developmental challenges that pertain to the utilization of molten salts. An understanding and knowledge of material or compatibility, cost of sourcing and preparing molten salt mixtures, the chemical (thermodynamic) properties, and the thermo-physical properties are required to evaluate the suitability of molten salts in any energy concept. For example, the European project, Energy Storage for Direct Steam Solar Power Plants (DISTOR), was initiated to identify high-temperature PCMs for integrating CSP plants with direct steam generation receiver [209]. The following property constraints are used to determine the suitability of molten salt materials for PCM applications [210]:

- Thermal transport property
  - Maximize the thermal conductivity of molten state: ($\gtrsim 1\ W.m^{-1}K^{-1}$)
  - Maximize the thermal conductivity of solid state: ($\gtrsim 2\ W.m^{-1}K^{-1}$)
- Thermodynamic property
  - Maximize the specific latent heat storage capacity: ($\gtrsim 450\ MJ.m^{-3}$)
  - Maximize the specific liquid heat capacity: ($\gtrsim 2\ MJ.m^{-3}K^{-1}$)
  - Minimize the system vapor pressure at maximum operating temperature: ($\lesssim 100\ Pa$)
  - Minimize the relative volume change upon melting: ($\lesssim 15\%$)

- Corrosion property
  - Minimize the corrosion rate: ($\lesssim 200\ \mu m.year^{-1}$)
  - Maximize the number of cycles: ($\gtrsim 10000\ cycles$)
- Economical aspect
  - Minimize the cost: < about 5000 (USD per ton)
  - Market availability in large quantity: > millions of ton

Aside from liquid thermal conductivity, many of these characteristics can be estimated reasonably well by experiments and theoretical approaches. The solid thermal conductivity and thermodynamic properties can be predicted by theoretical approaches [39, 60, 109, 133, 193, 194]. The corrosion characteristics of molten salts with structural materials can often be determined with experimental methods. However, the corrosion mechanisms are complicated by impurities affecting the redox potential. Thus, corrosion can also be challenging to model [211]. Additionally, the economic aspect largely follows the market supply and demand. For instance, the price of battery-grade lithium carbonate has constantly increased since 2014 due to the market shortages induced by growing demands in battery applications. The average price is now about 17,000 USD per metric ton [212]. However, as was alluded to, the thermal transport property of liquid thermal conductivity is relatively difficult to predict and measure experimentally. Therefore, to effectively design a PCMs for latent TES, accurate and reliable knowledge of molten salt thermal conductivity is essential. Furthermore, thermal conductivity is a primary property used in the most basic heat transfer calculations, and developing energy systems like CSP and molten salt reactors will require knowledge of this property.

A reliable database of thermo-physical properties of all molten salts would be a valuable resource for the scientific and engineering communities that could be utilized to design and optimize molten salt systems. To meet this need, several organizations have been developing property databases of molten salt properties [163, 173, 213–217]. Janz et al. provided an early compilation of molten salt properties in a series of reports [33]. While these reports are expansive, there is still a need for thermal conductivity data on additional molten salts, correcting or removing errant data, and adding new data with lower uncertainties. Most of the thermal conductivity correlations reported by Janz et al. and in other literature are empirically based and specific to discrete compounds or mixtures. These types of correlations are typically not useful when extrapolating to different molten salts. Other reviews on molten salt properties are usually application-specific and not comprehensive works of all molten salt families [39, 103, 184]. Notably, many studies cite the issues related to thermal conductivity

measurement difficulties and the reliability of existing data. Briefly, most of the experimental data sets reported in the literature are scattered or feature high uncertainties making it challenging for researchers to make reliable recommendations [10, 60]. Additionally, there are discrepancies between the sign of the temperature dependence of thermal conductivity reported by many experimental works compared to current theory and molecular dynamics predictions [60, 133]. Given the scatter in existing data and the difficulty of providing new experimental thermal conductivity data, a model of molten salts that does not depend on experimental thermal conductivity data would be ideal for developing a reliable molten salt property database.

Since it is difficult and costly to perform experimental measurements of thermal conductivity, computer simulation techniques such as Molecular Dynamics (MD), Monte Carlo, and other computational methodologies have been developed to provide a low-cost alternative to physical experiments [218–221]. MD has become an essential tool for understanding the properties of liquids and is often applied to study the properties of molten salts [120, 124, 133, 152, 220, 222, 223]. Unfortunately, most MD techniques predict thermal conductivity values that are larger than experimental results, have uncertainties that can be larger than experimental uncertainties, and are computationally intensive when applied to modeling higher order mixtures of molten salts [60, 224]. These methods also require knowledge regarding the intermolecular potential, which is relatively limited [225]. Therefore, these techniques are not feasible for developing a database at the time of this present work but can validate data and be used to better understand the behavior of molten salts. These techniques may become more valuable with increased computational power and more efficient modeling techniques.

Many different kinds of theoretical and empirical models have been developed to predict the thermal conductivity of molten salts. Empirical(or semi-empirical) models require correlation or fitting to experimental data sets. However, as mentioned, obtaining reliable experimental thermal conductivity data is challenging. Further, many empirical models have a limited theoretical basis since they are often constrained to specific mixtures, families of common anion salts, or chemically similar mixtures. As a result, empirical models are limited in their predictive capability [10, 196, 197]. Some models have been proposed using the Bridgeman equations. In Bridgeman models, the liquid is considered to have a quasi-crystalline structure with heat transported between adjacent lattice layers. The heat transfer rate depends on the sound velocity in the fluid [180]. Using the Bridgeman equations to analyze alkali nitrates, Turnbull [83] and Gustafsson et al. [103] found that values given by the model were too high, by approximately 25%. DiGuilio and Teja [39] noted that the realistic accuracy of these models is likely 20-40% due to the lack of reliable information on the sound velocity and

heat capacity. Some models use the assumption of a lattice structure, where vibration and diffusion primarily contribute to heat conduction. In the case where the diffusive component is negligible, only the vibrational contributions contribute to heat transfer. Yet, these models are not reliable for all families of salts [103, 184]. Other suggested models show a positive temperature dependence. For instance, Zhao et al. [109] developed a theoretical model based on free volume, assuming that the salt molecules are spherical particles, have cubic packing, and a molecular diameter instead of anionic/cationic radii. This model showed a slightly positive temperature dependence of thermal conductivity for molten nitrates and KCl, which is inconsistent with other models. Generally, predictions from these empirical and semi-empirical models are not transferable to all salt families.

Some relatively successful theoretical models for molten salt thermal conductivity are based on the corresponding states principle or the rough hard sphere theory. Nagasaka and Nagashima [94] applied Harada's corresponding state correlation [186] to thermal conductivity by comparing the model to experimental data of several molten salt families. The model was also used to predict the thermal conductivity of molten alkali metal fluorides, which could not be measured experimentally due to the corrosion of quartz and sapphire cells required for the forced Rayleigh scattering measurement technique. The model shows reasonable agreement with the experimental data and a decreasing thermal conductivity with increasing temperature. Unfortunately, specific parameters used in the model are not always known for each compound, which limits the application to additional salts. DiGuilio and Teja [39] proposed a model based on the rough hard-sphere theory of Li et al. [189]. This model successfully predicted the thermal conductivity of the chloride and nitrate families and showed good agreement with the reliable experimental data. This model also predicted a negative temperature dependence. Yet, the thermal conductivity of sodium chloride and sodium nitrate was determined by fitting the experimental data of the common anion family of salts. Unfortunately, sufficient reliable knowledge of each family of molten salts is not always available, which restricts the use of this model. Overall, rough hard sphere and corresponding states models have a reasonable predictive capability, and both suggest a negative trend with temperature but require supporting information that may be limited in availability.

Gheribi et al. [60] proposed a model based on the Boltzmann transport equation with the assumption that $(\partial ln\lambda/\partial T)_P$=0, suggesting that the thermal conductivity of molten salts does not depend significantly on temperature but on the coefficient of thermal expansion (or density). The model's predicted thermal conductivity was in good agreement with reliable experimental data for most molten alkali and alkaline earth metal halides, carbonates, nitrates/nitrites, sulfates, and hydroxides. Gheribi et al. assumed that the propagon (equivalent to phonons in crystals, see section 3) mean free path $< l_{pr.} >$ within atomic vibration

was proportional to the sum of the anionic and cationic radii and inversely proportional to the number of atoms per molecule $< l > \propto (r_a + r_c)/n_a$. This model introduced a dimensionless fitting constant K_{emp} into the equation. Gheribi et al. empirically determined $K_{emp} \sim 4.33$, limiting the applicability of the model when predicting multiple component mixtures, complex salts, and polymerizing salts. Therefore, it is desirable to develop a model that is independent of the experimental data.

In this work, we propose a model for the thermal conductivity of molten salts that is similarly derived from the Boltzmann transport equation but does not require fitting to any thermal conductivity data. Instead, we include a model for minimum thermal conductivity, often used in bulk metallic glasses, with a new proportionality constant that captures the number of cations and anions in each salt. With this formulation, the model can uniquely describe all salts, including complex and simple salts, without a singular K_{emp}. In this sense, the work herein is an improvement to Gheribi's initial ansatz, where the empirical constant K_{emp} is a limitation for predicting molten salt mixtures. In addition, there is no theoretical justification for Gheribi's assumption. Hence, this work aims to demonstrate the capability of the new theoretical model based on the kinetic theory that overcomes the previous limitations. Like the previous derivation, we also assume thermal conductivity depends strongly on density but weakly on temperature [224]. The model is, in principle, considered predictive and can predict the temperature-dependent thermal conductivity of all salts using the density, heat capacity, sound velocity, and melting temperature as inputs for the calculations.

A critical assessment of molten salt thermal conductivity data is provided through the collection of the experimental data available in the literature and comparison to the model's prediction, distinguishing between reliable and unreliable experimental data as suggested previously by DiGuilio [39] and Gheribi [60]. Computations are performed on salts from the fluoride, chloride, iodide, bromide, carbonate, nitrate/nitrite, sulfate, and hydroxide families to compare with the most reliable experimental data sets found in literature, when available. The accuracy of the proposed model shows prediction accuracy improvements compared to Gheribi's previous approach. The model was also applied to predict the thermal conductivity of molten salts that are lacking in reliable experimental data. Finally, we recommend a new database of molten salt conductivity for each family.

4.2 Experimental thermal conductivity: reliable and unreliable data sets

Thermal conductivity is one of the most challenging properties to determine with high accuracy and reliability using experimental techniques or MD simulation; this is particularly true in the case of molten salts [226]. For several decades, various experimental methods have been used to determine the thermal conductivity of molten salts. Experimental methods gen-

erally fall into two main categories: steady-state or transient methods. In the steady-state methods, the common measurement techniques include parallel plate and concentric cylinder methods [47, 55, 64]. Generally, these methods induce a thermal gradient through a layer of salt of known thickness with known heat flux. The thermal conductivity is determined using approximations to Fourier's law of conduction and the measured thickness, heat flux, and temperature difference through the specimen layer. The primary challenges with these techniques include competing convective heat transfer, thermal radiation corrections, accurately measuring the temperature difference through the specimen, and conduction heat losses from the heat source to the surrounding structure [36, 60, 67, 227–229]. Though, with carefully designed systems, these techniques have provided reasonably accurate data [47, 61, 92].

Literature suggests that transient methods are preferred over steady-state methods when measuring the thermal conductivity of high-temperature fluids due to fast measurement times and their potential to limit convective errors. Therefore, transient measurements provide much of the recommended data on molten salt thermal conductivity [58, 69, 70]. Typical transient methods include transient hot-wire, transient hot strip, laser flash, forced Rayleigh scattering, etc [59, 69, 71–75]. These techniques typically measure transient heat transfer through a material by a solution to the heat equation and provide thermal diffusivity measurements, not thermal conductivity. Therefore, transient methods also require information on the material's density and heat capacity to determine thermal conductivity. Additionally, these techniques are still challenging to use with many molten salts due to high temperatures, probe or container corrosion, and errors from competing modes of heat transfer. For example, fluoride salts react with many glasses and dielectric materials used as optical windows or probe electrical insulation, respectively [69, 71]. Additionally, recent results with the laser flash diffusivity technique have occasionally shown positive $(\partial ln\lambda/\partial T)_P$ [76, 77]. While many experimental results from transient techniques have been suggested to be reliable, these techniques still require careful consideration given the absence of a standardized measurement procedures [68, 78–80].

Because of the challenges associated with making thermal conductivity measurements of molten salts, the data reported in the literature can feature large deviations between studies and temperature dependence trends that disagree. For example, consider the experimental data for KNO_3 and $NaNO_3$, molten salts with a relatively large number of experimental data sets determined with different techniques. Figure 4.1 summarizes the thermal conductivity values of KNO_3 and $NaNO_3$ obtained by different investigators. These results show that the maximum deviation between reported values for the thermal conductivity of KNO_3 can achieve 50%. Similarly, the deviation between the reported values of $NaNO_3$ can be as high as 40%. The principle difference among reported data is the sign of the temperature

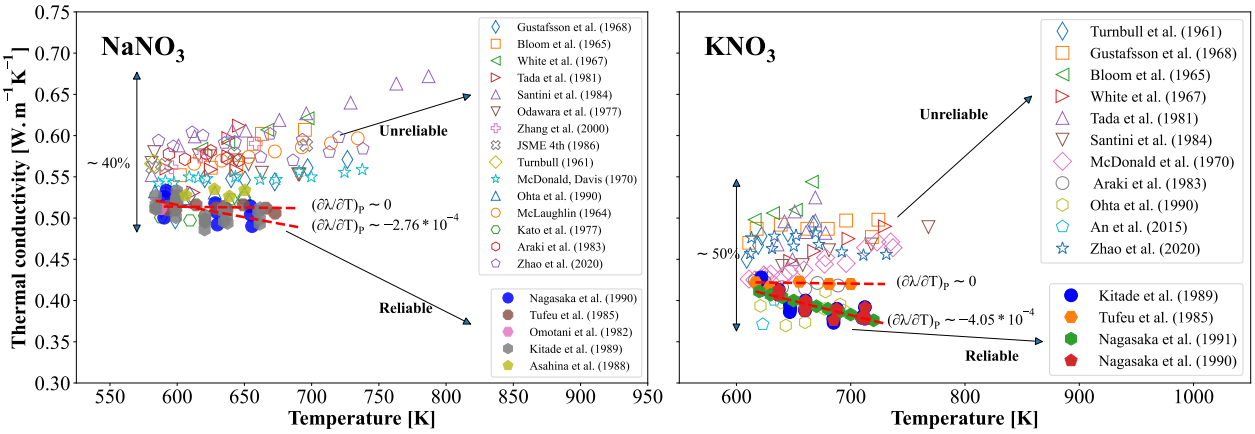

Figure 4.1 Thermal conductivity of molten $NaNO_3$ and KNO_3 as a function of temperature obtained via reliable (solid symbols) and non reliable (open symbols) experimental techniques.

dependence of thermal conductivity, $(\partial\lambda/\partial T)_P$, being either positive or negative. In the case of data considered reliable (denoted with solid symbols), the thermal conductivity at the melting temperature, λ_m, is in agreement for both salts. For instance, λ_m of KNO_3 is approximately 0.42 [W.m^{-1}K^{-1}]. However, the relative deviation between the reliable sets of data, detailed by the bounding red dashed lines, can be greater than 10% within the measured temperature range and increases when linearly extrapolating to higher temperatures. Despite the relatively large number of measurements made on KNO_3 and $NaNO_3$, it is clear that most data sets are likely unreliable. This also suggests that scatter and differing signs of $(\partial\lambda/\partial T)_P$ are expected to be present in other molten salt thermal conductivity data. Therefore, it is important to identify reliable data sets from the experimental work by careful checking and analysis.

KNO_3 is an appropriate case to compare the reliability of different measurement techniques given the relatively large number of available experimental studies. In order of reporting date, these data for KNO_3 loosely follow a trend of decreasing measured thermal conductivity with time. Turnbull et al. [83] used the transient hot-wire technique with an un-insulated wire, which likely led to the leakage of current during the measurement. Gustafsson et al. [103] measured by transient optical determination with a plane source technique. The measurement time was 10 s; therefore, the convective loss was negligible. A possible error of this technique could have been the current leakage from metallic heat sources into the molten salt; the investigators did not consider this. Bloom et al. [55], White et al. [49], Santini et al. [64], and McDonald et al. [50] employed either the steady-state concentric cylinders technique or parallel plates technique. It is expected that convection and radiation losses caused errors that the authors did not consider. For instance, Bloom et al. and Santini et al. underestimated

convection losses from the shape of the apparatus and neglected radiation losses through the molten salt gap. Regardless of the reasoning for the errors, these earlier correlations (open symbol) show a $(\partial\lambda/\partial T)_P > 0$ suggesting that heat losses may have biased the measurements given that losses should increase with temperature. Therefore, these results are considered unreliable.

Tufeu et al. [47] used a steady-state method with a silver coaxial cylinder cell and a carefully engineered specimen gap to minimize the convective and radiative heat transfer losses. The gap between the cylinders was 0.2 mm and the emissivity coefficient was 0.02. The reported data showed $(\partial\lambda/\partial T)_P \sim 0$. More recently, in the 1990s, Nagasaka et al. and coworkers [69, 72–75] used the forced Rayleigh scattering technique and the transient hot-wire technique with ceramic coated probes to determine the thermal conductivity of the molten salts. The characteristics of these methods included short measurement times and small sample temperature rises, therefore the effect of convection should be negligible. The researchers also carefully considered the radiation losses. All of these data sets show a $(\partial\lambda/\partial T)_P < 0$, a critical differentiating factor when considering the reliability of experimental data.

A $(\partial\lambda/\partial T)_P < 0$ is often associated with reliable data. DiGuilio and Teja [39] suggested that temperature dependence allows for easy verification of data's reliability. Galamba and Castro [225] stated that the data obtained by Nagashima and coworkers (Nagasaka, Nakazawa) were likely the most accurate at that time. In addition, the $(\partial\lambda/\partial T)_P < 0$ seen in more recent experimental data is consistent with the kinetic theory-based model proposed by Gheribi et al. [60]. Chliatzou et al. [40] pointed out the primary data selected as reference correlations of thermal conductivity for 13 inorganic salts, and all have a $(\partial\lambda/\partial T)_P < 0$. Therefore, in the context of this study, it is assumed that the reliable experimental data show $(\partial\lambda/\partial T)_P < 0$. Table 4.1 represents different experimental techniques and their features to determine the thermal conductivity of molten salts. The characteristics of each experimental technique are summarized along with notable references and the expected reliability. We consider the experimental works by Nagasaka and colleagues to be the most accurate data sets for comparison in this study, in accord with previous critical assessments.

4.3 Reliable representation of the temperature dependent thermal conductivity of simple and complex molten salts

A theoretical approach describing the thermal conductivity of simple molten salt compounds as a function of temperature has been proposed in a prior work [60]. This approach is, in many respects, predictive as it does not require experimental information on the thermal transport within the molten salt to parameterize the model. Only an accurate knowledge of several thermodynamic properties at their melting temperature are necessary: heat ca-

Table 4.1 Review of the characteristics of the most employed experimental techniques to measure the thermal conductivity and thermal diffusivity of molten salts along with their claimed accuracy

Category	Technique	Characteristics	Accuracy claimed	Reliability	Ref.
Transient method	Forced Rayleigh scattering	• Contact-free • Within 1 ms of measuring time • Less than 0.1 [K] temperature rise • A few cubic millimeters of sample	±3%	Reliable	[58]
	Transient hot-wire with liquid metal probe or coated probe	• Very short measuring time • Negligible of radiation effect • Carefully treat the convection errors	±3%	Reliable	[69, 71]
	Transient hot-wire without isolation	• Current leakage • Convective effects	±10%	Unreliable	[83, 91]
	Laser flash	• No special molten salt container • No Joule heating • Taking into account of radiation effect	±10%	Reliable	[105, 230]
	Pulse-heated flat plate	• Very short period ($< 1s$)	±10%	Reliable	[110]
	Wave-front-shearing interferometry	• Measurement within 10s • Negligible radiation errors • Studied convective effect	NaN	Reliable	[112]
	Optical interferometric	• Measurement within 10s • Negligible radiation errors • Current leakage	±2.6%	Unreliable	[103]
Steady state	Concentric-cylinders	• Very thin melting layer $\leq$ $1mm$ • Very low surface emissivity (Molybdenum or polished silver surface)	$\sim$ ±6%	Reliable	[47, 92]
	Coaxial cylinders	• Large melting layer $\geq$ $2.5mm$ • Heat losses (axial or end of apparatus vessel) • Affected by convection and radiation	±5%	Unreliable	[51, 54–56]
	Parallel-plates	• Suitable for solid materials • Heat losses due to high temperature	-	Unreliable	[64, 104]

pacity, density, thermal expansion, and sound velocity (or compressibility). Contrary to thermal conductivity, these properties are typically known for the large majority of molten salts. In a few cases (some complex molten salts), these thermodynamic properties can be predicted with appreciable accuracy from empirical relationships or trending analysis using the knowledge of the properties of similar molten salts. Briefly, this prior approach consists of a theoretical description of the temperature dependence of the thermal conductivity and a semi-empirical description of the magnitude of the thermal conductivity near the melting temperature. The theoretical expression of the temperature dependence of the thermal conductivity was derived from an empirical ansatz found in equilibrium and non-equilibrium molecular dynamics simulations [224]: at constant volume, the thermal conductivity is almost independent of temperature, which can be written as:

$$\left(\frac{\partial \lambda}{\partial T}\right)_V = 0 \tag{4.1}$$

Integration results in the following expression for the temperature dependence of the thermal conductivity at standard pressure (1 bar) [60]:

$$\lambda\left(T\right) = \lambda_m exp\left[-\alpha_m\left(\gamma_m + \frac{1}{3}\right)\left(T - T_m\right)\right] \tag{4.2}$$

where α_m, λ_m, and γ_m represent respectively the thermal expansion, the thermal conductivity, and the Grüneisen parameter, all taken at the melting temperature T_m. The Grüneisen parameter is an empirical parameter defined at the melting temperature as:

$$\gamma_m = \frac{\alpha_m c_{s,m}^2 M}{Cp_m} \tag{4.3}$$

where M, $c_{s,m}$, and Cp_m are the molecular weight, sound velocity, and heat capacity. Given that for most molten salts the term $\lambda_m,\ \alpha_m,\ \gamma_m$ is of the order of 10^{-4}, the first order Taylor expansion of Eq. 4.4 is considered an accurate approximation in a wide range of temperatures (up to or near the boiling point) :

$$\lambda\left(T\right) = \lambda_m\left[1 - \alpha_m\left(\gamma_m + \frac{1}{3}\right)\left(T - T_m\right)\right] \tag{4.4}$$

Thereafter, a formulation for the thermal conductivity at the melting temperature was proposed based on the kinetic theory and an ansatz on the mean free path of propagons, the quasi-particles associated with heat transport defined by Allen et al. [231]. Even though heat travels by collective vibrations in molten salts, they are distinct from phonons due to their lack of long-range ordering, unlike crystalline materials which have defined long-range

ordering [231]. Allen et al. described the distinction between propagons and phonons in heat transport at the quantum scale [231]. According to kinetic theory, the thermal conductivity within a material can be expressed:

$$\lambda_m = \frac{1}{3}\overline{Cv}_m c_{s,m} < l_{ph}. > \tag{4.5}$$

where $\overline{Cv}_m$ is the heat capacity per unit volume at the melting temperature and $< l_{ph}. >$ is the propagon mean free path assumed to be independent of temperature (volume). The second ansatz proposed in our prior study [60] is that the propagon mean free path is "universally" proportional to the average ionic radius, $\overline{r}_{ion}$, between constituting molten salt compounds:

$$< l_{pr}. >= K_{emp}\ \overline{r}_{ion} \tag{4.6}$$

By "universally," it is understood that K_{emp} is constant for all molten salts and therefore independent of the nature of interactions. Note that $\overline{r}_{ion}$ is simply defined as: $\left(\sum_i r_a^i + \sum_j r_c^j\right)/n$, where r_a^i and r_c^j are the radii of the anionic, i, and cationic, j, species. Thereafter, the thermal conductivity is expressed:

$$\lambda_m = K_{emp}\frac{Cv_m\ c_{s,m}}{3nV_m}\overline{r}_{ion} \tag{4.7}$$

K_{emp} was optimized to fit all the reliable experimental data reported for the thermal conductivity of molten KCl. It was determined that the optimal value of K_{emp} was 4.33.
Even though K_{emp} was optimized on the thermal transport properties of molten KCl only, this specific value can predict, with appreciable accuracy, the thermal conductivity of most molten salts with available experimental data. Nevertheless, from a theoretical point of view, assuming a "universal" definition of the propagon mean free path is questionable. Strictly speaking, the propagon mean free path should depend on the nature of the interactions within molten salts. Polymerizing molten salts such as BeF_2 [160] should have a lower propagon mean free path than fully dissociated molten salts like LiF. However, given the large discrepancy between the different reliable experimental datasets on simple molten salts (halides) and the relatively few reliable experimental datasets reported for complex molten salts, the reasonable predictive capability of the model was de facto admitted for all types of molten salts, including complex salts. Therefore, additional reliable experimental thermal conductivity data are necessary for both simple and complex molten salts before we can analyze the reliability of the assumptions behind our prior formulation [60] and its fine-tuned predictive capability.
In the present work, we propose an original theoretical approach to represent and predict the thermal conductivity of simple and complex molten salts as a function of temperature

without the empirical considerations leveraged in the prior formulation. The assumption that $(\partial\lambda/\partial T)_V = 0$ originates from molecular dynamics simulations performed in the framework of the Green-Kubo formalism [152, 220]. This was first demonstrated for simple molten salts [224] and later confirmed for complex molten salts [160, 232]. This fundamental equation governing the temperature dependence of the thermal conductivity of molten salts is not strictly empirical and can be justified by thermodynamic considerations. Indeed, from a thermodynamic point of view, at constant volume, the sound velocity within insulating materials is nearly independent of temperature or negligible compared to that at constant pressure. Then, the kinetic theory (Eq. 4.5) shows that the thermal conductivity is also nearly independent of temperature at constant volume. Therefore, Eq. 4.2 and its approximation given by Eq. 4.4 can be considered valid for any variety of molten salts.

We propose a formulation of the thermal conductivity based on the concept of a minimum thermal conductivity, λ_{min}. This assumption is the primary contribution of our new formulation. In amorphous solids, which, like liquids, lack the long-range order of crystals but may contain a certain amount of local short-range ordering, the thermal conductivity is often described through the Einstein minimum thermal conductivity model considering a single frequency [233]. Cahill–Pohl [234] further extended the model to include a range of frequencies. In general, the Cahill-Poll model has a strong predictive capability for thermal transport within non-metallic glasses, particularly those based on oxides. Neglecting the transversal component of the sound velocity, which is reasonable in the liquid state, the minimum thermal conductivity at the specific melting temperature is as [235]:

$$\lambda_{min} = k_B \; N_A^{2/3} \; (\frac{n}{M})^{2/3} \; \rho_m^{2/3} \; c_{s,m}, \tag{4.8}$$

Note that the parameters describing the minimum thermal conductivity are, in this case, identical to those describing its temperature dependence, which ensures a self-consistent description of the temperature-dependent thermal conductivity of molten salts when one describes λ_m by the minimum thermal conductivity model. Also, noting that Cv is close to $3nR$ ($R = N_A \; k_B$ being the gas constant), it is interesting to highlight that the minimum thermal conductivity expression is very similar to that derived in our prior work [60] from the kinetic theory (Eq. 4.7). The two expressions of thermal conductivity are proportional, $\lambda_{min} \propto \lambda^{kinetic}$, even though this proportionality depends on the average ionic radius of the molten salt compound. Based on this similarity, we assume that λ_m can be expressed:

$$\lambda_m(T) = \boldsymbol{K} \; \lambda_{min}(T) \tag{4.9}$$

where K is a proportionality constant typically greater than or equal to one. The more

complexity in the local structure, the closer K is to one. For polymerizing molten salts (e.g., BeF_2) that have a local structure close to that of glasses,in principle, $K \to 1$. Therefore, K must be a function of the local ordering, maximized when the molten salt is fully dissociated and at a minimum (equal to 1) when polymerizing. Simple molten salts (e.g., NaCl and LiF) are generally fully dissociated, while complex ones (AlF_3, UF_4, ThF_4) form complex anions where several anions surround one cation. The ratio n_s^+/n_s^- (n_s^+ and n_s^- being the number of cation and anion forming the salt compound) quantify, in first approximation, the degree complexity of the local ordering within molten salts. K can be directly expressed through this ratio:

$$\boldsymbol{K} = 1 + \frac{n_s^+}{n_s^-} \tag{4.10}$$

When coordination complexes, the ratio n_s^+/n_s^- significantly decreases, and in the case of polymerization, it becomes null. Therefore, for polymeric fluids, the thermal conductivity tends to its minimum value defined by Eq. 4.8.

In summary, in the proposed approach, the thermal conductivity is expressed as a function of temperature as follow:

$$\lambda\left(T\right) = \boldsymbol{K}\ \lambda_{min}\left[1 - \alpha_m\left(\gamma_m + \frac{1}{3}\right)\left(T - T_m\right)\right] \tag{4.11}$$

where λ_{min} is defined via Eq. 4.8. It is important to highlight that the proposed approach is predictive, as no prior information on thermal conductivity is necessary to parameterize the model. The only properties required to predict the thermal conductivity are the density, the heat capacity, the thermal expansion, and the sound velocity, all considered at the melting temperature of the salts.

4.4 Analysis Methodology

We performed a broad assessment of the proposed model's predictive capability by calculating the thermal conductivity of 25 different molten salts with reliable experimental data. These selected salts have data reported by Nagasaka et al. or Harada et al. [38, 58, 69, 72–75, 85, 94, 236]. Note that Harada et al. reported on nine salts, also evaluated by Nagasaka et al., for a total of 31 different experimental data sets. The other properties required by the model were taken from the works of Janz et al. [35] for density and Gheribi et al. [60] for the heat capacity and sound velocity. The model's accuracy was evaluated for all 25 molten salts using typical statistical measured. The model's accuracy was illustrated with Bland-Altman and correlation plots. The new model's predictions were also compared to that of Gheribi's previous approach. The initial assessment was chosen to demonstrate the model's accuracy

on both the thermal conductivity at the melting point and the temperature dependence of thermal conductivity for a range of molten salts from different families before considering each molten salt individually.

Model calculations were then carried out for all families of salts, separated by family and valency, where experimental data is available; grouping the salts into halides, divalent halides, carbonates, nitrates, nitrites, sulfates, and hydroxides. The density and heat capacity were computed in FactSage, a commercial thermodynamic equilibrium calculation software [179, 237]. The sound velocity was taken from Gheribi et al. [60]. The model's predictions are compared to both reliable and unreliable data reported in the literature and to the prediction of Gheribi's previous approach. The thermal conductivity of molten salts where there is no reliable experimental data was also predicted. Finally, a molten salt thermal conductivity database is provided based on the results obtained from the new model with all model parameters required for prediction.

4.5 Results and discussion

4.5.1 Broad assessment of the model

The proposed model's predictions and relative deviation to the experimental data from Nagasaka et al. and Harada et al. are shown in Bland-Altman plots, Figure 4.2 A) and B), respectively. The density data was from Janz [35], and the other parameters were taken from the previous work of Gheribi et al., aside from $MgCl_2$ [60]. The correlation for the sound velocity of $MgCl_2$ was recently re-assessed and provided in a separate work [238].

In Figure 4.2 A), 25 experimental data sets from literature, reported by Nagasaka and his co-workers [38, 58, 69, 72–75, 85, 94, 236], are compared to the model's prediction on a Bland-Altman plot. The mean relative error of the present model to the experimental data is 9.33%, while the average experimental error reported in the literature by Nagasaka is approximately 15%. The 95% confidence interval for the mean difference is shown in Figure 4.2, represented by the dashed lines $\pm 1.96SD$. All the predicted results are within the 95% confidence interval of Nagasaka et al., except for KI, which is slightly higher than the confidence limit. In Figure 4.2 B), the model's predictions are compared to 9 experimental thermal conductivity values reported by Harada et al. [59, 230]. In this case, the relative deviation of the model to experimental data is 8.04%. Note, KI reported by Harada et al. is nearly the same as the model's prediction, with a relative deviation of only 3.5%. In comparison, the relative deviation of the model to the value reported by Nagasaka et al. is approximately 38%. In the case of RbI, the model prediction agrees with Nagasaka et al.'s work, but it is low relative to the value reported by Harada et al. Even though both data sets are considered reliable, it is clear that large deviations for some salts still exist, which further illustrates the difficulty of relying

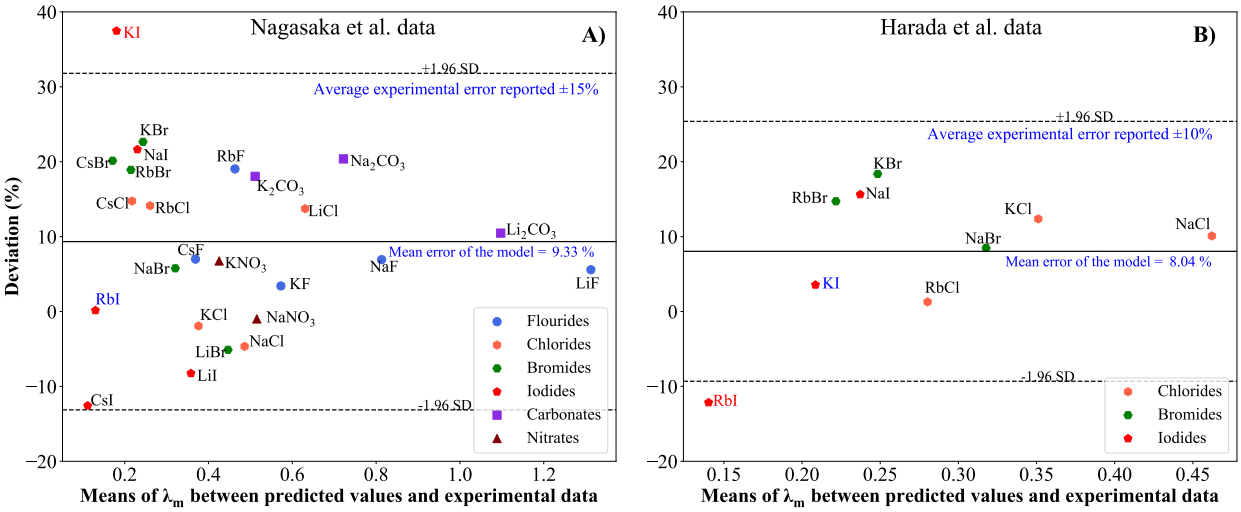

Figure 4.2 Quantification of the predictive capability of the present approach through a Bland-Altman plot representation. The means between the predicted and measured thermal conductivity (via reliable experimental techniques) at melting temperature reported by Nagasaka et al. (left) [38, 58, 69, 72–75, 85, 94, 236], and by Harada et al. [59, 230] are represented along with the 95% confidence limit. Note the experimental errors claimed by Nagasaka et al. fall in the range of 5% to 25% while Harada claimed the uncertainty was within 10%.

on experimental techniques when measuring molten salt thermal conductivity. Alternatively, the proposed model shows the capability of prediction within an average deviation of 10% for both simple and complex molten salts at the melting temperature. It also suggests that the model can be used with reasonable confidence to verify the reliability of experimental data. Figure 4.3 and Figure 4.4 show the thermal conductivity at the melting temperature and the slope of the thermal conductivity with temperature from the predictions. The reliable experimental data reported by Nagasaka et al. and Harada et al. are shown for comparison. Two dashed lines represent ±10% deviation from the experimental data. Figure 4.3 shows that our predictions are in good agreement for most simple and complex salts near or within this ±10% deviation. However, in some cases, the model overestimates the thermal conductivity for members of the iodide and carbonate families compared to Nagasaka's work. The discrepancy could be caused by errors in the model's thermo-physical property inputs or errors in experimental data. Note that the predictive accuracy is comparable to the experimental uncertainties claimed in the literature. Figure 4.4 shows the temperature dependence of thermal conductivity from the present model compared to experimental data from Nagasaka et al. and Harada et al. The shaded region represents the standard uncertainty from the experimental measurements of thermal conductivity. The predictions agree with most experimental data and are within the region of the experiments' standard uncertainty. Note

that all the experimental data have a negative or negligible temperature dependence, but the model can only predict a negative temperature dependence. In particular, the carbonate salt family, Li_2CO_3, Na_2CO_3 and K_2CO_3 show negligible temperature dependence. However, the model's predictions show a negative temperature dependence for these carbonates. If we observe the nitrate salts' experimental temperature dependence of thermal conductivity, a negative slope is shown for both $NaNO_3$ and KNO_3. Carbonates and nitrate are expected to behave similarly, suggesting that experimental errors may have affected the carbonate thermal conductivity data. With other empirically based models, errant data could bias the predicted thermal conductivity. However, our proposed model overcomes the limitation of relying on experimental measurements while still providing comparable accuracy to experimental techniques.

In Figure 4.5, the predicted thermal conductivity of molten salts at their melting temperature is compared to that of Gheribi et al. The dashed lines represent ±10% relative deviation from the proposed model's prediction of thermal conductivity to the Gheribi et al. prediction.

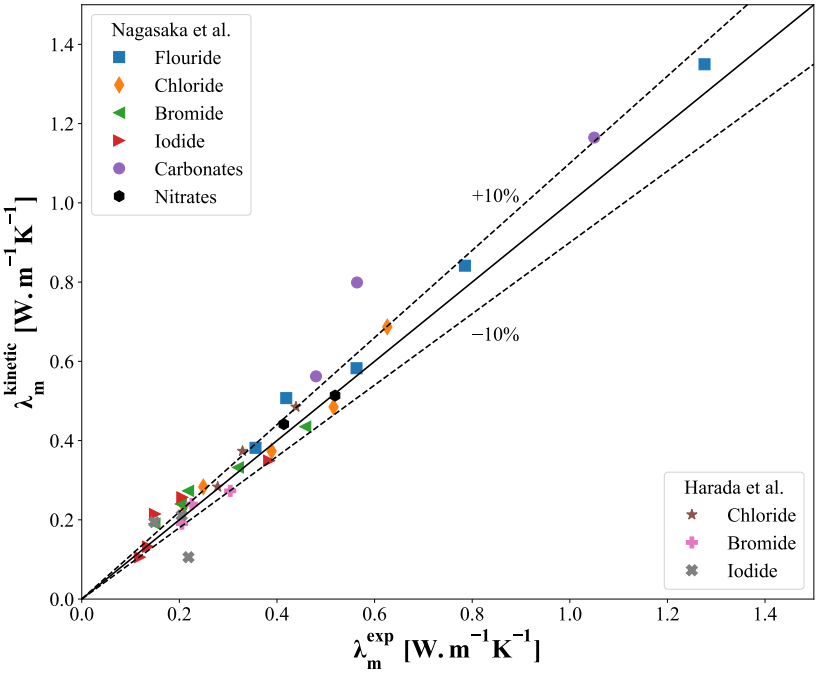

Figure 4.3 Correlation plot between predicted (y-axis) vs reliable experimental thermal conductivity (x-axis) taken near the melting temperature λ_m (see text for details). The two dashed lines represent a 10% error in the x-axis, which also highlights the accuracy of present model.

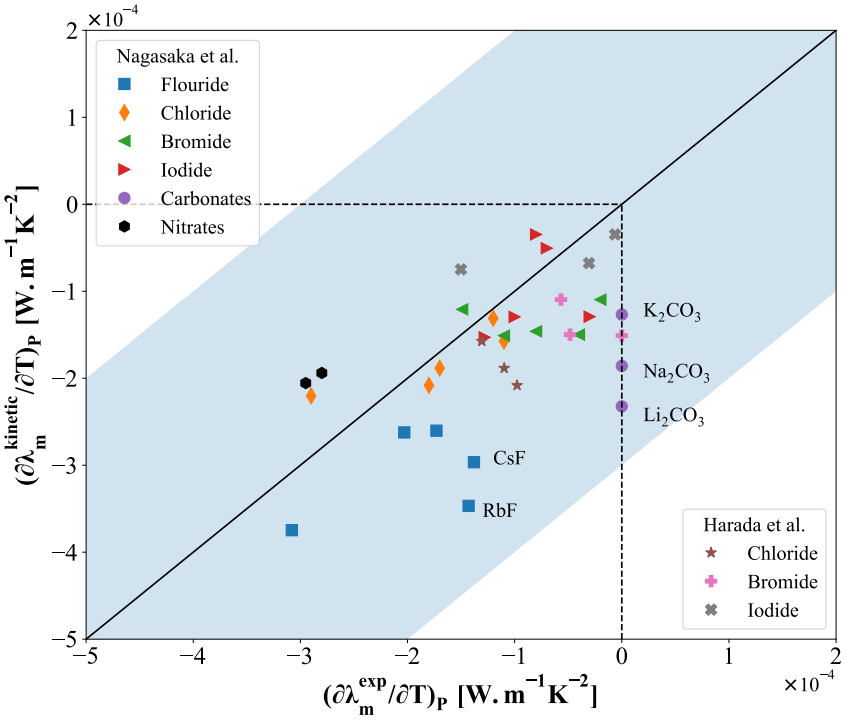

Figure 4.4 Correlation plot between predicted (y-axis) vs reliable experimental thermal conductivity of the temperature dependence $(\partial\lambda/\partial T)_P$. The light-blue region was determined from error analysis assuming a linear behavior of thermal conductivity with respect to temperature.

The results of the two models are in good agreement for most simple salts. The relative deviations for most of the salts, λ_m, are less than 10%. However, some members of divalent halides and some of the complex salts from the carbonate, sulfate, and hydroxide families have larger deviations. It is possible that the empirical constant $K_{emp} = 4.33$, proposed in the Gheribi et al. approach, is not suitable when extending the model to some complex salts. Alternatively, the theoretical formulation defines a unique $\boldsymbol{K}$ for each salt, potentially circumventing this previous limitation. This comparison shows that the proposed model agrees with the previously proposed theoretical model but provides the benefit of using the derived $\boldsymbol{K}$ for each salt instead of a discrete value. The derived $\boldsymbol{K}$ is particularly useful for extending the model to cases where $\boldsymbol{K} = 1$, such as the polymerizing salts like BeF_2, sulfate, and hydroxide salt families.

In general, the initial assessment of the proposed model demonstrates its accuracy for many molten salts. We observe reasonable agreement in comparison to reliable experimental data of thermal conductivity at the melting point and the experimental temperature dependence

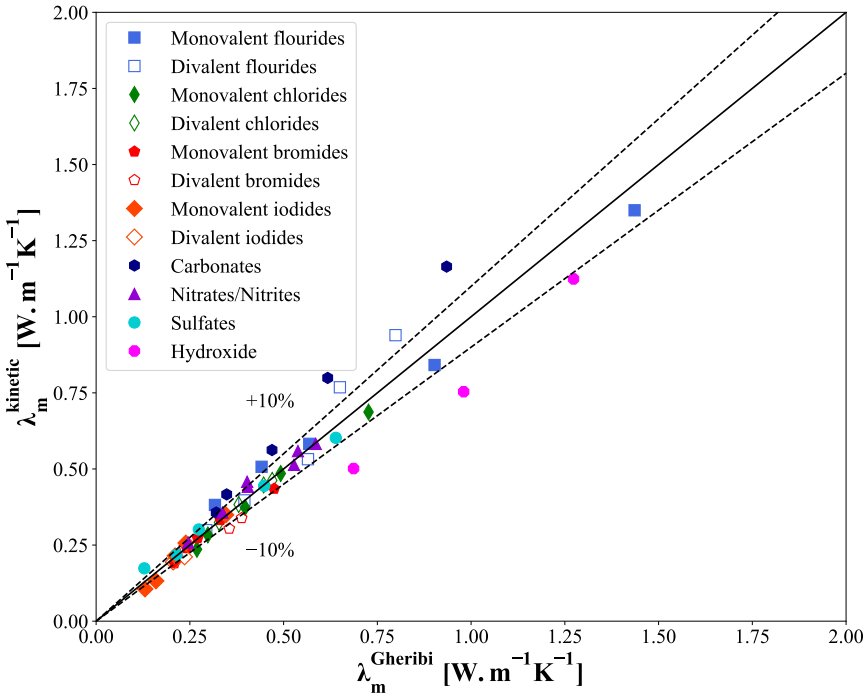

Figure 4.5 Correlation plot of predicted thermal conductivity between the present model (y-axis) and the Gheribi et al. approach (x-axis) taken near the melting temperature λ_m (see text for details). The two dashed lines represent a 10% error of x-axis. Note that this figure can be read to quantify the mean free path of phonon between two models.

of thermal conductivity. The proposed model agrees with the Gheribi et al. predictions for most simple salts, demonstrating that the new model is an acceptable modification. Notable differences occurred for divalent halides and complex salts, which is expected to be an improvement over the previous model, spanning from the new derivation of the magnitude of thermal conductivity proposed in the present formulation. In the following sections, both models are compared to experimental data, where available, for all salt families to test the accuracy of the proposed model.

The model was applied to monovalent halides, divalent halides, carbonates, nitrates, nitrites, sulfates, and hydroxides. The comparisons of predicted results and available experimental data found in the literature are presented in the following section. In each plot, error bars claimed by authors are included. The minimum error was assumed to be 5%; this is justified because it is expected that no experimental technique can provide an uncertainty less than 5% [239]. The solid symbols designate reliable experimental data sets, the open symbols designate unreliable experimental data sets, and the red dashed line represents the predic-

Table 4.2 The predicted thermal conductivity of molten salts (fluorides, chlorides, bromides, iodides). Model parameters for the thermal conductivity of molten salts are expressed as $\lambda(T) = \lambda_m + \lambda^{'}(T - T_m)$. Data reliability: reliable (R) or unreliable (UnR). For some salts, no experimental data is available, and predictions (Pre) are reported. The thermo-physical properties ($\rho = \rho + \rho^{'}T$, α, U, Cp) are also shown.

Salts	$\mathbf{T_m}$	$\boldsymbol{\rho}$	$\boldsymbol{\rho^{'}}$	$\boldsymbol{\alpha_m * 10^{-4}}$	$\mathbf{c_{s,m}}$	$\mathbf{Cp_m}$	$\boldsymbol{\lambda_m}$	$\boldsymbol{\lambda^{'} * 10^{-4}}$	**Data**
	[K]	[kg.m^{-3}]	[kg.m^{-3}.K^{-1}]	[K^{-1}]	[m.s^{-1}]	[J.mol^{-1}.K^{-1}]	[W.m^{-1}.K^{-1}]	[W.m^{-1}.K^{-2}]	**type**
Fluorides									
LiF	1118	2358	-0.490	2.68	2547.8	64.20	1.350	-3.75	R
NaF	1268	2755	-0.636	2.88	2085.5	70.20	0.841	-2.62	R
KF	1129	2646	-0.652	3.41	1816.4	66.90	0.583	-2.60	R
RbF	1048	3995	-1.021	3.49	1760.4	69.50	0.507	-3.47	R
CsF	955	4899	-1.280	3.85	1460.8	74.10	0.382	-2.97	R
BeF_2	1070	1972	-0.015	0.074	2547.8	87.90	0.626	-0.017	Pre
MgF_2	1536	3235	-0.524	2.16	2175.6	94.90	0.768	-1.67	R
CaF_2	1691	3179	-0.391	1.55	1710.3	99.90	0.532	-0.567	R
SrF_2	1673	4784	-0.751	2.13	1398.6	99.00	0.397	-0.728	Pre
BaF_2	1593	5775	-0.999	2.39	1174.6	99.30	0.299	-0.654	R
Chlorides									
LiCl	883	1884	-0.433	2.88	2038.1	65.02	0.687	-2.20	R
NaCl	1081	2139	-0.543	3.50	1743.7	69.62	0.485	-2.08	R
KCl	1045	2136	-0.583	3.82	1597.2	73.60	0.373	-1.88	R
RbCl	990	3121	-0.883	3.93	1292.1	73.40	0.283	-1.57	R
CsCl	918	3769	-1.065	3.82	1161.6	77.40	0.236	-1.31	R
$BeCl_2$	688	2276	-1.100	5.38	2408.6	181.92	0.351	-1.71	Pre
$MgCl_2$	987	1950	-0.271	1.80	2150.0	92.05	0.462	-1.04	UnR
$CaCl_2$	1055	2526	-0.423	2.03	2065.0	102.53	0.447	-1.15	UnR
$SrCl_2$	1148	3390	-0.578	2.12	1873.1	104.60	0.383	-1.19	UnR
$BaCl_2$	1235	4015	-0.681	2.15	1720.6	108.78	0.325	-1.08	UnR
Bromides									
LiBr	820	3065	-0.651	2.58	1470.7	65.27	0.435	-1.21	R
NaBr	1020	3175	-0.817	3.49	1324.4	68.00	0.332	-1.46	R
KBr	1007	2958	-0.825	3.88	1278.9	69.87	0.273	-1.50	R
RbBr	953	3739	-1.072	3.94	1188.2	72.80	0.240	-1.51	R
CsBr	909	4245	-1.223	3.91	1013.9	75.00	0.190	-1.10	R
$MgBr_2$	984	3087	-0.478	1.22	1965.6	76.94	0.354	-0.439	Pre
$CaBr_2$	1003	3618	-0.500	1.6	1767.8	112.97	0.339	-0.660	Pre
$SrBr_2$	916	4390	-0.745	2.01	1628.6	116.39	0.304	-0.896	Pre
$BaBr_2$	1123	5035	-0.924	2.31	1394.7	104.85	0.242	-0.899	Pre
Iodides									
LiI	722	3790	-0.919	2.93	1367.7	63.18	0.349	-1.53	R
NaI	935	3627	-0.949	3.46	1184.3	64.85	0.257	-1.29	R
KI	958	3359	-0.956	3.91	1144.2	70.30	0.215	-1.29	R
RbI	913	3950	-1.144	3.94	740.1	72.10	0.132	-0.505	R
CsI	894	4255	-1.183	3.72	634.7	71.00	0.106	-0.347	R
MgI_2	907	3642	-0.651	1.31	1350	74.22	0.205	-0.295	Pre
CaI_2	1052	4233	-0.751	1.16	1328.4	71.26	0.210	-0.310	Pre
SrI_2	788	4803	-0.885	2.16	1310.1	110.04	0.211	-0.677	Pre
BaI_2	1013	5222	-0.977	2.31	1292.4	112.97	0.194	-0.749	Pre

Table 4.3 The predicted thermal conductivity of molten salts (carbonates, nitrates/nitrites, sulfates and hydroxides) are recommended in the table.

Salts	$\mathbf{T_m}$	$\boldsymbol{\rho}$	$\boldsymbol{\rho'}$	$\boldsymbol{\alpha_m * 10^{-4}}$	$\mathbf{c_{s,m}}$	$\mathbf{Cp_m}$	$\boldsymbol{\lambda_m}$	$\boldsymbol{\lambda' * 10^{-4}}$	**Data**
	[K]	[kg.m^{-3}]	[kg.m^{-3}.K^{-1}]	[K^{-1}]	[m.s^{-1}]	[J.mol^{-1}.K^{-1}]	[W.m^{-1}.K^{-1}]	[W.m^{-1}.K^{-2}]	**type**
Carbonates									
Li_2CO_3	1008	2203	-0.373	2.04	2815.8	185.44	1.165	-2.32	R
Na_2CO_3	1127	2480	-0.449	2.27	2333.1	189.54	0.799	-1.86	R
K_2CO_3	1169	2414	-0.442	2.33	2011.7	205.50	0.562	-1.27	R
Rb_2CO_3	1110	3549	-0.641	2.26	1604.2	205.00	0.416	-0.930	UnR
Cs_2CO_3	883	4037	-0.561	1.59	1492.1	205.00	0.357	-0.508	UnR
Nitrates/Nitrites									
$LiNO_3$	527	2070	-0.549	3.07	1853.2	149.00	0.582	-1.47	R
$NaNO_3$	583	2334	-0.767	3.76	1807.5	155.60	0.513	-1.94	R
KNO_3	610	2335	-0.7601	3.90	1754.6	141.00	0.442	-2.06	R
$RbNO_3$	589	3137	-1.069	3.93	1499.9	146.00	0.357	-1.72	UnR
$CsNO_3$	690	3621	-1.166	4.14	1207.7	150.00	0.258	-1.19	UnR
$NaNO_2$	544	2226	-0.746	3.59	1906.2	99.79	0.559	-2.48	R
KNO_2	713	2167	-0.667	3.94	1887.3	102.00	0.458	-2.71	Pre
Sulfates									
Li_2SO_4	1132	2464	-0.406	2.03	2414.0	205.02	0.602	-1.18	Pre
Na_2SO_4	1157	2652	-0.503	2.33	2069.0	204.00	0.445	-1.06	UnR
K_2SO_4	1347	2475	-0.451	2.89	1721.0	201.46	0.301	-0.935	Pre
Rb_2SO_4	1347	3442	-0.665	2.61	1348.0	209.20	0.218	-0.535	Pre
Cs_2SO_4	1364	4300	-0.952	2.53	1176.0	206.69	0.174	-0.415	Pre
Hydroxides									
LiOH	735	1718	-0.457	3.31	3677.6	87.09	1.124	-5.82	UnR
NaOH	591	2068	-0.478	2.68	2926.2	86.02	0.754	-2.83	UnR
KOH	633	2013	-0.440	2.53	2486.0	87.00	0.501	-1.70	UnR

tions from Gheribi et al. Our proposed model is able to predict the thermal conductivity for any type of salt with existing knowledge of the required input properties. Notably, $BeCl_2$, $MgBr_2$, MgI_2, and CaI_2 lack data on their sound velocity, and this property was obtained by linear extrapolation of the same salt family as a function of the period (principal quantum number) [238]. The model uses the critically reviewed heat capacity, density, and coefficient of thermal expansivity provided in FactSage, a commercial software for thermodynamic equilibrium calculation [179, 237]. While the proposed model still relies on existing knowledge of other properties, the experimental data for these properties are generally more reliable and available than thermal conductivity data. Furthermore, it is possible to accurately predict

the density, heat capacity, coefficient of thermal expansivity, and sound velocity with existing modeling techniques. Nevertheless, the accuracy of the input property data is representative of the current model's accuracy and is expected to be near 15% or less. Complete uncertainty quantification of the input data and the propagation of those uncertainties for the proposed model is beyond this work's scope. Based on the results obtained from this work, we recommend a new database for molten earth metal halides and complex salts in Table 4.2 and Table 4.3 respectively.

4.5.2 Monovalent halides

Monovalent fluorides The predictions of monovalent fluorides and chlorides are illustrated in Figure A.1. Fluoride salts are a suitable candidate for PCM solar thermal energy storage systems because of their high latent heat capacity [240] and are of interest for nuclear applications. However, it is more difficult to experimentally determine their thermal conductivity using techniques that can be reliably applied to other salts, such as forced Rayleigh scattering. This difficulty is due to their corrosive behavior with most available optically transparent container cells and other electrically insulating materials commonly employed in high-temperature thermal conductivity measurements. Therefore, the reliable experimental data is relatively limited for fluoride salts compared to other salts. However, we observe that both λ_m and $(\partial\lambda/\partial T)_P$ from the present model agree with the available experimental data sets. Meanwhile, the present model is also generally closer to the experimental data and the predictions of Nagasaka et al. in comparison to the prediction of Gheribi et al. The predicted λ_m of the present model also falls within the error range claimed by experimental measurements and predictions.

Nagasaka [94] applied the law of corresponding states to estimate the thermal conductivity of monovalent fluoride salts based on reliable experimental data of the other molten halides [58]. The accuracy of Nagasaka's estimations are $\pm 15 \sim 20\%$ for monovalent fluorides and are considered reliable, despite the lack of experimental data for most fluorides. The present model's prediction agrees with Nagasaka's predictions. Outside of RbF, the present model also agrees better with Nagaska's predictions than Gheribi et al. LiF was the most studied salt in the family and includes results from different investigators with different experimental techniques. The reported experimental thermal conductivity of LiF at the melting temperature appears to be similar, and our predicted results agree with these reliable data sets.

Golyshev and Gonik [93] pointed out that a positive temperature dependence seen in previous experimental measurements could be caused by erroneous radiation and convection contributions due to a large melt layer. Experimental measurements that included corrections for these losses and showed a negative temperature dependence of thermal conductivity were con-

sidered reliable [89,92–94]. The results obtained by Smirnov et al. [56] showed a large positive temperature dependence, and the thermal conductivity values were considerably higher than others, even though they employed a small gap of 1.2 mm and platinum structure to reduce the convective and radiative heat transfer. A probable cause for their errors is conductive heat losses through the structure of the instrument spanning from the inadequate design of the top and bottom of their apparatus, as noted by Chliatzou et al. [40] Therefore, the data from Smirnov are considered unreliable as well as data from Sreenivasan et al. and Polyakov et al. [56, 88, 90]. However, Smirnov's data occasionally agree with the present model and other experimental data near the melting point, particularly those with lower melting points and higher thermal conductivity. This behavior is unsurprising since competing heat transfer mechanisms have more significant contributions at higher temperatures due to decreased fluid viscosity and increased thermal radiation.

The temperature dependence of thermal conductivity for RbF and CsF is slightly overestimated compared to Nagasaka et al. and the predictions fall outside the ±15% relative error at some temperatures. This magnitude of discrepancy was not observed in the predictions of other fluoride salts. However, Nagasaka et al. reported that their fluoride salt estimations may have errors ranging from ±15% to ±20%, and our model's predictions would fall within the recommended interval if the uncertainty was assumed to be ±20%. Unfortunately, we could only compare our model's predictions to Nagasaka's estimations for CsF and RbF. Nonetheless, the current agreement is reasonable considering the difficulty of fluoride measurements. Looking at the LiF data, the reliable data reported by Golyshev et al. had relative deviations over 50% at about 1200 [K]. Therefore, we can confirm that our predictions are comparable or better than existing empirical errors. Given the agreement with other fluorides, we suggest an accuracy of ±15% for the entire fluoride salt family, but more experimental data is necessary to verify this estimate.

Monovalent chlorides Figure A.1 compares the predicted and experimental thermal conductivity for molten alkali and alkaline earth metal chlorides. For most monovalent chlorides, reliable experimental data exists. When considering the reliability of available experimental data sets, the reliable data were identified using the same principles as the fluorides. The reliable data sets include the works of Nagasaka [58,72,94], Golyshev [92] and Harada [59]. In the figures, closed symbols depict these reliable data sets while open symbols represent unreliable data sets [51, 56, 83, 90, 95–98, 241]. The present model agrees better with experimental data, in comparison to the predictions of the Gheribi et al. model for all monovalent chloride salts, with the largest improvement of accuracy seen for KCl and CsCl. The predicted values of thermal conductivity and $(\partial\lambda/\partial T)_P$ have nearly the same values as the experimental data. Therefore, we have confidence that the accuracy of this model is less than 10% in the case

of monovalent chlorides.

It is noted that LiCl was successfully measured experimentally by Nagasaka et al. but the data featured a relatively large scatter, and deviation from the models' predictions, at higher temperatures. It was noted by Nagasaka that the quartz container cell turned slightly opaque due to corrosion of the quartz and sapphire cells, which likely affected the experimental values. This corrosive behavior is typical of Li cation salts [94]. Comparing the models' predictions to Nagasaka et al.'s experimental data at lower temperatures ($< 1200[K]$) is potentially a more reliable metric for the models' accuracy. The average and maximum relative deviations between the model's predictions and the empirical data of Nagasaka et al. at temperatures $< 1200[K]$ are 11.61% and 19.07%, respectively. Additionally, Roberston et al. [79] provided recent measurements of LiCl using a transient grating spectroscopy system designed to determine the molten fluoride thermal diffusivity and sound velocity. The thermal diffusivity measurements were performed around 1000 [K] for LiCl. It is shown that the magnitude of thermal conductivity and $(\partial\lambda/\partial T)_P$ from Robertson et al. agree well with the model's predictions. The average and maximum relative deviations between the model's predictions and the empirical data of Robertson et al. are 4.40% and 5.89%, respectively. The experiment used corrosion-resistant materials (namely diamond windows) to mitigate the effects of material interaction, which impacted the measurements by Nagasaka et al., so Robertson's data is considered more reliable. When considering the reliable data (Nagasaka $< 1200[K]$ and Roberton), it is expected that the model provides reasonable accuracy for LiCl, yet more data is necessary at higher temperatures for further validation.

Monovalent bromides Figure A.2 shows the predicted thermal conductivity for the monovalent bromide salt family compared to experimental values. Our predicted results agree with the reliable experimental data sets, which only include Nagasaka [73, 94] and Harada [59]. As mentioned, lithium cation salts are challenging to measure because of their corrosion of many cell materials. Therefore, Nagasaka [94] obtained the estimation values for LiBr by using the law of the corresponding state. The model's prediction has high accuracy in the cases of LiBr and NaBr, while the prediction values for other monovalent bromide salts are slightly over-estimated. For RbBr and KBr, the data from Harada et al. have slightly better agreement with the model compared to the data of Nakazawa et al. Other measurements from McDonald [241], Smirnov [56] and Lucks [95] are considered unreliable. Note that McDonald provided results reasonably close to the model's prediction and other experimental data but showed a slight positive temperature dependence. Further, the present model again shows slight improvements in accuracy over the Gheribi et al. model for CsBr and LiBr. Overall, the model's predictive accuracy is expected to be less than 15% for the monovalent bromide family salt.

Monovalent iodides Figure A.2 shows the predicted thermal conductivity for monovalent iodide salts compared to the experimental values. Once again, the present model shows agreement with existing reliable experimental data. The model shows improved accuracy compared to the Gheribi et al. model for RbI and CsI, and the present prediction has results nearly identical to the experimental data of Nakazawa and Nagasaka [74]. The predicted thermal conductivity of NaI and KI is higher than the experimental data of Nakazawa et al. [74] However, they are in good agreement with the experimental data obtained by Harada [59], similar to the results of KBr. Even though both experimental data sets are considered reliable, the deviation between two reliable data sets can achieve 100% for KI. As a result, we suggest that both experimental data sets should be reconsidered. Additionally, the accuracy of thermodynamic properties of heat capacity, density, and sound velocity should also be reconsidered before making a final assessment of the data's reliability.

4.5.3 Divalent molten salts

Divalent Fluorides Figure A.3 shows the experimental and predicted thermal conductivity for the divalent molten alkaline earth fluorides and chlorides. Unfortunately, no experimental data were found for molten alkaline earth bromides and iodides. For most divalent salts, our model's predictions are nearly the same as those from the Gheribi et al. model, except MgF_2, where our estimations are approximately 25% higher than the previous works prediction. Nevertheless, our present predictions are between the two reliable experimental data sets of Golyshev [93] and Khlebnikov [89]. We expect that the prediction accuracy of the present model is higher than our previous work for all divalent molten salts. The experimental data of Powell et al. [91], Golyshev [93] and Khlebnikov [89] for CaF_2 are considered reliable, and the present model's predictions are in between these three data sets. Conversely, the experimental measurements of Bystrai [96], Filatov [99], Green [242] and Savintsev [53] were considered to be unreliable. With the available data sets of divalent fluorides, the predictive accuracy of present model for this salt family is expected to be under 10%.

Divalent Chlorides There are no reliable experimental measurement data for divalent chlorides. The present model predicts almost the same λ_m and temperature dependence as the Gheribi et al. approach. The sound velocity of $MgCl_2$ was corrected by Gheribi et al. [238]. Therefore, the new thermal conductivity is shown in the figure. The present model's predicted thermal conductivity at the melting temperature is close to that of Bystrai et al. [96] and Green [242]. However, both are considered unreliable. Even through, Singh et al. [243] was considered the value of $MgCl_2$ of Green [242] as reliable data. Filatov et al. [99] employed the coaxial cylinders method to measure the thermal conductivity near the melting point; the data shows a high λ_m and a positive temperature dependence common in many

steady-state measurements. Due to the lack of reliable experimental data, the accuracy of the model could not be assess for the divalent chloride salts.

4.5.4 Complex molten salts

Carbonates Figure A.4 shows the comparison of experimental and predicted thermal conductivity for molten alkali metal carbonates. Only one reliable experimental data set was found for the molten carbonates, from Otsubo et al. [75] using the forced Rayleigh method, considered a reliable technique. All other experimental data are considered unreliable because of their positive temperature dependence [54, 97, 101, 244]. The present model's predictions agree with the reliable experimental data of Otsubo et al. We observe a relative deviation of 20% compared to the thermal conductivity predicted by the Gheribi et al. model. Compared to the reliable experimental data for Li_2CO_3, Na_2CO_3 from Otsubo et al., [75] the present model is within 10% relative deviation and shows accuracy improvement over the Gheribi et al. model. K_2CO_3 shows a higher predicted thermal conductivity than the Gheribi et al. model and the experimental measurements, but is still within the experiment's standard uncertainty. We conclude that the accuracy of the present model is higher than the Gheribi et al. model for molten alkali metal carbonates. We expect the present model's accuracy is approximately 10% for the carbonate salts.

Nitrates and nitrites Figure A.4 shows the predicted values and the experimental thermal conductivity data for molten alkali metal nitrates. The thermal conductivity of molten alkali metal nitrates has been studied extensively relative to other molten salts. The nitrate salts are also predominately used in CSP applications due to their low melting point and chemical stability in air environments. Typically, these applications use a mixture of binary salts referred to as solar salt, which constitutes of 60 wt% $NaNO_3$ and 40 wt% of KNO_3. This mixture is suitable and economical for the heat transfer and thermal energy storage medium for CSP, yet higher order systems that have potentially improved thermal properties are of interest. Due to their favorable properties (low melting point and low corrosion) and high interest, the nitrate salts are less difficult to measure experimentally and have a relatively large amount of experimental studies.

The most reliable experimental data are Omotani [70, 71], Nagasaka [38, 236], Tufeu [47] and Kitade [69] for $LiNO_3$, $NaNO_3$ and KNO_3. The comparisons with the present model's predictions show good agreement with the reliable experimental data reported; moreover, the model predicted the thermal conductivity of the nitrates salt with an accuracy of 10%. However, no reliable data was found for $RbNO_3$ and $CsNO_3$. Gustafsson et al. [103] employed the optical method to measure the nitrates salt, $RbNO_3$ and $CsNO_3$ had temperature dependence for thermal conductivity close to zero, similar to our predictions. Further, the measurements

of other salts by Gustafsson et al. and McDonald et al. were reasonably close compared to other experimental measurements but occasionally showed a positive temperature dependence, as was the case for $NaNO_3$ and KNO_3. Therefore, the $RbNO_3$ measurements were not considered reliable, despite their agreement with the model. Therefore, we suggest that these salts be further studied. The present model predicted lower thermal conductivity values than the experimental measurements of $CsNO_3$. This could be due to a relatively low thermal conductivity, inherently more difficult to measure experimentally than higher thermal conductivity molten salts. White et al., McDonald et al., and Gustafsson et al. reported thermal conductivity values that were higher than the reliable works for the other nitrate salts, and we expect that their results could be higher than the actual thermal conductivity of $CsNO_3$ as well.

Only one reliable experimental data set was found for sodium nitrite in the nitrite salt family, shown in Figure A.5. Our predicted estimations agree with the reliable experimental data, within 5% deviation. Tufeu [47] reported that the error of measurement was approximately 4% for $NaNO_2$. However, as mentioned, it is expected that experimental techniques can be expected to provide an accuracy of less than 5%. Other experimental data shows a positive temperature dependence or higher values are considered as unreliable [49, 50, 50, 55, 64, 76, 78, 83, 84, 102–104, 106–108, 111, 112, 230]. Overall, it is concluded that the prediction accuracy of our model is approximately 10% for the nitrate/nitrite salt family.

Sulfates Figure A.5 shows sodium sulfate's predicted and experimental data. Since Na_2SO_4 is a polymerizing salt, $\boldsymbol{K}$ is assumed to be one instead of the theoretical value of 1.4. The figure shows the predictions assuming both values with notably higher values when 1.4 is assumed. One reference was found in the literature. Creffield [113] applied the coaxial cylinder technique, and their method considered the effects of radiation with platinum-iridium cylinders. However, the measurements were taken with a gap size of 2 mm or larger, considered relatively large for this technique, and may have resulted in convection errors. Their reported correlation also shows an increasing trend with temperature, typical of many other coaxial cylinder measurements. Nonetheless, at the melting point, where the coaxial cylinder technique occasionally provides reliable data, the present model's predicted results agree with Creffield [113]. Given the reported experimental standard uncertainty of 8%, the prediction appears to be reasonable but inconclusive. No significant difference in performance was observed when comparing the present model with the Gheribi et al. model.

Hydroxides Figure A.6 shows the predicted results for some alkali metal hydroxides compared to the experimental data. The hydroxides are also known to be polymerizing salts; therefore, they have $\boldsymbol{K}$ of one. The figure also shows the model's prediction when polymerization is not considered, with notably higher thermal conductivity values. No reliable

experimental data was found for the hydroxide salts. Tye [104] showed a slightly positive temperature dependence for LiOH, with a lower thermal conductivity than the present model's prediction. Lucks [95] applied a steady-state technique, where the thickness of the liquid specimen was variable, using a movable heating plate. The uncertainty was likely less than 25%. The measurements reported a large positive temperature dependence for NaOH but a thermal conductivity relatively close to the model's prediction near the melting temperature. This value is also close to Touloukian et al. [114]. In the case of KOH, a relatively recent thermal conductivity measurement was reported by Wang [115] using a quasi-steady state technique with a reported uncertainty of 1.5%. This measurement is potentially reliable due to the minimization of the radiation effects and consideration of convective losses. The present model's prediction of KOH's thermal conductivity is nearly the same as the measurement reported by Wang at the melting point. Given the limited data, the model's accuracy was not assessed. The model also shows a significant difference compared to the Gheribi et al. model's prediction, predicting a lower thermal conductivity for all hydroxide salts considered. Though no experimental data were considered reliable, the present prediction is generally in better agreement with experiments compared to the previous model. This discrepancy may be due to the K_{emp} value used in the previous model, which is likely less capable considering complex and polymerizing salts.

4.6 Conclusion

Thermal conductivity is one of the most difficult thermophysical properties to be determined experimentally, but accurate knowledge is essential for many advanced energy applications, including TES, CSP, and nuclear energy. Though, significant discrepancies exist between experimental data sets, even for salts with a relatively high amount of experimental thermal conductivity data, such as $NaNO_3$ and KNO_3. Generally, this is caused by the difficulties of measuring high-temperature corrosive fluids. Furthermore, the thermal conductivity of molten salts is also relatively challenging to predict through MD and other computational methods. A reliable database and model of molten salt thermal conductivity would be highly beneficial to aid research and development of advanced energy applications.

This work proposed a theoretical model based on the kinetic theory that predicts the temperature-dependent thermal conductivity for pure molten salts. This model provides a theoretical basis for the thermal conductivity of pure salts, based on the concept of minimum thermal conductivity and the number of anions and cations, without any requirement for empirical fitting on thermal conductivity data. The model only needs density, heat capacity, and sound velocity data as inputs. The notable advantage of the present model is that it is derived from kinetic theory without any empirical fitting parameters, provides more accurate predictions than

the previous model, and can be considered more predictive. In contrast, the previous model from Gheribi et al. assumed a "universal" propagon (phonon) mean free path by introducing an empirical fitting constant, which limits the predictive capability for some families of salts. Moreover, the present model can be extended to a model for predicting the thermal conductivity of simple molten salt mixtures for binary, ternary, and higher orders by taking into account the mass fluctuation of the mixtures, as was done with the previous Gheribi model [44, 61, 133, 238]. The capability of the proposed theoretical model was initially assessed by comparing the model's predictions of thermal conductivity at the melting point and the temperature dependence of thermal conductivity to previous experimental data and the previous Gheribi et al. model for thermal conductivity. After the initial assessment, the predicted thermal conductivity was detailed for salts from the fluoride, chloride, iodide, bromide, carbonate, nitrate/nitrite, sulfate, and hydroxide families. Where available, comparisons were made to experimental data and the previous Gheribi et al. model. Lastly, we recommended a new thermal conductivity database for all these salts with the recommended property values.

The broad initial assessment of the model used two previous experimental studies as the basis for comparison. The experimental works of Nagasaka et al. and Harada et al. are considered reliable and cover the thermal conductivity of 25 different molten salts over 25 and 9 different measurements, respectively. The Bland Altman method compared experimental data and the model's prediction; the model agreed with the experimental measurements with an average deviation of less than 10%. The model also showed agreement with the experimentally determined thermal conductivity temperature dependence, with most predictions falling in or near a 10% relative deviation from the experimental data. Further, the new model showed reasonable agreement with the previously presented Gheribi et al. model, which uses an empirically derived fitting constant, K_{emp}, but showed notable differences for divalent halides and complex salts. This deviation was expected to be caused by the empirical derivation of the previous model in comparison to the new formulation from the concept of minimum thermal conductivity with a proportionality constant depending on the number of anions and cations in the salt. Overall, this broad initial assessment provided confidence in the new theoretical derivation and outlined the potential advantages of predicting the thermal conductivity of complex molten salts.

The model's predictions were compared with available experimental data, including monovalent halides, divalent halides, and complex molten salts. This model showed good agreement and accurate predictions with the most reliable experimental data for both simple and complex molten salts. The model's accuracy was superior to that of the previous Gheribi et al. model when compared to reliable experimental data. However, the model's accuracy was not

formally assessed due to the existing data limitations. We expect that the present model is comparable to or better than the Gheribi et al. model for all salts studied in this work, given the new theoretical derivation of $\boldsymbol{K}$. This is impactful since the present model better captures the influence of structure on the thermal conductivity of complex salts, divalent halides, and polymerizing salts. Many of these molten salts are of interest for emerging energy technologies, including nuclear energy and thermal energy storage. Further, the present model must capture the structural details when extending to molten salt mixtures, given that many mixtures of interest are complex or polymerizing. Detailed information on the structure and coordination of the salt mixtures will also be required to extend the model to these mixtures and capture the role of structure in thermal conductivity.

This work shows that our presented model accurately predicts the thermal conductivity of most pure molten salts given sufficient thermophysical properties. Nonetheless, it should be emphasized that the prediction accuracy depends on the accuracy of these input properties. As such, the formal error propagation of all property values into the model will be required to determine its uncertainty rigorously. Given the general agreement to reliable experimental data, the prediction uncertainties for all salts studied in this work are expected to be comparable to reliable measurement methods. Therefore, this model builds the foundation for a more detailed model of mixtures as well as provide input to molten salt databases used in engineering applications.

4.7 Acknowledgements

This research was supported by funds from the Natural Sciences and Engineering Research Council of Canada (NSERC) [funding reference number: RGPIN-2021-03279]. R.C.G acknowledges the support from The Ohio State University and Dr. Lei R. Cao for his advisory support.

CHAPTER 5 ARTICLE 2: A PREDICTIVE APPROACH FOR THE COMPOSITIONAL AND TEMPERATURE REPRESENTATION OF THERMAL CONDUCTIVITY IN MULTICOMPONENT MOLTEN SALTS SYSTEMS FOR ADVANCED ENERGY APPLICATIONS

Huiqiang Yang, Ryan C. Gallagher, Anh-Thu Phan, Patrice Chartrand, Aïmen E. Gheribi

Published in Materials Today Energy, October 16 2023, volume 38, 101441

My contributions to this article are: Conceptualization, Methodology, Validation, Software, Formal analysis, Investigation, Data curation, Writing – original draft, Visualization.

Abstract: This study presents a theoretical model, based on kinetic theory, for accurately predicting thermal conductivity in molten salt mixtures, a vital factor in designing advanced energy systems such as concentrating solar power, thermal energy storage, and advanced nuclear reactors. Applicable to non-complex, non-reciprocal systems, the model represents thermal conductivity with respect to composition and temperature. We evaluated the model using molecular dynamics simulations on binary systems from fluoride, chloride, bromide, iodide salt families. The model predictions were also compared against existing experimental datasets for those families as well as binary nitrates and carbonates. The model demonstrated an improvement in predictive accuracy over the ideal linear estimation and showed reasonable agreement with the reliable experimental data. Deviations from ideal conductivity, analyzed using the Redlich-Kister method, pointed to the molecular weight and thermal conductivity of individual compounds as primary influencing factors. When applied to predict the thermal conductivity of higher order eutectic salt mixtures relevant to energy applications, the model showed predictive accuracy comparable to empirical methods. The model was further applied to generate compositional mapping to quantify deviations from ideality over the compositional space. This advance enhances new molten salt mixtures evaluation efficiency and extends the model to complex mixtures.

5.1 Introduction

Molten salts (MSs) possess many thermo-physical properties that are well suited for use in advanced green energy technologies, including thermal energy storage (TES), concentrating

solar power (CSP), and molten salt reactors (MSRs) [207, 245–249]. These properties include a wide liquid temperature range, low pressures, high stability, high heat capacity, low viscosity, non-combustibility, and relatively low material costs [201, 214, 250]. For example, MS TES can help mitigate intermittency issues associated with renewable technologies such as wind and photovoltaic solar power by providing dispatchable power during times of high demand or low supply [251, 252]. MS CSP plants with TES have already been commercially demonstrated with nitrate salts [253]. Adopting higher temperature MSs like chloride mixtures could enable improved efficiency gains relative to existing MS CSP systems [13, 254]. MSRs offer potential benefits over traditional reactors, including lower pressures, higher temperatures, higher boiling points, and better radionuclide retention [6, 207, 255]. However, despite the potential advantages of MS energy technologies, collecting thermo-physical properties of new MS mixtures is generally challenging and costly, particularly for thermal conductivity [10, 40, 199, 213, 214] Therefore, the development of property databases and predictive models for MS mixtures is crucial for supporting the design and deployment of these technologies [173, 213, 214].

Accurate knowledge of the thermal conductivity of MSs is critical for the appropriate design and operation of energy systems. However, measurement challenges arise due to their high melting temperature, corrosiveness, and volatility, which can result in chemical interactions and measurement errors [40, 44, 199]. These properties can significantly impact thermal performance, efficiency, and safety of prospective energy systems [27, 256]. Moreover, empirical thermal conductivity data in the literature often feature larger uncertainties, scatter, discrepancies, and knowledge gaps compared to other properties influencing the thermal performance of advanced energy systems [34, 37, 40, 199, 256–258]. The need for accurate thermal conductivity data underscores the importance of developing new methodologies for determining the thermal conductivity of MSs for energy applications.

Numerous experimental methods have been developed to measure the thermal conductivity of MSs. These methods can be classified into steady-state methods and transient methods [40, 42, 44]. The steady-state methods include the coaxial cylinder [47, 50, 55, 56, 90, 92], parallel plate or comparative methods [62,64,259], and variable gap techniques [44,61,66,260]. Many of the data sets from steady-state methods are considered unreliable and show an incorrect temperature dependence of thermal conductivity, $(\partial\lambda/\partial T)_P > 0$ [39, 40, 60, 194, 261]. However, reliable data can be determined with carefully designed systems [40, 44, 47, 48, 61]. On the other hand, the transient state methods, including hot wire, laser flash, and forced Rayleigh scattering, are often recommended as the most reliable [50,65,71,76,80,87,200]. Yet, the transient methods can also be influenced by the effects of thermal radiation, and convection [200,262,263]. These competing heat transfer errors are expected to be the primary cause

of the large discrepancies between thermal conductivity data in the literature [40, 60, 199], making it difficult to rely on empirical data. While numerous measurement methods exist, few have consistently demonstrated reliability across all MS families, and their use for measuring large numbers of mixtures may not be practical.

Strategies like molecular dynamics(MD) or theoretical model predictions have been considered as alternatives to empirical measurement, but have largely been demonstrated for pure salts instead of mixtures [39, 60, 124, 133, 144, 152, 193, 194, 222, 223, 264]. The majority of MSs that are practical for energy applications are multicomponent mixtures. For instance, solar salt (60% $NaNO_3$ - 40% KNO_3 in weight) is used in modern CSP, chloride mixtures have been proposed for advanced CSP [250, 253, 265], and fluoride and chloride mixtures have been proposed for nuclear applications [199, 207, 256, 257, 266]. Yet, compared to the vast amount of possible mixture combinations, data on the thermal conductivity of binary and higher-order MS mixtures are relatively limited in the literature. Much of the existing empirical data also exhibit $(\partial\lambda/\partial T)_P > 0$ [34, 54, 56, 65, 80, 198, 267–269]. As a result, the empirical data of only a few mixtures have been compared to theoretical models and MD predictions [34, 47, 50, 54–56, 61, 65, 71, 75, 76, 80, 83, 86, 106, 133, 198, 200, 200, 222, 238, 267–269, 269–271]. A comprehensive understanding of the compositional and temperature dependence of MS mixtures is crucial for optimal system performance, but predicting their thermal conductivity remains challenging due to the complications of modeling of multiple component systems and the limited reliable validation data.

Early works relied on experimental data to describe the compositional dependence of MS mixtures, with varying success. Bloom et al. [55] measured the thermal conductivity of KNO_3-$NaNO_3$ mixtures summarized that the excess thermal conductivities of binary mixtures were negative and exhibited an increase proportional to the square of the difference between cationic radii, suggesting that the excess thermal conductivity primarily depends on differences in cation radii rather than cation masses. Later, Cornwell proposed that mixture thermal conductivity is influenced by several factors, such as cations/anion masses and the atomic radii, making it lower than values given by the ideal linear model [182]. Given these works, MS mixture thermal conductivity does not appear to be reliably predicted with a simple molar fraction-weighted sum of the pure component's thermal conductivity, often denoted as an ideal linear model.

$$\lambda^{id} = \sum_{i=1}^{n} X_i \, \lambda_i, \tag{5.1}$$

where λ^{id} represents the linear solution of thermal conductivity of salt mixtures, X_i denotes the unary component molar fraction, and λ_i corresponds to the thermal conductivity of each pure MS. Despite the evidence contradicting the reliability of ideal linear models, some later

works opted to apply these models [39, 47, 71, 193].

Smirnov et al. proposed that the thermal conductivity of common anion alkali halides and their mixtures varied inversely with molar volume, which is consistent with other models for pure salts [83, 103, 180, 181, 198]. However, the empirical data sets from Smirnov et al. were suggested to be unreliable, due to the substantial increase in thermal conductivity with temperature [40,44,199,200]. Given that heat losses are less significant at lower temperatures, the results of Smirnov et al. occasionally agree with reliable data near the melting point [264]. Several later works also implemented a molar volume dependence in predictive models for mixtures [39, 152, 193, 238].

Building on the empirical data, several works have attempted to develop theory-based thermal conductivity models of MS mixtures, such as the rough hard sphere model, unit cell models, and kinetic theory models. DiGuilio and Teja [39] developed a model for the thermal conductivity of pure MSs based on the rough hard-sphere theory of Li et al. [189], and applied it on mixtures of salts with a common anions using the ideal linear model. However, the experimental data of the mixtures considered in the study was generally not the same as in the ideal linear mixtures $\lambda^{Exp} \neq \lambda^{id}$, and the model is likely unreliable for all mixtures [50, 194]. Zhao et al. [194] developed a theoretical unit cell model to predict the thermal conductivity of binary MSs, where the thermal conductivity of a binary mixture would not be a linear function of each component's mole fraction. However, the pure MS's empirical data sets used in the study were considered unreliable, and it is challenging to verify the predictive capability of this binary mixture model. Muhmood et al. [195] extended the unit cell concept developed by Zhao et al. to ternary salt mixtures showing a negative temperature dependence of thermal conductivity. However, like the rough hard sphere models, the predictive reliability of the unit cell models on salt mixtures is still uncertain and must be validated on other systems.

Gheribi and Chartrand [133] presented a theoretical framework to predict the thermal transport properties of MS mixtures as a function of composition and temperature, based on prior work on a theoretical model of thermal conductivity for pure salts [60]. The model (Gheribi model) was derived from classical kinetic theory and demonstrated to be reliable for many pure MS compounds. Later the model was extended to mixtures [133, 238]. The model's predicted thermal conductivity of LiF-NaF-KF and LiCl-NaCl-KCl mixtures were compared with MD simulations and experimental data [61,133], showing that the thermal conductivity of MS mixtures was not a simple linear function of the pure components' mole fractions, agreeing with the theoretical model. However, the theoretical model included a constant derived from solid solutions, $\epsilon^{'}$, which was assumed to be "universal" for all ionic systems considered. This limits the model's reliability when predicting different MS mixtures, partic-

ularly in the case where large differences in the molar masses of cations exist, or in the case of complex salts.

Due to the difficulties and existing data discrepancies corresponding to experimental methods, computational simulations have been relied upon to determine the thermophysical properties of liquids, offering a cost-effective alternative [218–221]. Multiple works have successfully demonstrated that the thermal conductivity of pure MSs can be predicted accurately using kinetic theory-based models or MD simulations [39, 60, 124, 133, 144, 152, 193, 194, 222, 223]. Moreover, MD has been used to simulate the properties of MS mixtures, particularly for investigating multicomponent complexes in MS mixtures [147, 222, 238, 272, 273]. Despite the larger predicted thermal conductivity sometimes obtained by MD simulations, relative to the reliable experimental data, the compositional trend of the thermal conductivity predicted for mixtures provides a reasonable basis for comparison when evaluating the performance of theoretical models, such as the Gheribi model. As such, MD can allow for a preliminary understanding of the salt mixture's relative behavior with composition, but may not be reliable when predicting the magnitude of the mixture's thermal conductivity [120, 152].

In our previous work, we proposed a theoretical model for predicting the temperature-dependent thermal conductivity of pure MSs. The model modified the Gheribi kinetic theory model, by incorporating the concept of minimum thermal conductivity, which is often applied when predicting bulk non-metallic glasses [234]. The model proposed a proportionality constant equal to the ratio of the number of cations to anions in each salt and, therefore, does not require the universal constant used by Gheribi's original model. The predictions were compared to the reliable experimental data sets for halide, divalent halide, carbonates, nitrate, nitrite, sulfate, and hydroxide MSs, showing predictive accuracy comparable to the uncertainty of reliable empirical data, with an average predicted error of 10% or less for the compounds studied [264]. We propose that this model could be extended to predict the thermal conductivity of MS mixtures, in accordance with the original Gheribi model [61, 133, 238].

In this study, we introduce a new model that predicts the thermal conductivity of simple MS mixtures, not complex, polymerizing, or reciprocal, as a function of composition and temperature. We used equilibrium MD simulations for binary fluorides, chlorides, bromides, and iodides to validate the model's ability to capture the compositional dependence of thermal conductivity. For binary nitrate and carbonate systems, the model's predictions were compared against empirical data. The Redlich-Kister method was applied to quantify deviations from ideality in the binary salt systems. Furthermore, the model's predictions were applied to several higher-order MS mixtures relevant to advanced energy applications and contrasted with empirical data. Compositional mappings were also applied to identify the regions where the mixture deviated most significantly from ideality. By advancing the capability to accu-

rately predict the thermal conductivity of simple MS mixtures, this study holds the potential to expedite the evaluation of new mixtures for energy systems. It also lays the groundwork for future exploration into more complex mixtures.

5.2 Kinetic theory modeling for the molten salt mixture as a function of temperature and composition

The concept of minimum thermal conductivity is widely applied to characterize thermal transport in amorphous solids, like non-metallic glasses [234]. In the phonon-gas model for solids, phonons (collective vibrations) are treated as classical particles responsible for heat transport. However, amorphous materials lack the long-range ordering, heat is carried through harmonic couplings between non-correlated and delocalized atomic vibrations, referred to as "diffusons" [274]. This concept is also expected to be applicable to liquids like MSs given their local short-range ordering, but absence of long-range crystal ordering. By applying the Debye approximation of lattice vibration, Cahill et al. demonstrated that the minimum thermal conductivity in the canonical statistical ensemble (NVT) can be expressed as [234]:

$$\lambda_{min}^{NVT}(T) = (\frac{\pi}{6})^{1/3}\ k_B n_d^{2/3} \sum_i c_i (\frac{T}{\Theta_D^i})^3 \int_0^{\Theta_D^i/T} \frac{x^3 e^x}{(e^x-1)^2} dx, \tag{5.2}$$

where $n_d = (n_a N_A)/V$, c_i, and Θ_D^i represent the number density of atoms, the velocity of sound, and the Debye temperature for the three acoustic modes (two transversal and one longitudinal), $\Theta_D^i = c_i(\hbar/k_B)(6\pi n)^{1/3}$, respectively. At low temperatures, the minimum thermal conductivity model precisely exhibits the temperature-dependent behavior of non-metallic amorphous materials. However, it attains a plateau at high temperatures ($\geq \Theta_D^i$). By employing the Legendre transformation from the NVT (canonical) ensemble to the NPT (isobaric-isothermal) ensemble, the expression for the temperature-dependent thermal conductivity can be obtained:

$$\lambda_{min}^{NPT} = \lambda_{min}^{NVT} \left[1 - \alpha_0(\gamma_0 + \frac{1}{3})(T - T_0)\right], \tag{5.3}$$

where the α_0 and γ_0 are the thermal expansion coefficient, the Grüneisen parameter at temperature T_0. After applying this concept to MS, as demonstrated in recent works [152], the predicted temperature-dependent thermal conductivity for pure MSs is expressed.:

$$\lambda_{ms}(T) = \boldsymbol{K}\ \lambda_{min} \left[1 - \alpha_m \left(\gamma_m + \frac{1}{3}\right)(T - T_m)\right] \tag{5.4}$$

The minimum thermal conductivity at a specific melting temperature is [235]: $\lambda_{min} =$

$k_B\ (n_{liq})^{2/3}\langle c_s\rangle_{liq}$, where N_A, n_d, and c_s are the Avogadro constant, number density of atoms, and speed of sound at the melting temperature T_m of salts. $\boldsymbol{K}$ is a material constant, that refers to the degree of complexity of the chemical nature (location structure) for MSs which was established in our previous study [264], it can be represented as:

$$\boldsymbol{K} = 1 + \frac{n_s^+}{n_s^-}, \tag{5.5}$$

n_s^+ and n_s^- respectively denote the number of species involved in cationic and anionic complexes, with $n = 1$ corresponding to the case of free species. The ratio n_s^+/n_s^- represents the degree complexity of the local ordering within MSs. For instance, $\boldsymbol{K}$ =2 for LiF, NaCl, KBr, and $\boldsymbol{K}$ =1.5 for alkali carbonates Li_2CO_3, Na_2CO_3, and $\boldsymbol{K}$ =1.25 for the nitrates of $LiNO_3$. As the degree of complexity in MS increases, $\boldsymbol{K}\rightarrow 1$, which is the case for polymerizing MSs like BeF_2.

The ions in MSs act as scattering centers for phonons. In the case of mixed ions, there is a reduction of the mean free path of the phonons and the lattice thermal conductivity. This is due to the differences in atomic masses, cationic sizes, and neighbor coupling forces between the solute and solvent cations [133]. Ionic liquids share some similarities with solid solutions, where the disorder scattering parameter Γ describes the reduction of thermal conductivity when forming solutions. In the solid solutions, Abeles [275] showed that both the mass fluctuation term Γ_M and elastic strain field fluctuation term Γ_s contribute to the disorder scattering parameter [275–277]. However, only the mass fluctuation term is considered to be present in the disorder scattering parameter for liquid solutions. The disorder effect of the short-range quasi-crystalline lattice of the MS is induced by a mass fluctuation term g_{mass}. The thermal conductivity of any MS mixtures can be expressed as [133]:

$$\lambda(\underline{X}, T) = \lambda^k(\underline{X}, T)\left[1 - \delta_M^{\lambda}(\underline{X}, T)\right] \tag{5.6}$$

Where $\underline{X} = (X_1, X_2 ... X_n)$ represent the composition vector. λ^k is the kinetic thermal conductivity of MS mixtures that in supposing no local fluctuation of kinetic energy induced by the mass difference between host and solute ions. The expression of thermal conductivity of MS mixture derived from kinetic energy at a given temperature T is represented as:

$$\lambda^k(\underline{X}, T) = \boldsymbol{K}(\underline{X})\ k_B\ n_{liq}^{2/3}(\underline{X}, T_0)\ \langle c_s\rangle_{liq}(\underline{X}, T_0)\left[1 - \alpha(\underline{X}, T_0)\left(\gamma(\underline{X}, T_0) + \frac{1}{3}\right)(T - T_0)\right] \tag{5.7}$$

In which the material constant $\boldsymbol{K} = \sum_i X_i \boldsymbol{K_i}$, the molar volume ($V_m = M/\rho$), the thermal expansion with volume fraction ($\Phi_i = X_i V_i / \sum_i X_i V_i$), and the isothermal compressibility

($\chi = 1/(c_s^2\rho)$ are assuming to be ideal linear variation to the composition. δ_M^{λ} is the local fluctuation of kinetic energy effect upon the thermal transport. It was presented in the previous work [152, 238], can be expressed as:

$$\delta_M^{\lambda} = h_{diff}(\underline{X}, T)\ g_{mass}(\underline{X}) \tag{5.8}$$

The mass fluctuation parameter g_{mass} is defined by [275]:

$$g_{mass} = \sum_{i=1}^{N} X_i \left(1 - \frac{M_i}{\overline{M}(\underline{X})}\right)^2 \tag{5.9}$$

where $\overline{M} = \sum_i X_i\ M_i$ is the molecular weight of the MS mixtures, which also has a linear variation to the composition. And h_{diff} is the damping factor of heat carriers (diffusons), describes the attenuation of local kinetic energy fluctuation effects on the mean free path. It was derived from the kinetic theory in the prior work [152, 278], expressed as:

$$h_{diff} = \mu\ \frac{\lambda_{\sigma}(\underline{X}, T)}{k_B\ \langle c_s \rangle_{liq}(\underline{X}, T)\ n_{liq}^{2/3}(\underline{X}, T)}, \tag{5.10}$$

where μ is an adjusted constant that is approximately 1/2, it was demonstrated that h_{diff} is proportional constant between the mean free path and the average inter-ionic distance in our previous work [152], and eventually equivalent to a ratio of thermal conductivity. λ_{σ} is the effective thermal conductivity of the mixtures, assuming the mean free path of heat carriers equals to the average inter-ionic distance. The accuracy of prediction can be constrained due to the difficulty in calculating h_{diff} in compositional dependence, particularly for high order systems. Nevertheless, when $\boldsymbol{K} = 2$, and $\mu = 1/2$ in simple MS mixtures, h_{diff} is approximately equivalent to the ratio of λ_i/λ^{id}, where $\lambda^{id} = \sum_i X_i\lambda_i$ is the ideal linear behaviour of thermal conductivity of the mixtures. In summary, it can be assumed that the thermal conductivity of MS mixtures is directly proportional to the local fluctuation of kinetic energy. Where the quadratic terms (X_iX_j) have a negligible impact on this local fluctuation, therefore they can be confidently ignored in such instances. The proposed approach to the thermal conductivity of simple MS mixtures can be expressed as follow:

$$\lambda(\underline{X}, T) \simeq \lambda^k(\underline{X}, T) \left[1 - \sum_{i=1}^{N} \left(\frac{\lambda_i}{\lambda^{id}}\right) X_i \left(1 - \frac{M_i}{\overline{M}(\underline{X})}\right)^2\right] \tag{5.11}$$

The present model demonstrates excellent predictive capabilities with high accuracy for sim-

ple MS mixtures concerning their compositional and temperature dependence. Notably, no empirical fitting is necessary for these predictions. Only a few thermophysical properties, such as density, heat capacity, thermal expansion, and sound velocity, are required for pure MSs, and these can be obtained from the literature or precisely estimated. The compositional dependence of the parameters in the mixtures is estimated by applying an ideal linear behavior rule that takes advantage of leveraging the linear relationship between Gibbs energy and the pressure-temperature dependence. The model is expected to be extendable to include reciprocal and complex MS mixtures, which hold significant importance for energy applications.

Lastly, it is essential to address significant remarks regarding the microscopic origins of thermal transport in mixtures. It is well known that the movement of ions within ionic systems can significantly influence thermal conductivity [279–281]. However, in the proposed formalism, the compositional dependent thermal conductivity is described only through local fluctuations in kinetic energy. From a microscopic perspective, thermal transport in MS arises from fluctuations in energy current, charge current, and the interplay between energy and charge current fluctuations, as detailed in the Green-Kubo formalism (see Appendix B).

In Figure B.7, we present the results of MD simulations for NaCl-KCl as a function of composition at 1300 [K], directly comparing with predictions from our current model. The predicted results are in agreement with the MD results (λ_{GK}). Notably, two distinct flux tendenies are depicted: the energy flux (L_{ee}/T^2) and the thermo-electrical flux ($-A/BT^2$, A and B corresponds to the matrix determinants in Eq. B.5). In a ionic liquid, the thermal conductivity is the result of the combined contributions of these two fluxes. Thus, the obtained thermal conductivity of NaCl-KCl MS mixture exhibits an approximately linear trend in relation with compositional dependence. From a fundamental standpoint, both of these contributions are related to the local fluctuations of kinetic energy, which our current theoretical model is built upon. In other words, these fluctuations are directly attributed to variations in local velocity, thereby influencing both the local energy current and the local movement of ions (self-diffusion).

5.3 Model evaluation methodology

In a previous work [264], the reliability of pure MS thermal conductivity was reviewed. Figure 5.1 illustrates these two features on the available experimental data of thermal conductivity for LiF and NaCl. Across the available empirical datasets, there is a maximum deviation between data sets of more than 100% and 170% for LiF and NaCl, respectively, which are several times larger than the reported errors from experimental measurement. Moreover, these data sets showed disagreement on the temperature dependency. In accordance with

most findings in the literature [39, 40, 61, 199], the works of Nagasaka et al. and Harada et al. were considered to be the most reliable sources of empirical data. The mean relative error of the developed pure MS thermal conductivity model to reliable data sets was below 10%. As shown in the figure, the developed pure MS thermal conductivity model agrees with the reliable experimental data sets for LiF and NaCl. Given this agreement, these reliable end-member thermal conductivity empirical data for the initial comparison of the present MD simulations and the predictions using the present model for systems without reliable experimental data. These initial comparisons also verified that the present model for mixtures still provides reliable predictions for pure salts.

There are relatively few experimental data sets on the MS mixture's thermal conductivity and even less data covering the entire range of the compositions for the mixtures. Therefore, we employed a combined methodology to test the proposed thermal conductivity model's capability of predicting compositional behavior, comparing the present model to the MD simulated results for systems that did not have empirical data on mixtures in the literature, for example, the binary fluoride, chloride, bromide, and iodide salts. Details on the MD simulations performed are described in B.1. Smirnov et al. [56] reported on some salt mixtures, but all of these data sets were considered unreliable [40]. For the binary nitrates and carbonate mixtures, there were some empirical data sets available for comparison, in these cases the MD models were not applied.

Following the evaluation of the present model on the binary systems in comparison to the MD

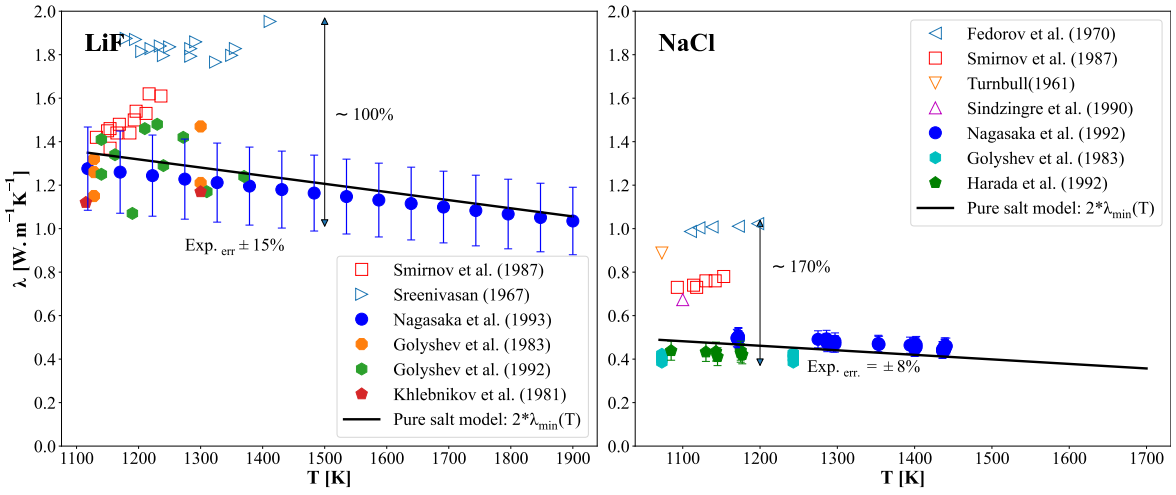

Figure 5.1 Predicted (solid line) thermal conductivity has a function of temperature in comparison with various reliable (solid symbols-Nagasaka et al. [87,94], Harada et al. [59],) and Golyshev et al. [92, 93], and nonreliable (open symbols - Sreenivasan [88] and Smirnov et al. [56], Fedorov et al. [51], Turnbull et al. [83] and Sindzingre et al. [98]) experimental data sets for MS LiF and NaCl.

and empirical data sets, the compositional dependence of thermal conductivity was estimated for additional systems. The principle purpose of this analysis was to consider the deviation from the linear model, which is often applied to predict mixtures and to quantify the influence of the pure compound molecular weight and thermal conductivity. A Redlich-Kister approach was used to estimate the deviation from linearity and support general trends that should be considered when estimating the thermal conductivity of simple salt mixtures.
Finally, several simple higher-order salts with empirical data were predicted using the present model to further test its predictive capability. Eutectic mixtures are of high interest due to their relatively low melting points, and much of the empirical thermal conductivity data for mixtures is provided for discrete mixtures, for example eutectic (46.5-11.5-42.0 mol% composition) LiF-NaF-KF. This also allowed for a comparison to the mixture's temperature dependence of thermal conductivity. For these mixtures, compositional mappings of thermal conductivity are also presented to predict the deviation from the linear ideal model.

5.4 Results and discussion

5.4.1 Prediction of thermal conductivity

Compositional dependence of binary salt mixtures

The predictions of the present model have been compared to all available experimental data sets of the thermal conductivity for simple binary mixtures that are available in the literature, as well as the results from MD simulations [39, 40, 61, 199]. As mentioned in the last section, simple MSs are those fully dissociated ions. For instance, the monovalent of fluorides, chlorides, bromides, and iodides. On the other hand, KCl-$MgCl_2$ system is a complex salt mixture, the population of Mg-Cl polymer increases with the increasing of faction $MgCl_2$ in the mixture [282]. The system LiF-BeF_2 is similar, where BeF_2 forms the polymers of $Be_2F_7^{3-}$, $Be_3F_{10}^{4-}$, $Be_4F_{13}^{5-}$, etc [160]. In the present work, only simple mixtures are considered.
Flourides Fluoride salt mixtures have significant interest in many advanced energy applications [214,283,284]. However, it is more challenging to determine the thermal conductivity using experimental methods techniques compared to other anionic salt mixtures [94]. For the fluoride salts considered here, MD simulations were used for comparison to the present model's predicted compositional dependence of thermal conductivity. Figure 5.2 shows the thermal conductivity predictions as a function of composition at 1300 [K] for three binary fluoride systems in comparison with MD simulations (left side), LiF-NaF, LiF-KF, and NaF-KF, using the present model. The two end-member thermal conductivities are using the corresponding MD simulation results. This allows us to validate the current model, and to gain insight into the variations in the thermal conductivity due to the mass fluctuations. The

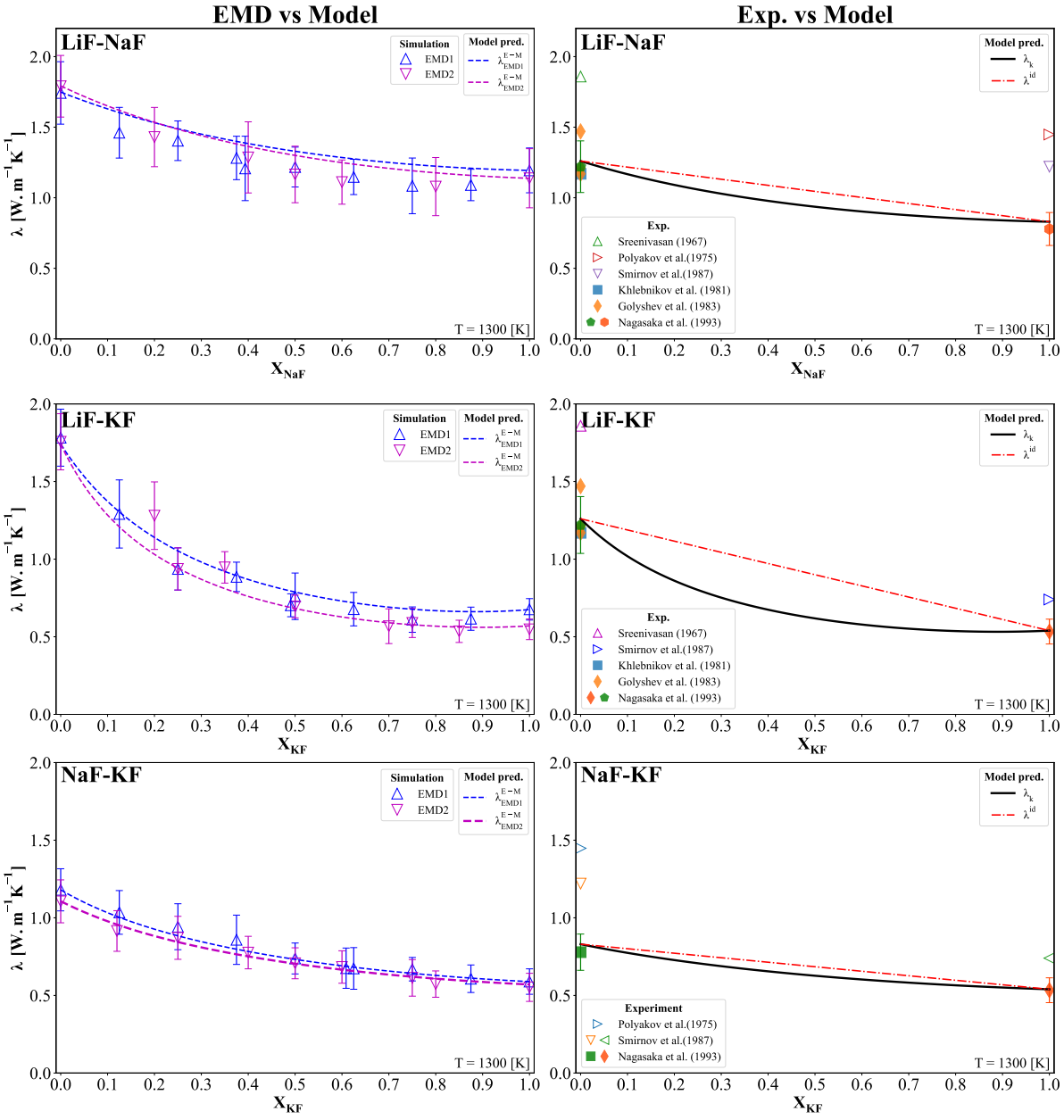

Figure 5.2 Predicted (solid line and dashed lines) thermal conductivity as a function of the composition of binary fluoride systems in comparison with ideal linear mixture(dot-dashed line), MD simulations, reliable (solid symbols) [92, 94, 267], and unreliable (open symbols) [56, 88, 90] experimental data sets.

reliable and unreliable experimental data sets near 1300 [K] for pure MS are also illustrated in the figures (right side). Despite the larger thermal conductivity of LiF and NaF predicted by MD simulations, the compositional behavior of the thermal conductivity for MS mixtures shows reasonable agreement over much of the compositional space for these mixtures.

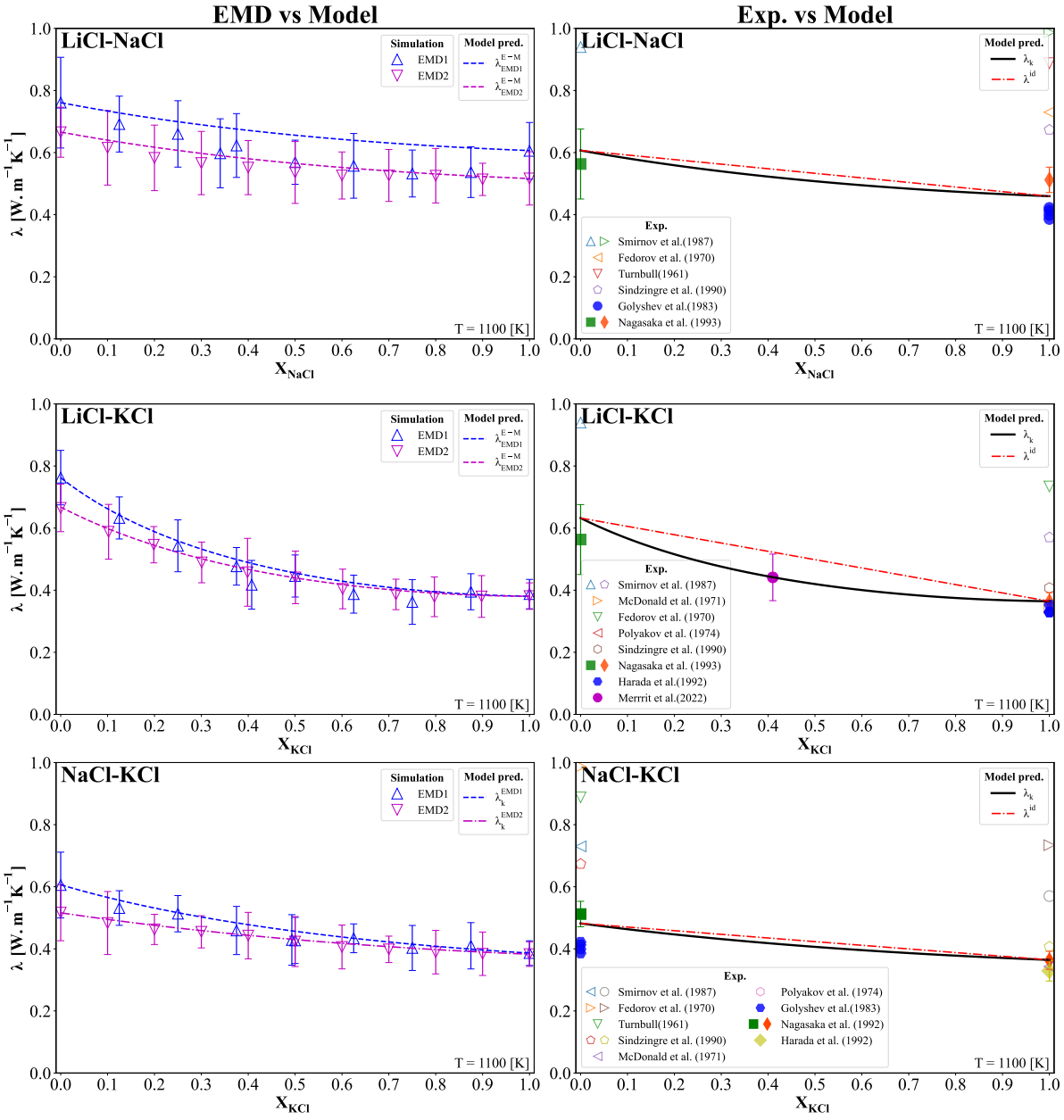

Figure 5.3 Predicted (solid line and dashed lines) thermal conductivity as a function of the composition of binary chloride systems in comparison with ideal linear mixture(dot-dashed line), MD simulations, reliable (solid symbols) [59, 87, 92, 200], and unreliable (open symbols) [50, 51, 56, 83, 90, 98] experimental data sets.

Two MD simulations of binary fluoride mixtures are shown in the figure (open markers). EMD1 was performed by the present work, while EMD2 utilized Ishii's [147] potential for the simulation. We observe that the results for these binary systems are very close to each other. In the figures on the left side, the dashed lines represent the predicted results using

the present model, but with the two end-member conductivity values taken from the MD simulation results. This allowed for a direct comparison of the compositional trends predicted by the model and by MD simulations. The two MD simulations have the error range of $\pm 15 - 30\%$. The results show that the compositional trends captured by the present model agree with those predicted by MD. On the right side in the figures, the predicted results from the present model by using the pure salt results of the previous work are shown by the solid black line, for the binary systems considered, whereas the red dot-dashed line represents the thermal conductivity of the ideal linear mixture. The predictions from the present model, not using the MD simulated end member conductivities, generally agree with MD simulation results for the KF-rich mixtures of LiF-KF and NaF-KF, but show more significant deviations for higher concentrations LiF and NaF, due to the MD simulations predicting higher end member conductivity, particularly LiF. However, it is noted that the deviations from linearity are qualitatively similar to the deviations predicted by MD.

There is a tendency toward a linear relationship between the thermal conductivity and the composition predicted for the LiF-NaF and NaF-KF systems. On the other hand, the present model's prediction of the LiF-KF system shows a more significant deviation from the ideal linear model's predicted thermal conductivity due to the larger difference in mass between the two constituents, a relationship that is also observed in the other systems considered in the present work. Further discussion regarding the deviations from linearity is provided in the following section. Additionally, we see that the thermal conductivity is nearly constant when the majority of the mixture consists of the higher molecular weight constituent (KF), but increases significantly as molar fraction approaches higher concentrations of the lower molecular weight component.

The present model's predictions agree well with Nagasaka's estimate for the pure salts, proving that the current model still holds for pure compounds. For the binary fluoride mixtures considered here, no reliable empirical data was available. The predicted results were also compared with the only available empirical data for these mixtures, reported by Smirnov et al. [56] and the results are shown in Figure B.1 in the Appendix. However, the empirical data was considered unreliable.

Chlorides Chloride salts are one of the most attractive HTF/TES materials for next-generation CSP plants because of their low costs, higher, and wider working temperature ranges [12–14, 16]. Figure 5.3 illustrates the thermal conductivity of three binary chloride systems in comparison to the MD simulations (left side), LiCl-NaCl, LiCl-KCl, and NaCl-KCl, as a function of composition at 1100 [K]. There was no reliable empirical thermal conductivity data that could be used to validate the predicted thermal conductivity for these

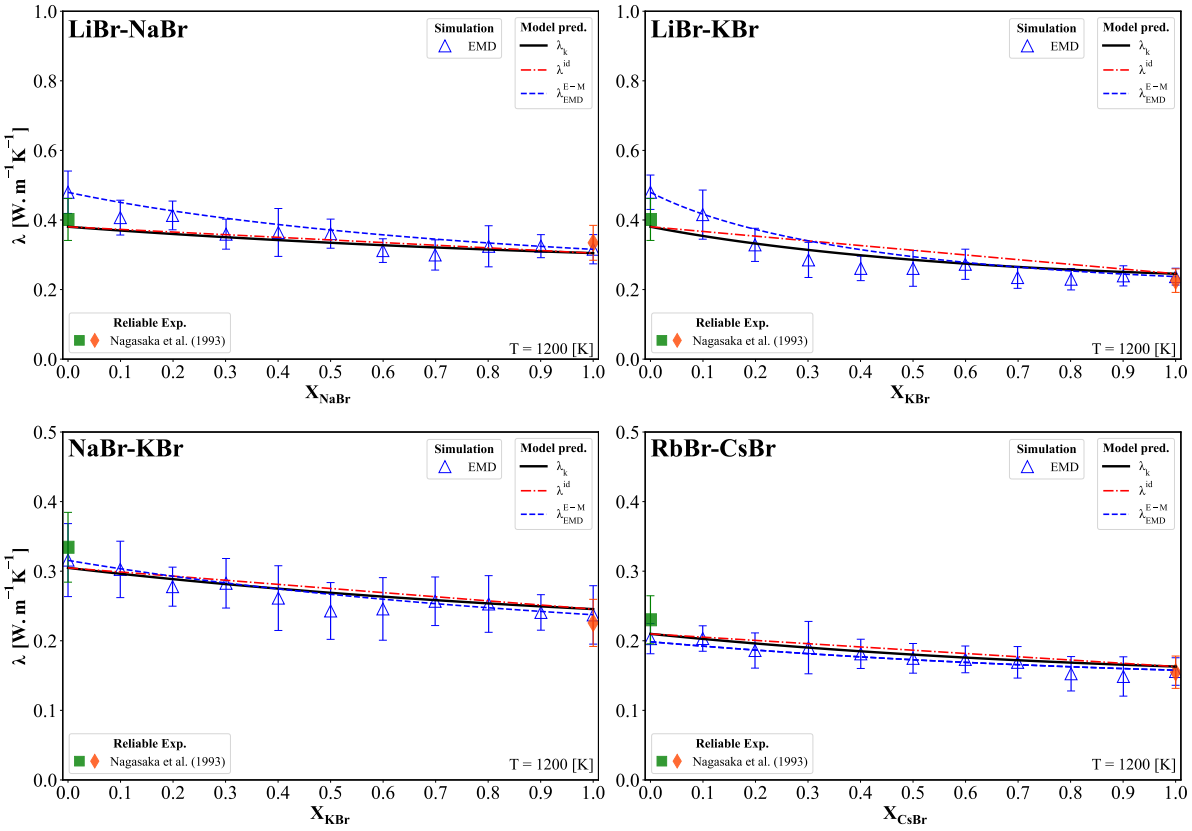

Figure 5.4 Predicted (solid line and dashed lines) thermal conductivity as a function of the composition of binary bromide and binary iodide systems in comparison with ideal linear mixture(dot-dashed line), MD simulations, reliable (solid symbols) [73] experimental data sets.

mixtures, aside from one mixture of LiCl-KCl from Merritt et al. [200]. Therefore, MD simulations were used for comparison. In addition, the reliable experimental data sets for pure MS are also illustrated in the same figures (right side).

The results show that the model using MD predicted end-member conductivity agrees with the compositional trends predicted by MD simulations. The results of the MD simulation's thermal conductivity also show lower relative deviations from the reliable experimental data sets for the pure chloride salts than the pure fluoride salts. The Li rich salts also show the largest relative deviation from the reliable data. The error in the MD simulation ranged from $\pm 15 - 30\%$ and the present model's predicted results for these chloride binary systems are within the error bounds of the MD simulated results for all the systems considered here.

The LiCl-NaCl and NaCl-KCl systems show a nearly linear relationship between the composition and thermal conductivity. The LiCl-KCl system shows more significant deviations from the linear behavior for Li rich mixtures, which is consistent with the behavior of the LiF-KF system. Moreover, the binary chloride systems show smaller deviations from linear

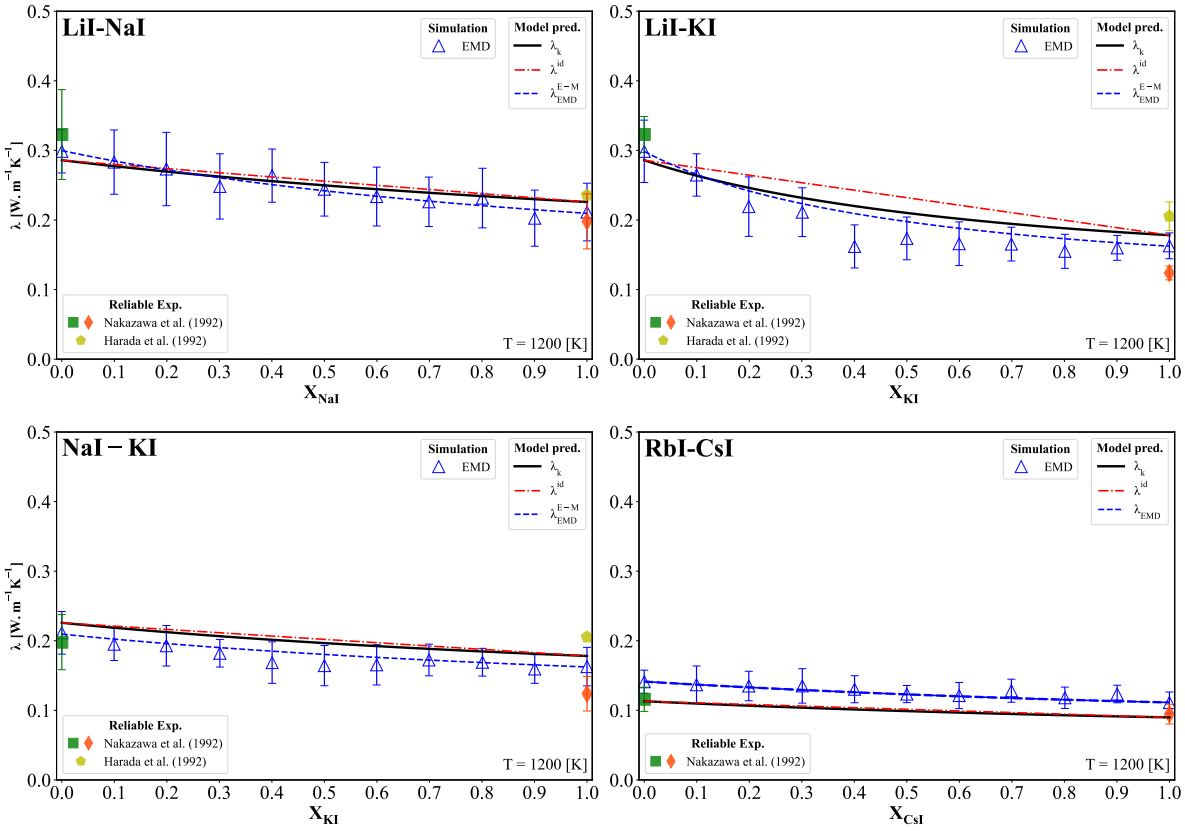

Figure 5.5 Predicted (solid line and dashed lines) thermal conductivity as a function of the composition of binary bromide and binary iodide systems in comparison with ideal linear mixture(dot-dashed line), MD simulations, reliable (solid symbols) [59,74] experimental data sets.

behavior than binary fluoride systems for the same cation mixtures. This is due to the lower mass ratio of M_i/M as the molar mass of the anion grows, causing smaller deviations in the thermal conductivity along the compositions, a trend that persists in the other salt families considered here.

The present model's predictions agree with the empirical data for the pure salts. Binary chloride mixtures with empirical data found in the literature were NaCl-CsCl and LiCl-KCl. NaCl-CsCl is shown in Figure B.1 in the Appendix, which was reported by Smirnov et al. Apart from the significantly larger magnitude of thermal conductivity values for both pure NaCl and CsCl, we observed that the trend of thermal conductivity as a function of composition was in agreement with our prediction. However, as stated already, the data from Smirnov et al. is likely unreliable. The LiCl-KCl data from Merritt et al., however, shows strong agreement with the present model [200].

Bromides Figure 5.4 shows the thermal conductivity predictions of four binary bromide

systems using the present model, LiBr-NaBr, LiBr-KBr, NaBr-KBr, and RbBr-CsBr, as a function of composition at 1200 [K]. Both the predicted results and MD simulations show nearly linear behavior of thermal conductivity with composition for all the systems considered, aside from LiBr-KBr. The nearly linear thermal conductivity predicted by the present model is primarily due to the larger anionic molar mass(lower M_i/M), compared to F^- and Cl^-. The LiBr-KBr also shows the largest deviation from the ideal model, caused by the larger relative difference in the compound molar masses. Meanwhile, the present model's predictions are also in agreement with the reliable experimental for the pure MSs. Only the NaBr-CsBr system has been found in the literature, which is reported by Smirnov et al. [56]. Figure B.1 shows the comparisons of the predicted results to the experimental data.

Iodides Figure 5.5 shows the thermal conductivity of four binary iodide systems, LiI-NaI, LiI-KI, NaI-KI, and RbI-CsI, as a function of composition, in comparison with MD simulations. Both the predicted results and MD simulations show a nearly linear behavior of thermal conductivity with composition for all systems considered, aside from LiI-KI. The predicted results of the thermal conductivity by the present model are also in agreement with MD simulations, with larger deviations occurring for the thermal conductivity of LiI-KI mixtures. Regarding the comparison to empirical data, the present model's predicted thermal conductivity for pure salt KI is in between the empirical data of Nakazawa et al., and Harada et al. [59, 74]. In a prior assessment, it was suggested that the data by Harada, which shows slightly better agreement with the present model seemed more realistic than that of Nakazawa et al. [74]. Only empirical data on the NaI-CsI system has been found in the literature, which is reported by Smirnov et al. [56]. Figure B.1 shows the comparisons of the predicted results to the experimental data sets.

Nitrates For advanced energy systems, nitrate salts are of great interest, Today, all commercial CSP facilities employ nitrate-based MS mixtures as TES medium and the secondary MS loop of next-generation MS nuclear reactors. Nitrate mixtures also have more empirical data available in the literature, relative to the fluorides, chlorides, iodide, and bromide mixtures. Therefore, the present model was compared to existing empirical data. Figure 5.6 shows the thermal conductivity predictions as a function of composition for six binary nitrate salt systems using the present model compared to the available experimental data sets.
The systems $LiNO_3$ - $NaNO_3$ and $NaNO_3$ - KNO_3 both had reliable data [47, 70, 71]. Both systems showed a linear behavior. As such, Omotani et al. [70,71] considered both systems to be linearly dependent on the composition. The present model's predictions agree with these reliable data sets and show that the ideal linear model is adequate for predicting the thermal

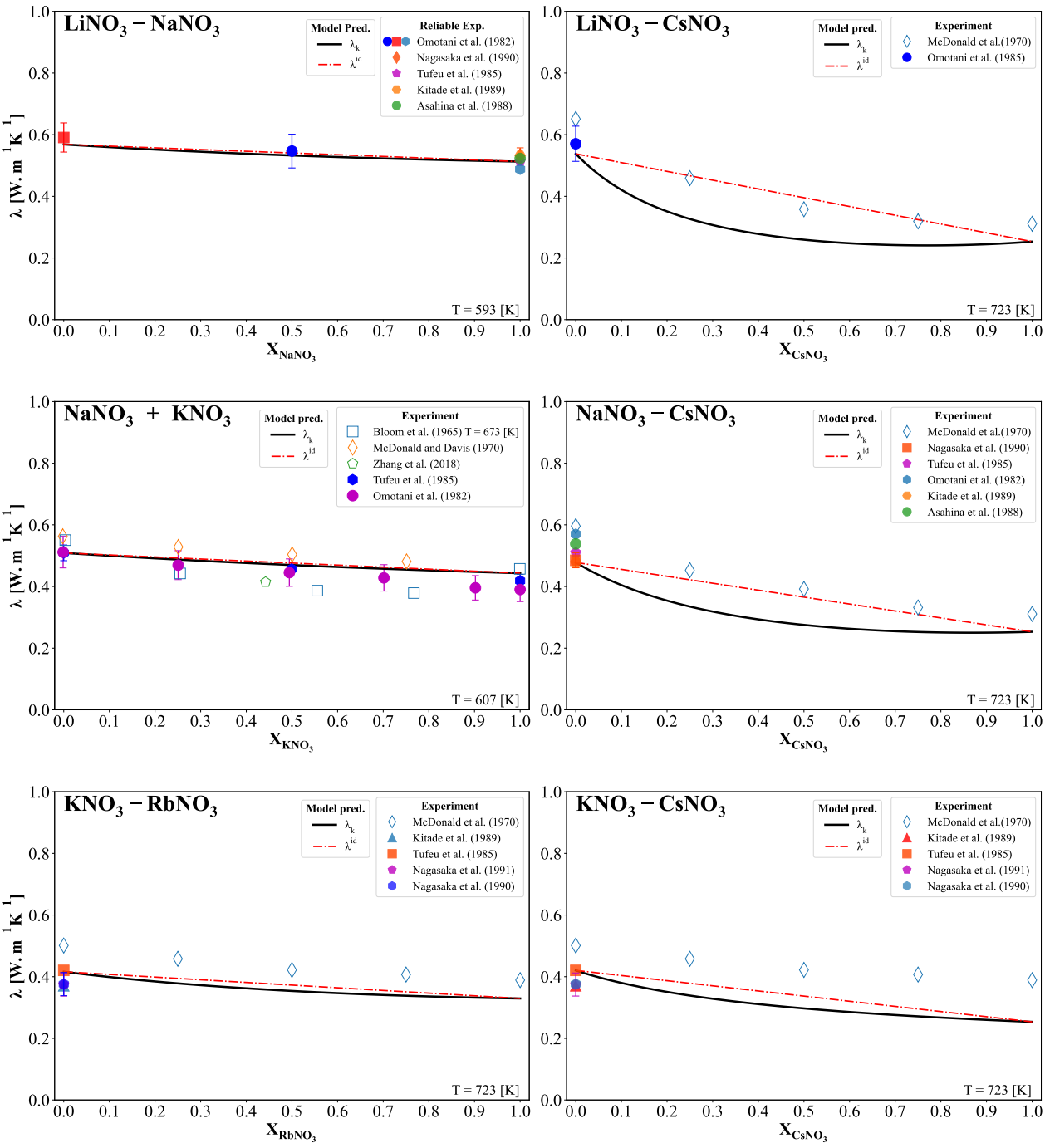

Figure 5.6 Predicted (solid line) thermal conductivity as a function of the composition of binary nitrate systems in comparison with reliable (solid symbols), unreliable (open symbols) experimental data sets.

conductivity of these particular mixtures. However, the results show that the other three nitrate systems considered have a tendency for significant deviation from ideality. Consistent with the other systems, the mixtures with larger molecular weight differences and differences

in pure salt conductivity, like the $LiNO_3$-$CsNO_3$ system, show the greatest deviations from the linear rule solution.
McDonald et al. [50] used a concentric cylinder apparatus to determine the thermal conductivity of pure and mixed molten nitrate salts at 723 [K]. The empirical compositional dependence of thermal conductivity for the mixtures agrees with the predictions of the present model, aside from the $LiNO_3$-$CsNO_3$ and $NaNO_3$-$CsNO_3$ systems, where deviations from linearity occur. However, those data were considered unreliable due to the larger values obtained and slight positive temperature dependency, so these systems may require additional studies.

Carbonates Molten carbonates are considered also one of the most promising TES/HTF mediums for advanced energy applications [285–288]. Figure 5.7 shows the thermal conductivity predictions of Li_2CO_3-Na_2CO_3 and Li_2CO_3-K_2CO_3 by the present model in comparison with experimental datasets. Two compositions (50%:50% and 47%:53%) have been experimentally determined for the binary system Li_2CO_3-Na_2CO_3, and our predictions are in agreement with the works reported by Fuji and his colleagues (Zhang and Fuji [106] and Wicaksonno et al. [271]) at 1000 [K]. The works presented by Otsubo et al. [75] for the pure Li_2CO_3 and Na_2CO_3 were considered reliable data. Yet, their experimental result of the thermal conductivity for the mixture 50% Li_2CO_3-50% Na_2CO_3 was significantly lower than other works, which could be due to the errors of the experimental measurements.
In the case of Li_2CO_3-K_2CO_3, because of the mass difference between Li^+ and K^+ cations, it shows larger deviations from linearity, and predictions from the present model agree with the values reported by Ostubo et al. However, the works reported by Wicaksono et al., and Zhang and Fuji showed near linear behavior. Additionally, the studies from Araki et al. [65] appeared to be compositionally independent. Given these discrepancies, it is unclear if the model agrees with the carbonate salts' empirical data, and the collection of new empirical data or MD should be considered in future works.

Thermal conductivity deviation from ideal linear mixing

To quantify the impact of composition on the thermal conductivity of MS mixtures is to assess the deviations from a linear rule behavior, which can be expressed by [133]:

$$D_\lambda = 1 - \lambda^{id}/\lambda_{ref} \tag{5.12}$$

where λ^{id} and λ_{ref} are the thermal conductivity of ideal linear behavior and the thermal conductivity of the reference pure salt values, respectively, which are both dependent on

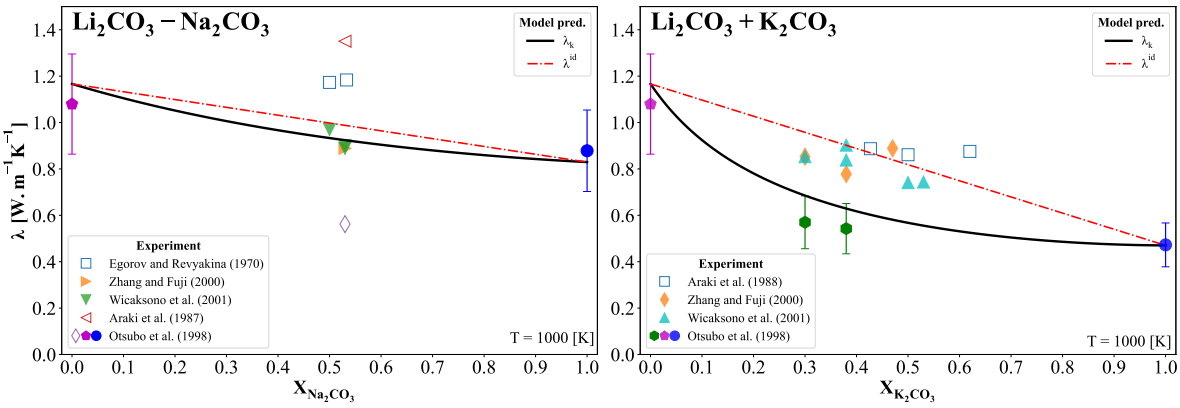

Figure 5.7 Predicted (solid line) thermal conductivity as a function of the composition of binary carbonate systems in comparison with reliable (solid symbols), unreliable (open symbols) experimental data sets.

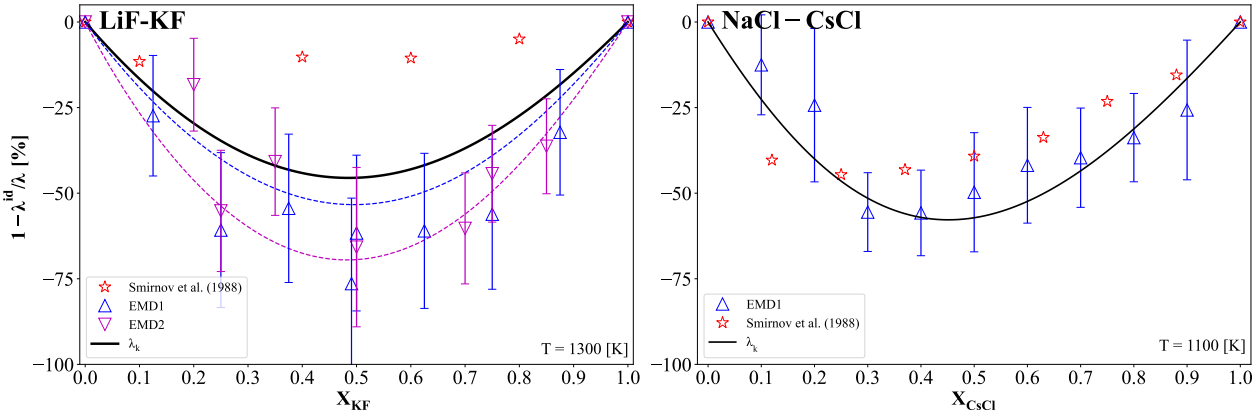

Figure 5.8 Deviation of predicted (solid line) thermal conductivity as a function of the composition of binary LiF-KF and NaCl-CsCl systems in comparison with MD simulations, unreliable (open symbols) experimental data sets.

the composition and temperature. Differences in the molecular weight and thermal conductivity of the pure components are the main contributors to the linearity deviation. As mentioned, for the MS mixtures, the ideal linear rule assumption of the thermal conductivity with composition is considered as a first approximation in most studies. Thus, a composition to linear rule behavior is a practical basis for assessing the potential advantages provided by the present model [44].

Figure 5.8 illustrates the deviations of two examples of binary systems, LiF-KF and NaCl-CsCl, which show relatively large deviations from linearity in comparison to the other systems considered here. In the fluoride binary system of LiF-KF, we use the values of pure salt from MD simulations as the reference pure conductivity for the present model, the dashed lines

Table 5.1 The equation $\Delta\lambda/\lambda(X)[\%] = X_1X_2(L_0 + L_1(X_1 - X_2))$ describe the deviations of the system from ideal linear behavior, where $L_0(T) = L_0^0 + L_0^1T$ and $L_1(T) = L_1^0 + L_1^1T$ are both the fitting constants as a function of temperature. The composition of maximum deviation X^*_{max} and the values of the simple binary mixtures of fluoride, chloride, bromide, and iodide are shown in the table.

Simple binary systems	L_0 [%]		L_1 [%]		M_1/M_2	X^*_{max}	$\Delta\lambda/\lambda(X^*_{max})[\%]$
Fluorides	L_0^0	$10^{-2}L_0^1$	L_1^0	$10^{-2}L_1^1$			T=1300 [K]
LiF-NaF	-23.11	-1.78	-0.93	-0.07	0.62	0.51	-12
LiF-KF	-90.67	-6.97	-5.48	- 0.42	0.45	0.51	**-46**
LiF-RbF	-224.12	-17.24	-59.76	-4.60	0.25	0.56	***-115***
LiF-CsF	-459.50	-35.35	-112.18	-8.63	0.17	0.56	***-235***
NaF-KF	-18.33	-1.41	-0.97	0.07	0.72	0.51	-9
NaF-RbF	-73.48	-5.65	-14.71	-1.13	0.40	0.55	**-37**
NaF-CsF	-177.99	-13.69	-27.67	-2.13	0.28	0.54	***-91***
KF-RbF	-22.94	-1.76	-6.97	-0.54	0.56	0.58	-12
KF-CsF	-72.46	-5.57	-22.01	-1.69	0.38	0.57	**-37**
RbF-CsF	-13.46	-1.04	-0.27	-0.02	0.69	0.50	-7
Chlorides							T=1100 [K]
LiCl-NaCl	-9.75	-0.89	-0.39	-0.04	0.73	0.51	-5
LiCl-KCl	-37.23	-3.38	-1.51	-0.14	0.57	0.51	-19
LiCl-RbCl	-120.78	-10.98	-14.71	-1.34	0.35	0.54	***-61***
LiCl-CsCl	-229.91	-20.90	-53.15	-4.83	0.25	0.55	***-117***
NaCl-KCl	-8.22	-0.75	-0.17	-0.02	0.78	0.51	-4
NaCl-RbCl	-51.49	-4.68	-6.27	-0.57	0.48	0.53	**-26**
NaCl-CsCl	-114.80	-10.44	-23.92	-2.17	0.35	0.55	***-58***
KCl-RbCl	-18.06	-1.64	-2.99	-0.27	0.62	0.53	-9
KCl-CsCl	-55.33	-5.03	-12.93	-1.18	0.44	0.55	**-28**
RbCl-CsCl	-8.55	-0.78	-0.72	-0.07	0.72	0.52	-4
Bromides							T=1200 [K]
LiBr-NaBr	-4.81	-0.40	-0.10	-0.01	0.85	0.50	-2
LiBr-KBr	-19.16	-1.6	-1.60	-0.13	0.73	0.51	-10
LiBr-RbBr	-46.26	-3.85	-2.91	-0.24	0.53	0.51	**-23**
LiBr-CsBr	-98.51	-8.21	-6.2	-0.52	0.41	0.51	***-50***
NaBr-KBr	-4.56	-0.38	-0.29	-0.02	0.86	0.51	-2
NaBr-RbBr	-20.36	-1.70	-1.28	-0.11	0.62	0.51	-10
NaBr-CsBr	-54.51	-4.54	-3.43	-0.29	0.48	0.52	**-28**
KBr-RbBr	-7.39	-0.62	-1.08	-0.09	0.72	0.53	-4
KBr-CsBr	-28.21	-2.35	-4.13	-0.34	0.56	0.53	-14
RbBr-CsBr	-6.94	-0.58	-0.14	-0.01	0.78	0.50	-4
Iodides							T=1200 [K]
LiI-NaI	-4.83	-0.40	-0.30	-0.02	0.89	0.51	-2
LiI-KI	-20.74	-1.73	-3.56	-0.30	0.81	0.54	-11
LiI-RbI	-76.74	-6.39	-9.88	-0.82	0.63	0.53	**-39**
LiI-CsI	-132.22	-11.02	-15.62	-1.30	0.52	0.52	***-66***
NaI-KI	-5.41	-0.45	-0.64	-0.05	0.90	0.53	-3
NaI-RbI	-40.18	-3.35	-3.85	-0.32	0.71	0.52	-20
NaI-CsI	-78.03	-6.50	-5.78	-0.48	0.58	0.52	**-39**
KI-RbI	-14.94	-1.25	-0.16	-0.01	0.78	0.50	-8
KI-CsI	-39.30	-3.28	-0.41	-0.03	0.64	0.50	-20
RbI-CsI	-5.18	-0.43	-0.05	0	0.82	0.50	-3

represent the deviations of the predicted mixtures by using MD simulations in comparison to the thermal conductivity of pure salt from the previous work (black solid line) [264]. It can be observed that the deviations from linearity predicted by the present model agree with the MD simulations (dashed lines), and are primarily fall within the error bounds. The present model (black solid line) also predicts deviations that are smaller in magnitude than those values in MD simulations, likely due to the larger values obtained by MD simulations for LiF. The it can be seen that the empirical data for the LiF-KF system has a maximum deviation from linearity around -10%, in disagreement with the present model. For the chloride binary system of NaCl-CsCl, the model predicts a similar deviation range to the MD simulation results, approximately -58% for $X_{0.45}$.

Table 5.1 summarizes the maximum deviation and the corresponding composition for simple binary MS mixtures of the fluoride family, chloride family, bromide family, and iodide family, with additional systems not assessed in the prior sections. The Redlich-Kister equation [289] $X_1X_2(L_0 + L_1(X_1 - X_2)$ quantifies the excess behavior from ideal linear behavior according to the compositions of the binary mixtures. The Redlich-Kister method is widely used in the CALPHAD (CALculation of PHAse Diagrams) to map the compositional dependence of free energy for multicomponent systems because it is symmetrical, L_0 describes the symmetry of the systems, L_1 describes the degree of departure from the symmetry. The results further demonstrate that the present model predicts an increasing deviation from the ideal with an increasing molar mass difference between two compounds in a binary system. Moreover, the deviation of the thermal conductivity decreases with the increase of anionic mass.

5.4.2 Predictions of thermal conductivity for eutectic salt mixtures

The compositions at the eutectic point are more interesting to the energy industry due to their lower melting points. Various binary, ternary, and high-order simple MS mixtures have been predicted in comparison with experimental data sets. Here we present the predicted temperature-dependent thermal conductivity for mixtures with available experimental data and relevance to advanced energy applications.

Eutectic binary systems

Figure 5.9 compares the binary mixtures for $(LiCl)_{0.59}$ - $(KCl)_{0.41}$ and $(NaCl)_{0.5}$ - $(KCl)_{0.5}$ with experimental data sets that are both reliable and unreliable as a function of temperature. Merrit et al. [200] used a modified transient hot-wire needle probe to determine the thermal conductivity of fluoride and chloride MSs. The temperature dependency $(\partial\lambda/\partial T)_P$ of $(LiCl)_{0.59}$ - $(KCl)_{0.41}$ system showed a negative sign, approximately $-4.26 * 10^{-4}$, which

is slightly less than both unary LiCl and KCl from Nagasaka e al. [87], $-2.9 * 10^{-4}$ *and* $-1.7 * 10^{-4}$ $[W.m^{-1}K^{-2}]$ respectively. The errors reported by these experimental measurements were between the range of ± 14.2 to 17.8%. Our predictions are within the intervals of the reported errors, with better agreement near the higher temperature data. The data reported by Smirnov et al. [56] for both systems showed positive temperature-dependent and larger values, as well as the value reported by Turnbull [83] for the eutectic salt mixture of LiCl-KCl.

Two carbonates binary systems of $(Li_2CO_3)_{0.533}$ - $(Na_2CO_3)_{0.467}$ and $(Li_2CO_3)_{0.62}$ - $(K_2CO_3)_{0.38}$ were found in the literature. The results reported by Otsubo et al. were nearly independent of temperature for both binary systems, which could be caused by the experimental measurements. Moreover, Otsubo et al. reported a significantly smaller thermal conductivity than other experimental works for $(Li_2CO_3)_{0.533}$ - $(Na_2CO_3)_{0.467}$. The values reported for $(Li_2CO_3)_{0.533}$ - $(Na_2CO_3)_{0.467}$, by Egorov et Revyakina [54] and Araki et al. [65], showed higher magnitudes of thermal conductivity with positive temperature dependencies, shown in Figure 5.10. Our predictions are in general agreement with the works reported by Zhang and Fuji [106, 271].

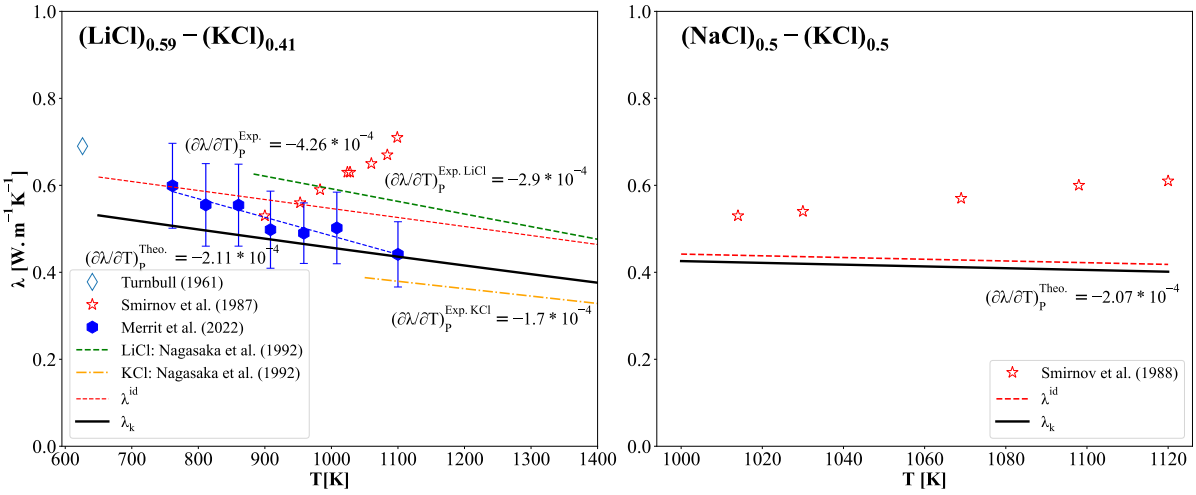

Figure 5.9 Predicted (solid line) thermal conductivity as a function of the temperature of $(LiCl)_{0.59}$ - $(KCl)_{0.41}$ and $(NaCl)_{0.5}$ - $(KCl)_{0.5}$ in comparison with reliable (solid symbols) and unreliable (open symbols) experimental data sets.

The data sets presented by Zhang and Fuji [106, 271] seem to be relatively large and close to the unreliable dataset of Araki et al. [65] for the system Li_2CO_3-K_2CO_3 near the melting temperature, which can be seen in Figure 5.10. The works reported by Otsubo et al. seemed to have slightly increasing (nearly constant) thermal conductivity for Li_2CO_3-Na_2CO_3, although the predicted results are in agreement with their results at high temperatures (greater

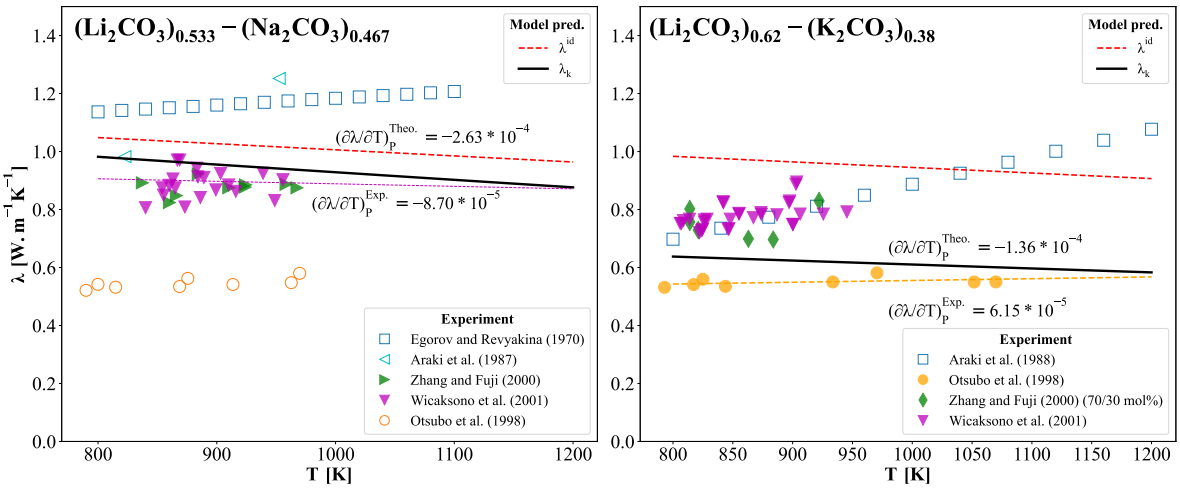

Figure 5.10 Predicted (solid line) thermal conductivity as a function of the temperature of carbonates in comparison with the reliable (solid symbols), unreliable (open symbols) experimental data sets.

than 950 K). Given that the empirical data from reliable data sets inconsistently agree with the model for the two mixtures considered, it is suggested that the carbonate systems require further investigation empirically or with MD.

Ternary and high order systems

LiF − NaF − KF Figure 5.11 shows the available experimental measurements in the literature in comparison with the calculations of the ideal linear rule and predictions of the present model. There is a discrepancy between the experimental data sets. The results reported by Lane et al. [270], and Janz et al. [34] were substantially larger than those from more recent works. Inversely, the works presented by Ewing et al. [198] were relatively low, and temperature independent. Smirnov et al. [56], Khokhlov et al. [267], An et al. [76], and Robertson et al. [80] show a positive temperature dependence of the thermal conductivity, therefore we consider these works unreliable. However, the magnitudes thermal conductivity reported these investigators are close to that of the reliable datasets around 750-800 [K], close to the melting temperature. The results reported by Gallagher et al. [61], Rudenko et al. [86], and Merrit et al. [200] show a negative temperature dependence, which we consider reliable. The uncertainty reported by Merrit et al. is between $\pm 14.5 \sim 16.9\%$. Our predictions agree with these data sets. Gallagher et al. [61] provided a $(\partial\lambda/\partial T)_P$ of the average low bounding data, $-2.12 * 10^{-4}$ $[W.m^{-1}K^{-2}]$, which is in good agreement with the present model, approximately $-2.64 * 10^{-4}$ $[W.m^{-1}K^{-2}]$. The ideal linear calculation is illustrated by the dashed line, which is approximately 40% larger than the present model predictions, as well

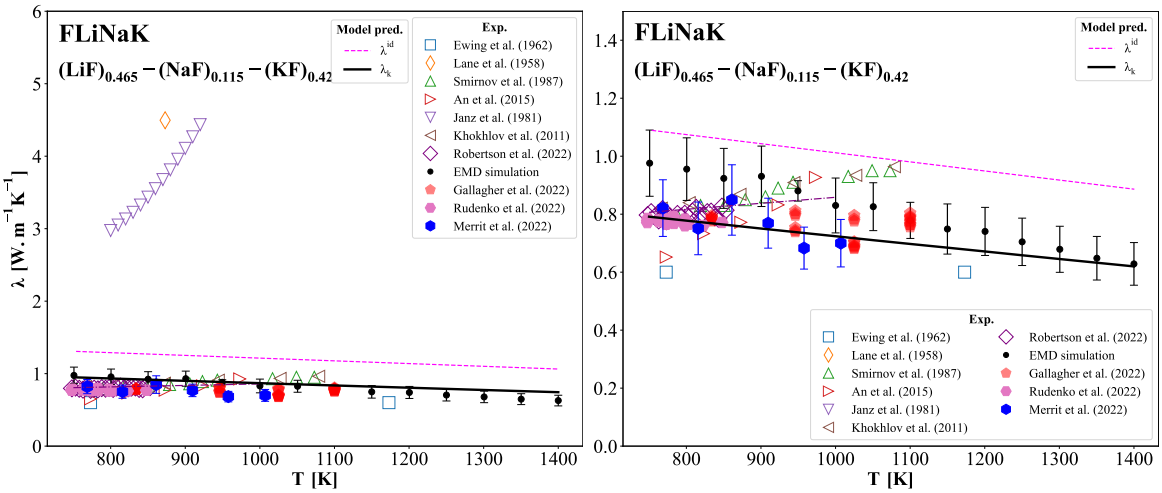

Figure 5.11 Predicted (solid line) thermal conductivity as a function of the temperature of FLiNaK ($(LiF)_{0.465}$-$(NaF)_{0.115}$-$(KF)_{0.42}$) in comparison with the ideal linear mixture (dashed lines), reliable (solid symbols), unreliable (open symbols) experimental data sets.

as most of the experimental datasets. The MD simulations [61] show a negative temperature dependency but larger in magnitude, the reason could be the overestimated values for pure LiF and NaF by EMD simulation.

Figure B.2 illustrates a compositional mapping of the predicted thermal conductivity of the LiF-NaF-KF at 1300 [K] (left) and the corresponding deviation from a linear rule behavior (right). The results show the composition gradient of the thermal conductivity close to LiF has a relatively large magnitude, which means that as the LiF concentration increases, the thermal conductivity rapidly increases. In contrast, for KF, the conductivity rapidly drops as the concentration increases. This behavior is primarily caused by the relatively large molecular weight and low conductivity of KF and the small molecular weight and high thermal conductivity of LiF, as mentioned in the previous section. The thermal conductivity and molecular weight of NaF are between those of LiF and KF, resulting in little changes in the composition gradient and deviation. The composition 54%LiF - 46%KF has a maximum deviation from linearity of roughly -48%, and the deviation progressively reduces to 0% at the corner of NaF. The deviation at the system eutectic is approximately -40%.

$NaF - KF - MgF_2$ The temperature dependency of NaF-KF-MgF_2 in comparison with ideal linear calculations and the only experimental datasets available in the literature is shown in Figure 5.12. The predictions of the present model agree with these experimental datasets reported by Merrit et al. [200], who mentioned that there were only 5 data points measured in a narrow temperature range of $967-1000[K]$, this is one potential contribution to

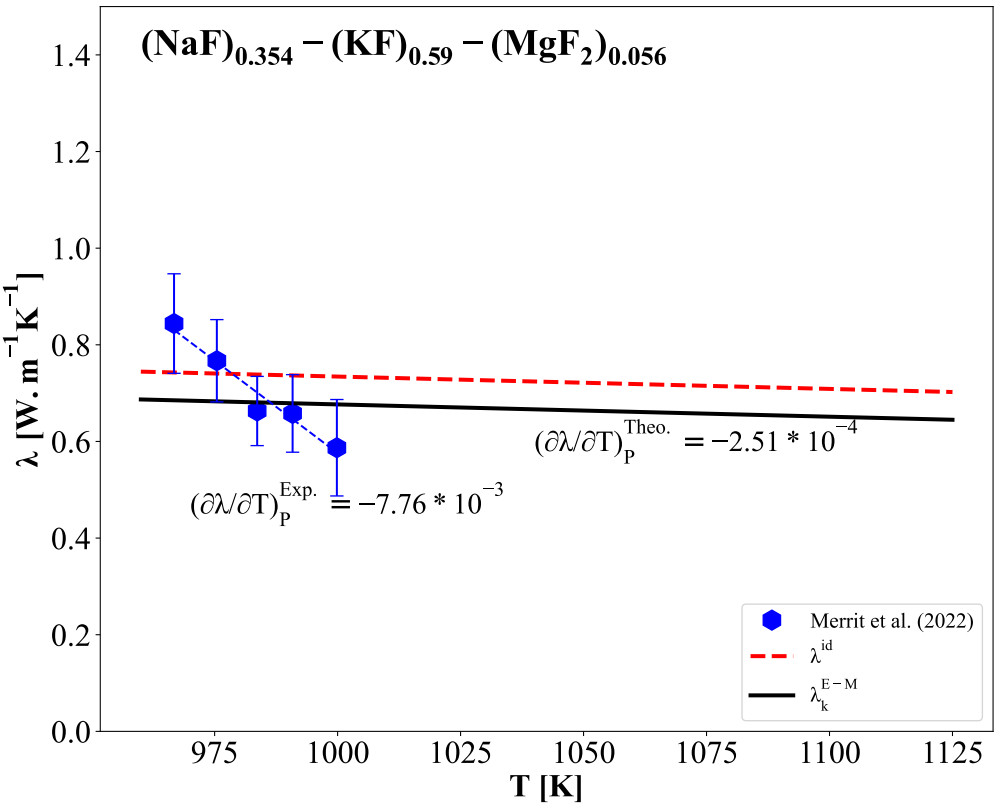

Figure 5.12 Predicted (solid line) thermal conductivity as a function of the temperature of FMgNaK ($(NaF)_{0.354}$-$(KF)_{0.59}$-$(MgF_2)_{0.056}$) in comparison with the ideal linear calculations and the only experimental datasets.

the significant temperature dependency $(\partial\lambda/\partial T)_P$, approximately $-7.76 * 10^{-3}[W.m^{-1}K^{-2}]$. If the measurements were obtained over larger temperature range or with lower uncertainty, the slope may prove to be less significant, as noted by Merritt et al. The result of $(\partial\lambda/\partial T)_P$ obtained by the model is $-2.51 * 10^{-4}$ $[W.m^{-1}K^{-2}]$, which seems more reasonable given the $(\partial\lambda/\partial T)_P$ of the pure salts are $-2.62 * 10^{-4}$, $-2.60 * 10^{-4}$, and $-1.67 * 10^{-4}$ $[W.m^{-1}K^{-2}]$ for NaF, KF, and MgF_2, respectively. Lastly, the results show that the present model predictions are approximately 10% lower than the ideal linear calculations.

Figure B.3 shows a compositional mapping of the predicted thermal conductivity of the NaF-KF-MgF_2 in composition at 1000 [K] (left) and the corresponding deviation from a linear rule behavior (right). The system of $(NaF)_{0.354}$ - $(KF)_{0.59}$ - $(MgF_2)_{0.056}$ (FMgNaK) is also shown in the figure. The thermal conductivity of NaF and MgF_2 are of the same magnitude, therefore the thermal conductivity gradient slowly decreases with increasing KF. The maximum deviation is around 6%, found in the binary mixture of NaF-KF. However, we note that many divalent metals dissolved in alkali halides and form the complex anions. For instance, MgF_2 in NaF/KF can be treated as containing Na^+, F^- and the complex anions

MgF_4^{2-} [290]. It is possible that the current model may not be fully representative of this system if complex anions have large effects of conductivity.

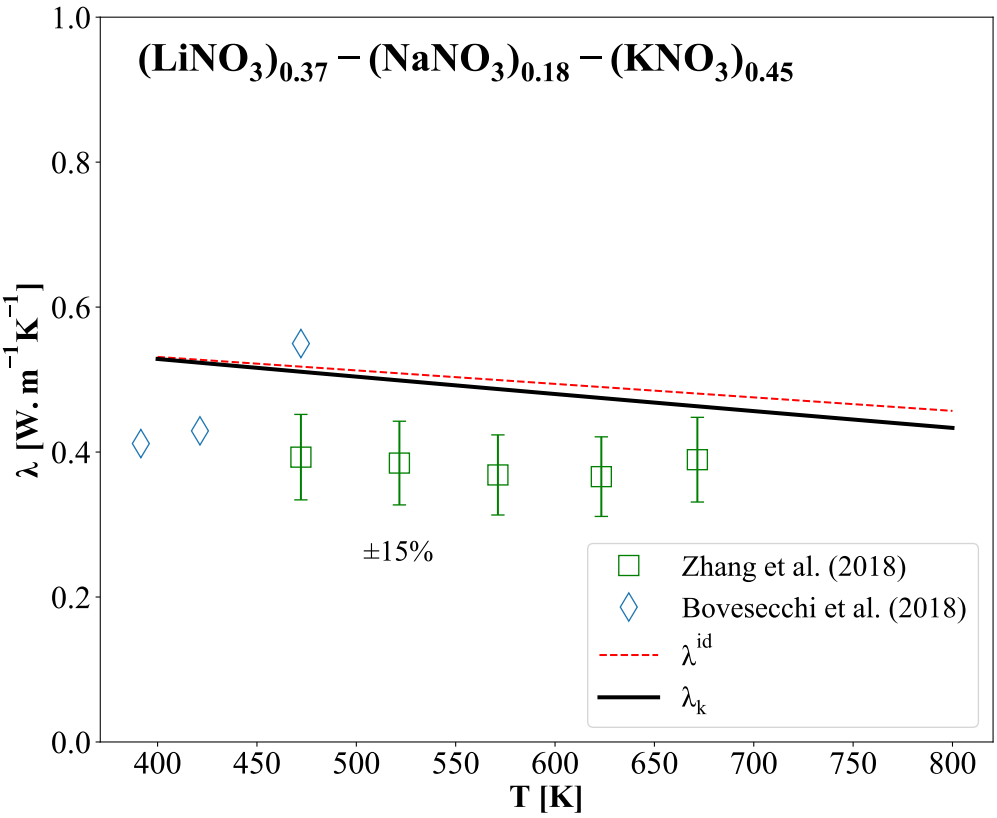

Figure 5.13 Predicted (solid line) thermal conductivity as a function of the temperature of (LiNaK)NO_3 ($(LiNO_3)_{0.37}$-$(NaNO_3)_{0.18}$-$(KNO_3)_{0.45}$) in comparison with the ideal linear calculations and the only experimental datasets.

$LiNO_3 - NaNO_3 - KNO_3$ Figure 5.13 shows the temperature dependent of the system $(LiNO_3)_{0.37}$-$(NaNO_3)_{0.18}$-$(KNO_3)_{0.45}$ in comparison with two experimental datasets. Bovesecchi et al. [268] built a new thermal conductivity probe for and reported three data points. However, the reported thermal conductivity had a significant positive dependence on the temperature. As the investigator pointed out, this was primarily caused by free convection errors during measurement. Therefore, the measurements are suggested to be unreliable at high temperatures. Zhang et al. [269] applied the laser flash analysis to determine the thermal diffusivity of several nitrate salt mixtures. The experimental values of thermal conductivity of this ternary nitrates system are lower than our predictions, as was the case for the binary nitrates solar salt ($NaNO_3$-KNO_3 60/40 wt%) they measured, which were about 15% lower

than the present model's predictions. However, the predicted values of the present model show good agreement with those reliable experimental data sets in Figure 5.6.
A compositional mapping of the predicted thermal conductivity of the ternary nitrates system in composition at 1000 [K] and the corresponding deviation from a linear rule behavior(right) is shown in Figure B.4. The orientation of the thermal conductivity and deviation gradients are similar to fluoride and chloride ternary systems, depending on the pure constituent molecular weight and conductivity. However, the maximum deviation is less than 5%, mainly due to the greater molecular weight of the NO_3^- anion and a lower thermal conductivity magnitude for the mixtures, relative to the F^- and Cl^- anion salts. As such, some investigators were successful when applying the linear rule behavior to calculate the thermal conductivity of the nitrate mixtures, and the present model may not present significant advantages when modeling the nitrate systems [39, 47, 75, 193].

$NaNO_3 - KNO_3 - CsNO_3$ Figure 5.14 compares the predicted results to the only experimental datasets reported by Zhang et al. [269]. The data sets are consistent with our predictions near lower temperatures(assuming a minimum of 15% uncertainty from the diffusivity measurement). However, the empirical thermal conductivity increases slightly at high temperatures, which is likely due to the difficulty of measurement at high temperatures, owing to increased contributions from competing convective and radiative heat transfer. Nonetheless, the model shows reasonable agreement, in the lower temperatures that showing an apparent downward trend with temperature, and is within the error intervals. The present model also shows improved accuracy over the linear model.
A compositional mapping of the predicted thermal conductivity of the $NaNO_3$-KNO_3-$CsNO_3$ in composition at 500 [K] and the corresponding deviation from a linear rule behavior(right) is shown in Figure B.5. The gradient of the thermal conductivity decreases from the side of $NaNO_3$-KNO_3 to $CsNO_3$, which is caused by the thermal conductivity of $CsNO_3$ being significantly lower than the other two nitrate salts. The thermal conductivity for pure salts of this ternary nitrates system is 0.529, 0.462, and 0.280 $[W.m^{-1}K^{-1}]$ for $NaNO_3$, KNO_3, and $CsNO_3$, respectively. As in other systems, the maximum deviation orients in the direction of the components with the maximum molecular weight differences. The deviation gradient is not as symmetric as Li-Na-K cation mixtures, since the molecular weight of Cs is much greater than Na and K. Therefore, the deviation gradient direction orients to KNO_3-$CsNO_3$ side. The maximum deviation of $NaNO_3$-KNO_3-$CsNO_3$ is approximately -25%.

$Li_2CO_3 - Na_2CO_3 - K_2CO_3$ The ternary carbonate system of $(Li_2CO_3)_{0.435}$-$(Na_2CO_3)_{0.315}$-$(K_2CO_3)_{0.25}$ is illustrated in Figure 5.15. The system's predicted conductivity shows a -35%

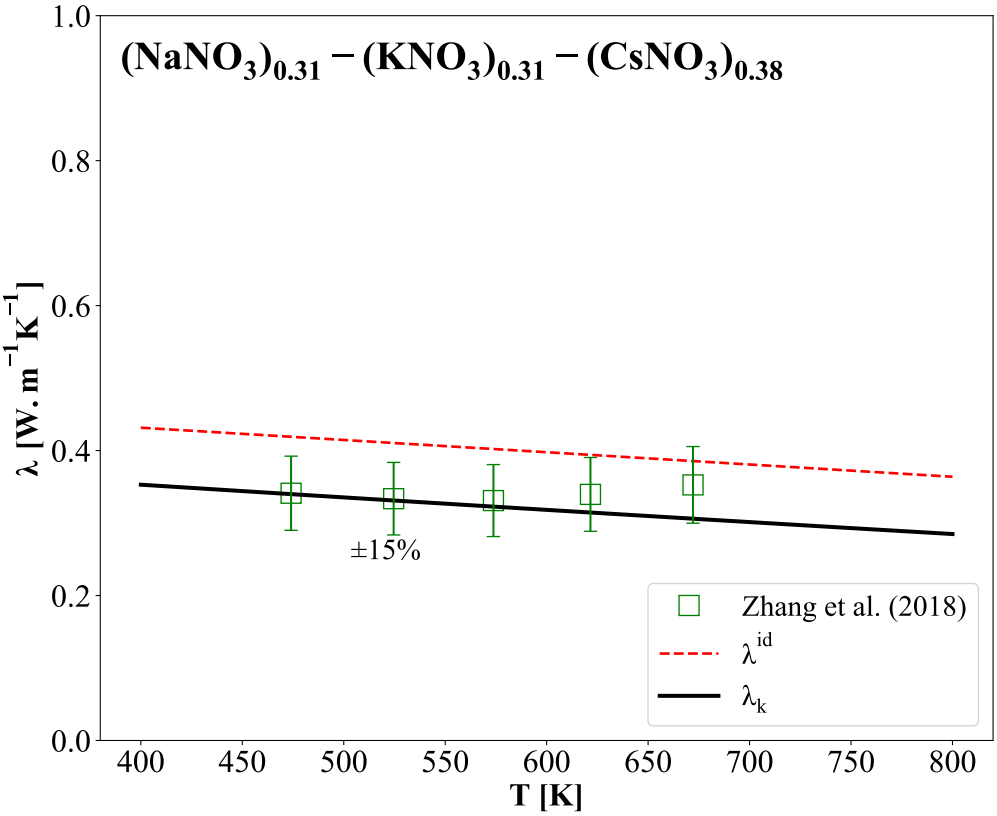

Figure 5.14 Predicted (solid line) thermal conductivity as a function of the temperature of $(NaNO_3)_{0.435}$-$(KNO_3)_{0.315}$-$(CsNO_3)_{0.25}$ in comparison with the ideal linear calculations and the only experimental dataset.

deviation from the ideal linear calculation. Three experimental data sets were reported in the literature. The data sets reported by Otsubo et al. [75] and Zhang et al. [291] both showed a $(\partial\lambda/\partial T)_P \sim 0$, with a potentially positive trend. The results reported by Araki et al. [65] agree in magnitude with the present model's predictions for two data points. However, their results of the binary carbonates system showed significant positive temperature dependency, and therefore, the datasets reported by Araki et al. [65] are considered unreliable. The ideal linear model (red dashed line) predicts a thermal conductivity that is larger than both reliable data sets, whereas the present model's predictions are in between both reliable datasets and suggested that it is potentially more reliable for this salt mixture.

A compositional mapping of the predicted thermal conductivity of the Li_2CO_3 - Na_2CO_3 - K_2CO_3 in composition at 800 [K] and the corresponding deviation from a linear rule behavior(right) is shown in Figure B.6. Because of the doubling of the cationic molecular weight, we observed that the deviation gradient of this ternary carbonates system is not as symmetric as other Li-Na-K mixtures. The maximum deviation from linearity is found along the binary

Li_2CO_3-K_2CO_3 of -46 % at the composition of 54/46 %.

$(\mathbf{LiNO_3})_{0.3} - (\mathbf{NaNO_3})_{0.16} - (\mathbf{KNO_3})_{0.28} - (\mathbf{CsNO_3})_{0.26}$ Zhang et al. [269] have evaluated the ternary, quaternary nitrates system as a potential candidate of HTF/TES for solar energy systems. This quaternary system featured a low melting temperature of 368 [K]. Figure 5.16 shows the comparison between this experimental data, the ideal linear calculations, and the predictions of the present model for the quaternary nitrates system of $(LiNO_3)_{0.3}$-$(NaNO_3)_{0.16}$-$(KNO_3)_{0.28}$-$(CsNO_3)_{0.26}$. We observe that the $(\partial\lambda/\partial T)_P \sim 0$, with a potentially positive trend, for the experimental data sets. The empirical results are in reasonable agreement with the model's predictions at higher temperatures. Overall, the deviations are slightly above the cited error intervals, but still comparable to modern experimental methods. Moreover, once again the ideal linear calculations are significantly large to experimental data and our predictions.

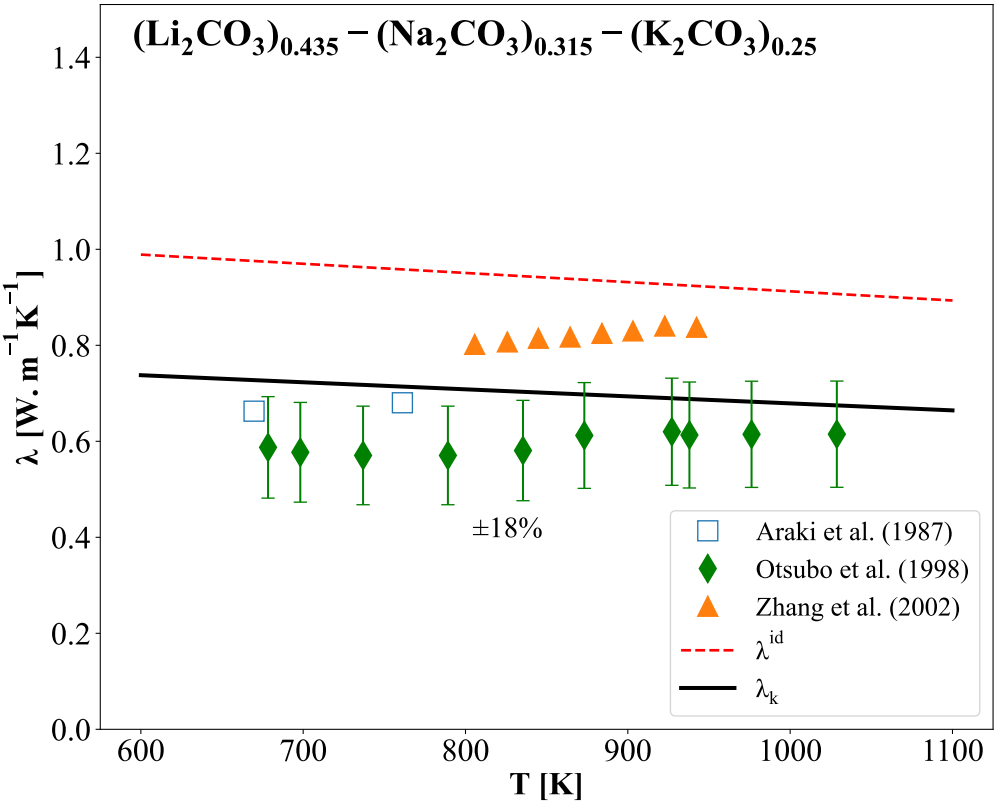

Figure 5.15 Predicted (solid line) thermal conductivity as a function of the temperature of Li_2CO_3 - Na_2CO_3 - K_2CO_3 in comparison with the ideal linear calculations and the reliable (solid symbol), and unreliable (open symbol) experimental data sets.

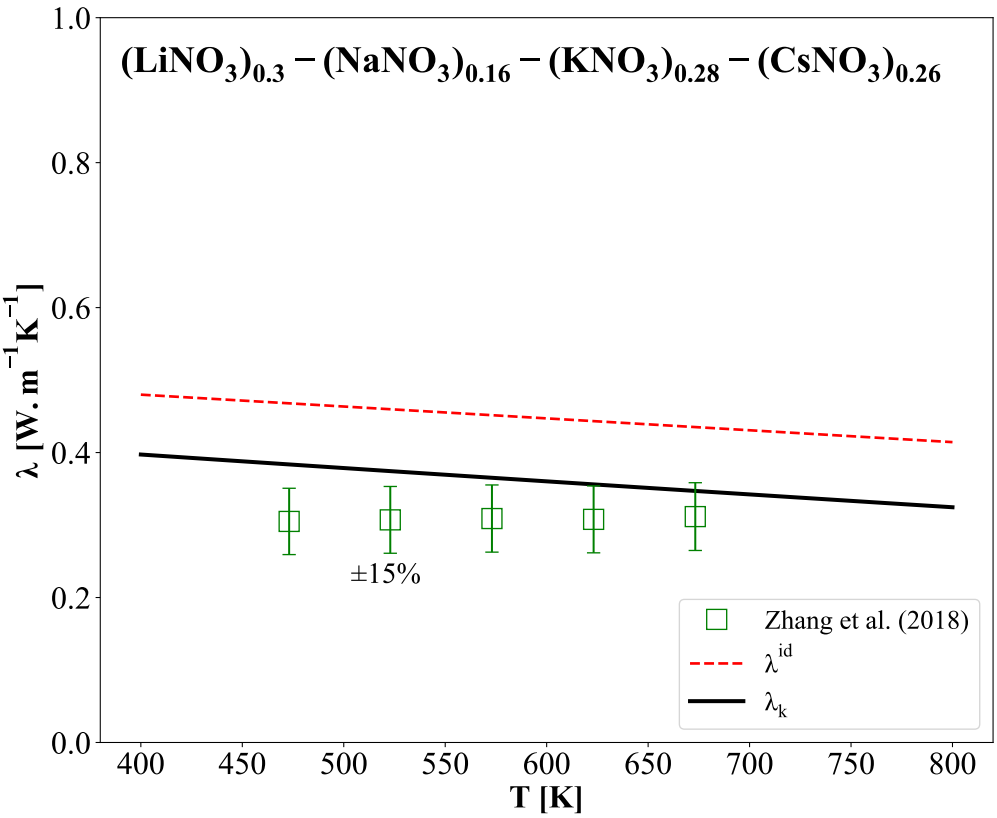

Figure 5.16 Predicted (solid line) thermal conductivity as a function of the temperature of $(LiNO_3)_{0.3}$-$(NaNO_3)_{0.16}$-$(KNO_3)_{0.28}$-$(CsNO_3)_{0.26}$ in comparison with the ideal linear calculations and the only experimental data sets.

5.5 Conclusion

One of the most important properties in the design of advanced MS systems is thermal conductivity since it plays the role of evaluating the efficiency of heat transfer. MS mixtures feature many more interesting thermo-physical properties than pure salts for industrial applications, such as lower melting temperature, higher heat capacity, lower viscosity, etc. However, it is challenging to determine the thermal conductivity of MSs accurately. In addition, the often used linear rule behavior does not apply to the thermal conductivity of all MS mixtures.

A theoretical model derived from the kinetic theory was proposed to predict accurately the thermal conductivity for any simple, non-reciprocal MS mixture. Because of the limited availability of the experimental data sets of the thermal conductivity for MS mixtures, numerous MD simulations were performed for the binary fluoride, chloride, bromide, and iodide salt families to validate the proposed model's accuracy in determining compositional dependence. The predicted results were also compared to the available experimental data sets for binary

nitrates and carbonates salts. The model was also applied to several higher-order eutectic mixtures that have existing empirical data, showing reasonable agreement. While additional empirical data is necessary to fully validate the model. The predicted results were in agreed with most of the reliable experimental data sets and the MD simulated predictions with the model's predicted results were within or near the reported error intervals. Therefore, the proposed model is expected to have a predictive capability comparable to most experimental datasets.

Only an accurate knowledge of several thermodynamic properties at their melting temperatures is required for the prediction using this model. These properties include heat capacity, density, thermal expansion, and sound velocity. Most of these parameters can be obtained from the MS database; therefore, the computational cost is relatively low. In our previous work, the thermal conductivity of pure salts was found to have an average deviation of 10% for over 50 MSs. In such cases, this current model may yield predictions with a similar level of accuracy for MS mixtures.

We also found several notable trends that are relevant when considering the thermal conductivity of mixtures. First, the deviations show significant deviations from the linear rule behavior when there is a large difference between the molecular weight and thermal conductivity for pure salt constituents. The magnitude of non-ideality generally decreases with increasing molecular weight. Considering mixtures with the same cations, an increase in anionic weight correlated with decreases in the deviations from the linear calculation. Likewise, the same anion salts showed decreasing deviations from ideality with increasing molecular weight of the cations. Moreover, compositional mappings of the predicted thermal conductivity of the ternary systems and the corresponding deviation from linear rule calculations were performed, showing that these trends also persists in the higher-order mixtures.

Lastly, it is expected that the proposed model for predicting the thermal conductivity of MS mixtures has the capability to predict all kinds of MS mixtures with accuracy comparable to experimental methods. It is anticipated that the model could be extended to the reciprocal and complex of MS mixtures, which are of high importance to energy applications. The current model can be extended to complex MS mixtures, such as KCl-$MgCl_2$, NaF-AlF_3 which forms a complex compound or polymer chains within the mixtures. Therefore, is introduced a new parameter named "complex rate" to describe the mass fluctuation associated with the complexity structures. Follow on work will be considered to validate this. This current work further demonstrates the capability of a theoretical model and database for simple MS mixture thermal conductivity, in support of advanced energy applications.

5.6 Acknowledgments

This research was supported by funds from the Natural Sciences and Engineering Research Council of Canada (NSERC) [funding reference number: RGPIN-2021-03279]. R.C.G acknowledges the support from The Ohio State University. This research was enabled in part by support provided by Calcul Québec (www.calculquebec.ca) and the Digital Research Alliance of Canada (alliancecan.ca)

CHAPTER 6 ARTICLE 3: EXTENDING THE KINETIC THEORY–BASED THERMAL CONDUCTIVITY MODEL TO RECIPROCAL MOLTEN SALT MIXTURES WITH SHORT–RANGE ORDERING VIA THE MODIFIED QUASI–CHEMICAL MODEL IN THE QUADRUPLET APPROXIMATION

Huiqiang Yang, Anh-Thu Phan, Aïmen E. Gheribi, Patrice Chartrand

Published in Solar Energy Materials and Solar Cells, June 11 2025, volume 292, 113724

My contributions to this article are: Conceptualization, Methodology, Validation, Software, Formal analysis, Investigation, Data curation, Writing – original draft, Visualization.

Abstract: Molten salts are among the most promising materials for advanced energy systems in the renewable energy and nuclear fields, with thermal conductivity being a critical property that directly impacts the efficiency of heat transfer processes. However, reliable experimental data on the thermal conductivity for molten salt mixtures is scarce, requiring the use of atomistic simulations and robust theoretical frameworks to fill this gap. This study extends a previously developed kinetic theory-based model for common-anion molten salt mixtures to reciprocal molten salt mixtures (i.e., LiF-KCl). To account for the effects of first-nearest neighbor short-range ordering between cations and anions, pair fractions in the Modified Quasi-chemical Model in the Quadruplet Approximation was employed. The current model fills an important gap in the modeling of thermal conductivity for reciprocal molten salt mixtures, since no existing model has accurately characterized their thermal conductivity. Predicted results were compared with various equilibrium molecular dynamics simulations performed in this work for solutions involving Li^+, Na^+, K^+ / F^-, Cl^-, and with existing experimental measurements. The model also predicted the thermal conductivity of reciprocal molten salt mixtures proposed in the literature as potential phase change materials. The current model demonstrated excellent predictive capability and accuracy of thermal conductivity for both monoatomic and polyatomic anion reciprocal molten salt mixtures, with an estimated error margin up to 20%. This advancement will significantly contribute to improving the statement of knowledge of reciprocal molten salt thermal conductivity and provide valuable tools for evaluating the thermal conductivity of molten salt mixtures in engineering applications.

6.1 Introduction

The goal of achieving carbon neutrality was established before 2050 for most countries by the Paris Agreement [25]. Renewable energy and nuclear energy are two primary sources to decarbonizing the electric power sector. Molten salt reactor is one of the Generation IV advanced nuclear reactor, in which molten salt serves as the primary nuclear coolant and/or fuel materials. However, more recently, the wind, photovoltaic and molten salt power tower multisource renewable energy cogeneration systems have become very popular to combat CO_2 emissions. Molten salts have been extensively used in metal production for over a century. For example, the Hall-Héroult process for aluminum production utilizes molten cryolite (Na_3AlF_6) as an electrolyte [292]. Similarly, metals such as titanium (Ti), zirconium (Zr), and magnesium (Mg) are produced using eutectic mixtures of NaCl-KCl as the electrolyte in their respective electrolysis processes [2]. Despite the wide applications of molten salts in industry, some of the properties still remains not well understood, in particular the thermal conductivity.

The thermal conductivity of molten salts plays a critical role in the efficiency of heat transfer in fluid mechanics. For instance, the Prandtl number, defined as $Pr = \mu Cp/\lambda$ quantifies the efficiency of heat transfer within a fluid, while the Nussel number ($Nu = hD/\lambda$) offers key insight into the relative performance of convective versus conductive heat transfer. High thermal conductivity ensures uniform temperature distribution, preventing hot spots and overheating. As a results, the system could remain safe and efficient. Over the past several decades, the thermal conductivity of molten salts has been studied through experimental techniques, numerical simulations, and modeling. Measuring thermal conductivity through experiments is difficult and costly. Major challenges arise in accurately estimating heat losses through convection, conduction, and radiation at high temperatures. Errors caused by chemical reactions further contribute to the uncertainties [40,60,61]. Therefore, experimental datasets often appear scattered, inconsistent, and in disagreement regarding temperature dependence. For instance, the eutectic molten fluoride salt mixture - FLiNaK ($(LiF)_{0.465}$-$(NaF)_{0.115}$-$(KF)_{0.42}$), which is of important interest for nuclear reactors, the discrepancy in experimental datasets is as high as 500% at around 900 [K] from individual studies [76]. Moreover, extensive experimental measurements have been carried out to to determine the thermal conductivity of pure molten salts. However, molten salt mixtures are more of interest in practical engineering due to the enhanced properties. Experimental datasets for molten salt mixtures are unfortunately quite limited, particularly for reciprocal molten salt mixtures that contain more than one cation and more than one anion. For instance, molten LiF-KCl solutions involve two cations Li^+ and K^+, and two anions, F^- and Cl^-.

Molecular dynamics (MD) simulations offer a cost-effective way to estimate the thermal

conductivity of pure and mixed molten salts. This technique also eliminates hazards linked to high-temperature measurements. However, several challenges persist, including the need for the accurate interatomic potentials and the significant computational resources required for high-order salt mixtures. Additionally, simulations can only be performed for one specific composition at a specific temperature in each run, making it time-consuming and really challenging to explore variations in composition and temperature, which are common in simulations of practical engineering processes. Despite these challenges, MD simulations can help to understand of the mixing behavior and assist in validating developing models, which is the case in the present work.

Several studies have reviewed different categories of available models to predict thermal conductivity [39,60,94,194]. Most of these models provide relatively accurate predictions of thermal conductivity for unary molten salt. To date, the most commonly employed to estimate the thermal conductivity of molten salt mixtures is the ideal mixing rule, $\lambda^{id} = \sum_{i=1}^{N} X_i \lambda_i$, which provided relatively good results for some salts, such as nitrate salt mixtures [39]. This model is convenient to use, only the mole fraction (X_i) and the thermal conductivity of pure molten salt (λ_i) are required of each component (i), but the reliability should be verified due to the limited availability of thermal conductivity datasets for molten salt mixtures in the literature. Additionally, it is not based on thermodynamic theory [44]. Smirnov et al. [56] proposed a model that the thermal conductivity of molten salt mixtures of common anion is inversely proportional to their molar volume. However, the experimental measurements from the study are not recommended, as they exhibited a strong positive temperature dependence on thermal conductivity, likely resulting from the improper design of the apparatus of heat losses through convection, conduction and radiation [40]. Zhao et al. [194] presented a model based on theoretical unit cell for binary mixtures, the predicted results have been compared to some experimental datasets which were not recommended, making it challenging to verify the reliability. Gheribi and Chartrand [152] developed a theoretical model based on earlier work on classical kinetic theory. The model was validated by Equilibrium MD (EMD) simulations, which showed good agreement for ternary salt LiF-NaF-KF and LiCl-NaCl-KCl common-anion mixtures. However, a "universal" constant was assumed to be effective for all ionic mixtures, which restricted the model's wide application in different molten salt mixtures. This is especially true for molten salt mixture with large differences in the molar mass of ions and common-ion complex salt mixtures, such as LiF-CsF and LiF-BeF_2 respectively. Most of these models are tailored to a specific salt family and their mixtures. These models showed to be able to predict some of the salt mixtures with common-anion mixtures, but their reliability stills need to be questioned for applying to other salt mixtures. To the best of our knowledge, no existing model can accurately predict the thermal conductivity across a wide

range of molten salt mixtures. Indeed, there is currently no model of thermal conductivity available for reciprocal molten salt mixtures.

To better illustrate reciprocal system and reciprocal solutions, Figure 6.1 presents the composition of the LiF-LiCl-KF-KCl reciprocal mixture, typically plotted on a square. The pure salts are found at the four corners of the neutral plane of the four elements (Li-K-F-Cl). The four sides represent compositions in binary common-cation (LiF-LiCl, KF-KCl) and common-anion (LiF-KF, LiCl-KCl) mixtures. Within the square, four ions (Li^+, K^+, F^- and Cl^-) all are involved as reciprocal solutions. There is an infinite number of combinations of three or four of the four pure salts that can reproduce a given composition inside the reciprocal square (except on the sides where there is only one combination that defines the composition, this renders the previously mentioned ideal mixing rule questionable). To predict the thermal conductivity of a specific reciprocal mixture, the cationic fractions (X_C) and anionic fractions (X_A) should be defined, where C and A denote the cation and anion, respectively. By accounting the ionic charges, the equivalent site fractions (Y_C and Y_A) can be also determined, as be discussed in the next section. Therefore, the pair fractions ($X_{C/A}$) that involve the interactions of the first-nearest-neighbor (FNN) in the solution of Li^+, K^+, F^- and Cl^-, are defined as the ratio of the number of moles of (Li^+/F^-, Li^+/Cl^- and K^+/F^-, K^+/Cl^-) pairs to the total number of moles [293].

Let us consider an example of two monovalent reciprocal mixtures with the following nominal mole fractions: $(LiF)_{0.4}$-$(KF)_{0.1}$-$(KCl)_{0.5}$ and $(LiCl)_{0.4}$-$(KF)_{0.5}$-$(KCl)_{0.1}$. Using the ideal mixing rule model, thermal conductivity values of these two mixtures at 1300 [K] are calculated to be 0.727 [$W.m^{-1}K^{-1}$] and 0.538 [$W.m^{-1}K^{-1}$], respectively, with a deviation of 35.13%. However, both mixtures have the same ionic fractions at point R in Figure 6.1, specifically $Y_{Li^+} = 0.4$, $Y_{K^+} = 0.6$, and $Y_{F^-} = 0.5$, $Y_{Cl^-} = 0.5$, the exchange reaction $LiCl_{liq} + KF_{liq} \rightleftharpoons LiF_{liq} + KCl_{liq}$ associated to $\Delta g^{0,EX}_{Li,K/F,Cl}$ should proceed to equilibrium at constant n_{Li^+}, n_{K^+}, n_{F^-} and n_{Cl^-}, temperature and pressure, providing a unique internal FNN pair fractions composition from the multitudes of input combinations of the four salts that give the same sets of n_{Li^+}, n_{K^+}, n_{F^-} and n_{Cl^-}. Consequently, their thermal conductivity should be only one value at this composition. This discrepancy highlights a fundamental issue with using nominal mole fractions for reciprocal molten salt mixtures (within the composition square) when applying the ideal mixing rule. Multiple combinations of nominal mole fractions can lead to identical ionic fractions, yet yield different thermal conductivity values. A same problem arises when directly applying nominal mole fractions to our previous thermal conductivity model for common-anion molten salt mixtures into reciprocal salt mixtures. Within the composition square, a specific point can represent an infinite number of nominal mole fraction combinations, resulting in an infinite number of predicted thermal conductiv-

ity values. In contrast, at the sides of the composition square, only a single composition is uniquely defined. This indicates that nominal mole fractions are well-suited for describing common-ion mixtures only, but not for reciprocal molten salt mixtures. For instance, at point O, the nominal composition of the common-anion mixture is $(LiF)_{0.4}$-$(KF)_{0.6}$, with ionic fractions $Y_{Li^+} = 0.4$, $Y_{K^+} = 0.6$, and $Y_{F^-} = 1$. Using Equation 6.4, the pair fractions are calculated as $X_{Li^+/F^-} = Y_{Li^+} * Y_{F^-} = 0.4$, and $X_{K^+/F^-} = 0.6$. These pair fractions are identical to the nominal mole fractions of the common-anion salt mixture.

The aim of this study is to address the existing gap by extending our previous work on thermal conductivity model for common-anion molten salt mixtures to reciprocal molten salt solutions. In this extension, the use of nominal mole fractions for each component in reciprocal molten salt mixtures is no longer feasible. Instead, pair fractions, which account for the interactions between first nearest neighbors (FNN) of different cations and anions, are considered. The first approach, the Temkin model, assumes random mixing of cations and anions within their respective sublattices, providing one set of FNN pair fraction from a unique set of equivalent ionic fraction. However, results from the EMD simulations in this work reveal deviations from random mixing, highlighting the effects of FNN short-range ordering interactions. The second approach is the Modified Quasi-chemical Model in the Quadruplet Approximation (MQMQA) [41], in which the Gibbs energy minimization is performed with the EQUILIB Module of FactSage^{TM} [294], finds the set of FNN pair fractions from a unique set of equilibrium ionic fractions at a fixed temperature. It evaluates combined FNN and second nearest neighbor (SNN) short-range orders. In the ideal case where $\Delta g^{EX} = 0$, the MQMQA approach reduces to the Temkin model when all common-ion interactions are ideal. Furthermore, in common-anion mixtures, the pair fractions predicted by the MQMQA approach are identical to the nominal mole fractions. Additionally, the MQMQA approach has been extensively used to derive model parameters for the thermodynamics and phase diagrams of various molten salt systems, including both common-ion and reciprocal molten salts [168, 170, 177, 178]. A detailed discussion of the pair fractions in the Temkin model and the MQMQA approach is presented in the next section.

The MQMQA model was specifically developed to estimate pair fractions, with numerous parameters obtained and many molten salt mixtures optimized. Building on these advancements, we aim to modify the previous model for common-anion molten salt mixtures to account for reciprocal effects. Most parameters in the model will be adjusted to incorporate compositional variations affecting by the FNN pair fractions. Additionally, as part of this work and in the context of extending the FTsalt Database of FactSage^{TM} from version 8.3 to 8.4, which already included different excess volume parameters, we have introduced several new parameters, such as thermal expansion and bulk modulus of pure salts, to enable the

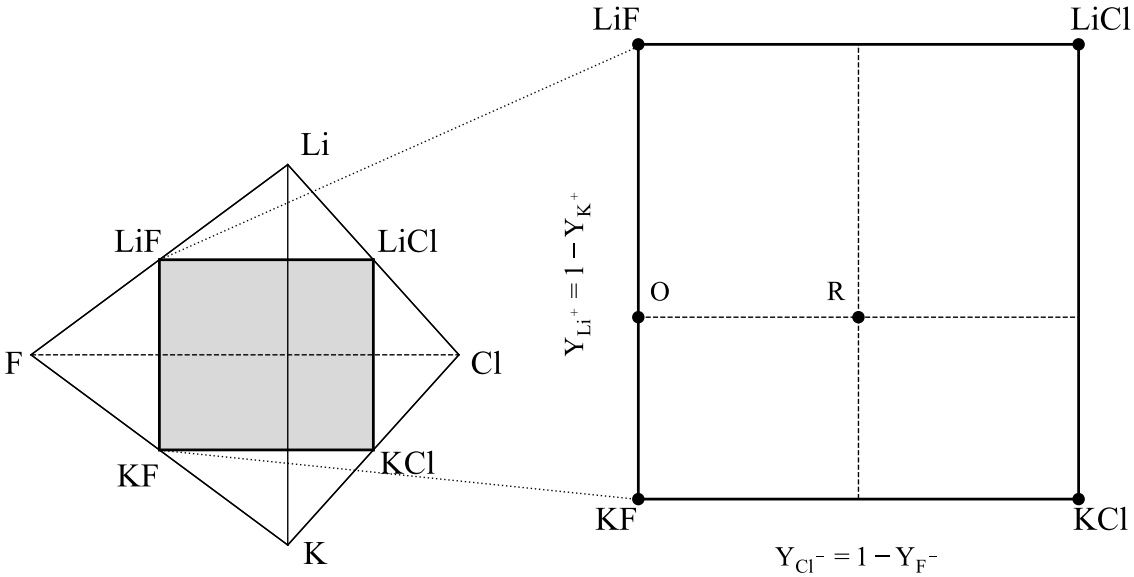

Figure 6.1 Neutral plane representation of Li, K, F, and Cl, along with the composition square for the Li^+, K^+ / F^-, Cl^- reciprocal solution. Point R illustrates an example of a reciprocal composition defined by the cationic and anionic fractions. Point O represents a common-anion mixture of $(LiF)_{0.4}$-$(KF)_{0.6}$.

precise calculations of sound velocity for both pure molten salts and molten salt mixtures.

6.2 From nominal fractions to FNN pair fractions in the Temkin model and MQMQA approach

It is important to clearly define the various types of fractions mentioned in this paper. In our previous work on common-anion mixtures [295], there is no constraint on the nominal mole fractions applied in the model, since only one single combination uniquely defines a composition (representing the sides of the compositional square). However, in the case of reciprocal molten salt solutions (Li^+, K^+ / F^-, Cl^-), where two or more different cations (Li^+, K^+) and two and more anions (F^-, Cl^-) are forming in the melt (inside the compositional square), understanding the concept of FNN pair fractions becomes essential. Let's again see the example mentioned above $(LiF)_{0.4}$-$(KF)_{0.1}$-$(KCl)_{0.5}$.

- Nominal fraction (X_i [mol/mol]): This refers to the initial mole fraction of each component in the melt, representing the starting proportions of each ionic species before any interactions are considered, like input moles in an experiment. In the example mixture above, $X_{LiF} = 0.4$, $X_{KF} = 0.1$, and $X_{KCl} = 0.5$.

- Cationic and anionic site (or mole) fractions (X_C and X_A): In the Temkin and quasi-chemical models, it is assumed that cations and anions reside on the cation sublattice

and the anion sublattice, respectively. The cationic and anionic site fractions are defined [296]:

$$X_{C_1} = \frac{n_{C_1}}{n_{C_1} + n_{C_2}} = 1 - X_{C_2},$$
$$X_{A_1} = \frac{n_{A_1}}{n_{A_1} + n_{A_2}} = 1 - X_{A_2}, \tag{6.1}$$

where n_i is the number of moles of ion i in the solution. In the example, we have X_{Li^+} = 0.4/(0.4 + 0.5 + 0.1) = 0.4, X_{K^+} = 0.6, X_{F^-} = (0.4 + 0.1)/(0.4 + 0.1 + 0.5) = 0.5, and X_{Cl^-} = 0.5.

- Equivalent site fractions (Y_C and Y_A): These fractions account for ionic charges ($|q_i|$) to ensure an equal number of equivalents on each sublattice. For instance, in pure $CaCl_2$, $q_{Ca^{2+}} = 2q_{Cl^-}$ The equivalent cationic and anionic fractions are given [215]:

$$Y_{C_1} = \frac{q_{C_1} * n_{C_1}}{q_{C_1} * n_{C_1} + q_{C_2} * n_{C_2}} = 1 - Y_{C_2}, \tag{6.2}$$
$$Y_{A_1} = \frac{q_{A_1} * n_{A_1}}{q_{A_1} * n_{A_1} + q_{A_2} * n_{A_2}} = 1 - Y_{A_2}, \tag{6.3}$$

this is a monovalent reciprocal mixture, we have $|q_i| = 1$ for all ions. Therefore, Y_{Li^+} = 0.4, Y_{K^+} = 0.6, Y_{F^-} = 0.5, and Y_{Cl^-} = 0.5.

- Pair fractions of FNN in the Temkin model ($X_{C/A}^{Temkin}$): The Temkin model assumed random mixing of cations on cationic sites and anions on anionic sites. Therefore, the FNN pair fractions can be estimated based on the random mixing between cations and anions. The following equation gives the probability of the FNN pair in the Temkin model,

$$X_{C/A} = Y_C * Y_A \tag{6.4}$$

Consequently, the pair fractions for each component in the Temkin model are given as: $X_{LiF}^{Temkin} = Y_{Li^+} * Y_{F^-}$ = 0.4*0.5 = 0.2, $X_{LiCl}^{Temkin} = Y_{Li^+} * Y_{Cl^-}$ = 0.2, and $X_{KF}^{Temkin} = Y_{K^+} * Y_{F^-}$ = 0.6*0.5 = 0.3, $X_{KCl}^{Temkin} = Y_{K^+} * Y_{Cl^-}$ = 0.3, these values are independent of temperature in Temkin model.

- Pair fractions in the MQMQA approach ($X_{C/A}^{MQMQA}$) [41]: The MQMQA uses an internal composition of quadruplets, formed by two cations and two anions, to reproduce the Gibbs energy of a multi-component solution. Each quadruplet has a Gibbs energy function, the equilibrium quadruplet composition is obtained by minimizing the Gibbs energy at constant temperature and pressure, and moles of ions. From the equilibrium

quadruplet fractions, FNN pair fractions can be computed. The expression for the pair fraction in the MQMQA ($X_{C/A}^{MQMQA}$) is shown:

$$X_{C/A}^{MQMQA} = X_{(C_1)_2/(A_1)_2}^{Quad} + \frac{1}{2}X_{C_1C_2/(A_1)_2}^{Quad} + \frac{1}{2}X_{(C_1)_2/A_1A_2}^{Quad} + \frac{1}{4}X_{C_1C_2/A_1A_2}^{Quad} + ... \quad (6.5)$$

where $X_{C_1C_2/A_1A_2}^{Quad}$ are the quadruplet fractions.

For a detailed explanation of "quadruplets", please refer to the works of Pelton et al. [41, 215, 296].

Table 6.1 Calculated equilibrium pair fractions in the MQMQA approach for the nominal fraction of $(LiF)_{0.4}$-$(KF)_{0.1}$-$(KCl)_{0.5}$ molten salt mixture as a function of temperature, starting from the liquidus temperature (around 950 [K]), compared to the pair fractions in the Temkin model.

$X_{C/A}^{MQMQA} \backslash T$ [K]	950	1150	1350	1550	$X_{C/A}^{Temkin}$ (all T)
X_{LiF}^{MQMQA}	0.2896	0.2742	0.2633	0.2554	0.2
X_{LiCl}^{MQMQA}	0.1157	0.1312	0.1420	0.1499	0.2
X_{KF}^{MQMQA}	0.2104	0.2258	0.2367	0.2446	0.3
X_{KCl}^{MQMQA}	0.3843	0.3688	0.3580	0.3501	0.3

The pair fractions in the MQMQA approach and the Temkin model (temperature independent), for $(LiF)_{0.4}$-$(KF)_{0.1}$-$(KCl)_{0.5}$, are presented in Table 6.1 as a function of temperature. The significant deviation is primarily attributed to the interaction caused by the short-range ordering in the FNN. Furthermore, as the temperature increases, the solution becomes more disordered and are more likely to reside in their respective sites in a random manner, approaching the ideal case of random mixing described by the Temkin model. Please note that if the nominal composition is $(LiCl)_{0.4}$-$(KF)_{0.5}$-$(KCl)_{0.1}$ (as presented in the previous section), the ionic fraction of Li^+, K^+, F^-, and Cl^- in the melt will be the same with those of the example composition in the table, resulting in identical pair fractions in the MQMQA.

6.3 Equilibrium molecular dynamics simulations for Li^+, Na^+, K^+ / F^-, Cl^-

The methodology for determining thermal conductivity using equilibrium molecular dynamics (EMD) has been extensively described in previous works, along with the force field formalism used to model inter-ionic interactions. These details will not be repeated here, please refer to [124, 144, 238, 278, 295] for further information. In brief, we first carried out two series of simulations in the NPT ensemble at the target temperature of 1300 [K] to generate thermally equilibrated configurations, with the simulation time of 2 ns. Then, a new series of EMD

simulations was performed in the NVT based on the thermally equilibrated configurations obtained in the NPT simulations, with simulation time of 10 ns. In both NPT and NVT simulations, the temperature was controlled by a Nosé-Hoover thermostat, and the pressure in the NPT simulations was controlled using an extension of the Martyna barostat [297]. The relaxation times for both the thermostat and barostat were set to 0.5 ps. All simulations were performed using periodic boundary conditions and the minimum image convention.
The determination of thermal conductivity is based on the GK approach, where the Onsager phenomenological coefficients are calculated via EMD (L_{nm}), and the thermal conductivity is obtained through the autocorrelation function in thermodynamic equilibrium, defined as [98]:

$$L_{mn}(\tau) = \frac{1}{3k_B V} \int_0^\tau \langle \mathbf{J}_m(t) \cdot \mathbf{J}_n(0) \rangle \, dt \tag{6.6}$$

where n, and m are indices that can that the values e and/or z_i, corresponding to the energy current and the mass current of ion i, respectively.
The standard error associated with the thermal conductivity was calculated using a block averaging method. For a detailed explanation, refer to [298]. The number of blocks, 20, was chosen in our studies to be proportional to the total simulation time and was determined following a convergence test.
The thermal conductivity is calculated from the simulated phase trajectory using the Green-Kubo formalism [299], which enables the interpretation of thermal conductivity based on energy and charge fluctuations from EMD simulations. The total NVT run was divided into 20 blocks of 0.5 ns, and the transport coefficients were computed independently for each block. In order to ensure convergence of thermal conductivity, a correlation time (τ) of 5 ps was chosen. The thermal conductivity of a thermally equilibrated system is determined by averaging the values of all the blocks, which can be written as follows:

$$\lambda(n_{ion_i}, T) = \lim_{\tau \to \infty} \langle \lambda \ (\tau, T, n_{ion_i}) \rangle_{all \ blocks} \tag{6.7}$$

To simulate the phase trajectory, the Polarizable Ion Model (PIM) force field was employed, with parameters for the Li^+, Na^+, K^+ / F^-, Cl^- systems determined *ab initio* molecular dynamics, based on reproducing forces and dipoles obtained through DFT calculations. Notably, the PIM force field has demonstrated high accuracy in simulating both salt families, and numerous studies have utilized it to derive thermal conductivity values with remarkable precision [122, 133, 144, 152]. Three reciprocal mixtures have been simulated using the PIM EMD for the fluoride and chloride families. The simulated mixtures include (Li^+, Na^+) / (F^-, Cl^-); (Li^+, K^+) / (F^-, Cl^-); and (Na^+, K^+) / (F^-, Cl^-). To generate the phase trajectory required for extracting thermal conductivity using the Green-Kubo (GK) method at

1300 [K], well above the melting point of the pure molten salt. The simulations were performed with compositions varying in increments of 0.25 mole fraction for both cations and anions. This approach ensures comprehensive coverage of the entire compositional range of the reciprocal mixtures. In each simulation, a total of 864 ions (432 cations and 432 anions) were included, with the equilibrium volume determined by a prior simulation in the isobaric-isothermal statistical ensemble (NPT) at the corresponding temperatures and a pressure of 10^5 Pa. Two sets of NPT simulations were initially performed at the designed simulating temperature. These simulations generated thermally equilibrated configurations. Following this, a new series of EMD simulations were conducted in the canonical statistical ensemble (NVT) to determine the thermal conductivity of the mixtures, using the configurations obtained from the previous NPT simulations. The volume in the NVT simulations remained fixed.

6.4 Model of thermal conductivity for common-anion and common-cation molten salt mixtures with pair fractions ($\mathbf{X}_{C/A}$)

In our previous work [295], we proposed a thermal conductivity model for simple common-anion molten salt mixtures. The model showed a reduced thermal conductivity, which is attributed to the specific characteristics of the ions, such as the atomic masses, ionic sizes, and neighbor coupling forces between host and solute atoms. A mass fluctuation term (Γ) is included to account for the disorder effect within the short-range quasi-crystalline lattice of the liquid salt solutions. The formulation is given as follows [295]:

$$\lambda(\underline{X_i}, T) \simeq \lambda^k(\underline{X_i}, T) \left[1 - \underbrace{\sum_{i=1}^{N} \left(\frac{\lambda_i^0(T)}{\lambda^{id}(T)} \right) X_i \left(1 - \frac{M_i}{\overline{M}(\underline{X_i})} \right)^2}_{\text{Mass fluctuation } (\Gamma)} \right] \tag{6.8}$$

where $\underline{X_i}$, N, λ_i^0, λ^{id}, M_i and $\overline{M}$ represent the vector of nominal mole fractions, total number of components, thermal conductivity of the i component of pure molten salt, ideal thermal conductivity (based on the ideal mixing rule), molar mass of the i component, and the molar mass of the mixture, respectively. The thermal conductivity of molten salt mixture as a function of temperature dependence without considering the mass fluctuation term is expressed:

$$\lambda^{k}(\underline{X_i}, T) = \boldsymbol{K}(\underline{X_i})\, k_B\, n_{d\ liq}^{2/3}(\underline{X_i}, \mathbf{T_{m,i}})\, \langle c_s \rangle_{liq}(\underline{X_i}, \mathbf{T_{m,i}}) \left[1 - \alpha(\underline{X_i}, \mathbf{T_{m,i}}) \left(\gamma(\underline{X_i}, \mathbf{T_{m,i}}) + \frac{1}{3}\right)(T - \mathbf{T_{m,i}})\right], \tag{6.9}$$

where k_B, $n_{d\ liq} = (n_a \mathbf{N_A})/V(\mathbf{T_{m,i}}, \underline{X_i})$, n_a, $\mathbf{N_A}$, c_s, α, and γ are the Boltzmann constant, number density of atoms, number of atoms, Avogadro number, speed of sound, thermal expansivity and the Grüneisen parameter at the melting point ($\mathbf{T_{m,i}}$). $\boldsymbol{K}$ is an introduced material constant to characterize the complexity of the chemical nature (local structure) of unary molten salts, as established in our previous study [264]. It is defined as:

$$\boldsymbol{K} = 1 + \frac{n_s^+}{n_s^-}, \tag{6.10}$$

n_s^+ and n_s^- the number of species involved in cationic and anionic ions, respectively. For example, in the case of LiF, $\boldsymbol{K} = 1 + 1/1 = 2$, and for $NaNO_3$ $\boldsymbol{K} = 1 + 1/4 = 1.25$. For the case of polymerizing molten salts such as BeF_2, $\boldsymbol{K} = 1$.
As a result, the model can be expressed in terms of pair fractions (denoted as $X_{C/A}$), leading to the following equation for common-anion mixtures:

$$\lambda(\underline{X_{C/A}}, T) \simeq \lambda^{k}(\underline{X_{C/A}}, T) \left[1 - \sum_{C=1}^{N_C} \left(\frac{\lambda_{C/A}^{0}(T)}{\lambda^{id}(T)}\right) X_{C/A} \left(1 - \frac{M_{C/A}}{\overline{M}(\underline{X_{C/A}})}\right)^2\right] \tag{6.11}$$

Similarly, for the case of common-cation mixtures, replace $\sum_{C=1}^{N_C}$ with $\sum_{A=1}^{N_A}$. It is important to note that in our previous work [295], we validated the predicted thermal conductivity only for common-anion molten salt mixtures.

6.5 Modeling the temperature and composition dependence of thermal conductivity of reciprocal molten salt mixtures with the MQMQA

The sound velocity has been firstly evaluated using the pure molten salt model [264] as a function of temperature, rather than using its value at the melting point. The expression gives:

$$c_s = \left(\frac{\beta_T C_p}{\rho C_v}\right)^{0.5}, \tag{6.12}$$

where β_T, C_p, and C_v represents the isothermal bulk modulus, the specific heat capacity at constant pressure, and the specific heat capacity at volume constant. All these values can be obtained using the EQUILIB Module of FactSage^{TM}, which determines the equilibrium val-

ues of Cp, Cv, ρ, β_T for a salt component at a given temperature and pressure through Gibbs energy minimization [294], it also calculates all equilibrium quadruplet mole fractions. From the thermodynamic and volumetric model parameters in the FTsalt Database of FactSage^{TM}, numerical derivatives can be computed mathematically with at least 6 digital precisions of these parameters based on the value of Gibbs energy. Figure C.1 (in the Appendix C) illustrates the sound velocity calculated using the latest FTsalt Database [169, 177, 300] of FactSage^{TM} 8.4. The results show excellent agreement with the experimental measurements reported by Prissiajnyi et al. [301] as a function of composition at 1100 [K]. The supplementary materials (Appendix D1) demonstrate that we successfully reproduced the sound velocity of pure salts, common-ion mixtures, and reciprocal mixtures, achieving accuracy comparable to experimental measurements. Eventually, the λ^k can be simplified by using these temperature-dependent parameters, a general formulation can be written as follows:

$$\lambda^k(\underline{X_{C/A}}, T) = \boldsymbol{K}(\underline{X_{C/A}})\ k_B\ n_{d\ liq}^{2/3}(\underline{X_{C/A}}, T)\ \langle c_s \rangle_{liq}(\underline{X_{C/A}}, T) \tag{6.13}$$

In this general expression, the FNN pair fractions can be estimated using various methods, including EMD simulations, experimental techniques (for example, spectroscopy), and theoretical models (for example, Temkin, quasi-chemical models). The thermal conductivity values obtained from these methods differ from one another due to differences in FNN pair fractions. Compared to Equation 6.9, Equation 6.8 no longer requires the melting temperature of the pure salts.

As previously mentioned, nominal mole fractions can not be directly applied to predict the thermal conductivity of reciprocal salt mixtures, where more than one cation and more than one anion are present. Since in a reciprocal salt solution, the FNN short-range ordering interactions can be very strong between cation-anion, causing considerable deviations in the FNN pair fractions from the random mixing (Temkin model). These interactions are notably complex due to the significant impact of both FNN and second-nearest-neighbor (SNN) short-range ordering [41]. Reciprocal salt solutions of fluoride and chloride mixtures have been performed in EMD in this work, showing a clear occurrence of FNN short-range ordering. The extent of the reactions is determined by the exchange reactions of Gibbs energy ($\Delta g^{0,\ EX}$) [177, 296]:

$$AF + BCl = ACl + BF \qquad \Delta g^{0,\ EX}, \tag{6.14}$$

where A, B represent different cations.

In this paper, we extend the thermal conductivity model for common-ion mixtures to reciprocal molten salt mixtures by incorporating the FNN short-range ordering pairs within the MQMQA approach, in terms of temperature and compositional dependence. The current

model can be represented using the pair fractions in the MQMQA approach ($X_{C/A}^{MQMQA}(T)$) defined in Equation 6.5 as follows:

$$\lambda(\underline{X_{C/A}^{MQMQA}}(T),T) \simeq \lambda^{k}(\underline{X_{C/A}^{MQMQA}}(T),T)\Bigg[1-\sum_{C=1}^{N_C}\sum_{A=1}^{N_A}\left(\frac{\lambda_{C/A}^{0}(T)}{\lambda^{id}(\underline{X_{C/A}^{MQMQA}}(T),T)}\right) X_{C/A}^{MQMQA}(T)\left(1-\frac{M_{C/A}}{\overline{M}(\underline{X_{C/A}^{MQMQA}}(T))}\right)^{2}\Bigg], \tag{6.15}$$

please note that the pair fractions $X_{C/A}^{MQMQA}$ are temperature dependent at a same composition. The kinetic theory based thermal conductivity of liquid salt mixtures without considering the mass fluctuation in pair fraction is expressed:

$$\lambda^{k}(\underline{X_{C/A}^{MQMQA}}(T),T) = \boldsymbol{K}(\underline{X_{C/A}^{MQMQA}}(T))\; k_B\; n_{d\;liq}^{2/3}(\underline{X_{C/A}^{MQMQA}}(T),T)\; \langle c_s\rangle_{liq}(\underline{X_{C/A}^{MQMQA}}(T),T) \tag{6.16}$$

where $\lambda_{C/A}^{0}(T)$ represents the thermal conductivity of each pure component, determined using Equation 6.16. $\lambda^{id}(X_{C/A}^{MQMQA}(T),T)$ is the thermal conductivity calculated from the pair fractions in the MQMQA approach using the ideal mixing rule with the calculated equilibrium pair fraction vector of MQMQA. In the case of simple common-ion mixtures, where there are no interatomic interactions, pairs fractions in the MQMQA model ($X_{C_1C_2/A}^{MQMQA}$) are identical to those of nominal fractions.

6.6 Results and discussion

Most available experimental works found in the literature are on pure molten salts and some eutectic compositions of common-ion molten salt mixtures. These experimental datasets are scarce and show disagreement in their temperature dependence, which is attributed to differences in experimental techniques and measurement conditions. Various studies [39, 40, 60] emphasize that datasets exhibiting a negative temperature dependence are considered reliable. The works reported by Nagasaka et al. [38, 58, 58, 69, 72–75, 94, 236] and Harada et al. [59, 230] were selected as reliable references in our previous model development. In this work, since there are few experimental measurements of thermal conductivity for reciprocal molten salt mixtures, numerous EMD simulations have been performed to validate the developed model. Very few experimental datasets on the thermal conductivity of reciprocal molten salt solutions are available in the literature. The same methodology used in our previous work was applied [295]. Initially, we calibrated the thermal conductivity of pure molten

salts to match the EMD results for the pure salts of LiF, NaF, KF, LiCl, NaCl, and KCl. Subsequently, we assessed the thermal conductivity behaviors of reciprocal liquid solutions along with the compositions. Some common-cation mixtures were simulated meanwhile using EMD, the model was further evaluated for some common-cation mixtures (available in the supplementary materials - Appendix D2) in comparison with the common-cation mixtures simulated by EMD.

The aim of this work is to model the thermal conductivity of reciprocal molten salt mixtures in considering interatomic interactions of FNN short-range ordering between different cations and anions within melt. The predictions of the current model showed less than 20% error compared to EMD simulation results for the three reciprocal mixtures of fluoride and chloride, which demonstrated higher accuracy than the ideal mixing rule (λ^{id}). Moreover, the predictions are assessed by comparing it to available experimental data in the literature for the HITEC salt and the mixture of NaF-NaCl-KCl for solar energy application. Finally, the current model's predictive capability is further demonstrated by its capability to estimate the thermal conductivity of reciprocal molten salt PCMs, which were proposed for energy storage applications, accounting both for temperature and compositional dependence. It is expected that the current model also validates for the molten mixtures of polyatomic salt mixtures, such as nitrates, carbonates. Overall, the current model provides significant benefit in the estimation for the efficient assessment of thermal conductivity. Its potential applications include serving as a valuable reference for molten salt databases and helping to as a powerful tool for molten salt materials evaluations across diverse compositions and temperatures in industrial settings.

6.6.1 Model evaluation and validation using EMD results and experiential data

(Li^+, Na^+, K^+) / (F^-, Cl^-) reciprocal solutions

EMD simulations for three reciprocal molten salt solutions including (Li^+, Na^+) / (F^-, Cl^-), (Li^+, K^+) / (F^-, Cl^-), and Na^+, K^+) / (F^-, Cl^-) have been performed with an increment of 0.25 mole fraction of cation and anion at 1300 [K]. The EMD results have the error range of ± 15-30%. To provide a clear representation of the data's accuracy, a 20% error margin was applied to each EMD result for visualization purposes. The cations (Li^+, Na^+, K^+) and anions (F^-, Cl^-) will exchange in between, and forming LiF, LiCl, NaF, NaCl, KF, and KCl with different pair fractions. The Gibbs energy of exchange, $\Delta g^{EX}_{C_1C_2/FCl}$ has a strong impact on the equilibrium pair fractions. For example, in the case of LiF-KCl, $LiF + KCl \rightleftharpoons LiCl + KF$, $|\Delta g^{EX}_{C_1C_2/FCl}| = 57.4$ [kJ/mol] at 1300 [K], LiF and KCl pairs predominate in the melt.

a. (Li^+, Na^+) / (F^-, Cl^-) reciprocal mixture

Figure 6.2 presents the predicted thermal conductivities for the LiF-NaCl and NaF-LiCl mixtures as a function of composition. The red dashed line corresponds to predictions based on end-member parameters calibrated (λ_{cal}) to the EMD results instead of our assessed values [264]. This calibration approach provides insights into the behaviors of compositional dependence of reciprocal molten salt solutions. As shown in the sub-figures, the predictions from the present model exhibit high accuracy, closely matching the compositional trends and predicted values within a margin of 20%. The black solid line represents the model's predictions, which align well with reliable experimental datasets for the end members. Although no experimental data are currently available in the literature for the reciprocal mixture (Li^+, Na^+ / F^-, Cl^-), we are confident with reliability of the model's predictions (black solid line) with an accuracy of approximately 20%. At the nominal composition $X_{nominal} = 0.5$, the predicted thermal conductivity is identical for both molten reciprocal LiF-NaCl and NaF-LiCl mixtures, with $\lambda_{C/A}^{MQMQA} = 0.5501$ [W.m^{-1}K^{-1}], since their pair fractions are identical. In addition, both mixtures exhibit significant deviations from ideal mixing calculations. The LiF-NaCl mixture, in particular, exceeds the predicted thermal conductivity value by 57%. These deviations are attributed to the large differences in molar masses and thermal conductivities between the pure salts, which contribute to the observed discrepancies.

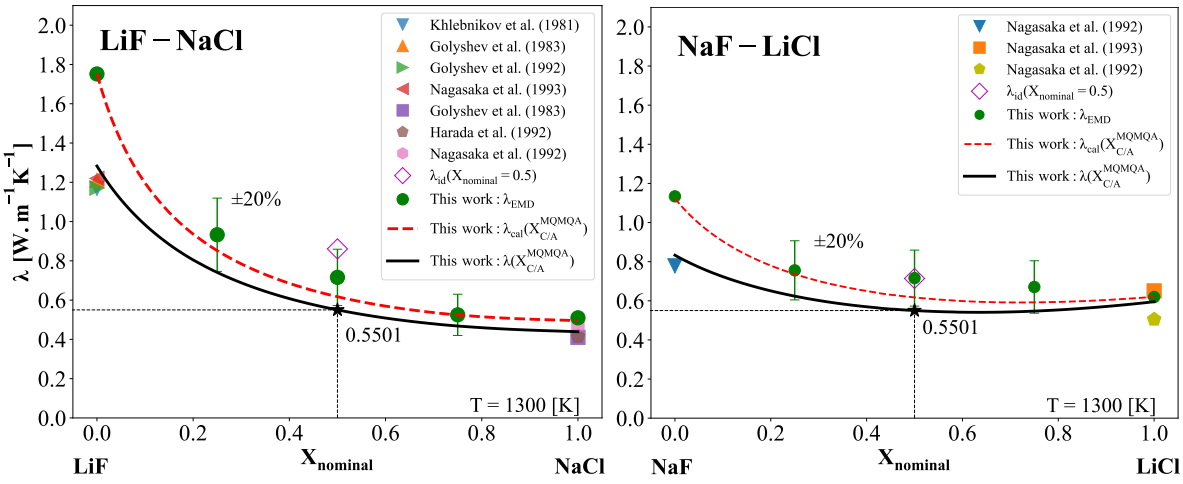

Figure 6.2 Predicted thermal conductivity values of reciprocal Li^+, Na^+ / F^-, Cl^- molten salt mixtures in comparison to EMD results and to recommended experimental results at 1300 [K] reported by Khlebnikov et al. [89], Golyshev et al. [92, 93], Nagasaka et al. [87, 94], Harada et al. [59]. At the nominal composition $X_{nominal} = 0.5$, both reciprocal mixtures have an identical thermal conductivity of $\lambda_{LiNa/FCl}^{MQMQA} = 0.5501$ [W.m^{-1}K^{-1}].

Table 6.2 presents the comparison between the ionic fractions, the pair fractions calculated by the Temkin model, and those calculated using the MQMQA approach. The results reveal notable differences between random mixing and the pair fractions in the FNN short-range

ordering of MQMQA approach. These deviations arise from the contribution of interatomic exchange of the Gibbs energy (Δg^{EX}). The magnitude of $|\Delta g^{EX}|$, determines the extent of deviation from the random mixing (Temkin model). For instance, at a nominal composition of $(LiF)_{0.5}$ – $(NaCl)_{0.5}$, the random mixing assumption predicts equal contributions of 0.25 [mol/mol] for each pure component. However, with $|\Delta g^{EX}_{LiNa/FCl}| = 35.4$ [kJ/mol] at 1300 [K] (Calculated by FactSage^{TM}), LiF and NaCl dominate in the melt, $X^{MQMQA}_{LiF} = 0.2889$ and $X^{MQMQA}_{NaCl} = 0.2889$. It is observed that the fractional difference (y) remains consistent across the components, reflecting an increase of probability of FNN cation-anion pairs from random mixing (Temkin model $X^{Temkin}_{C/A} = Y_C * Y_A$) to non-random mixing (MQMQA). For instance, as demonstrated in the example above, the relationships are $X_{LiF} = Y_{Li^+}{}^*Y_{F^-} + y$, $X_{NaCl} = Y_{Na^+}{}^*Y_{Cl^-} + y$, $X_{NaF} = Y_{Na^+}{}^*Y_{F^-} - y$, and $X_{LiCl} = Y_{Li^+}{}^*Y_{Cl^-} - y$ [296, 302], where the largest difference between two approaches is shown by $|y| = 0.0389$. Thus, the MQMQA approach offers a more accurate representation of molten salt behavior compared to the random mixing assumption by considering the effects of FNN and SNN short-range ordering interactions and $|\Delta g^{EX}_{LiNa/FCl}|$.

Table 6.2 Comparison of different ionic fractions of Li^+, Na^+ / F^-, Cl^- with their corresponding random mixing fractions and pair fractions estimated by the MQMQA approach at 1300 [K].

Cationic and anionic fractions	**Fractions**	**LiF**	**NaF**	**LiCl**	**NaCl**
0.75 Li^+, 0.25 Na^+ / 0.75 F^-, 0.25 Cl^-	Random mixing (Temkin)	0.5625	0.1875	0.1875	0.0625
	FNN per MQMQA	0.5836	0.1664	0.1664	0.0836
	Difference ($\|y\|$)	0.0211	0.0211	0.0211	0.0211
0.75 Li^+, 0.25 Na^+ / 0.25 F^-, 0.75 Cl^-	Random mixing (Temkin)	0.1875	0.5625	0.0625	0.1875
	FNN per MQMQA	0.2099	0.5401	0.0401	0.2099
	Difference ($\|y\|$)	0.0224	0.0224	0.0224	0.0224
0.5 Li^+, 0.5 Na^+ / 0.5 F^-, 0.5 Cl^-	Random mixing (Temkin)	0.25	0.25	0.25	0.25
	FNN per MQMQA	0.2889	0.2111	0.2111	0.2889
	Difference ($\|y\|$)	0.0389	0.0389	0.0389	0.0389
0.25 Li^+, 0.75 Na^+ / 0.75 F^-, 0.25 Cl^-	Random mixing (Temkin)	0.1875	0.0625	0.5625	0.1875
	FNN per MQMQA	0.2086	0.0414	0.5414	0.2086
	Difference ($\|y\|$)	0.0211	0.0211	0.0211	0.0211
0.25 Li^+, 0.75 Na^+ / 0.25 F^-, 0.75 Cl^-	Random mixing (Temkin)	0.0625	0.1875	0.1875	0.5625
	FNN per MQMQA	0.0874	0.1626	0.1626	0.5874
	Difference (y)	0.0249	0.0249	0.0249	0.0249

b. (Li^+, K^+) / (F^-, Cl^-) reciprocal mixture

Figure 6.3 compares the EMD simulation results with the calibrated predictions (red dashed line) for the reciprocal mixtures LiF-KCl and KF-LiCl, alongside the predictions of the present model (black solid line). The predictions from the current model align well with the EMD results, both in terms of compositional trends and thermal conductivity values,

with deviations within a 20% error margin. At $X_{nominal} = 0.5$, both mixtures have a same thermal conductivity value of 0.3757 [$W.m^{-1}K^{-1}$]. In the reciprocal mixture of LiF-KCl, the estimated thermal conductivity value based on the ideal mixing rule is approximately 0.8 [$W.m^{-1}K^{-1}$], which shows a significant large deviation at $X_{nominal} = 0.5$, exceeding 110%. This discrepancy arises from the substantial differences in molar masses and thermal conductivities of the end members (LiF and KCl), as well as the very important Gibbs energy of exchange within the solution. For both the LiF-KCl and KF-LiCl mixtures, the model predictions are slightly smaller than the EMD results. This dependency can be explained by two factors: 1. The EMD simulations employed the PIM method, which tends to overestimate thermal conductivity for LiF by about 38% compared to the recommended experimental data, as the non-polarizable nature of LiF. The small Li^+/F^- pair fractions in the melt may slightly increase the EMD results of the reciprocal melts. 2. The exchange of different cations and anions in the solution forms new salts, which likely helps stabilize the overall solution by reducing the mass fluctuations. For example, two new salts, LiCl and KF, are formed in the solution within the LiF-KCl melt. The overestimated LiF contributions in the EMD results may have influenced these outcomes, as a similar issue was observed in the reciprocal mixture of (Li^+, Na^+ / F^-, Cl^-). These two observations, however, require validation through further investigations with additional reciprocal mixtures.

Table 6.3 presents a comparison between the ionic fractions of the mixture and the pair fractions calculated using the MQMQA approach at 1300 [K]. Since the ionic fractions are identical to those in Table 6.3, the random mixing fractions remain unchanged and are not repeated here. However, a comparison between the two tables reveals that for the nominal composition of $(LiF)_{0.5}$ - $(NaCl)_{0.5}$, and $(LiF)_{0.5}$ - $(KCl)_{0.5}$, the pair fractions of Li^+, K^+/ F^-, Cl^- is larger than that of Li^+, Na^+ / F^-, Cl^-, which can be attributed to the greater magnitude of $|\Delta g^{EX}|$.

Table 6.3 Comparison of different ionic fractions of Li^+, K^+ / F^-, Cl^- with their corresponding random mixing fractions and pair fractions estimated by the MQMQA approach at 1300 [K].

Cationic and anionic fractions	**Fractions**	**LiF**	**KF**	**LiCl**	**KCl**
0.75 Li^+, 0.25 K^+/0.75 F^-, 0.25 Cl^-	FNN per MQMQA	0.5868	0.1536	0.1536	0.1060
0.75 Li^+, 0.25 K^+/0.25 F^-, 0.75 Cl^-	FNN per MQMQA	0.2232	0.5208	0.0329	0.2232
0.5 Li^+, 0.5 K^+ / 0.5 F^-, 0.5 Cl^-	Random mixing (Temkin)	0.25	0.25	0.25	0.25
	FNN per MQMQA	0.3140	0.1860	0.1860	0.3140
	Difference ($\|y\|$)	0.064	0.064	0.064	0.064
0.25 Li^+, 0.75 K^+/0.75 F^-, 0.25 Cl^-	FNN per MQMQA	0.2245	0.0313	0.5196	0.2245
0.25 Li^+, 0.75 K^+/0.25 F^-, 0.75 Cl^-	FNN per MQMQA	0.1122	0.1479	0.1479	0.5920

c. (Na^+, K^+) / (F^-, Cl^-) reciprocal mixture

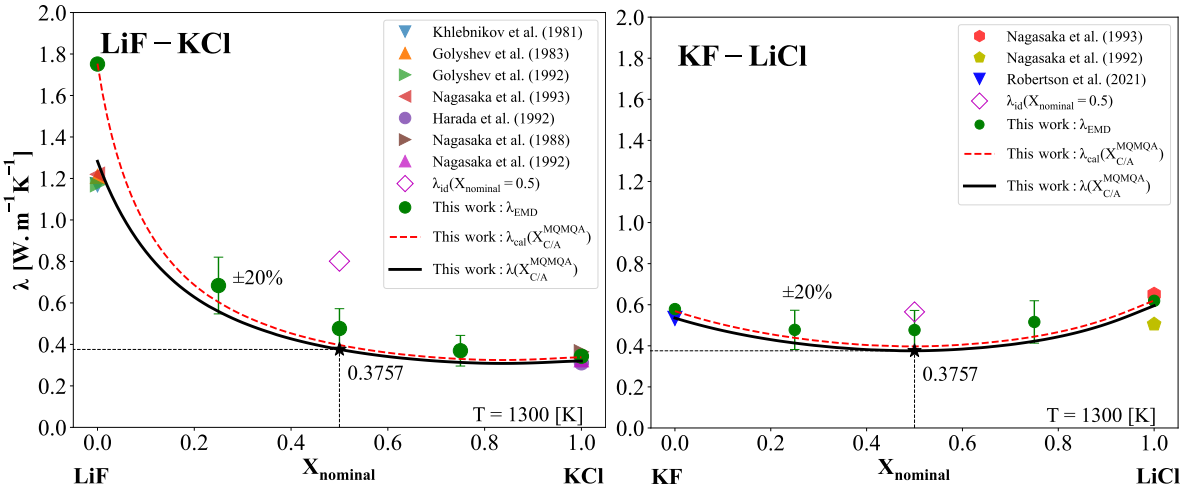

Figure 6.3 Predicted thermal conductivity values of reciprocal (Li^+, K^+ / F^-, Cl^-) molten salt mixture in comparison to EMD results and to recommended experimental results at 1300 [K] reported by Khlebnikov et al. [89], Golyshev et al. [92, 93], Nagasaka et al. [58, 87, 94], Harada et al. [59], Robertson et al. [80]. At the nominal composition $X_{nominal} = 0.5$, both reciprocal mixtures have an identical thermal conductivity of $\lambda^{MQMQA}_{LiK/FCl} = 0.3757$ [W.m^{-1}K^{-1}].

Figure 6.4 presents a comparison between the calibrated predictions (red dashed line) and the EMD results, demonstrating good agreement for both reciprocal mixtures, NaF-KCl and KF-NaCl. The black solid line represents the predictions from the present model at 1300 [K]. In the absence of LiF in the solutions, the predicted values are in closer alignment with the EMD data. In the KF-NaCl mixture, the deviation is relatively small, because of the insignificant difference in thermal conductivity between the two pure end-members and in their molar masses. Furthermore, as shown in Table 6.4, the pair fractions in this mixture exhibit less deviation from random mixing compared to the other two reciprocal mixtures, indicating a smaller Gibbs energy of exchange interaction, with $|\Delta g^{EX}_{NaK/FCl}| = 22$ [kJ/mol]. Which reveals that the effect of FNN short-range ordering on thermal conductivity is less significant in this melt.

In summary, this current model demonstrates strong predictive capability of thermal conductivity for reciprocal mixtures with high accuracy, in consistence with EMD results. However, for mixtures containing LiF, the predicted results were somewhat underestimated compared to the EMD results. This understatement may be due to the overestimated value of pure LiF, which is non-polarizable. This may also be attributed to interatomic interactions between different cations and anions, potentially reducing the effects of mass fluctuation. Overall, predictions for the three reciprocal mixtures show less than 20% error compared to EMD simulations. Consequently, this model shows promise for predicting thermal conductivity in

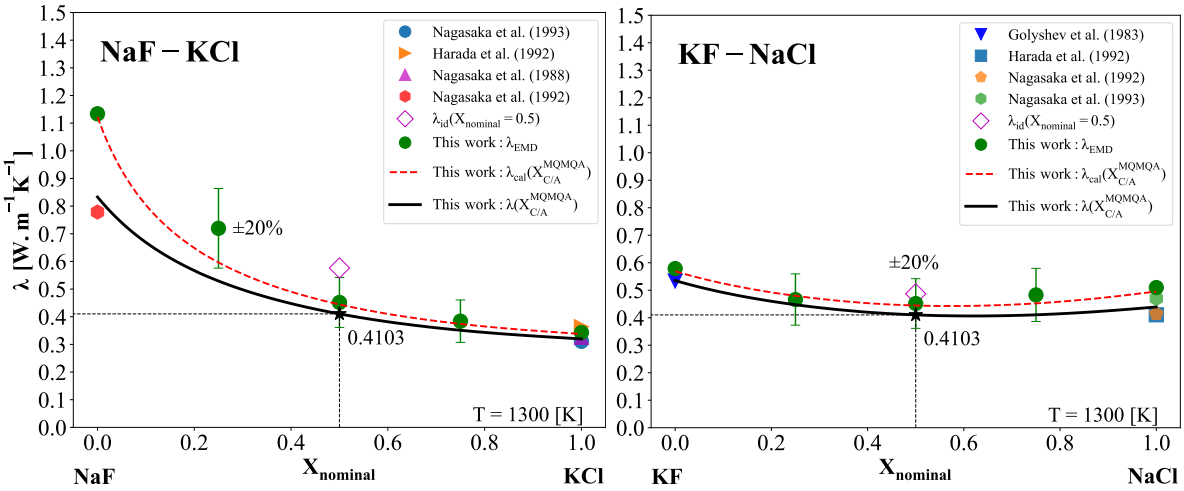

Figure 6.4 Predicted values of reciprocal Na^+, K^+ / F^-, Cl^- mixtures in comparison to MD results and two end member of reliable experimental results at 1300 [K] reported by Nagasaka et al. [58, 87, 94], Golyshev et al. [92], Harada et al. [59]. At the nominal composition $X_{nominal} = 0.5$, both reciprocal mixtures have an identical thermal conductivity of $\lambda^{MQMQA}_{NaK/FCl} = 0.4103$ [W.m^{-1}K^{-1}].

Table 6.4 Comparison of different ionic fractions of Na^+, K^+ / F^-, Cl^- with their corresponding random mixing fractions and pair fractions estimated by the MQMQA approach at 1300 [K].

cationic and anionic fractions	Fractions	NaF	KF	NaCl	KCl
0.75 Na^+, 0.25 K^+/0.75 F^-, 0.25 Cl^-	FNN per MQMQA	0.5819	0.1681	0.1681	0.0819
0.75 Na^+, 0.25 K^+/0.25 F^-, 0.75 Cl^-	FNN per MQMQA	0.2010	0.5490	0.0490	0.2010
0.5 Na^+, 0.5 K^+/0.5 F^-, 0.5 Cl^-	FNN per MQMQA	0.2759	0.2241	0.2241	0.2759
0.25 Na^+, 0.75 K^+/0.75 F^-, 0.25 Cl^-	FNN per MQMQA	0.1995	0.0505	0.5505	0.1995
0.25 Na^+, 0.75 K^+/0.25 F^-, 0.75 Cl^-	FNN per MQMQA	0.0770	0.1730	0.1730	0.5770

other reciprocal molten salt mixtures across temperatures and compositions with an error of less than 20%. In addition, it is also expected to be applicable to polyatomic salt mixtures such as nitrates and carbonates. The additional predicted compositions for these three reciprocal mixtures align with the EMD results, which are provided in the Appendix C.

Reciprocal salt mixtures in energy applications

Two reciprocal molten salt mixtures relevant to energy applications have been identified in the literature: HITEC salt ($(NaNO_3)_{0.07}$-$(NaNO_2)_{0.53}$-$(KNO_3)_{0.40}$ weight fraction, or 0.066:0.616:0.318 in mole fraction) and $(NaCl)_{0.48}$-$(KCl)_{0.36}$-$(NaF)_{0.16}$ (mole fraction). In this subsection, we evaluate the predictions of the current model by comparing them to experimental data from both mixtures.

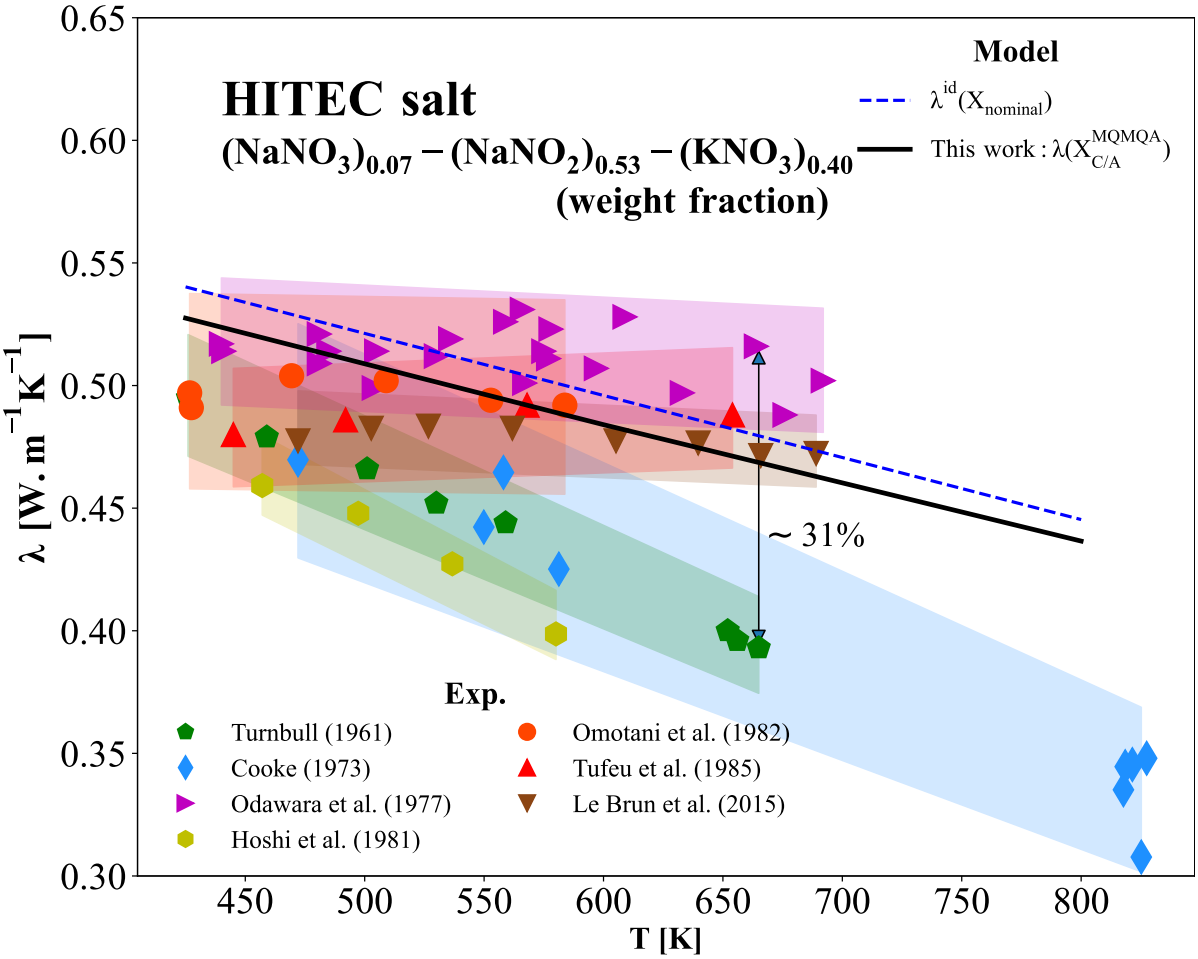

Figure 6.5 Predicted thermal conductivity values of HITEC salt mixture ($(NaNO_3)_{0.07}$-$(NaNO_2)_{0.53}$-$(KNO_3)_{0.40}$ weight fraction, corresponding to approximately 0.066:0.616:0.318 in mole fraction) in comparison to the recommanded experimental datasets reported by Turnbull [83], Cooke [66], Odawara et al. [112], Hoshi et al. [303], Omotani et al. [71], Tufeu et al. [47] and Le Burn et al. [304], as a function of temperature.

HITEC salt is one of the most interesting heat transfer fluids in heat recovery process since several decades, it was also the HTF in the test concentrating solar power in Themis [305, 306]. Various experimental measurements of thermal conductivity have been performed since half a century. In Figure 6.5, we can observe that these experimental results showed a non-positive slope with temperature, which were considered as reliable measurements. The HITEC salt mixtures consists of Na^+, K^+, NO_3^-, and NO_2^-, as both the cations and anions are neighbouring elements, relatively heavy ions. The mass fluctuation term (Γ) is relatively small. In the MQMQA approach, the pair fractions are 0.2442 for $NaNO_3$, 0.2671 for KNO_3, 0.3139 for $NaNO_2$, and 0.1748 for KNO_2 at 430 [K]. In comparison, the pair fractions in Temkin model are 0.285, 0.226, 0.273, 0.216, respectively. The predictions of the current

model are represented by the black solid line, compared to the solution based on the ideal mixing rule. As shown in the figure, the predictions of the current model are consistent with the ideal mixing rule. It is worth noting that the model demonstrates better accuracy, showing excellent agreement with the experimental results reported by Odawara et al. [112], Omotani et al. [71], and Le Brun et al. [304]. This is to be understood within the challenging context of experimentally determining thermal conductivity at high temperatures, where even recommended datasets can show deviations of up to 31% for the HITEC salt between investigators for the HITEC salt. Even more so, if the measurements were conducted under ambient conditions, $NaNO_2$ is unstable in the presence of air (O_2) at high temperatures, leading to the formation of $NaNO_3$ instead of maintaining the initial weight fractions, which will could further distort the result.

The ternary NaCl-KCl-NaF eutectic salt mixtures was proposed by Wang et al. [307] for the design of a thermo-economical candidate PCMs for next generation CSP plants with supercritical CO_2 Brayton cycle. The thermal diffusivity (α_{dif}) of this salt mixture was experimentally measured using the laser flash analysis technique. The thermal conductivity was then calculated [307] using the corresponding equation $\lambda = \rho\ Cp\ \alpha_{dif}$.

A comparison between experimental measurements and the current model's predictions is shown in Figure 6.6. The experimental data show a pronounced positive temperature dependence, with values near the melting point approximately 100% higher than our model predictions. These results may be unreliable, as DiGuilio and Teja [39] noted that datasets indicating a positive temperature dependence in thermal conductivity are potentially inaccurate. For reference, thermal conductivities for the four pure salts from the work of Nagasaka et al. [87, 94, 100] and the ideal mixing rule solutions are also included, starting from their respective melting temperatures. The experiments by Nagasaka and co-workers are widely regarded as reliable by multiple studies [39, 40, 60]. Interestingly, all pure salts exhibit a clear negative temperature dependence, consistent with expected behavior. The pair fractions in the MQMQA approach of each component in this mixture are 0.1185 for NaF, 0.5215 for NaCl, 0.0415 for KF, and 0.3185 for KCl at 1000 [K]. In comparison, the pair fractions estimated by Temkin model are 0.1024, 0.5376, 0.0576, 0.3024, respectively. The predicted results exhibit negative temperature dependence. Furthermore, the values for the mixture lie between those of the pure salts. Based on these findings, we are confident that the current model provides reliable predictions for the ternary mixture $(NaCl)_{0.48}$-$(KCl)_{0.36}$-$(NaF)_{0.16}$, which are likely more accurate than the experimental results.

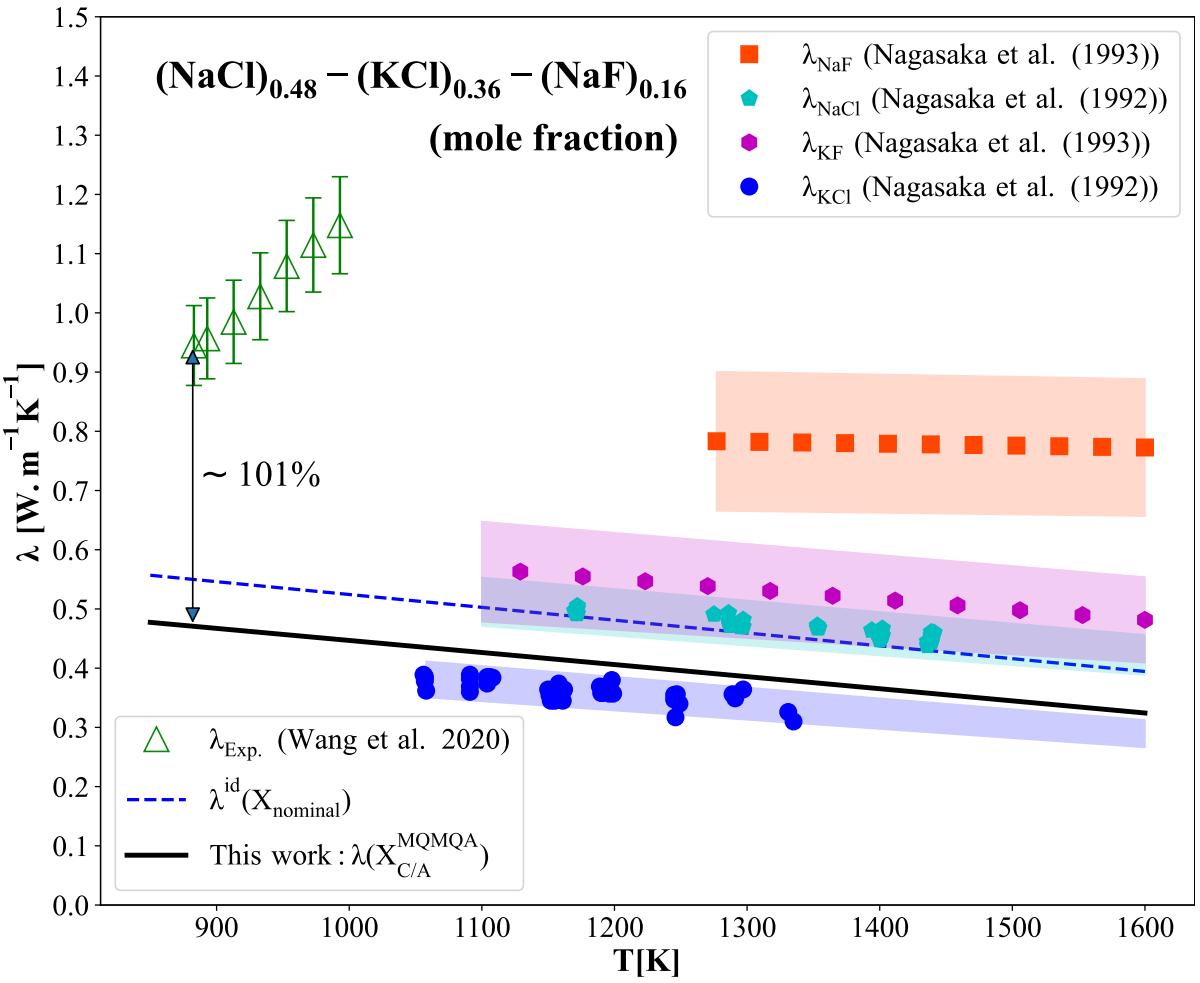

Figure 6.6 Predicted thermal conductivity values for the ternary salt $(NaCl)_{0.48}$-$(KCl)_{0.36}$-$(NaF)_{0.16}$ (mole fraction) molten mixture compared with recommended experimental data four pure salts reported by Nagasaka et al. [87, 94] as a function of temperature.

6.6.2 Thermal conductivity predictions for molten salt PCMs

Thermal energy storage system is one of the most critical systems that makes renewable energy plants such as PV, wind, and CSP that provide stable and dispatchable power generation. Nowadays, it has become popular also integrating into conventional power plants to improve the thermal cycle efficiency. Molten salt thermal energy storage systems using PCMs feature a high energy density at high temperatures. However, thermal conductivity, as the key parameter that determines the charging/discharging performance, their knowledge is still very limited. Opolo et al. [308] and Lin et al. [309] reviewed the different molten salts that serve as latent heat thermal energy storage medium. Unfortunately, some of thermal conductivity values are not available, particularly for the reciprocal molten salt mixtures, such as the thermal conductivity values of the eutectic compositions of $LiNO_3$-NaCl, $LiNO_3$-

KCl, and Na_2CO_3-NaCl-KCl, are unavailable either experimentally or as estimates. Here, we would like to employ the current model to predict the liquid salt as temperature and composition dependence. In the reciprocal mixture of $LiNO_3$-NaCl, the solution products are

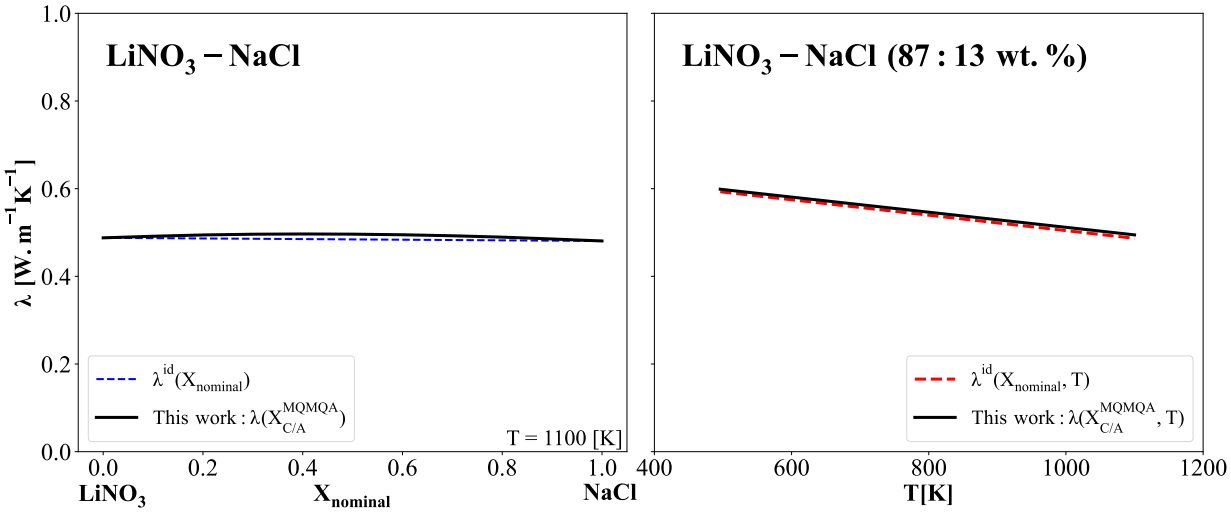

Figure 6.7 Predicted thermal conductivity values for reciprocal $LiNO_3$-NaCl molten mixture as a function of composition at 1100 [K] and temperature dependence for the designed composition of 87:13 w.t% or 0.85:0.15 in mole fraction.

LiCl, $LiNO_3$, NaCl, $NaNO_3$ (other products such as $NaNO_2$, $NaClO_4$, $LiNO_2$, and $LiClO_4$ are listed in the FTsalt Database, but their concentrations appear to be negligible, on the order of 10^{-7}, therefore, they were neglected in the predictions.). Figure 6.7 presents the predicted values as a function of composition and temperature. The temperature was set to 1100 [K], slightly above the melting point of NaCl. Composition-dependent behavior closely follows the ideal mixing rule, as the molecular weights and thermal conductivities of the four components show no significant differences. A very slight positive deviation may arise from minor inaccuracies in the input properties. The predicted thermal conductivity of $LiNO_3$-NaCl (87:13 wt.%) mixture at 496 [K] is to be approximately 0.599 [$W.m^{-1}K^{-1}$]. At this temperature, the FNN pair fractions in the MQMQA model are 0.1072 for LiCl, 0.7429 for $LiNO_3$, 0.0427 for NaCl, and 0.1072 for $NaNO_3$.

Figure 6.8 illustrates a similar reciprocal salt mixture, $LiNO_3$-KCl, showing the predicted values as a function of composition and temperature. The predicted values align closely with the behavior described by the ideal mixing rule, because of the close values of the molecular weights and thermal conductivities. These outcomes further support the statement that molten mixtures of lithium, sodium, and potassium nitrate salts can be estimated with good accuracy using the ideal mixing rule, as reported by DiGuilio and Teja [39]. The thermal conductivity of $LiNO_3$-KCl (58.1:41.9 wt.% or 0.6:0.4 in mole fraction) is approximately

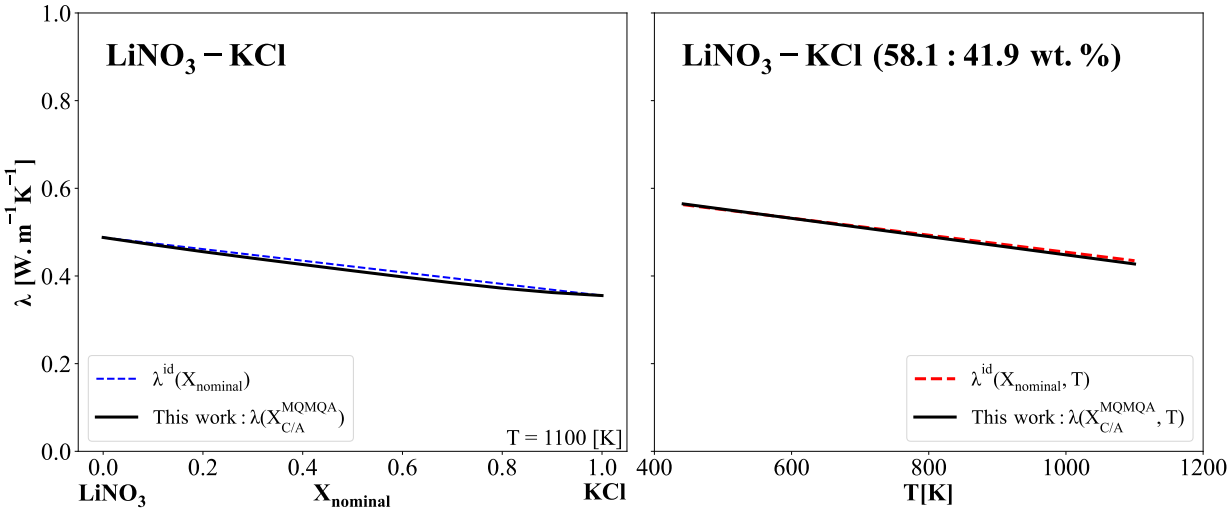

Figure 6.8 Predicted thermal conductivity values for reciprocal $LiNO_3$-KCl molten mixture as a function of composition at 1100 [K] and temperature dependence for the designed compositionof 58.1:41.9 wt.% or 0.6:0.4 in mole fraction.

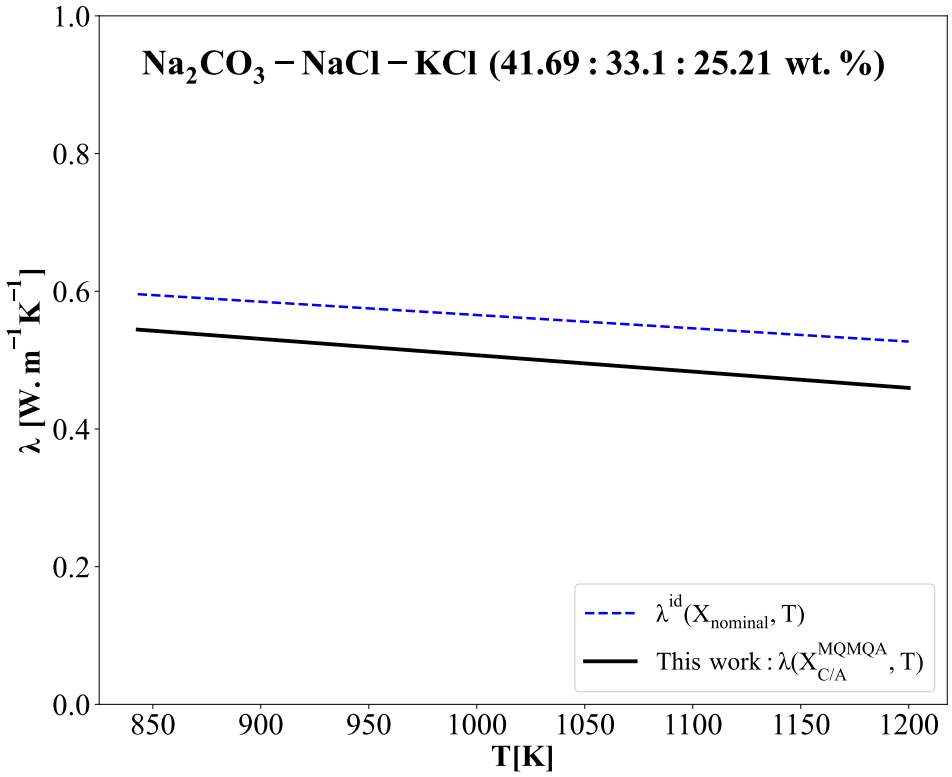

Figure 6.9 Predicted thermal conductivity values for reciprocal Na_2CO_3-NaCl-KCl (41.69:33.1:25.21 wt.% or 0.303:0.436:0.261 in mole fraction) molten mixture as a function of temperature for the designed composition compared to the ideal mixing rule estimations.

0.564 [$W \cdot m^{-1}K^{-1}$] at 445 [K]. The FNN pair fractions obtained from the MQMQA model at this temperature are 0.2180, 0.3819, 0.1821, and 0.2180 for LiCl, $LiNO_3$, KCl, and KNO_3, respectively.

The last reciprocal mixture examined consists of ternary mixtures of Na_2CO_3-NaCl-KCl with a composition of 41.69:33.1:25.21 wt.% or 0.303:0.436:0.261 in mole fraction. In the MQMQA model, the FNN pair fractions at 845 [K] are 0.4070 for NaCl, 0.3036 for Na_2CO_3, 0.2093 for KCl, and 0.0802 for K_2CO_3. The thermal conductivity values are approximately 10% lower than those predicted by the ideal mixing rule, as shown in Figure 6.9, which primarily results from the significant mass and thermal conductivity difference between carbonate salt and chloride salt, as well as the FNN pair fractions. The thermal conductivity at 845 [K] is estimated to be approximately 0.544 [$W.m^{-1}K^{-1}$]. The predictions of the current model could be assumed comparable to reliable experimental measurements. Further experimental work is recommended to support our predictions.

6.7 Comparisons of predictions from the present model and previous model

In our previous models [264, 295] for estimating thermal conductivity, parameters such as thermal expansivity, bulk modulus, Grüneisen parameter, sound velocity, etc were evaluated at the melting point rather than at the actual molten salt temperature. In this work, we consider the actual temperature and estimate these parameters by incorporating additional models. Which not only simplifies the application but also leads to a more accurate estimation of thermal conductivity.

To further emphasize the predictive capability and accuracy of the current model, we will compare the predicted thermal conductivity of randomly selected pure molten salts and common-anion molten salt mixtures with the values obtained from previous models [264,295]. Figure 6.10 compares the thermal conductivity predictions from the current model (black solid line) with those from the previous model for pure molten salts (red dashed line). The comparison is made for four pure unary salts: monovalent LiF, divalent $MgCl_2$, and lithium carbonate, and sodium nitrate. The analysis of the experimental datasets is not repeated here, please refer to the previous work [264]. These four sub-figures demonstrate that the predicted accuracy is consistent with the previous model. However, the predictive capability of the current model is enhanced, as it does not require the melting temperature, unlike the previous model. This feature is particularly advantageous for molten salt mixtures, as their liquidus temperature is typically lower than the melting temperature of pure salts.

The predicted thermal conductivity from the current model (black solid line) is shown in Figure 6.11 for two commonly studied common-anion molten salt mixtures: Li_2CO_3-Na_2CO_3 (composition dependent) and FLiNaK (temperature dependent). The predictions are com-

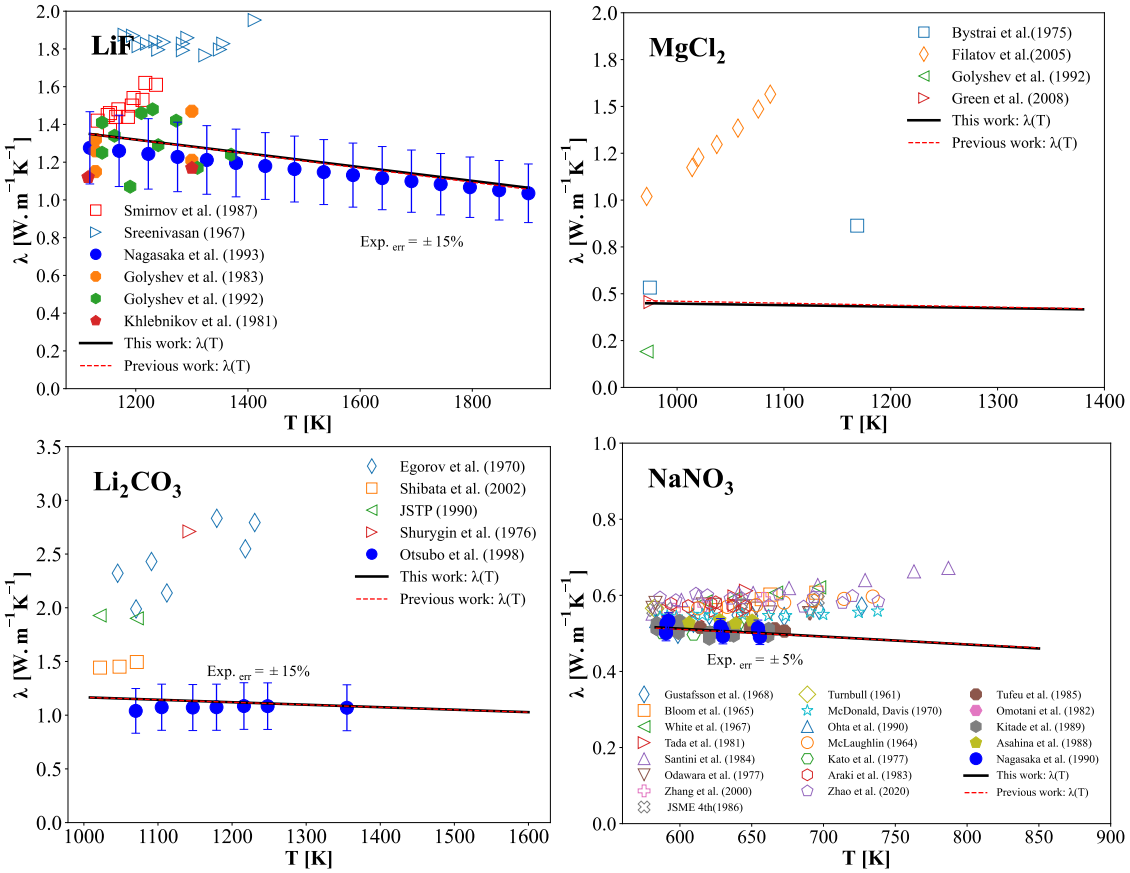

Figure 6.10 Predicted thermal conductivity for four pure molten salts of monovalent LiF, divalent $MgCl_2$, Li_2CO_3, and $NaNO_3$ using the present model, compared to previous work [264], and experimental works reported by Smirnov et al. [56], Sreenivasan [88], Nagasaka et al. [94, 100], Golyshev et al. [92, 93], Khlebnikove et al. [89], Bystrai et al. [96], Filatov et al. [99], Green et al. [242], Egorov et al. [54], Shibata et al. [101], Shurygin et al. [97], Otsubo et al. [75], Gustafsson et al. [103], Bloom et al. [55], White et al. [49], Tada et al. [230], Santini et al. [64], Odawara et al. [112], Zhang et al. [106], JSME [102], Turnbull [83], McDonald and Davis [50], Ohta et al. [107], McLaughlin [84], Kato et al. [63], Araki et al. [65], Zhao et al. [109], Tufeu et al. [47], Omotani et al. [71], Kitade et al. [69], and Asahina et al. [110].

pared with those obtained from the previous model for common-anion molten salt mixtures (red dashed line) [295]. Both mixtures show results that closely align with previous work. However, the FLiNaK mixture exhibits a slight deviation at high temperatures (above 1200 [K]), which may be attributed to the assumption of ideal linear variation in the composition of thermal expansion and isothermal compressibility in the previous model. Indeed, the current model appears to be more consistent with the recommended experimental data for FLiNaK. In the Li_2CO_3-Na_2CO_3 mixture, it can be observed that the deviations are identical to the results obtained from the previous model. This, in turn, explains that the pair frac-

tions in the MQMQA approach used in the current model are equal to the nominal fractions for common-ion molten salt mixtures. In other words, the current model is identical to the previous model for common-ion molten salt mixtures. Overall, the present model has shown enhanced predictive capability and improved accuracy.

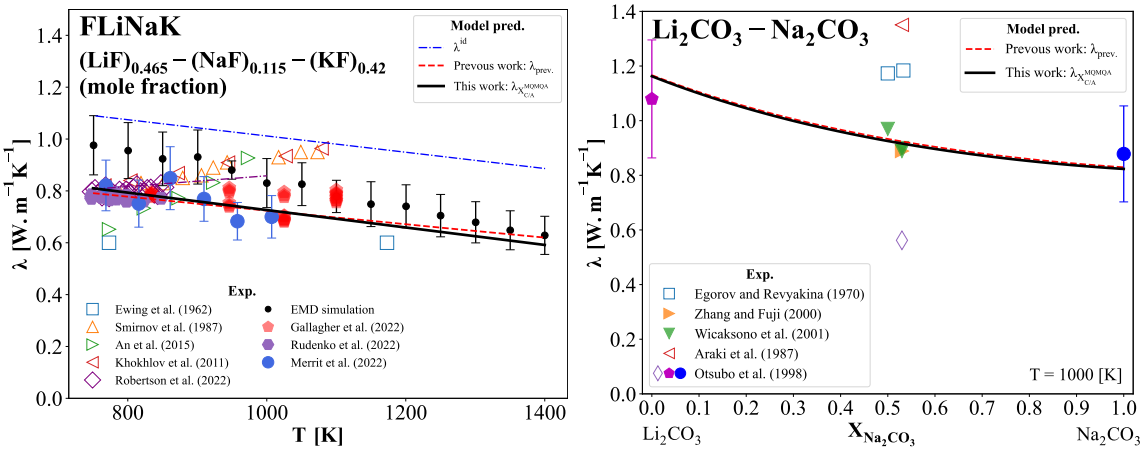

Figure 6.11 Predicted thermal conductivity of common-anion molten salt mixtures of FLiNaK as a function of temperature, and Li_2CO_3-Na_2CO_3 as a function of composition at 1000 [K]. The predictions of the present model (black solid line) are compared with the previous model (red dashed line) [295], and experimental works reported by Ewing et al. [198], Smirnov et al. [56], An et al. [76], Khokhlov et al. [267], Roberston et al. [80], Gallagher et al. [61], Rudenko et al. [86], Merrit et al. [200], Egorov et Revyakina [54], Zhang and Fuji [291], Wicaksono et al. [271], Araki et al. [65], and Otsubo et al. [75]. The datasets for FLiNaK reported by Lane et al. [270] and Janz [34] are not included in the figure.

6.8 Conclusion

In this study, we extended our previously developed kinetic-based thermal conductivity model, initially developed for common-anion mixtures, to include reciprocal molten salt mixtures. This extension incorporates the effects of FNN short-range ordering interactions between cation-anion pairs, using the MQMQA approach. This adaptation is crucial because directly applying nominal mole fractions to reciprocal salt mixtures poses a fundamental challenge: a specific (equivalent) ionic fraction can correspond to an infinite number of possible nominal mole fractions in reciprocal salt solutions.

Thermal conductivity is one of the most difficult parameters to determine, both experimentally and through EMD simulations. Only two experimental studies on reciprocal mixtures were found in the literature, and there is currently no model available that describes the thermal conductivity of reciprocal molten salt mixtures. Numerous EMD simulations of Li^+, Na^+, K^+ / F^-, Cl^- mixtures were conducted to validate the present model. The predicted

results showed good agreement with EMD results, with a predictive error of up to 20%. The predictions for HITEC salt align well with reliable experimental measurements, confirming the model's suitability for polyatomic reciprocal salt mixtures.

The model requires only a few thermophysical parameters, such as heat capacity, density, and sound velocity, and exhibits strong predictive capabilities for reciprocal salt mixtures, also including both common-anion and common-cation mixtures. This was demonstrated through its predictions of thermal conductivities for reciprocal molten salt PCMs suggested in the literature as a function of composition and temperature. We expect that the current model will also be able to predict thermal conductivity in other heavy-ion and complex anionic reciprocal salt mixtures. We believe that this work will make a significant contribution to the assessment of thermal conductivity in molten salt mixtures for engineering applications, providing valuable reference data for molten salt databases. Future work will focus on extending the model to molten salt solid solutions.

6.9 Acknowledgments

The authors would like to thank Dr. Christian Robelin and Dr. Kun Wang for valuable discussions on the MQMQA approach. This research was supported by the Natural Sciences and Engineering Research Council of Canada (NSERC) [funding reference number: RGPIN-2021-03279]. This research was enabled in part by support provided by Calcul Québec (www.calculquebec.ca) and the Digital Research Alliance of Canada (alliancecan.ca)

CHAPTER 7 GENERAL DISCUSSIONS

The developed model is based on the kinetic theory of thermal conductivity for molten salts and aims to provide reliable predictions for various industrial applications, including metal and materials production, MSR, CSP, TES in advanced energy systems. Accurate knowledge of the thermal conductivity of molten salt mixtures is essential for optimizing heat transfer efficiency, ensuring operational safety, and achieving cost-effectiveness.

This model overcomes the limitations associated with determining the thermal conductivity of molten salts through experimental techniques or numerical estimations. In particular, it addresses challenges in industrial processes where temperature and composition changes frequently occur, for instance in metal production and recycling, MSRs, or HTFs in CSP systems. Furthermore, the model addresses the gaps related to the reliance on empirical fitting constants specific to a given salt family, which often neglect interatomic interactions. This research focused on 58 salts commonly used in industry, including halides, divalent halides, carbonates, nitrates/nitrites, sulfates, and hydroxides, as well as their mixtures.

In this thesis, we focus on developing a theoretical model for the thermal conductivity of molten salts, while omitting an examination of convective, and radiative heat transfer mechanisms. As mentioned earlier in introduction chapter, these two heat transfer mechanisms depend on extrinsic quantities, which are defined by the external factors of the geometry of the system, the materials of container, the temperature, and other variables, each of them have their own degree of importance on the rate of heat transfer.

In the convective heat transfer mode, the heat transfer coefficient (h [W.m^{-2}]) of the system depends on the thermal conductivity of the fluid, as seen from the Nusselt relationship ($Nu = h_{cv}L/\lambda$). In industrial applications, forced convection is typically presence, and the Nusselt number is also directly defined by the Reynolds number, Prandtl number, and an empirical constant of flow and geometry. Various convection correlations for flow in circular pipes can be referred to Kuchibhotla et al. [310]. Let's consider again the molten salt receiver during the operation, where the molten salt heat exchange tube surface receives as high as approximately 1.5 [MW$_{th}$.m^{-2}] of heat flux in certain areas from solar field, it is sensitive to damage due to the relatively low thermal conductivity of the molten solar salt, with our estimation around 0.443 [W.m^{-1}K^{-1}] at 500°C with de developed model. The heat transfer coefficient is given by $h = -\lambda_{MS}(dT/dy)_w/(T_w - T_{MS})$ (w denotes wall) [311], as seen to increase the performance of molten salt receiver, either by increasing the temperature gradient ($(dT/dy)_w$) or increasing the thermal conductivity of the fluid (λ_{MS}), since the maximum input heat flux is limited due to the receiver tube material and the temperature

of decomposition of solar salt. However, increasing the temperature gradient will obviously increasing the friction along the pipe, leading to higher pumping power consumption [311]. Let's make a rough calculation to assess the importance of the thermal conductivity of the HTF in influencing the molten salt receiver's performance. In a commercial molten salt power plant, we assumed that the velocity of the fluid in the tube is 2 [m/s] to ensure turbulent flow, and the tube diameter of 0.0508 [m], the density, heat capacity and viscosity values are taken from Zavoico [312]. The Dittus-Boelter equation ($Nu = 0.023Re^{0.8}Pr^{0.4}$) was applied to determine the Nusselt number, from which we can determine the heat transfer coefficient, is approximately h = 4724 [W.m^{-2}K^{-1}]. If the thermal conductivity of the molten molten is 0.51 [W.m^{-1}K^{-1}] (which is the minimum requirement of new molten salt HTF development in the US [313]) at 500°C, heat transfer coefficient is about 5140 [W.m$^{-2}K^{-1}$]. The thermal conductivity of molten salt is expected to be as high as possible, when λ_{MS} = 1 [W.m^{-1}K^{-1}], the heat transfer coefficient can reach 7700 [W.m^{-2}K^{-1}]. This increased heat transfer coefficient can be potentially reducing the receiver damage. In addition, the reported thermal conductivity of solar salt by Zavoico [312] is 0.538 [W.m^{-1}K^{-1}] at 500 °C, which is approximately 21% larger than our estimation, and has a positive temperature dependence. These deviations will prevent the receiver from achieving the nominal power capacity and may potentially put the receiver in unsafe operation, for example overheating. Please note that the correlation of the Nusselt number depending of the characteristics of the heat exchanger. Here, it is just a simple demonstration of the important role of the HTF in the heat transfer engineering application.

7.1 Thermal conductivity model for pure molten salts

The development of the model followed three sub-objectives presented earlier. The first objective was to establish an accurate model for the thermal conductivity of pure molten salts, which would serve as a foundation for further developments in the model of molten salt mixtures. After evaluating various modeling approaches, the lower minimum thermal conductivity model in the classic kinetic theory was selected for this research. A key parameter ($\boldsymbol{K}$) was introduced into the model to describe the degree of complexity of chemical nature of the salt. This parameter (dimensionless) is directly related to the ratio of the number of atoms of the salt to the number of anionic species, it is not a fitting parameter and varies between 1 to 2, with $\boldsymbol{K} = 2$ for monovalent salts, and $\boldsymbol{K} = 1$ for the polymerized salts.
To validate the model, hundreds of experimental datasets were collected and carefully analyzed. The datasets from Nagasaka and co-workers [38, 58, 72, 87, 94, 100, 236] and Harada and colleagues [59] were identified as the most suitable for the validating the developed model. These datasets exhibited a characteristic negative temperature dependence, which

was recognized as an indicator of reliable experimental measurements [39].

Since the experimental measurements are conducted at high temperatures, the contribution of conduction, convection, and radiation heat transfer influence the observed thermal conductivity, often resulting in larger values. Conduction losses primarily arise from the improper design of the apparatus, where heat escapes through its structural components. Additionally, the fluid density decreases at high temperatures, resulting in significant heat transfer through convection. Radiation can also contribute a major portion of heat transfer at high temperatures, which is reflected in a positive temperature dependence of thermal conductivity, with the slope influenced by the emissivity of the container walls [57, 92].

These factors challenge the accurate determination of the rate of heat transfer and become significant as the measurement temperature increases [40]. To reduce radiative heat transfer, researchers have applied materials with low emissivity coefficient around 0.02, such as silver or platinum, and minimized the measurement gap. Despite these precautions, some experimental thermal conductivity values still exhibit a positive temperature dependence in recent studies [76, 80, 307].

In the first study, we applied the Bland-Altman method to evaluate the accuracy of the model in comparison to experimental datasets for 25 salts reported by Nagasaka et al. and Harada et al. These salts include monovalent and complex compounds such as fluorides, chlorides, bromides, iodides, carbonates, and nitrates. The mean relative error of the model was 9.33% for Nagasaka et al. and 8.04% for Harada et al. with respect to these experimental datasets, while the experimental measurement error reported by Nagasaka averaged around 15%.

Two salts fell outside the 95% confidence interval: KI, which was 38% higher than the value reported by Nagasaka et al., but showed only a 3.5% deviation from Harada et al.'s data. Conversely, RbI matched the Nagasaka dataset with no deviation but exhibited about a -12% difference from Harada's data. These discrepancies highlighted the challenges in accurately determining the thermal conductivity of molten salts experimentally.

In general, the model demonstrated its reliability in predicting the thermal conductivity of monovalent molten salts, with an estimated error around $\pm 15\%$. The accuracy of this model depended on the precision of the following properties: heat capacity, density, thermal expansivity, and sound velocity. In this study, all of these properties were obtained through FactSage^{TM} with the FTsalt Database version 8.4.

We extended our evaluation to include thermal conductivity predictions at melting temperatures and their temperature dependence by comparing them against experimental datasets available in the literature. In some cases, predictions slightly overestimated the thermal conductivity at the melting point, particularly for certain iodide and carbonate compounds, such as KI and K_2CO_3. These discrepancies could be attributed to the input parameters

for thermo-physical properties and/or the intrinsic uncertainties within the experimental measurements. Importantly, the predictive accuracy of the model was within the range of experimental uncertainties reported in the literature, thereby assuring its reliability.
Specifically, the temperature dependence of thermal conductivity for carbonate salts (Li_2CO_3, Na_2CO_3, and K_2CO_3) showed minimal variation according to the reported experimental data, which were almost independent of temperature $(\partial\lambda/\partial T)_P \simeq 0$. However, our predictions exhibited a negative temperature dependency of thermal conductivity for these salts. This discrepancy may explained by some unpredictable errors during the experimental measurements.
For molten nitrate salts, such as $NaNO_3$ and KNO_3, experimental datasets consistently showed a negative temperature dependence, which aligned with the expected trend and our predictions. The results established the accuracy and predictive capability of thermal conductivity for pure molten salts, while additional investigations are recommended to clarify these observed inconsistencies. Since the polyatomic salts (nitrate salts) are less stable than monoatomic salts (for example, NaCl), nitrate salts can potentially decompose to nitrite salts (NO^{2-}) at higher temperature, which affects the values obtained in the temperature dependence.
The model is expected to have similar predictive capabilities for other salt families, and has been successfully validated across various salt families, including monovalent halides, divalent halides, carbonates, nitrates, nitrites, sulfates, and hydroxides. The predictions are generally reliable and comparable to the recommended experimental datasets. However, some thermal conductivity values may be slightly under or overestimated due to a lack of accurate thermo-physical property data. For example, $BeCl_2$, $MgBr_2$, MgI_2, and CaI_2, whose sound velocity data is unavailable in the literature, had their sound velocity values estimated through linear extrapolation using other salts in the same family. Therefore, improving the accuracy of input thermo-physical properties will enhance the precision of the model's predictions.

7.2 Extending the molten salt thermal conductivity model for pure salt to common-ion molten salt mixtures

Secondly, we developed a model for simple common-ion molten salt mixtures based on previous work discussed in Chapter 4. In molten salt mixtures, variations in ion mass, size, and inter-ionic coupling forces could lead to a reduction in thermal conductivity. This reduction is largely due to mass fluctuations and the varying thermal conductivities of the pure salt components within the mixture. Given the scarcity of experimental data for molten salt mixtures, we performed hundreds of EMD simulations using PIM for various compositions,

including common-anion mixtures of fluorides, chlorides, bromides, and iodides (chapter 5). The developed model was validated against both EMD results and available experimental datasets. The results showed good agreement with EMD simulations and a significant improvement over the commonly used ideal linear mixing rule, through comparative analysis of common-anion mixtures of different salt families, including fluorides, chlorides, bromides, iodides, nitrates, and carbonates. We found that the primary factors influencing the thermal conductivity of salt mixtures are the molecular mass and the thermal conductivity of the end-members. Both factors play an important role in determining the deviation from the ideal mixing rule.

For instance, for binary fluoride mixtures such as LiF-NaF and NaF-KF, the model generally predicted a near-linear relationship between composition and thermal conductivity, meaning that a proportional variation in thermal conductivity with mixture compositions. However, the LiF-KF mixture demonstrated notable deviations from this trend due to the substantial difference in mass between lithium and potassium ions. This mass difference resulted in a less straightforward thermal conductivity trend, reflecting how the molar mass disparity between constituents affects ideal linear behavior. Moreover, the thermal conductivity of their end-members also contributed to the deviation.

Interestingly, the binary chloride mixtures exhibited smaller deviations from linearity compared to binary fluoride mixtures with same cationic compositions. This can be attributed to the lower mass ratio ($M_i/\overline{M}$), as the molar mass of chloride anion is heavier than fluorine. This observation suggests that a heavier anionic molar mass reduces variations in thermal conductivity along with its compositional dependence, a trend consistent with other salt families examined in this study. Notably, the model's predictions showed good agreement with empirical data from Merritt et al. [200] for the LiCl-KCl mixture, further supporting the model's reliability for this chloride mixture. As the anionic mass increases further in the binary mixtures of bromides (LiBr-NaBr,LiBr-KBr, NaBr-KBr, and RbBr-CsBr) and iodides (LiI-NaI, LiI-KI, NaI-KI, and RbI-CsI), the deviation from linearity was observed to be much smaller than in the fluorides.

The model was expected to be applicable to common-anion of polyatomic anions mixtures such as nitrates, carbonates, and sulfates. As the anionic mass increased, with less variation in the cationic masses and the thermal conductivity of pure $NaNO_3$ and KNO_3, the compositional dependence of their mixtures exhibited a near-linear behavior. This explains why the ideal mixing rule is feasible for estimating the thermal conductivity of $NaNO_3$-KNO_3 mixtures that suggested by DiGuilio [39]. However, when considering mixtures between $LiNO_3$ and $CsNO_3$, both the cationic masses and the thermal conductivity of the pure salts have significant differences, the deviations can reach as much as -100%. On the other hand, ex-

perimental datasets for carbonate mixtures were very sparse with limited data available. It was challenging to verify the current model's reliability for molten carbonate mixtures. The same issue has occupied in the modeling of pure molten carbonate salts. Nevertheless, we believe the model can still provide reasonable accuracy for carbonates as well. Additional experimental work is recommended to validate our predictions for carbonate mixtures.
The analysis of fluoride, chloride, bromide, iodide, and nitrate salt mixtures revealed a general trend where thermal conductivity of molten salt mixtures varied linearly with composition in mixtures composed of components with similar molar masses. Deviations from linearity were predominantly observed in the mixtures where there were significant disparities in molar mass between the constituents, such as Li-K/X, Li-Rb/X, or Li-Cs/X pairs. This effect was most pronounced in mixtures with large differences in cationic mass and thermal conductivity of the end-members.

The study included the validation of the current model for common-cation mixtures. Over a hundred EMD simulations were performed due to the lack of experimental datasets on common-cation mixtures. The common-cation binary mixtures included LiF-LiCl, LiF-LiBr, LiF-LiI, LiCl-LiBr, LiCl-LiI, NaF-NaCl, NaF-NaBr, and KF-KCl. Overall, the model's predictions aligned well with the EMD results, as observed in the mixtures of light anions such as LiF-LiCl, NaF-NaCl, and KF-KCl. This alignment demonstrated the model's ability to capture the thermal conductivity behavior across various compositions, highlighting its accuracy in predicting the common-cation and common-anion mixtures with similar ionic masses.
However, large deviations occupied in mixtures that contains heavier anions like Br^- and I^-, where the EMD results displayed greater instability and dispersion. This discrepancy likely arose from the significant mass differences among the ions, potential inaccuracies in the force field parameters for Br^- and I^- ions, or insufficient relaxation time during the EMD simulations. Thus, the thermal conductivity values for LiF-LiBr and LiF-LiI mixtures were slightly larger compared to other common-cation mixtures. Nevertheless, it can be observed that large deviations from ideal mixing rule occupied in both mixtures in their compositional dependence. Which indicated that ion mass plays a significant role in conductivity predictions, particularly when large mass disparities exist. This tendency was consistent with trends observed in other studies on common-anion molten salt mixtures, which emphasized the influence of mass fluctuations on thermal transport properties. Larger mass differences of the anions led to more significant deviations from linearity, thereby greatly reducing in thermal conductivity in these mixtures.
The model was validated by using the EMD results of the Polarizable Ion Model (PIM) framework. Some limitations were observed when applied to non-polarizable salt, LiF. The

EMD results provided higher thermal conductivity values with greater scatter compared to the recommended experimental data. The overestimated values indicate the uncertainties that occurs when using PIM for non-polarizable salt mixtures. Nevertheless, the model's predictions perfectly matched the EMD values for the NaF-NaCl, NaF-NaBr, and KF-KCl mixtures, emphasizing the model's robustness in common-cation molten salt mixtures of Na^+/F^-, Cl^- and K^+/F^-, Cl^-. These findings confirmed that the model accurately captures thermal conductivity behavior within the mixtures where mass differences between ions were less important, yielding more stable and reliable predictions.

In brief, the current model demonstrated its accuracy in predicting the thermal conductivity for simple common-ion monovalent and poly-anionic molten salt mixtures, validated by numerous experimental datasets of common-ion mixtures. The consistent agreement between the model's predictions and EMD results further proved its reliability. Given this feature, the model showed promising potential for predicting thermal conductivity in polyatomic common-ion mixtures, such as nitrates and carbonates. These insights established a solid foundation for further exploration of complex molten salt mixtures (for example, KCl-$MgCl_2$) and reciprocal molten salt mixtures (for example, LiF-KCl). Thus, the model can be expanded to a wider ranger of molten salt applications in processes simulations and practical engineering.

7.3 Thermal conductivity model for reciprocal molten salt mixtures

The final sub-objective is to extend the model for common-ion molten salt mixtures to reciprocal molten salt mixtures, which contains more than one cation and more than one anion, for example molten LiF-KCl mixture. Due to the lack of experimental data on the thermal conductivity of reciprocal molten salt mixtures, for this study, three reciprocal mixtures were simulated using EMD: Li^+, Na^+ / F^-, Cl^-; Li^+, K^+ / F^-, Cl^-; and Na^+, K^+ / F^-, Cl^-, with nine different compositions covering the entire composition range (inside the reciprocal composition square), each incrementing by 0.25 ionic mole fraction of cations and anions.

EMD offers advantages in determining the thermal conductivity of molten salts. However, obtaining accurate values across a range of compositions requires extensive computational effort and time, because each simulation can only simulate a specific composition at a given temperature per run. Such a limitation restricts the utilization in industrial processes, where temperature and compositions of molten salts changes rapidly according to system conditions. Moreover, there is still lacking of accurate knowledge of force field on certain molten salts.

To address these challenges, modeling provides an efficient alternative solution in the variation of temperature and composition. One of the popular approaches is using the MQMQA,

which offers several advantages. First, since there is an infinite number of combinations of three or four of the four pure salts that can reproduce a specific composition, the nominal mole fraction (X_i) is no longer valid for reciprocal molten salt mixtures. Fortunately, the MQMQA approach was developed specifically to estimate the pair fractions that consider the interactions of the FNN and SNN short-range ordering within reciprocal melts. Second, Gibbs energy minimization performed with the EQUILIB module of FactSage^{TM}, which finds the set of FNN pair fractions from a unique set of equilibrium ionic fractions at a fixed temperature and evaluates combined FNN and SNN short-range orders. This provides a more realistic estimation compared to the random mixing assumption of the Temkim model. Additionally, the MQMQA approach has been widely applied to predict thermodynamic properties and phase diagrams for many molten salt mixtures, including both common-ion and reciprocal molten salt mixtures [169, 178]. Leveraging these strengths, we build on the pair fraction framework in the MQMQA approach to extend our previous model for reciprocal molten salt mixtures.

The predicted results of calibrating the thermal conductivity of end members to EMD results aligned well with the EMD results, with a maximum error of approximately 20% for three reciprocal molten salt mixtures, Li^+, Na^+ / F^-, Cl^-, Li^+, K^+ / F^-, Cl^-, and Na^+, K^+ / F^-, Cl^-. The predictions were significantly more accurate compared to the commonly used ideal mixing rule, with deviations of up to 150% for the Li^+, K^+ / F^-, Cl^- mixture near the equimolar composition. In the Li^+, Na^+ / F^-, Cl^- and Li^+, K^+ / F^-, Cl^- mixtures, predictions were slightly underestimated compared to the EMD results. This could be attributed to two main factors: first, the PIM was used in the EMD simulations, since LiF is not polarizable, which led to EMD result for LiF that were approximately 38% larger than the recommended dataset reported by Nagasaka et al. [94]. The significant presence of pair fraction of LiF in the melt (as seen in the tables in Chapter 6) contributed to slightly higher values in the EMD results. Secondly, mass fluctuation effects may be reduced or compensated within the melt due to interactions between different cations and anions, as other new pure components are formed in the solution.

In contrast, for the Na^+, K^+ / F^-, Cl^- mixture, predictions were better match the EMD results, as LiF was absent from the melt. However, further experimental work or additional EMD simulations were recommended to confirm the impact of mass fluctuations in reciprocal molten salts, especially for mixtures with large differences in molar mass and thermal conductivity. Overall, we were confident in the predictive capability of the present reciprocal molten salt model.

In addition, we compared the nominal mole fractions of the mixture with the pair fractions calculated by using the random mixing of Temkin model and by using the MQMQA approach

for these reciprocal mixtures. The pair fractions of Temkin model remained the same across all three mixtures, as the nominal molar fractions were unchanged and independent of temperature. In contrast, the pair fractions in the MQMQA approach showed slight deviations from that of Temkin model, due to the consideration of the FNN and SNN short-range orders and the Gibbs free energy of exchange, $\Delta g^{exchange}_{AB/FCl}$. The mixture of Li^+, K^+ / F^-, Cl^- exhibited the most negative value of $\Delta g^{exchange}_{LiK/FCl} = -57$ [kJ/mol], indicating that the reactions are dominated by LiF and KCl, which prevail within the melt. This may also be another factor contributing to the significant deviation of this reciprocal mixture from the ideal mixing rule. Moreover, the pair fractions in the MQMQA approach are temperature dependent.

The model demonstrated its predictive capability for monoatomic fluoride and chloride reciprocal mixtures. It was expected to be suitable for predicting the behavior of polyatomic anion molten salt mixtures with the similar accuracy, such as nitrates, carbonates, and sulfates. The predicted results were also compared to a ternary reciprocal mixture of $(NaCl)_{0.48}$-$(KCl)_{0.36}$-$(NaF)_{0.16}$ (mole fraction), which was proposed for renewable energy applications and experimentally measured using the Laser Flash technique, as reported by Wang et al. [307]. The reported experimental datasets showed a strong positive temperature dependence, which may be considered as non-recommended data due to inadequate estimation of heat losses [39]. Additionally, the thermal conductivity of the mixture was approximately 100% larger than our predictions near the melting point. Unfortunately, only one experimental dataset was available in the literature.

To better illustrate the reliability of the current model, the recommended experimental datasets for the four pure components (NaF, NaCl, KF, KCl) were compared. The predictions for the mixtures showed a negative temperature dependence, consistent with the pure components, and the thermal conductivities were of the same order of magnitude. Another reciprocal salt mixture available in the literature was HITEC salt ($(NaNO_3)_{0.07}$-$(NaNO_2)_{0.53}$-$(KNO_3)_{0.40}$ weight fraction), a nitrate/nitrite mixture. As demonstrated by Diguilio and Teja [39], the ideal mixing rule accurately estimated the thermal conductivity of nitrate salt mixtures. Therefore, the advantage of the current model could not be effectively demonstrated for this mixture. However, predictions were closer to the most recent recommended experimental data than ideal mixing rule. Which once more reinforce the predictive accuracy of the current model. In addition, a noticeable discrepancy in the thermal conductivity reported by different investigators can be observed at high temperatures. This may be due to the fact that most experimental works were conducted under ambient conditions, where $NaNO_2$ was exposed to air (O_2) and can quickly convert to $NaNO_3$ at high temperatures. This reaction could influence the final thermal conductivity results of this reciprocal mixtures. Furthermore, additional reciprocal molten salt phase-change materials (PCMs), for which

the thermal conductivities in the liquid phase were still unknown or not well-defined, were investigated. These mixtures included Na_2CO_3-KCl-NaCl, $LiNO_3$-NaCl, and $LiNO_3$-KCl. The predictive capability of the extended model were well illustrated by predicting the thermal conductivity of these reciprocal mixtures, with temperature and composition dependencies. Importantly, one of the highlights is modifying the sound velocity to be temperature-dependent rather than fixed at the melting point in the last work, the model's applicability was enhanced. We then used this final reciprocal model to predict the thermal conductivity of various pure salts, including monovalent, divalent, and complex salts, and common-ion mixtures. Comparisons with previous models showed nearly identical results, with improved predictions for some common-ion mixtures. In other words, this final model was applicable for predicting the thermal conductivity of pure salts, common-ion mixtures, reciprocal mixtures, and complex mixtures (with their local structures precisely represented).

To conclude, we have developed a thermal conductivity model of molten salts based on kinetic theory. The model has demonstrated its strong predictive capabilities across a wide range of molten salts, including pure salts, simple common-ion mixtures, complex mixtures, and reciprocal molten salt mixtures. The model accounts for interatomic structural effects, particularly for complex and reciprocal molten salt mixtures. Importantly, the model does not require any empirical fitting constants. The input properties require the heat capacity, thermal expansivity, and sound velocity, which are readily available in the literature or molten salt databases. The predicted accuracy is generally within 20%, depending on the precision of the input parameters. We believe this model will be valuable for the design of new molten salt materials, and provide a reliable tool for quickly estimating thermal conductivity values in engineering applications.

7.4 Extended work on thermal conductivity modeling of complex molten salt solutions

As a part of this project, the model has been extended to the complex molten salt solution. This supplementary study was included in the Appendix E. My contributions to this work are particularly significant but not majority. Therefore, it is worth to include a discussion as a complement of this project, since it's in the scope of this thesis. In addition, many industrial processes generally involve complex molten salt solutions.

The same methodology was applied to extend the latter model for complex molten salt mixtures. In common-ion molten salt mixtures, short-range ordering is primarily dominated by first-nearest neighbors (FNN). However, in complex molten salt solutions, the strong FNN and second-nearest neighbors (SNN) interactions contribute to the formation of intricate coordination complexes and polymer chains. This leads to a reduction in thermal conductivity,

as the mobility of the complex ions decreases and the mean free path of the phonons shortens. To account for this effect, a new parameter was introduced into the model to describe the local structure within molten salt solutions: "complexion rate", which represented the mass weighted fraction of total mass coordination complexes and polymers in relation to the mass of the mixture. Given the lack of experimental data available in the literature, numerous EMD simulations were performed to gain a better understanding of how local structural behavior behaves and influences the overall thermal conductivity. The commonly used complex molten salt mixtures in the industry of KCl-$MgCl_2$ and NaF-AlF_3 were simulated and analyzed using EMD, and the results were compared with the model predictions.

In the case of the KCl-$MgCl_2$ mixture, the molar masses and thermal conductivities of the end-members are 74.55 and 95.21 [g/mol], and 0.36 and 0.45 [$W.m^{-1}K^{-1}$], respectively. As previously mentioned, the differences in molar mass and thermal conductivity of the end-members have a significant impact on the deviation of thermal conductivity from linearity. If the relationship between two compounds of the mixture is validated, $\lambda_{MgCl_2}/M_{MgCl_2} \simeq \lambda_{KCl}/M_{KCl}$, and the thermal conductivity of the melt behavior as a function of composition would be expected to follow the ideal mixing rule if the local structure of the melt were not considered, meaning that the melt is assumed to be fully dissociated of K^+, Mg^{2+}, and Cl^- ions. However, the EMD simulation results showed that a negative deviation from linearity of approximately 25% near $X_{MgCl_2} = 0.5$. The results revealed the presence of the complex ions within the melt, such as $MgCl_3^-$, $MgCl_4^{2-}$, $Mg_2Cl_5^-$, $Mg_2Cl_6^{2-}$,$Mg_3Cl_7^-$, $Mg_3Cl_8^{2-}$,$Mg_4Cl_9^-$, $Mg_4Cl_{10}^{2-}$ complexes ions, as well as neutral complexes like Mg_5Cl_{10}, Mg_6Cl_{12} (which resemble long polymer chains) [282]. The higher the $MgCl_2$ content in the melt, the greater the predominance of these neutral complexes. The predicted results showed an improvement over the case of full dissociated ions, with an error of approximately 10% compared to the EMD results.

The thermal conductivity in the compositional dependence of the NaF-AlF_3 mixture behaves differently from that of KCl-$MgCl_2$, primarily due to the significant differences in end-member's thermal conductivities and masses, which lead to larger deviations from linearity. The prediction results were compared to two distinct force fields (FF1 and FF2) from EMD simulations, as well as experimental data from Khokhlov et al. [314].

The EMD estimations, experimental measurements, and the predictions from the modified model were in good agreement. FF1 was based on NMR experimental technique [315], may provide more reliable predictions for local structure. However, FF2 covered the entire composition range, exhibiting a better fit with the data. Despite this, both force fields are in good agreement with each other up to $X_{MgCl_2} = 0.4$.

The EMD simulation revealed the behavior of the local structure in the melt. Simulation

results showed that, as the AlF_3 concentration increases, complex fluoroaluminate ions (such as AlF_4^-, AlF_5^{2-}, AlF_6^{3-}), dimers, trimers, tetramers, and polymers become prevalent. In terms of theoretical predictions, the models exhibited significant variability in the calculated excess thermal conductivity, which depends on the force field applied. For instance, using the local structures obtained by FF1, the modified model predicted a minimum excess thermal conductivity of approximately -75% near $X_{AlF_3} = 0.3$, whereas the EMD results showed deviations from ideality reaching up to -160% around $X_{AlF_3} = 0.4$. In contrast to the local structure of FF2, the model predicted a minimum excess of about -170% near $X_{AlF_3} = 0.4$, with the EMD simulations yielding excess values closer to -100%. However, the experimental data revealed a minimum deviation occurring at $X_{AlF_3} = 0.5$, approximately -120%.

The formation of heavier complex anions contributed to this variability as anticipated by FF2. This emphasizes the formation of higher coordination states, such as AlF_6 and dimers, rather than lower coordination species like AlF_4 and AlF_5 at higher AlF_3 concentrations. Consequently, the excess thermal conductivity of complex mixtures is primarily determined by the force field's assumptions on local structural configurations. Thus, accurate knowledge of local structural configuration in complex mixture is crucial for the predictive reliability of the current model.

According to the findings, the formalism employed in this research could offer robust predictions for thermal transport in the common-ion complex melts, as long as their local structural configurations are accurately represented. For example, in the NaF-AlF_3 mixture, improving the local structure could enhance the accuracy of predicting thermal transport properties. The considerable differences in thermal conductivity across the compositional range, along with variations in structural complexity, highlight the importance of accurate force fields and their parameters in simulating realistic thermal transport characteristics in ionic melts.

CHAPTER 8 CONCLUSION

This chapter presents an overview of the research conducted on the modeling of thermal conductivity in molten salts, highlighting significant contributions made in this area. Key advancements include the enhancement of predictive capabilities and a deeper understanding of how local structures within the systems influence thermal conductivity. The model's limitations have been carefully evaluated to define its fundamental scope. Additionally, recommendations for future research are offered enhance the model's predictive capabilities and accuracy, including the potential extension of the model to encompass oxide and solid solutions. These recommendations provide a pathway to improve the reliability of the model and its potential applications across diverse industrial and research contexts.
To begin with, it is essential to highlight the main contributions of this thesis:

- In this research project, we introduced a theoretically based thermal conductivity model of molten salts that does not rely on any empirical fitting parameters or any knowledge of the same salt family. This is the first available model that accurately predicts thermal conductivity values comparable to reliable experimental measurements for both pure molten salts and common-ion molten salt mixtures, in terms of temperature and composition dependence.

- This model has been extended to the thermal conductivity predictions for reciprocal and complex molten salt solutions by several considerations, particularly the sound velocity of the pure salt has been modified to be temperature-dependent, and the pair fractions in the MQMQA have been employed to model the FNN and SNN structure of reciprocal salts from their thermodynamic properties. This updated model represents the first to consider the effects of local structures in molten salt thermal conductivity predictions in the literature. The capability of predicting the thermal conductivity of complex molten salt solutions has been demonstrated in Appendix E, and accurate information on the formed complex ions and polymer chains is required for the model. Notably, this extended model can predict the thermal conductivity of pure molten salts and common-ion molten salt mixtures with slightly improved accuracy.

The developed model has been validated against available experimental data and EMD simulations for common-ion, reciprocal and complex molten salt solutions, confirming its predictive accuracy and robustness. This advancement greatly enhances the ability to predict the thermal conductivity of molten salts and their mixtures. We believe it will yield substantial benefits for simulations and practical engineering applications in advanced energy systems

and industrial processes.

8.1 Summary of works

This thesis aimed to develop a thermal conductivity model for molten salts based on kinetic theory, specifically targeting advanced energy applications. This developed model exhibits predictive capabilities for a broad range of pure and mixed molten salts, including monovalent halides, divalent halides, nitrate/nitrite, carbonates, sulfates, and hydroxides, without requiring empirical fitting parameters. The model successfully predicts thermal conductivity as a function of temperature and composition with an error margin less than 20%, which is comparable to the most recommended experimental studies. Furthermore, it integrates characteristics and interatomic interactions within the melt, a first in this area of research.

Initially, a foundational model was developed for pure molten salts. This model, based on kinetic theory, predicts thermal conductivity as a function of temperature (from the melting point upward) while avoiding reliance on empirical fitting parameters. A key theoretical parameter was introduced into the concept of minimum thermal conductivity, defined by the number of cations and anions. This parameter effectively captures the structural characteristics of pure salts, providing a basis for extending the model to predict the thermal conductivity of molten salt mixtures.

The accuracy of this pure molten salt model was validated against 25 and 9 reliable experimental datasets reported by Nagasaka et al. and Harada et al., respectively. The Bland-Altman method was employed to assess the reliability of the model in predicting thermal conductivity both at the melting point and its temperature dependence. The comparison results showed an average deviation of approximately less than 10%. The model's predictions aligned well with the recommended experimental datasets across various salt families, including fluorides, chlorides, bromides, iodides, nitrates/nitrites, carbonates, sulfates, and hydroxides. This predictive accuracy is largely attributed to the input parameters of heat capacity, density, thermal expansivity, and sound velocity.

Despite minor discrepancies with some salts, the agreement with recommended experimental datasets demonstrates that its accuracy is comparable to that of established reliable experimental techniques. Consequently, this pure molten salt model provides a strong foundation for extending thermal conductivity predictions to molten salt mixtures, making it a valuable tool for predicting and optimizing thermal conductivity in diverse molten salt systems important for high-temperature energy applications.

Building on the previous model for pure molten salts, a composition-dependent model was developed for simple molten salt mixtures, which includes a mass fluctuation term within the disorder scattering parameter. Molten salt mixtures demonstrate enhanced thermophysical

properties compared to pure salts, making them highly valuable for industrial applications. Given the limited experimental data available for molten salt mixtures, extensive EMD simulations were performed, focusing on binary mixtures with common anions and common cations to validate the model.

The model's predictions closely matched both reliable experimental data and EMD simulation results within acceptable error margins, illustrating predictive accuracy comparable to reliable experimental outcomes. This model represents a significant improvement over the commonly used ideal mixing rule, with deviations from ideality being highly sensitive to the molecular weights and thermal conductivities of the constituent salts. An important achievement is that the model successfully predicts properties of common-cation mixtures, for which no prior data was available.

Lastly, the interatomic interactions associated with FNN and SNN short-range ordering were incorporated into the model for reciprocal molten salt mixtures. While EMD simulations can accurately capture local structures within these melts, they are computationally intensive, especially for high-order and complex molten salt mixtures. Moreover, EMD simulations are constrained to analyzing only one specific molten salt composition at a fixed temperature during each run, making it impractical to simulate an industrial process where both parameters vary over time.

As a viable alternative, the MQMQA approach offers a realistic solution by efficiently accounting for interatomic interactions. In this approach, pair fractions determined by the MQMQA model are governed by the Gibbs energy of exchange and the FNN short-range ordering, which in turn governs the pair fractions of each constituent. The model was validated through extensive EMD results across three reciprocal molten salt mixtures: Li^+, Na^+ / F^-, Cl^-; Li^+, K^+ / F^-, Cl^-; and Na^+, K^+ / F^-, Cl^-. The model demonstrated strong alignment with the simulation results, with prediction errors within 20%. This work notably establishes the first theoretical model for thermal conductivity in reciprocal molten salt mixtures that incorporates FNN short-range ordering effects, as estimated through the MQMQA approach.

Additionally, the same methodology was extended to complex molten salt mixtures where ions and polymer chains form within the melt (i.e. LiF-BeF_2, NaF-AlF_3). These complex ions further reduce transport properties, so a "complex rate" parameter describing the local structures in the melt was introduced. The results revealed that the variations in local structural significantly influence thermal conductivity (see the supplementary work in the Appendix E). This is the first instance in which local structure effects have been incorporated into the model, providing an advantage over atomistic simulation methods by enabling more efficient predictions of temperature and compositional dependencies.

8.2 Limitations

This thesis presents a thermal conductivity model that extends from pure molten salts to complex and reciprocal molten salt mixtures. However, certain limitations arose through these extensions and modifications. The key limitations are summarized below:

- Sound velocity data for pure molten salts: The model analyzed only 58 molten salts starting from their melting temperatures. A significant limitation lies in the availability of accurate sound velocity data for other salts. For some salts, sound velocity was obtained through extrapolation due to a lack of reliable data, raising concerns about its accuracy. Additionally, sound velocity in the liquid phase remains unknown for certain salts, such as AlF_3. To expand the model's applicability, a comprehensive and reliable database of sound velocities for a broader range of salts is essential.

- Phase transitions in salt mixtures: The model for molten mixtures (simple, complex, and reciprocal mixtures) does not account for phase transitions. To simplify the analysis, the sound velocity of pure molten salt was modified to be temperature-dependent, based on thermal conductivity over a range from 300 [K] below to 600 [K] above its melting point. However, liquidus transitions in salt mixtures are not considered. Consequently, the predictive accuracy may be limited when a phase transition occurs at the temperature of interest for the salt mixtures.

- Limitations in reciprocal molten salt solutions: The model is not yet feasible for all complex reciprocal molten salt systems due to the unavailability of certain thermodynamic models. Unfortunately, many of them have not yet been developed or optimized, which constrains the application in such cases. Currently, the need of coordination data should be obtained through atomistic simulations, experimental techniques, or specific models for particular salt mixtures.

- Local structure in complex molten salt solutions: The local structural configurations within the melt are crucial for providing accurate predictions in complex molten salt mixtures. A limitation of the current model is its reliance on reliable coordination data, which can vary significantly depending on the method used, for example experimental techniques (NMR spectroscopy), EMD, and various models. As shown in the appendix E (supplementary work), the local structural configurations were determined by the force fields from EMD simulations. For reliable predictions, it is important to have high-quality coordination data for complex mixtures.

These limitations indicate areas where further research and data collection would be valuable

for enhancing the model's robustness and extending its applicability across more molten salt systems.

8.3 Future research

Building on the identified limitations, the thermal conductivity model developed in this thesis has significant potential for further enhancement and can be expanded in several promising directions. One of the most impactful directions would be to extend the model to solid salt solutions. Solid salts play an important role in many applications where phase transitions and high thermal conductivity values are essential, such as in thermal energy storage systems and electrochemical devices (batteries). Developing a reliable model for solid-state salt thermal conductivity would greatly contribute to the current research on molten salts, thereby bridging the gap between the liquid and solid phases for practical engineering applications.

Secondly, we only consider the conductive heat transfer mechanism in this project. As seen in last chapter, the convective and radiative heat transfer mechanisms will also be present under the same conduction, and influence significantly the heat transfer at high temperatures. The integration of both heat transfer modes will be another focus, in particular, the radiative heat transfer mechanism becomes more significant at high temperatures, which will substantially increase the heat transfer.

Thirdly, molten salts are corrosive, and held in alloy material containers, and chemical reactions in between will occur upon contact. Some products will be released through reactions, and some potential impurities in the salt, both of them will influence our predictions. Therefore, another future direction is to consider the possible effects of both chemical reactions and impurities on the thermal conductivity of the melt.

Furthermore, establishing a reliable database of sound velocity across a broader range of salts would be vital for future work. Currently, our database includes sound velocity data for only 58 salts, some of which were derived through extrapolation from other salts within the same family. Indeed, many salts still lack reliable experimental datasets for their sound velocity, which limits the broader applicability of the model. Enhancing the accuracy of sound velocity would significantly improve the model's predictive reliability.

Finally, to address phase transitions in molten salt mixtures, the next step involves integrating the current thermal conductivity model into FactSage^{TM}. By leveraging FactSage^{TM}'s extensive phase transition database, this integration would enhance the model's accuracy in capturing thermal conductivity variations across the entire range of composition and temperature. This modeling process is efficient, producing thermal conductivity mappings in a short time while being user-friendly. This technique would facilitate predictions for multi-phase

molten salt systems, particularly during solid-liquid transitions, making the model more robust against compositional and temperature variations and more accessible for practical applications within the FactSage^{TM} environment.

REFERENCES

[1] A. Association *et al.*, *Aluminum: properties and physical metallurgy*. ASM international, 1984.

[2] M. Gaune-Escard, *Molten salts: from fundamentals to applications*. Springer Science & Business Media, 2002, vol. 52.

[3] A. B. Zavoico, "Solar Power Tower Design Basis Document, Revision 0."

[4] Phoenix TV "A Close Look at China". (2024) Visiting the "super mirror" power plant. Accessed on 2025-08-09. [Online]. Available: https://ishare.ifeng.com/c/vs/v006TQi8XjmKyAWibAb8k9J4FxvSzy0xamAcKKms5puW4XVtKOoCXDTTh6V--PJdYx5c0

[5] D. G. Lovering, *Molten salt technology*. Springer, 2014.

[6] M. Rosenthal, P. Kasten, and R. Briggs, "Molten-salt reactors—history, status, and potential," *Nuclear Applications and Technology*, vol. 8, no. 2, pp. 107–117, 1970.

[7] H. MacPherson, "Development of materials and systems for the molten-salt reactor concept," Univ. of Tennessee, Knoxville, Tech. Rep., 1972.

[8] A. Perry, "Physics program for molten-salt breeder reactors." Oak Ridge National Lab., Tenn., Tech. Rep., 1967.

[9] W. Grimes, "Molten-salt reactor chemistry," *Nuclear Applications and Technology*, vol. 8, no. 2, pp. 137–155, 1970.

[10] D. F. Williams, "Assessment of candidate molten salt coolants for the advanced high temperature reactor (AHTR)," 2006.

[11] C. Forsberg, G. Zheng, R. G. Ballinger, and S. T. Lam, "Fusion blankets and fluoride-salt-cooled high-temperature reactors with flibe salt coolant: common challenges, tritium control, and opportunities for synergistic development strategies between fission, fusion, and solar salt technologies," *Nuclear Technology*, vol. 206, no. 11, pp. 1778–1801, 2020.

[12] M. Mehos, C. Turchi, J. Vidal, M. Wagner, Z. Ma, C. Ho, W. Kolb, C. Andraka, and A. Kruizenga, "Concentrating solar power Gen3 demonstration roadmap," National Renewable Energy Lab.(NREL), Golden, CO (United States), Tech. Rep., 2017.

[13] W. Ding, H. Shi, A. Jianu, Y. Xiu, A. Bonk, A. Weisenburger, and T. Bauer, "Molten chloride salts for next generation concentrated solar power plants: Mitigation strategies against corrosion of structural materials," *Solar Energy Materials and Solar Cells*, vol. 193, pp. 298–313, 2019.

[14] K. Niedermeier, J. Flesch, L. Marocco, and T. Wetzel, "Assessment of thermal energy storage options in a sodium-based CSP plant," *Applied thermal engineering*, vol. 107, pp. 386–397, 2016.

[15] K. Vignarooban, P. Pugazhendhi, C. Tucker, D. Gervasio, and A. M. Kannan, "Corrosion resistance of Hastelloys in molten metal-chloride heat-transfer fluids for concentrating solar power applications," *Solar Energy*, vol. 103, pp. 62–69, 2014.

[16] J. Gasia, L. Miró, and L. F. Cabeza, "Review on system and materials requirements for high temperature thermal energy storage. Part 1: General requirements," *Renewable and Sustainable Energy Reviews*, vol. 75, pp. 1320–1338, 2017.

[17] B. Zalba, J. M. Marín, L. F. Cabeza, and H. Mehling, "Review on thermal energy storage with phase change: materials, heat transfer analysis and applications," *Applied thermal engineering*, vol. 23, no. 3, pp. 251–283, 2003.

[18] M. Kenisarin and K. Mahkamov, "Solar energy storage using phase change materials," *Renewable and sustainable energy reviews*, vol. 11, no. 9, pp. 1913–1965, 2007.

[19] Y. Dutil, D. R. Rousse, N. B. Salah, S. Lassue, and L. Zalewski, "A review on phase-change materials: Mathematical modeling and simulations," *Renewable and sustainable Energy reviews*, vol. 15, no. 1, pp. 112–130, 2011.

[20] W. Su, J. Darkwa, and G. Kokogiannakis, "Review of solid–liquid phase change materials and their encapsulation technologies," *Renewable and Sustainable Energy Reviews*, vol. 48, pp. 373–391, 2015.

[21] B. E. Rapp, *Microfluidics: modeling, mechanics and mathematics*. William Andrew, 2016.

[22] G. F. Hewitt, G. L. Shires, and T. Bott, *Process heat transfer*. Begell House, 1994.

[23] J. Fourier, "Théorie analytique de la chaleur. Paris, English transl.: The Analytical Theory of Heat," 2003.

[24] T. L. Bergman, A. S. Lavine, F. P. Incropera, and D. P. DeWitt, *Introduction to heat transfer*. John Wiley & Sons, 2011.

[25] M.-T. Huang and P.-M. Zhai, "Achieving Paris Agreement temperature goals requires carbon neutrality by middle century with far-reaching transitions in the whole society," *Advances in Climate Change Research*, vol. 12, no. 2, pp. 281–286, 2021.

[26] V. Nunes, C. Queirós, M. Lourenço, F. Santos, and C. N. De Castro, "Molten salts as engineering fluids-A review: Part I. Molten alkali nitrates," *Applied energy*, vol. 183, pp. 603–611, 2016.

[27] V. M. Nunes, M. J. Lourenço, F. J. Santos, and C. A. Nieto de Castro, "Importance of accurate data on viscosity and thermal conductivity in molten salts applications," *Journal of Chemical & Engineering Data*, vol. 48, no. 3, pp. 446–450, 2003.

[28] M. X. Ho and C. Pan, "Experimental investigation of heat transfer performance of molten HITEC salt flow with alumina nanoparticles," *International journal of heat and mass transfer*, vol. 107, pp. 1094–1103, 2017.

[29] A. Elsheikh, S. Sharshir, M. E. Mostafa, F. Essa, and M. K. A. Ali, "Applications of nanofluids in solar energy: a review of recent advances," *Renewable and Sustainable Energy Reviews*, vol. 82, pp. 3483–3502, 2018.

[30] Z. Li, L. Cui, B. Li, and X. Du, "Mechanism exploration of the enhancement of thermal energy storage in molten salt nanofluid," *Physical Chemistry Chemical Physics*, vol. 23, no. 23, pp. 13 181–13 189, 2021.

[31] J. C. Ard, J. A. Yingling, T. J. Johnson, J. Schorne-Pinto, M. Aziziha, C. M. Dixon, M. S. Christian, J. W. McMurray, and T. M. Besmann, "Development of the molten salt thermal properties database- thermochemical (MSTDB - TC), example applications, and LiCl- RbCl and UF_3-UF_4 system assessments," *Journal of Nuclear Materials*, vol. 563, p. 153631, 2022.

[32] G. J. Janz, C. Solomons, and H. J. Gardner, "Physical Properties And Constitution Of Molten Salts-Electrical Conductane, Transport, And Cryoscopy," *Chemical Reviews*, vol. 58, no. 3, pp. 461–508, 1958.

[33] G. J. Janz, C. B. Allen, N. Bansal, R. Murphy, and R. Tomkins, "Physical properties data compilations relevant to energy storage, 2. Molten salts: Data on single and multi-component salt systems," *Nasa Sti/recon Technical Report N*, vol. 80, p. 10643, 1979.

[34] G. J. Janz and R. Tomkins, "Physical properties data compilations relevant to energy storage. IV. Molten salts: data on additional single and multi-component salt systems," National Standard Reference Data System, Tech. Rep., 1981.

[35] G. J. Janz, "Thermodynamic and transport properties for molten salts: correlation equations for critically evaluated density, surface tension, electrical conductance, and viscosity data," *Journal of Physical and Chemical Reference Data*, vol. 17, 1988.

[36] G. Janz, "High-temperature calibration quality data: molten salts and metals," in *Materials Science Forum*, vol. 73. Trans Tech Publ, 1991, pp. 707–714.

[37] G. J. Janz, *Molten salts handbook*. Elsevier, 2013.

[38] Y. Nagasaka and A. Nagashima, "The Temperature Dependence of the Thermal Conductivity of Molten Salts," *ECS Proceedings Volumes*, vol. 1990, no. 1, p. 230, 1990.

[39] R. DiGuilio and A. S. Teja, "A rough hard-sphere model for the thermal conductivity of molten salts," *International journal of thermophysics*, vol. 13, no. 5, pp. 855–871, 1992.

[40] C. D. Chliatzou, M. J. Assael, K. Antoniadis, M. L. Huber, and W. A. Wakeham, "Reference correlations for the thermal conductivity of 13 inorganic molten salts," *Journal of physical and chemical reference data*, vol. 47, no. 3, p. 033104, 2018.

[41] A. D. Pelton, P. Chartrand, and G. Eriksson, "The modified quasi-chemical model: Part IV. Two-sublattice quadruplet approximation," *Metallurgical and Materials Transactions A*, vol. 32, pp. 1409–1416, 2001.

[42] A. Palacios, L. Cong, M. Navarro, Y. Ding, and C. Barreneche, "Thermal conductivity measurement techniques for characterizing thermal energy storage materials–A review," *Renewable and Sustainable Energy Reviews*, vol. 108, pp. 32–52, 2019.

[43] A. Z. Zhao and J. E. Garay, "High temperature liquid thermal conductivity: a review of measurement techniques, theoretical understanding, and energy applications," *Progress in Materials Science*, p. 101180, 2023.

[44] R. C. Gallagher, "Measuring and Predicting the Thermal Conductivity of Molten Salts for Nuclear Energy Applications," Ph.D. dissertation, The Ohio State University, 2022.

[45] D. Zhao, X. Qian, X. Gu, S. A. Jajja, and R. Yang, "Measurement techniques for thermal conductivity and interfacial thermal conductance of bulk and thin film materials," *Journal of Electronic Packaging*, vol. 138, no. 4, p. 040802, 2016.

[46] V. D. Golyshev and M. A. Gonik, "A standard reference material for thermal conductivity of semitransparent melts," *High Temperatures-High Pressures*, vol. 33, no. 6, pp. 639–646, 2001.

[47] R. Tufeu, J. Petitet, L. Denielou, and B. Le Neindre, "Experimental determination of the thermal conductivity of molten pure salts and salt mixtures," *International journal of thermophysics*, vol. 6, no. 4, pp. 315–330, 1985.

[48] I. Veneraki, V. Deshko, and O. Khlebnikov, "Determination of thermoconductivity of sodium-chloride in liquid-state," pp. 212–214, 1976.

[49] L. R. White and H. T. Davis, "Thermal conductivity of molten alkali nitrates," *The Journal of Chemical Physics*, vol. 47, no. 12, pp. 5433–5439, 1967.

[50] J. McDonald and H. T. Davis, "Thermal conductivity of binary mixtures of alkali nitrates," *The Journal of Physical Chemistry*, vol. 74, no. 4, pp. 725–730, 1970.

[51] V. I. Fedorov and V. I. Machuev, "Thermal conductivity of fused salts," *Teplofizika vysokikh temperatur*, vol. 8, no. 4, pp. 912–914, 1970.

[52] P. V. Polyakov and E. M. Hildebrandt, "Study of the Thermal Conductivity of Melts in the KCl–$MgCl_2$ System," *Teplofizika vysokikh temperatur*, vol. 12, no. 4, pp. 892–893, 1974.

[53] P. Savintsev, V. Khokhlov, and M. Smirnov, "Thermal Conductivity of Binary Mixtures of Cesium, Barium, and Lanhanum Chlorides," *Teplofizika Vysokikh Temperatur*, vol. 16, no. 3, pp. 644–646, 1978.

[54] Egorov and M. P. Revyakina, "Investigation of the thermal conductivity of carbonates in a mixture of carbonates and magnesium oxide," *Teplofizika vysokikh temperatur*, vol. 8, no. 6, pp. 1299–1302, 1970.

[55] H. Bloom, A. Doroszkowski, and S. Tricklebank, "Molten salt mixtures. IX. The thermal conductivities of molten nitrate systems," *Australian Journal of Chemistry*, vol. 18, no. 8, pp. 1171–1176, 1965.

[56] M. Smirnov, V. Khokhlov, and E. Filatov, "Thermal conductivity of molten alkali halides and their mixtures," *Electrochimica acta*, vol. 32, no. 7, pp. 1019–1026, 1987.

[57] R. M. DiGuilio, *The thermal conductivity of molten salts and concentrated aqueous salt solutions*. Georgia Institute of Technology, 1991.

[58] Y. Nagasaka, T. Hatakeyama, M. Okuda, and A. Nagashima, "Measurement of the thermal diffusivity of liquids by the forced Rayleigh scattering method: Theory and experiment," *Review of scientific instruments*, vol. 59, no. 7, pp. 1156–1168, 1988.

[59] M. Harada, A. Shioi, T. Miura, and S. Okumi, "Thermal conductivities of molten alkali metal halides," *Industrial & engineering chemistry research*, vol. 31, no. 10, pp. 2400–2407, 1992.

[60] A. E. Gheribi, J. A. Torres, and P. Chartrand, "Recommended values for the thermal conductivity of molten salts between the melting and boiling points," *Solar energy materials and solar cells*, vol. 126, pp. 11–25, 2014.

[61] R. C. Gallagher, A. Birri, N. G. Russell, A.-T. Phan, and A. E. Gheribi, "Investigation of the thermal conductivity of molten LiF-NaF-KF with experiments, theory, and equilibrium molecular dynamics," *Journal of Molecular Liquids*, p. 119151, 2022.

[62] R. Tye, J. Bourne, and A. Destarlais, "Thermal energy storage material thermophysical property measurement and heat transfer impact," Tech. Rep., 1976.

[63] Y. Kato, K. Kobayasi, N. Araki, and K. Furukawa, "An accuracy analysis of the thermal diffusivity measurement of molten salts by stepwise heating and improved apparatus," *Journal of Physics E: Scientific Instruments*, vol. 10, no. 9, p. 921, 1977.

[64] R. Santini, P. Cerisier, J. Pantaloni, and L. Tadrist, "Measurement of thermal conductivity of molten salts in the range 100-500°C," *Int. J. Heat Mass Transfer;(United Kingdom)*, vol. 27, no. 4, 1984.

[65] N. Araki, M. Matsuura, A. Makino, T. Hirata, and Y. Kato, "Measurement of thermophysical properties of molten salts: mixtures of alkaline carbonate salts," *International journal of thermophysics*, vol. 9, no. 6, pp. 1071–1080, 1988.

[66] J. Cooke, "Development of the variable-gap technique for measuring the thermal conductivity of fluoride salt mixtures." OAK RIDGE NATIONAL LAB., TENN., Tech. Rep., 1973.

[67] R. C. Gallagher, A. Birri, N. Russell, and N. D. B. Ezell, "Design and performance a variable gap system for thermal conductivity measurements of high temperature, corrosive, and reactive fluids," *International Journal of Heat and Mass Transfer*, vol. 192, p. 122763, 2022.

[68] B. Merritt, M. Seneca, S. Larson, K. Davis, and T. Munro, "Measurements of the thermal conductivity of reference liquids using a modified transient hot-wire needle probe," *International Journal of Heat and Mass Transfer*, vol. 189, p. 122674, 2022.

[69] S. Kitade, Y. Kobayashi, Y. Nagasaka, and A. Nagashima, "Measurement of the thermal conductivity of molten KNO_3 and $NaNO_3$ by the transient hot-wire method with ceramic-coated probes," *High Temperatures-High Pressures*, vol. 21, no. 2, pp. 219–224, 1989.

[70] T. Omotani and A. Nagashima, "Thermal conductivity of molten salts, HTS and the lithium nitrate-sodium nitrate system, using a modified transient hot-wire method," *Journal of Chemical and Engineering Data*, vol. 29, no. 1, pp. 1–3, 1984.

[71] T. Omotani, Y. Nagasaka, and A. Nagashima, "Measurement of the thermal conductivity of KNO_3-$NaNO_3$ mixtures using a transient hot-wire method with a liquid metal in a capillary probe," *International Journal of Thermophysics*, vol. 3, no. 1, pp. 17–26, 1982.

[72] Y. Nagasaka, N. Nakazawa, and A. Nagashima, "Experimental determination of the thermal diffusivity of molten alkali halides by the forced Rayleigh scattering method. I. Molten LiCl, NaCl, KCl, RbCl, and CsCl," *International Journal of Thermophysics*, vol. 13, no. 4, pp. 555–574, 1992.

[73] N. Nakazawa, Y. Nagasaka, and A. Nagashima, "Experimental determination of the thermal diffusivity of molten alkali halides by the forced Rayleigh scattering method. II. Molten NaBr, KBr, RbBr, and CsBr," *International journal of thermophysics*, vol. 13, no. 5, pp. 753–762, 1992.

[74] N. Y. Nakazawa, N. and A. Nagashima, "Experimental determination of the thermal diffusivity of molten alkali halides by the forced Rayleigh scattering method. III. molten NaI, KI, RbI, and CsI," *International journal of thermophysics*, vol. 13, no. 5, pp. 763–772, 1992.

[75] S. Otsubo, Y. Nagasaka, and A. Nagashima, "Experimental study on the forced rayleigh scattering method using CO_2 laser (3rd report, measurement of molten single carbonates and their binary and ternary mixtures)," *Nihon Kikai Gakkai Ronbunshu, B Hen/Transactions of the Japan Society of Mechanical Engineers, Part B*, vol. 64, no. 619, pp. 806–813, 1998.

[76] X.-H. An, J.-H. Cheng, H.-Q. Yin, L.-D. Xie, and P. Zhang, "Thermal conductivity of high temperature fluoride molten salt determined by laser flash technique," *International Journal of Heat and Mass Transfer*, vol. 90, pp. 872–877, 2015.

[77] Y. Grosu, L. González-Fernández, U. Nithiyanantham, and A. Faik, "Wettability control for correct thermophysical properties determination of molten salts and their nanofluids," *Energies*, vol. 12, no. 19, p. 3765, 2019.

[78] A. Z. Zhao, M. C. Wingert, and J. E. Garay, "Frequency-domain hot-wire measurements of molten nitrate salt thermal conductivity," *Journal of Chemical & Engineering Data*, vol. 66, no. 1, pp. 262–270, 2020.

[79] S. G. Robertson and M. P. Short, "Design and performance of a molten fluoride salt-compatible optical thermophysical property measurement system," *Review of Scientific Instruments*, vol. 92, no. 6, p. 064905, 2021.

[80] S. G. Robertson, R. Wiser, W. Yang, D. Kang, S. Choi, E. Baglietto, and M. P. Short, "The curious temperature dependence of fluoride molten salt thermal conductivity," *Journal of Applied Physics*, vol. 131, no. 22, p. 225102, 2022.

[81] M. J. Assael, K. D. Antoniadis, and W. A. Wakeham, "Historical evolution of the transient hot-wire technique," *International journal of thermophysics*, vol. 31, pp. 1051–1072, 2010.

[82] H. M. Roder, "A transient hot wire thermal conductivity apparatus for fluids," *Journal of research of the National Bureau of Standards*, vol. 86, no. 5, p. 457, 1981.

[83] A. Turnbull, "The thermal conductivity of molten salts. I. A transient measurement method," *Australian J. Appl. Sci.*, vol. 12, 1961.

[84] E. McLaughlin, "The thermal conductivity of liquids and dense gases," *Chemical Reviews*, vol. 64, no. 4, pp. 389–428, 1964.

[85] N. Nakazawa, Y. Nagasaka, and A. Nagashima, "Measurement of the thermal diffusivity of molten salts by the forced Rayleigh scattering method," *High Temperatures-High Pressures*, vol. 23, no. 5, pp. 595–604, 1991.

[86] A. Rudenko, A. Redkin, E. Il'ina, S. Pershina, P. Mushnikov, Y. Zaikov, S. Kumkov, Y. Liu, and W. Shi, "Thermal Conductivity of FLiNaK in a Molten State," *Materials*, vol. 15, no. 16, p. 5603, 2022.

[87] Y. Nagasaka, N. Nakazawa, and A. Nagashima, "Experimental determination of the thermal diffusivity of molten alkali halides by the forced Rayleigh scattering method. I. Molten LiCl, NaCl, KCl, RbCl, and CsCl," *International Journal of Thermophysics*, vol. 13, no. 4, pp. 555–574, 1992.

[88] K. Sreenivasan, "Ph.D thesis," *University of Pennsylvania*, 1967.

[89] I. V. O. Khlebnikov, A. Alabovski and V. Sokolov, "," *Prom. Teplotekh5*, pp. 97–101, 1981.

[90] P. V. Polyakov, "Thermal conductivities of NaF-AlF_3 melts," *Teplofizika vysokikh temperatur*, vol. 13, no. 3, pp. 661–663, 1975.

[91] K. M. I.Powell, J.Bryant, "Proceedings of the Symposiumon Transport Properties of Fluids and Fluid Mixtures," 1979, p. pp.1.2/1–1.2/18.

[92] V. D. Golyshev, M. A. Gonik, V. Petrov, and Y. M. Putilin, "Experimental investigation of the thermal-conductivity of transparent melts," *Teplofizika vysokikh temperatur*, vol. 21, no. 5, pp. 899–903, 1983.

[93] V. Golyshev and M. Gonik, "High-temperature thermophysical properties of non-scattering semitransparent materials III: thermal conductivity of melts," *High Temperatures-High Pressures*, vol. 24, no. 6, pp. 677–688, 1992.

[94] Y. Nagasaka and A. Nagashima, "Corresponding states correlation for the thermal conductivity of molten alkali halides," *International journal of thermophysics*, vol. 14, pp. 923–936, 1993.

[95] C. Lucks and H. Deem, "Apparatus for Measuring the Thermal Conductivity of Liquids at Elevated Temperatures: Thermal Conductivity of Fused NaOH to 600°C," *Preprint*, no. 56SA31, 1956.

[96] G. Bystrai and V. Desyatnik, "Thermal conductivity of alkali metal chlorides," *Teplofizichcskie Issledovaniya Zhidkostei*, pp. 34–8, 1975.

[97] V. L. P.M. Shurygin, V.P. Buzovkin, "Study of the thermal conductivity of molten oxides," *Teplofiz. Vysok. Temp*, vol. 14, p. 1101–1105, 1976.

[98] P. Sindzingre and M. Gillan, "A computer simulation study of transport coefficients in alkali halides," *Journal of Physics: Condensed Matter*, vol. 2, no. 33, p. 7033, 1990.

[99] E. Filatov, A. Kodintsev, and V. Khokhlov, "Thermal conductivity of molten and crystalline alkali-earth chlorides near phase transition temperature," *Rasplavy*, pp. 11–15, 2005.

[100] Y. Nagasaka and A. Nagashima, "The thermal conductivity of molten $NaNO_3$ and KNO_3," *International Journal of Thermophysics*, vol. 12, no. 5, pp. 769–781, 1991.

[101] H. Shibata, H. Ohta, and H. Yoshida, "Thermal diffusivity of molten carbonates at elevated temperatures," *High Temperature Materials and Processes*, vol. 21, no. 3, pp. 139–142, 2002.

[102] J. S. Mech., "JSME Data Book Heat Transfer 4th Edition," 1986.

[103] S. E. Gustafsson, N.-O. Halling, and R. A. Kjellander, "Optical determination of thermal conductivity with a plane source technique," *Zeitschrift für Naturforschung A*, vol. 23, no. 5, pp. 682–686, 1968.

[104] R. Tye, A. Desjarlais, and J. Bourne, "Thermophysical Property Measurements on Thermal Energy Storage Materials," in *Proc. Seventh Symposium on Thermophysical Properties*. ASME New York, 1977, pp. 189–197.

[105] Y. Tada, M. Harada, M. Tanigaki, and W. Eguchi, "Laser flash method for measuring thermal conductivity of liquids—application to low thermal conductivity liquids," *Review of Scientific instruments*, vol. 49, no. 9, pp. 1305–1314, 1978.

[106] X. Zhang and M. Fujii, "Simultaneous measurements of the thermal conductivity and thermal diffusivity of molten salts with a transient short-hot-wire method," *International journal of thermophysics*, vol. 21, pp. 71–84, 2000.

[107] H. Ohta, G. Ogura, Y. Waseda, and M. Suzuki, "Thermal diffusivity measurements of molten salts using a three-layered cell by the laser flash method," *Review of scientific instruments*, vol. 61, no. 10, pp. 2645–2649, 1990.

[108] N. Araki, M. Ochi, and K. Kobayashi, "Measurement Method of Thermal Diffusivity of Liquids by Stepwise Radiative Heating: Part 2, Thermal Loss Characteristics and Measurement of Molten Salts," *Journal of the Japan Society of Mechanical Engineers, Series B*, vol. 49, no. 441, pp. 1058–1067, 1983.

[109] Q.-g. Zhao, S.-y. Miao, H. Guo, and Y.-t. Wu, "Temperature dependence of density and thermal conductivity of single molten salts," *Applied Thermal Engineering*, vol. 171, p. 115084, 2020.

[110] T. Asahina, M. Kosaka, and K. Tajiri, "Thermal diffusivity measurement of molten nitrates by pulse-heated flat plate method," *Kagaku Kogaku Ronbunshu*, vol. 14, no. 5, pp. 616–621, 1988.

[111] Y. Iwadate, K. Kawamura, and I. Okada, "Thermal conductivity of molten KNO_3-$NaNO_2$ mixtures measured with wave-front shearing interferometry," *Nippon Kagaku Kaishi*, vol. 1982, no. 6, pp. 969–976, 1982.

[112] O. Odawara, I. Okada, and K. Kawamura, "Measurement of the thermal diffusivity of HTS (a mixture of molten sodium nitrate-potassium nitrate-sodium nitrite; 7-44-49 mole%) by optical interferometry," *Journal of Chemical and Engineering Data*, vol. 22, no. 2, pp. 222–225, 1977.

[113] G. K. Creffield and A. J. Wickens, "Thermal conductivity of anhydrous borax, boric oxide, and sodium sulfate," *Journal of Chemical and Engineering Data*, vol. 20, no. 3, pp. 223–225, 1975.

[114] Y. Touloukian, R. Powell, C. Ho, and P. Klemens, "Thermophysical properties of matter-the tprc data series- volume 2. thermal conductivity-nonmetallic solids," Thermophysical and Electronic Properties Information Analysis Center, Tech. Rep., 1971.

[115] F.-k. Wang, X.-w. Fan, and Z.-g. Liu, "Testing for thermal properties of new phase-change thermal storage material," *Chem. Eng.(China)*, vol. 36, no. 10, pp. 58–61, 2008.

[116] G. Chen, "Perspectives on molecular-level understanding of thermophysics of liquids and future research directions," *Journal of Heat Transfer*, vol. 144, no. 1, p. 010801, 2022.

[117] D. Marx and J. Hutter, "*Ab initio* molecular dynamics: Theory and implementation," *Modern methods and algorithms of quantum chemistry*, vol. 1, no. 301-449, p. 141, 2000.

[118] M. Sangster and M. Dixon, "Interionic potentials in alkali halides and their use in simulations of the molten salts," *Advances in Physics*, vol. 25, no. 3, pp. 247–342, 1976.

[119] H. Wang, "Molecular Dynamics Simulations of Molten Salts: Force Field Evaluation and Development," 2 2022.

[120] T. Porter, M. M. Vaka, P. Steenblik, and D. Della Corte, "Computational methods to simulate molten salt thermophysical properties," *Communications Chemistry*, vol. 5, no. 1, p. 69, 2022.

[121] M. Wilson and P. Madden, "Polarization effects in ionic systems from first principles," *Journal of Physics: Condensed Matter*, vol. 5, no. 17, p. 2687, 1993.

[122] P. A. Madden, R. Heaton, A. Aguado, and S. Jahn, "From first-principles to material properties," *Journal of Molecular Structure: THEOCHEM*, vol. 771, no. 1-3, pp. 9–18, 2006.

[123] M. Salanne, B. Rotenberg, S. Jahn, R. Vuilleumier, C. Simon, and P. A. Madden, "Including many-body effects in models for ionic liquids," *Theoretical Chemistry Accounts*, vol. 131, pp. 1–16, 2012.

[124] A. Gheribi, D. Corradini, L. Dewan, P. Chartrand, C. Simon, P. Madden, and M. Salanne, "Prediction of the thermophysical properties of molten salt fast reactor fuel from first-principles," *Molecular Physics*, vol. 112, no. 9-10, pp. 1305–1312, 2014.

[125] J. Ocádiz-Flores, A. E. Gheribi, J. Vlieland, K. Dardenne, J. Rothe, R. J. Konings, and A. L. Smith, "New insights and coupled modelling of the structural and thermodynamic properties of the LiF-UF_4 system," *Journal of Molecular Liquids*, vol. 331, p. 115820, 2021.

[126] K. Tang and J. P. Toennies, "An improved simple model for the van der Waals potential based on universal damping functions for the dispersion coefficients," *The Journal of chemical physics*, vol. 80, no. 8, pp. 3726–3741, 1984.

[127] M. P. Allen and D. J. Tildesley, *Computer Simulation of Liquids*. Oxford University Press, 06 2017.

[128] Y. Ishii, S. Kasai, M. Salanne, and N. Ohtori, "Transport coefficients and the Stokes–Einstein relation in molten alkali halides with polarisable ion model," *Molecular Physics*, vol. 113, no. 17-18, pp. 2442–2450, 2015.

[129] D. Fu, C. Zhang, G. Wang, H. Na, and Y. Wu, "An update review of molecular dynamic study on thermal physical properties of molten salt," *Solar Energy Materials and Solar Cells*, vol. 273, p. 112916, 2024.

[130] D. Dickel, M. Nitol, and C. Barrett, "LAMMPS implementation of rapid artificial neural network derived interatomic potentials," *Computational Materials Science*, vol. 196, p. 110481, 2021.

[131] J. Weber, "Fluctuation dissipation theorem," *Physical Review*, vol. 101, no. 6, p. 1620, 1956.

[132] S. R. De Groot and P. Mazur, *Non-equilibrium thermodynamics*. Courier Corporation, 2013.

[133] A. E. Gheribi and P. Chartrand, "Thermal conductivity of molten salt mixtures: Theoretical model supported by equilibrium molecular dynamics simulations," *The Journal of chemical physics*, vol. 144, no. 8, p. 084506, 2016.

[134] M. Salanne, R. Vuilleumier, P. A. Madden, C. Simon, P. Turq, and B. Guillot, "Polarizabilities of individual molecules and ions in liquids from first principles," *Journal of Physics: Condensed Matter*, vol. 20, no. 49, p. 494207, 2008.

[135] R. S. DeFever, H. Wang, Y. Zhang, and E. J. Maginn, "Melting points of alkali chlorides evaluated for a polarizable and non-polarizable model," *The Journal of Chemical Physics*, vol. 153, no. 1, 2020.

[136] D. Corradini, D. Marrocchelli, P. A. Madden, and M. Salanne, "The effect of dispersion interactions on the properties of LiF in condensed phases," *Journal of Physics: Condensed Matter*, vol. 26, no. 24, p. 244103, 2014.

[137] R. J. Heaton, R. Brookes, P. A. Madden, M. Salanne, C. Simon, and P. Turq, "A first-principles description of liquid BeF_2 and its mixtures with LiF: 1. Potential development and pure BeF_2," *The Journal of Physical Chemistry B*, vol. 110, no. 23, pp. 11 454–11 460, 2006.

[138] N. Ohtori, M. Salanne, and P. A. Madden, "Calculations of the thermal conductivities of ionic materials by simulation with polarizable interaction potentials," *The Journal of chemical physics*, vol. 130, no. 10, 2009.

[139] M. Anderson, K. Sridharan, D. Morgan, P. Peterson, P. Calderoni, R. Scheele, A. Casekka, and B. McNamara, "Heat transfer salts for nuclear reactor systems-chemistry control, corrosion mitigation, and modeling," Univ. of Wisconsin, Madison, WI (United States); Univ. of California ..., Tech. Rep., 2015.

[140] M. Salanne, C. Simon, H. Groult, F. Lantelme, T. Goto, and A. Barhoun, "Transport in molten LiF-NaF-ZrF_4 mixtures: A combined computational and experimental approach," *Journal of Fluorine Chemistry*, vol. 130, no. 1, pp. 61–66, 2009.

[141] M. Salanne, C. Simon, P. Turq, and P. A. Madden, "Heat-transport properties of molten fluorides: Determination from first-principles," *Journal of Fluorine Chemistry*, vol. 130, no. 1, pp. 38–44, 2009.

[142] V. Sarou-Kanian, A.-L. Rollet, M. Salanne, C. Simon, C. Bessada, and P. A. Madden, "Diffusion coefficients and local structure in basic molten fluorides: in situ NMR measurements and molecular dynamics simulations," *Physical Chemistry Chemical Physics*, vol. 11, no. 48, pp. 11 501–11 506, 2009.

[143] C. Merlet, P. A. Madden, and M. Salanne, "Internal mobilities and diffusion in an ionic liquid mixture," *Physical Chemistry Chemical Physics*, vol. 12, no. 42, pp. 14 109–14 114, 2010.

[144] M. Salanne, D. Marrocchelli, C. Merlet, N. Ohtori, and P. A. Madden, "Thermal conductivity of ionic systems from equilibrium molecular dynamics," *Journal of Physics: Condensed Matter*, vol. 23, no. 10, p. 102101, 2011.

[145] C. Bessada, O. Pauvert, L. Maksoud, D. Zanghi, V. Sarou-Kanian, M. Gobet, A. Rollet, A. Rakhmatullin, M. Salanne, C. Simon *et al.*, "In Situ Experimental Approach of Speciation in Molten Fluorides: A Combination of NMR, EXAFS, and Molecular Dynamics," *Molten Salts Chemistry and Technology*, pp. 219–228, 2014.

[146] E. Sooby, A. Baty, O. Beneš, P. McIntyre, N. Pogue, M. Salanne, and A. Sattarov, "Candidate molten salt investigation for an accelerator driven subcritical core," *Journal of nuclear materials*, vol. 440, no. 1-3, pp. 298–303, 2013.

[147] Y. Ishii, K. Sato, M. Salanne, P. A. Madden, and N. Ohtori, "Thermal conductivity of molten alkali metal fluorides (LiF, NaF, KF) and their mixtures," *The Journal of Physical Chemistry B*, vol. 118, no. 12, pp. 3385–3391, 2014.

[148] M. Levesque, V. Sarou-Kanian, M. Salanne, M. Gobet, H. Groult, C. Bessada, P. A. Madden, and A.-L. Rollet, "Structure and dynamics in yttrium-based molten rare earth alkali fluorides," *The Journal of Chemical Physics*, vol. 138, no. 18, 2013.

[149] J. Dai, D. Long, P. Huai, and Q. Li, "Molecular dynamics studies of the structure of pure molten ThF_4 and ThF_4-LiF-BeF_2 melts," *Journal of Molecular Liquids*, vol. 211, pp. 747–753, 2015.

[150] D. Corradini, Y. Ishii, N. Ohtori, and M. Salanne, "DFT-based polarizable force field for TiO_2 and SiO_2," *Modelling and Simulation in Materials Science and Engineering*, vol. 23, no. 7, p. 074005, 2015.

[151] A. E. Gheribi, M. Salanne, and P. Chartrand, "Thermal transport properties of halide solid solutions: Experiments vs equilibrium molecular dynamics," *The Journal of chemical physics*, vol. 142, no. 12, 2015.

[152] ——, "Formulation of temperature-dependent thermal conductivity of NaF, β-Na_3AlF_6, $Na_5Al_3F_{14}$, and molten Na_3AlF_6 supported by equilibrium molecular dynamics and density functional theory," *The Journal of Physical Chemistry C*, vol. 120, no. 40, pp. 22 873–22 886, 2016.

[153] S. Wang, H. Luo, H. Deng, S. Xiao, and W. Hu, "A molecular dynamics study of the transport properties of LiF-BeF_2-ThF_4 molten salt," *Journal of Molecular Liquids*, vol. 234, pp. 220–226, 2017.

[154] H. Shishido, N. Yusa, H. Hashizume, Y. Ishii, and N. Ohtori, "Thermal design investigation for a flinabe blanket system," *Fusion Science and Technology*, vol. 72, no. 3, pp. 382–388, 2017.

[155] B. Li, S. Dai, and D.-e. Jiang, "Molecular dynamics simulations of structural and transport properties of molten NaCl-UCl_3 using the polarizable-ion model," *Journal of Molecular Liquids*, vol. 299, p. 112184, 2020.

[156] A. E. Gheribi, K. Machado, D. Zanghi, C. Bessada, M. Salanne, and P. Chartrand, "On the determination of ion transport numbers in molten salts using molecular dynamics," *Electrochimica Acta*, vol. 274, pp. 266–273, 2018.

[157] A. E. Gheribi, A. Serva, M. Salanne, K. Machado, D. Zanghi, C. Bessada, and P. Chartrand, "Study of the partial charge transport properties in the molten alumina via molecular dynamics," *ACS omega*, vol. 4, no. 5, pp. 8022–8030, 2019.

[158] F. Wu, S. Roy, A. S. Ivanov, S. K. Gill, M. Topsakal, E. Dooryhee, M. Abeykoon, G. Kwon, L. C. Gallington, P. Halstenberg *et al.*, "Elucidating ionic correlations beyond simple charge alternation in molten $MgCl_2$-KCl mixtures," *The journal of physical chemistry letters*, vol. 10, no. 24, pp. 7603–7610, 2019.

[159] J. Wu, H. Ni, W. Liang, G. Lu, and J. Yu, "Molecular dynamics simulation on local structure and thermodynamic properties of molten ternary chlorides systems for thermal energy storage," *Computational Materials Science*, vol. 170, p. 109051, 2019.

[160] A. Smith, E. Capelli, R. Konings, and A. Gheribi, "A new approach for coupled modelling of the structural and thermo-physical properties of molten salts. Case of a polymeric liquid LiF-BeF_2," *Journal of Molecular Liquids*, vol. 299, p. 112165, 2020.

[161] J.-X. Dai, W. Zhang, C.-L. Ren, and X.-J. Guo, "Prediction of dynamics properties of ThF_4-based fluoride molten salts by molecular dynamic simulation," *Journal of Molecular Liquids*, vol. 318, p. 114059, 2020.

[162] A. Smith, "Structure-property relationships in actinide containing molten salts – A review: Understanding and modelling the chemistry of nuclear fuel salts," *Journal of Molecular Liquids*, vol. 360, p. 119426, 2022.

[163] J. Jerden, "Molten salt thermophysical properties database development: 2019 update," Argonne National Lab.(ANL), Argonne, IL (United States), Tech. Rep., 2019.

[164] G. Lambotte and P. Chartrand, "Thermodynamic optimization of the (Na_2O+ SiO_2+ NaF+ SiF_4) reciprocal system using the modified quasichemical model in the quadruplet approximation," *The Journal of Chemical Thermodynamics*, vol. 43, no. 11, pp. 1678–1699, 2011.

[165] S. Benalia, "Modèle thermodynamique pour les chromates, molybdates et tungstates de sodium et de potassium impliqués dans la corrosion des aciers à haute température," Ph.D. dissertation, Polytechnique Montréal, August 2023.

[166] C. Robelin and P. Chartrand, "Thermodynamic evaluation and optimization of the (NaF+AlF_3+CaF_2+BeF_2+Al_2O_3+BeO) system," *The Journal of Chemical Thermodynamics*, vol. 57, pp. 387–403, 2013.

[167] D. Lindberg, R. Backman, and P. Chartrand, "Thermodynamic evaluation and optimization of the (NaCl+Na_2SO_4+Na_2CO_3+KCl+K_2SO_4+K_2CO_3) system," *The Journal of Chemical Thermodynamics*, vol. 39, no. 7, pp. 1001–1021, 2007.

[168] E. Renaud, C. Robelin, M. Heyrman, and P. Chartrand, "Thermodynamic evaluation and optimization of the (LiF+NaF+KF+MgF_2+CaF_2+SrF_2) system," *The Journal of Chemical Thermodynamics*, vol. 41, no. 5, pp. 666–682, 2009.

[169] C. Robelin, P. Chartrand, and A. D. Pelton, "Thermodynamic evaluation and optimization of the ($NaNO_3$+KNO_3+Na_2SO_4+K_2SO_4) system," *The Journal of Chemical Thermodynamics*, vol. 83, pp. 12–26, 2015.

[170] E. Renaud, C. Robelin, A. E. Gheribi, and P. Chartrand, "Thermodynamic evaluation and optimization of the Li, Na, K, Mg, Ca, Sr/F, Cl reciprocal system," *The Journal of Chemical Thermodynamics*, vol. 43, no. 8, pp. 1286–1298, 2011.

[171] J. W. McMurray and S. S. Raiman, "Thermodynamic modeling of the K-KCl and Mg-$MgCl_2$ binary systems using the CALPHAD method," *Solar Energy*, vol. 170, pp. 1039–1042, 2018.

[172] K. Wang, Z. Fei, J. Wang, Z. Wu, C. Li, and L. Xie, "Thermodynamic description of the AgCl-$CoCl_2$-$InCl_3$–KCl system," *Materials Chemistry and Physics*, vol. 163, pp. 73–87, 2015.

[173] J. W. Mcmurray, T. M. Besmann, J. Ard, B. FItzpatrick, M. Piro, J. Jerden, M. Williamson, B. S. Collins, B. R. Betzler, and A. L. Qualls, "Multi-physics simulations for molten salt reactor evaluation: Chemistry modeling and database development," Oak Ridge National Lab.(ORNL), Oak Ridge, TN (United States), Tech. Rep., 2018.

[174] O. Beneš and P. Souček, "Molten salt reactor fuels," in *Advances in Nuclear Fuel Chemistry*. Elsevier, 2020, pp. 249–271.

[175] M. Beilmann, O. Beneš, R. Konings, and T. Fanghänel, "Thermodynamic investigation of the (LiF + NaF + CaF_2 + LaF_3) system," *The Journal of Chemical Thermodynamics*, vol. 43, no. 10, pp. 1515–1524, 2011.

[176] O. Beneš, J. Van der Meer, and R. Konings, "Modelling and calculation of the phase diagrams of the LiF-NaF-RbF-LaF_3 system," *Calphad*, vol. 31, no. 2, pp. 209–216, 2007.

[177] P. Chartrand and A. D. Pelton, "Thermodynamic evaluation and optimization of the Li, Na, K, Mg, Ca//F, Cl reciprocal system using the modified quasi-chemical model," *Metallurgical and Materials Transactions A*, vol. 32, pp. 1417–1430, 2001.

[178] ——, "Thermodynamic evaluation and optimization of the LiF-NaF-KF-MgF_2-CaF_2 system using the modified quasi-chemical model," *Metallurgical and Materials Transactions A*, vol. 32, pp. 1385–1396, 2001.

[179] E. B. C. Bale, "Fact-Web suite of interactive programs," https://www.crct.polymtl.ca/factweb.php, accessed 04.22.

[180] P. W. Bridgman *et al.*, "Physics of high pressure," 1952.

[181] J. F. Kincaid and H. Eyring, "Free volumes and free angle ratios of molecules in liquids," *The Journal of Chemical Physics*, vol. 6, no. 10, pp. 620–629, 1938.

[182] K. Cornwell, "The thermal conductivity of molten salts," *Journal of Physics D: Applied Physics*, vol. 4, no. 3, p. 441, 1971.

[183] F. Lindemann, "About the Calculation of Molecular Own Frequencies," *Physical Magazine*, vol. 11, p. 609–612, 1910.

[184] M. R. Rao, "Thermal Conductivity of Liquids," *Phys. Rev.*, vol. 59, pp. 212–212, Jan 1941.

[185] J. Horrocks and E. McLaughlin, "Temperature dependence of the thermal conductivity of liquids," *Transactions of the Faraday Society*, vol. 59, pp. 1709–1716, 1963.

[186] M. Harada, M. Tanigaki, and Y. Tada, "Law of corresponding states of uniunivalent molten salts," *Industrial & Engineering Chemistry Fundamentals*, vol. 22, no. 1, pp. 116–121, 1983.

[187] R. E. Young and J. P. O'Connell, "An empirical corresponding states correlation of densities and transport properties of 1-1 alkali metal molten salts," *Industrial & Engineering Chemistry Fundamentals*, vol. 10, no. 3, pp. 418–423, 1971.

[188] D. Chandler, "Rough hard sphere theory of the self-diffusion constant for molecular liquids," *The Journal of Chemical Physics*, vol. 62, no. 4, pp. 1358–1363, 1975.

[189] S. Li, "The thermal conductivity of liquid hydrocarbons," 1984.

[190] M. Assael and W. Wakeham, "Vibrating-wire viscometry on liquids at high pressure," *Fluid phase equilibria*, vol. 75, pp. 269–285, 1992.

[191] F. Ciotta, J. M. Trusler, and V. Vesovic, "Extended hard-sphere model for the viscosity of dense fluids," *Fluid Phase Equilibria*, vol. 363, pp. 239–247, 2014.

[192] J. O. Hirschfelder, C. F. Curtiss, and R. B. Bird, *The molecular theory of gases and liquids*. John Wiley & Sons, 1964.

[193] M. Z. Hossain, M. H. Kassaee, S. Jeter, and A. S. Teja, "A new model for the thermal conductivity of molten salts," *International Journal of Thermophysics*, vol. 35, no. 2, pp. 246–255, 2014.

[194] Q.-G. Zhao, S.-J. Liu, H. Guo, and X. Chen, "A theoretical model for predicting the thermal conductivity of binary molten salts," *International Journal of Heat and Mass Transfer*, vol. 92, pp. 639–642, 2016.

[195] L. Muhmood, "Modeling for Thermal Conductivity of Ternary Molten Nitrate Salts Using Unit Cell Concept," *International Journal of Thermophysics*, vol. 41, no. 9, pp. 1–12, 2020.

[196] V. Ignatiev, A. Merzlyakov, V. Afonichkin, V. Khokhlov, and A. Salyulev, "Transport properties of molten-salt reactor fuel mixtures: the case of Na, Li, Be/F and Li, Be, Th/F salts," in *Seventh Information Exchange Meeting on Actinide and Fission Product Partitioning and Transmutation, 14th-16th October, Jeju, Republic of Korea*, 2002.

[197] A. Redkin, Y. Zaikov, O. Tkatcheva, and A. Shuryghin, "A physical model of molten salt data," *Zeitschrift für Naturforschung A*, vol. 63, no. 7-8, pp. 462–466, 2008.

[198] C. Ewing, J. Spann, and R. Miller, "Radiant Transfer of Heat in Molten Inorganic Compounds at High Temperatures." *Journal of chemical and engineering data*, vol. 7, no. 2, pp. 246–250, 1962.

[199] J. Magnusson, M. Memmott, and T. Munro, "Review of thermophysical property methods applied to fueled and un-fueled molten salts," *Annals of Nuclear Energy*, vol. 146, p. 107608, 2020.

[200] B. Merritt, M. Seneca, B. Wright, N. Cahill, N. Petersen, A. Fleming, and T. Munro, "Thermal Conductivity Characterization of Fluoride and Chloride Molten Salts Using a Modified Transient Hot-Wire Needle Probe," *International Journal of Thermophysics*, vol. 43, no. 10, p. 149, 2022.

[201] R. W. Bradshaw, D. B. Dawson, W. De la rosa, R. Gilbert, S. H. Goods, M. J. Hale, P. Jacobs, S. A. Jones, G. J. Kolb, J. E. Pacheco *et al.*, "Final test and evaluation results from the solar two project," Sandia National Lab.(SNL-NM), Albuquerque, NM (United States); Sandia ..., Tech. Rep., 2002.

[202] C. W. Forsberg, P. F. Peterson, H. Zhao *et al.*, "An advanced molten salt reactor using high-temperature reactor technology," in *Proceedings of ICAPP*, vol. 4, 2004.

[203] M. Liu, N. S. Tay, S. Bell, M. Belusko, R. Jacob, G. Will, W. Saman, and F. Bruno, "Review on concentrating solar power plants and new developments in high temperature thermal energy storage technologies," *Renewable and Sustainable Energy Reviews*, vol. 53, pp. 1411–1432, 2016.

[204] U. Pelay, L. Luo, Y. Fan, D. Stitou, and M. Rood, "Thermal energy storage systems for concentrated solar power plants," *Renewable and Sustainable Energy Reviews*, vol. 79, pp. 82–100, 2017.

[205] Y. Lin, G. Alva, and G. Fang, "Review on thermal performances and applications of thermal energy storage systems with inorganic phase change materials," *Energy*, vol. 165, pp. 685–708, 2018.

[206] B. Mignacca and G. Locatelli, "Economics and finance of molten salt reactors," *Progress in Nuclear Energy*, vol. 129, p. 103503, 2020.

[207] J. Serp, M. Allibert, O. Beneš, S. Delpech, O. Feynberg, V. Ghetta, D. Heuer, D. Holcomb, V. Ignatiev, J. L. Kloosterman *et al.*, "The molten salt reactor (MSR) in generation IV: overview and perspectives," *Progress in Nuclear Energy*, vol. 77, pp. 308–319, 2014.

[208] R. M. Saeed, K. L. Frick, A. Shigrekar, D. Mikkelson, and S. Bragg-Sitton, "Mapping thermal energy storage technologies with advanced nuclear reactors," *Energy Conversion and Management*, vol. 267, p. 115872, 2022.

[209] V. Morisson, M. Rady, E. Palomo, and E. Arquis, "Thermal energy storage systems for electricity production using solar energy direct steam generation technology," *Chemical Engineering and Processing: Process Intensification*, vol. 47, no. 3, pp. 499–507, 2008.

[210] A. E. Gheribi, A. D. Pelton, and J.-P. Harvey, "Determination of optimal compositions and properties for phase change materials in a solar electric generating station," *Solar Energy Materials and Solar Cells*, vol. 210, p. 110506, 2020.

[211] J. Zhang, C. W. Forsberg, M. F. Simpson, S. Guo, S. T. Lam, R. O. Scarlat, F. Carotti, K. J. Chan, P. M. Singh, W. Doniger *et al.*, "Redox potential control in molten salt systems for corrosion mitigation," *Corrosion Science*, vol. 144, pp. 44–53, 2018.

[212] "Average lithium carbonate price," https://www.statista.com/statistics/606350/battery-grade-lithium-carbonate-price/, accessed 04.22.

[213] M. S. Sohal, M. A. Ebner, P. Sabharwall, and P. Sharpe, "Engineering database of liquid salt thermophysical and thermochemical properties," Idaho National Lab.(INL), Idaho Falls, ID (United States), Tech. Rep., 2010.

[214] R. Serrano-López, J. Fradera, and S. Cuesta-López, "Molten salts database for energy applications," *Chemical Engineering and Processing: Process Intensification*, vol. 73, pp. 87–102, 2013.

[215] A. D. Pelton, "A database and sublattice model for molten salts," *Calphad*, vol. 12, no. 2, pp. 127–142, 1988.

[216] M. Bernagozzi, A. S. Panesar, and R. Morgan, "Molten salt selection methodology for medium temperature liquid air energy storage application," *Applied Energy*, vol. 248, pp. 500–511, 2019.

[217] K. Yasuda, T. OKUBO, O. Takeda, S. Natsui, and H. Sekimoto, "Activity report on information-gathering of database literatures for molten salts," *Electrochemistry*, pp. 20–00 058, 2020.

[218] C. A. Nieto de Castro and M. J. V. Lourenço, "Towards the Correct Measurement of Thermal Conductivity of Ionic Melts and Nanofluids," *Energies*, vol. 13, no. 1, p. 99, 2019.

[219] M. Revere and M. Tosi, "Structure and dynamics of molten salts," *Reports on Progress in Physics*, vol. 49, no. 9, p. 1001, 1986.

[220] M. Salanne, C. Simon, P. Turq, N. Ohtori, and P. Madden, "Modeling of molten salts," in *Molten Salts Chemistry*. Elsevier, 2013, pp. 1–16.

[221] A.-L. Rollet and M. Salanne, "Studies of the local structures of molten metal halides," *Annual Reports Section" C"(Physical Chemistry)*, vol. 107, pp. 88–123, 2011.

[222] N. Galamba, C. Nieto de Castro, and J. F. Ely, "Thermal conductivity of molten alkali halides from equilibrium molecular dynamics simulations," *The Journal of chemical physics*, vol. 120, no. 18, pp. 8676–8682, 2004.

[223] Z. Rong, J. Ding, W. Wang, G. Pan, and S. Liu, "*Ab initio* molecular dynamics calculation on microstructures and thermophysical properties of NaCl-$CaCl_2$-$MgCl_2$ for concentrating solar power," *Solar Energy Materials and Solar Cells*, vol. 216, p. 110696, 2020.

[224] N. Ohtori, T. Oono, and K. Takase, "Thermal conductivity of molten alkali halides: Temperature and density dependence," *The Journal of chemical physics*, vol. 130, no. 4, p. 044505, 2009.

[225] N. Galamba, C. N. de Castro, I. Marrucho, and J. Ely, "A corresponding states approach for the prediction of surface tension of molten alkali halides," *Fluid phase equilibria*, vol. 183, pp. 239–245, 2001.

[226] C. N. de Castro, "Thermal conductivity of molten materials. is experiment necessary?" in *Proc. TEMPMEKO*. Citeseer, 2004, pp. 49–58.

[227] C. A. Nieto de Castro and M. J. V. Lourenço, "Towards the correct measurement of thermal conductivity of ionic melts and nanofluids," *Energies*, vol. 13, no. 1, 2020.

[228] J. Healy, J. De Groot, and J. Kestin, "The theory of the transient hot-wire method for measuring thermal conductivity," *Physica B+ c*, vol. 82, no. 2, pp. 392–408, 1976.

[229] R. A. Perkins, D. G. Friend, H. Roder, and C. Nieto de Castro, "Thermal conductivity surface of argon: A fresh analysis," *International journal of thermophysics*, vol. 12, no. 6, pp. 965–984, 1991.

[230] Y. Tada, M. Harada, M. Tanigaki, and W. Eguchi, "Laser flash method for measuring thermal conductivity of liquids. Application to molten salts," *Industrial & Engineering Chemistry Fundamentals*, vol. 20, no. 4, pp. 333–336, 1981.

[231] P. B. Allen, J. L. Feldman, J. Fabian, and F. Wooten, "Diffusons, locons and propagons: Character of atomie yibrations in amorphous Si," *Philosophical Magazine B*, vol. 79, no. 11-12, pp. 1715–1731, 1999.

[232] A. Gheribi, D. Corradini, L. Dewan, P. Chartrand, C. Simon, P. Madden, and M. Salanne, "Prediction of the thermophysical properties of molten salt fast reactor fuel from first-principles," *Molecular Physics*, vol. 112, no. 9-10, pp. 1305–1312, 2014.

[233] A. Einstein, "Eine Beziehung zwischen dem elastischen Verhalten und der spezifischen Wärme bei festen Körpern mit einatomigem Molekül," *Annalen der Physik*, vol. 339, no. 1, pp. 170–174, 1911.

[234] D. G. Cahill, S. K. Watson, and R. O. Pohl, "Lower limit to the thermal conductivity of disordered crystals," *Physical Review B*, vol. 46, no. 10, p. 6131, 1992.

[235] D. R. Clarke, "Materials selection guidelines for low thermal conductivity thermal barrier coatings," *Surface and Coatings Technology*, vol. 163, pp. 67–74, 2003.

[236] Y. Nagasaka and A. Nagashima, "The thermal conductivity of molten $NaNO_3$ and KNO_3," *International Journal of Thermophysics*, vol. 12, no. 5, pp. 769–781, 1991.

[237] C. Bale, E. Bélisle, P. Chartrand, S. Decterov, G. Eriksson, A. Gheribi, K. Hack, I.-H. Jung, Y.-B. Kang, J. Melançon, A. Pelton, S. Petersen, C. Robelin, J. Sangster, P. Spencer, and M.-A. Van Ende, "FactSage thermochemical software and databases, 2010–2016," *Calphad*, vol. 54, pp. 35–53, 2016.

[238] A. E. Gheribi, A. T. Phan, and P. Chartrand, "A theoretical framework for reliable predictions of thermal conductivity of multicomponent molten salt mixtures: KCl-NaCl-$MgCl_2$ as a case study," *Solar Energy Materials and Solar Cells*, vol. 236, p. 111478, 2022.

[239] U. Mardolcar and C. Nieto de Castro, "The measurement of thermal conductivity at high temperatures," *High Temperatures. High Pressures (Print)*, vol. 24, no. 5, pp. 551–580, 1992.

[240] J. Kesseli and D. Lacy, "Advanced solar receiver conceptual design study," in *22nd Intersociety Energy Conversion Engineering Conference*. American Institute of Aeronautics and Astronautics, 1987, p. 9221.

[241] J. McDonald and H. T. Davis, "Determination of the thermal conductivities of several molten alkali halides by means of a sheathed hot-wire technique," *Physics and Chemistry of Liquids*, vol. 2, no. 3, pp. 119–134, 1971.

[242] D. W. Green, "Perry's chemical engineers' handbook, 9th edition," *2019 McGraw-Hill Education*, 2019.

[243] D. Singh, T. Kim, W. Zhao, W. Yu, and D. M. France, "Development of graphite foam infiltrated with $MgCl_2$ for a latent heat based thermal energy storage (LHTES) system," *Renewable Energy*, vol. 94, pp. 660–667, 2016.

[244] J. S. of Thermophysical Properties, "Thermophysical properties handbook," 1990.

[245] A. Caraballo, S. Galán-Casado, Á. Caballero, and S. Serena, "Molten salts for sensible thermal energy storage: a review and an energy performance analysis," *Energies*, vol. 14, no. 4, p. 1197, 2021.

[246] E. González-Roubaud, D. Pérez-Osorio, and C. Prieto, "Review of commercial thermal energy storage in concentrated solar power plants: Steam vs. molten salts," *Renewable and sustainable energy reviews*, vol. 80, pp. 133–148, 2017.

[247] M. T. Islam, N. Huda, A. Abdullah, and R. Saidur, "A comprehensive review of state-of-the-art concentrating solar power (CSP) technologies: Current status and research trends," *Renewable and Sustainable Energy Reviews*, vol. 91, pp. 987–1018, 2018.

[248] P. N. Haubenreich and J. Engel, "Experience with the molten-salt reactor experiment," *Nuclear Applications and technology*, vol. 8, no. 2, pp. 118–136, 1970.

[249] D. LeBlanc, "Molten salt reactors: A new beginning for an old idea," *Nuclear Engineering and design*, vol. 240, no. 6, pp. 1644–1656, 2010.

[250] G. Mohan, M. B. Venkataraman, and J. Coventry, "Sensible energy storage options for concentrating solar power plants operating above 600°C," *Renewable and Sustainable Energy Reviews*, vol. 107, pp. 319–337, 2019.

[251] M. M. Rahman, A. O. Oni, E. Gemechu, and A. Kumar, "Assessment of energy storage technologies: A review," *Energy Conversion and Management*, vol. 223, p. 113295, 2020.

[252] G. Alva, Y. Lin, and G. Fang, "An overview of thermal energy storage systems," *Energy*, vol. 144, pp. 341–378, 2018.

[253] A. G. Fernández, J. Gomez-Vidal, E. Oró, A. Kruizenga, A. Solé, and L. F. Cabeza, "Mainstreaming commercial CSP systems: A technology review," *Renewable energy*, vol. 140, pp. 152–176, 2019.

[254] M. Liu, J. Gomez, C. Turchi, N. Tay, W. Saman, and F. Bruno, "Determination of thermo-physical properties and stability testing of high-temperature phase-change materials for CSP applications," *Solar Energy Materials and Solar Cells*, vol. 139, pp. 81–87, 2015.

[255] S. Cantor, "Physical properties of molten-salt reactor fuel, coolant, and flush salts," Oak Ridge National Lab., Tenn., Tech. Rep., 1968.

[256] J. W. Mcmurray, K. Johnson, C. Agca, B. R. Betzler, D. J. Kropaczek, T. M. Besmann, D. Andersson, and N. Ezell, "Roadmap for thermal property measurements of Molten Salt Reactor systems," Oak Ridge National Lab.(ORNL), Oak Ridge, TN (United States), Tech. Rep., 2021.

[257] R. R. Romatoski and L.-W. Hu, "Fluoride salt coolant properties for nuclear reactor applications: A review," *Annals of Nuclear Energy*, vol. 109, pp. 635–647, 2017.

[258] Y. Bie, Z. Xu, Z. Li, T. Xu, and J. Tu, "Effects of molten salt multi-thermophysical properties on performance of the latent heat thermal energy storage system and synergetic optimization investigation," *Solar Energy Materials and Solar Cells*, vol. 255, p. 112277, 2023.

[259] J. Cooke, "Experimental determination of the thermal conductivity of molten lithium from 320 to 830°C," *The Journal of Chemical Physics*, vol. 40, no. 7, pp. 1902–1909, 1964.

[260] L. Cooper and S. Claiborne, "Measurement of the thermal conductivity of FLiNaK," 1952.

[261] Q.-G. Zhao, C.-X. Hu, S.-J. Liu, H. Guo, and Y.-T. Wu, "The thermal conductivity of molten $NaNO_3$, KNO_3, and their mixtures," *Energy Procedia*, vol. 143, pp. 774–779, 2017.

[262] N. Srinivasan, X. Xiao, and S. Seetharaman, "Radiation effects in high-temperature thermal diffusion measurements using the laser-flash method," *Journal of applied physics*, vol. 75, no. 5, pp. 2325–2331, 1994.

[263] R. Rusconi, W. C. Williams, J. Buongiorno, R. Piazza, and L.-W. Hu, "Numerical analysis of convective instabilities in a transient short-hot-wire setup for measurement of liquid thermal conductivity," *International Journal of Thermophysics*, vol. 28, pp. 1131–1146, 2007.

[264] H. Yang, R. Gallagher, P. Chartrand, and A. E. Gheribi, "Development of a molten salt thermal conductivity model and database for advanced energy systems," *Solar Energy*, vol. 256, pp. 158–178, 2023.

[265] W. Ding and T. Bauer, "Progress in research and development of molten chloride salt technology for next generation concentrated solar power plants," *Engineering*, vol. 7, no. 3, pp. 334–347, 2021.

[266] R. Roper, M. Harkema, P. Sabharwall, C. Riddle, B. Chisholm, B. Day, and P. Marotta, "Molten salt for advanced energy applications: A review," *Annals of Nuclear Energy*, vol. 169, p. 108924, 2022.

[267] V. Khokhlov, I. Korzun, V. Dokutovich, and E. Filatov, "Heat capacity and thermal conductivity of molten ternary lithium, sodium, potassium, and zirconium fluorides mixtures," *Journal of nuclear materials*, vol. 410, no. 1-3, pp. 32–38, 2011.

[268] G. Bovesecchi, P. Coppa, and S. Pistacchio, "A new thermal conductivity probe for high temperature tests for the characterization of molten salts," *Review of Scientific Instruments*, vol. 89, no. 5, p. 055107, 2018.

[269] P. Zhang, J. Cheng, Y. Jin, and X. An, "Evaluation of thermal physical properties of molten nitrate salts with low melting temperature," *Solar Energy Materials and Solar Cells*, vol. 176, pp. 36–41, 2018.

[270] J. A. Lane, H. G. MacPherson, and F. Maslan, *Fluid fuel reactors: Molten salt reactors, aqueous homogeneous reactors, fluoride reactors, chloride reactors, liquid metal reactors and why liquid fission.* Addison-Wesley Pub. Co., 1958.

[271] H. Wicaksono, X. Zhang, S. Fujiwara, and M. Fujii, "Measurements of thermal conductivity and thermal diffusivity of molten carbonates," *Kyushu University Institutional Repository*, vol. 15, no. 2, pp. 165–168, 12 2001.

[272] K. Takase, Y. Matsumoto, K. Sato, and N. Ohtori, "Thermal conductivity in molten alkali halides: composition dependence in mixtures of (Na-K) Cl," *Molecular Simulation*, vol. 38, no. 5, pp. 432–436, 2012.

[273] M.-T. Nguyen, V.-A. Glezakou, J. Lonergan, B. McNamara, P. D. Paviet, and R. Rousseau, "*Ab initio* molecular dynamics assessment of thermodynamic and transport properties in (K, Li) Cl and (K, Na) Cl molten salt mixtures," *Journal of Molecular Liquids*, vol. 326, p. 115262, 2021.

[274] P. B. Allen, J. L. Feldman, J. Fabian, and F. Wooten, "Diffusons, locons and propagons: Character of atomie vibrations in amorphous Si," *Philosophical Magazine B*, vol. 79, no. 11-12, pp. 1715–1731, 1999.

[275] B. Abeles, "Lattice thermal conductivity of disordered semiconductor alloys at high temperatures," *Physical Review*, vol. 131, no. 5, p. 1906, 1963.

[276] G. A. Slack, "Effect of isotopes on low-temperature thermal conductivity," *Physical Review*, vol. 105, no. 3, p. 829, 1957.

[277] A. E. Gheribi, S. Poncsák, R. St-Pierre, L. I. Kiss, and P. Chartrand, "Thermal conductivity of halide solid solutions: Measurement and prediction," *The Journal of Chemical Physics*, vol. 141, no. 10, p. 104508, 2014.

[278] A. E. Gheribi, A. T. Phan, H. Yang, R. C. Gallagher, and P. Chartrand, "The role of the local structure on the thermal transport within dissociated and complexed molten salt mixtures," *Journal of Molecular Liquids*, p. 125239, 2024.

[279] Y. Zhou, S. Xiong, X. Zhang, S. Volz, and M. Hu, "Thermal transport crossover from crystalline to partial-crystalline partial-liquid state," *Nature communications*, vol. 9, no. 1, p. 4712, 2018.

[280] B. Wu, Y. Zhou, and M. Hu, "Two-channel thermal transport in ordered-disordered superionic Ag_2Te and its traditionally contradictory enhancement by nanotwin boundary," *The Journal of Physical Chemistry Letters*, vol. 9, no. 19, pp. 5704–5709, 2018.

[281] Y. Zhou and S. Volz, "Thermal transfer in amorphous superionic Li_2S," *Physical Review B*, vol. 103, no. 22, p. 224204, 2021.

[282] W. Liang, G. Lu, and J. Yu, "Composition-dependent microstructure evolution in liquid $MgCl_2$-KCl: A first-principles molecular dynamics study," *Journal of Molecular Liquids*, vol. 309, p. 113131, 2020.

[283] C. Le Brun, "Molten salts and nuclear energy production," *Journal of nuclear materials*, vol. 360, no. 1, pp. 1–5, 2007.

[284] S. Flueckiger, Z. Yang, and S. V. Garimella, "An integrated thermal and mechanical investigation of molten-salt thermocline energy storage," *Applied Energy*, vol. 88, no. 6, pp. 2098–2105, 2011.

[285] N. Navarrete, R. Mondragón, D. Wen, M. E. Navarro, Y. Ding, and J. E. Juliá, "Thermal energy storage of molten salt–based nanofluid containing nano-encapsulated metal alloy phase change materials," *Energy*, vol. 167, pp. 912–920, 2019.

[286] R. I. Olivares, C. Chen, and S. Wright, "The thermal stability of molten lithium-sodium-potassium carbonate and the influence of additives on the melting point," *Journal of solar energy engineering*, vol. 134, no. 4, 2012.

[287] G. Pan, X. Wei, C. Yu, Y. Lu, J. Li, J. Ding, W. Wang, and J. Yan, "Thermal performance of a binary carbonate molten eutectic salt for high-temperature energy storage applications," *Applied Energy*, vol. 262, p. 114418, 2020.

[288] S. I. Stepanov and A. V. Boyarintsev, "Reprocessing of spent nuclear fuel in carbonate media: Problems, achievements, and prospects," *Nuclear Engineering and Technology*, 2022.

[289] O. Redlich and A. Kister, "Algebraic representation of thermodynamic properties and the classification of solutions," *Industrial & Engineering Chemistry*, vol. 40, no. 2, pp. 345–348, 1948.

[290] A. Pelton, "A complex ion model for molten halides," *Canadian Journal of Chemistry*, vol. 49, no. 24, pp. 3919–3934, 1971.

[291] X. Zhang, H. Wicaksono, S. Fujiwara, and M. Fujii, "Measurements of Thermal Conductivity and Thermal Diffusivity of Molten Carbonates," *High Temperatures-High Pressures*, vol. 34, pp. 617–625, 01 2002.

[292] K. Grjotheim, *Aluminium electrolysis: The chemistry of the Hall-Heroult process, 3rd*, 1977.

[293] A. D. Pelton, S. A. Degterov, G. Eriksson, C. Robelin, and Y. Dessureault, "The modified quasichemical model I—Binary solutions," *Metallurgical and Materials Transactions B*, vol. 31, pp. 651–659, 2000.

[294] C. W. Bale, E. Bélisle, P. Chartrand, S. A. Decterov, G. Eriksson, A. Gheribi, K. Hack, I.-H. Jung, Y.-B. Kang, J. Melançon *et al.*, "Reprint of: FactSage thermochemical software and databases, 2010-2016," *Calphad*, vol. 55, pp. 1–19, 2016.

[295] H. Yang, R. C. Gallagher, A.-T. Phan, P. Chartrand, and A. E. Gheribi, "A predictive approach for the compositional and temperature representation of thermal conductivity in multicomponent molten salt systems for advanced energy applications," *Materials Today Energy*, vol. 38, p. 101441, 2023.

[296] Y. Dessureault and A. Pelton, "Contribution to the quasi-chemical model of reciprocal molten salt solutions," *Journal de chimie physique*, vol. 88, pp. 1811–1830, 1991.

[297] G. J. Martyna, D. J. Tobias, and M. L. Klein, "Constant pressure molecular dynamics algorithms," *The Journal of chemical physics*, vol. 101, no. 5, pp. 4177–4189, 1994.

[298] H. Flyvbjerg and H. G. Petersen, "Error estimates on averages of correlated data," *The Journal of Chemical Physics*, vol. 91, no. 1, p. 461, 1989.

[299] R. Kubo, "The fluctuation-dissipation theorem," *Reports on progress in physics*, vol. 29, no. 1, p. 255, 1966.

[300] C. W. Bale, P. Chartrand, S. Degterov, G. Eriksson, K. Hack, R. B. Mahfoud, J. Melançon, A. Pelton, and S. Petersen, "FactSage thermochemical software and databases," *Calphad*, vol. 26, no. 2, pp. 189–228, 2002.

[301] V. Prissiajnyi, V. Vasilescu, and S. Sternberg, "Ultrasonic velocity and compressibility in reciprocal fused salt pairs (Cd, K, Cl, Br) and (Li, K, Cl, Br)," *The Journal of Chemical Thermodynamics*, vol. 3, no. 6, pp. 867–876, 1971.

[302] T. Førland, *Thermodynamic Properties of Systems of Fused Salts*. Institute of Inorganic Chemistry, Technical University of Norway, 1962.

[303] M. Hoshi, T. Omotani, and A. Nagashima, "Transient method to measure the thermal conductivity of high-temperature melts using a liquid-metal probe," *Review of Scientific Instruments*, vol. 52, no. 5, pp. 755–758, 1981.

[304] N. Le Brun and C. N. Markides, "A Galinstan-Filled Capillary Probe for Thermal Conductivity Measurements and Its Application to Molten Eutectic KNO_3 - $NaNO_3$ - $NaNO_2$ (HTS) up to 700 K," *International Journal of Thermophysics*, vol. 36, pp. 3222–3238, 2015.

[305] G. Janz, "Melting and premelting properties of the KNO_3-$NaNO_2$-$NaNO_3$ eutectic system. vol. 28," *J Chem Eng*, pp. 201–202, 1983.

[306] J. Mochinaga, K. Igarashi, and Y. Iwadate, "Molar volumes of the molten $NaNO_3$—KNO_3—$NaNO_2$ system," *Journal of chemical and engineering data (Print)*, vol. 30, no. 3, pp. 274–276, 1985.

[307] Y. Wang, X. Li, N. Li, C. Ling, Z. Tang, and Z. Li, "Thermal transport and storage performances of NaCl–KCl–NaF eutectic salt for high temperatures latent heat," *Solar Energy Materials and Solar Cells*, vol. 218, p. 110756, 2020.

[308] M. Opolot, C. Zhao, M. Liu, S. Mancin, F. Bruno, and K. Hooman, "A review of high temperature (>= 500°C) latent heat thermal energy storage," *Renewable and Sustainable Energy Reviews*, vol. 160, p. 112293, 2022.

[309] Y. Lin, G. Alva, and G. Fang, "Review on thermal performances and applications of thermal energy storage systems with inorganic phase change materials," *Energy*, vol. 165, pp. 685–708, 2018.

[310] A. Kuchibhotla, D. Banerjee, and V. Dhir, "Forced convection heat transfer of molten salts: A review," *Nuclear Engineering and Design*, vol. 362, p. 110591, 2020.

[311] H. Benoit, L. Spreafico, D. Gauthier, and G. Flamant, "Review of heat transfer fluids in tube-receivers used in concentrating solar thermal systems: Properties and heat transfer coefficients," *Renewable and Sustainable Energy Reviews*, vol. 55, pp. 298–315, 2016.

[312] A. B. Zavoico, "Design basis document," *Sandia National Laboratories, SAND2001-2100, Albuquerque, NM*, 2001.

[313] T. Liu, W. Liu, and X. Xu, "Properties and heat transfer coefficients of four molten-salt high temperature heat transfer fluid candidates for concentrating solar power plants," in *IOP conference series: earth and environmental science*, vol. 93, no. 1. IOP Publishing, 2017, p. 012023.

[314] V. A. Khokhlov, E. Filatov, A. Solheim, and J. Thonstad, "Thermal conductivity in cryolitic melts-new data and its influence on heat transfer in aluminum cells," in *Light Metals: Proceedings of Sessions, TMS Annual Meeting (Warrendale, Pennsylvania)*, 1998, pp. 501–506.

[315] K. Machado, D. Zanghi, V. Sarou-Kanian, S. Cadars, M. Burbano, M. Salanne, and C. Bessada, "Study of NaF-AlF_3 Melts by Coupling Molecular Dynamics, Density Functional Theory, and NMR Measurements," *The Journal of Physical Chemistry C*, vol. 121, no. 19, pp. 10 289–10 297, 2017.

[316] S. Nosé, "A unified formulation of the constant temperature molecular dynamics methods," *The Journal of chemical physics*, vol. 81, no. 1, pp. 511–519, 1984.

[317] D. C. Rapaport and D. C. R. Rapaport, *The art of molecular dynamics simulation*. Cambridge university press, 2004.

[318] P. Stepanov, "Speed of sound and adiabatic compressibility of binary sodium halide mixtures," *High Temperature*, vol. 56, pp. 689–693, 2018.

[319] V. P. Stepanov, "Speed of sound in binary molten mixtures of potassium halides," *High Temperature*, vol. 57, pp. 842–847, 2019.

[320] M. Smirnov, V. Minchenko, and A. Bukharov, "Sound absorption in molten alkali chlorides, bromides, iodides and their mixtures," *Electrochimica acta*, vol. 33, no. 2, pp. 213–220, 1988.

[321] M. B. Schreuder, J. A. Ocadiz Flores, A. E. Gheribi, O. Benes, J.-C. Griveau, E. Colineau, R. J. Konings, and A. L. Smith, "Experimental and computational exploration of the NaF-ThF_4 fuel system: Structure and thermochemistry," *The Journal of Physical Chemistry B*, vol. 125, no. 30, pp. 8558–8571, 2021.

[322] P. W. Bridgman, "The thermal conductivity of liquids under pressure," in *Proceedings of the American Academy of Arts and Sciences*, vol. 59, no. 7. JSTOR, 1923, pp. 141–169.

[323] S. Khrapak, "Bridgman formula for the thermal conductivity of atomic and molecular liquids," *Journal of Molecular Liquids*, vol. 381, p. 121786, 2023.

[324] Q.-G. Zhao, C.-X. Hu, S.-J. Liu, and X. Chen, "A unit-cell model for predicting the viscosity of binary molten salts," *International Journal of Heat and Mass Transfer*, vol. 107, pp. 484–488, 2017.

[325] M. Ausloos, "Thermal Conductivity," in *Encyclopedia of Materials: Science and Technology*, K. J. Buschow, R. W. Cahn, M. C. Flemings, B. Ilschner, E. J. Kramer, S. Mahajan, and P. Veyssière, Eds. Oxford: Elsevier, 2001, pp. 9151–9155.

[326] A. Z. Zhao, M. C. Wingert, R. Chen, and J. E. Garay, "Phonon gas model for thermal conductivity of dense, strongly interacting liquids," *Journal of Applied Physics*, vol. 129, no. 23, 2021.

[327] D. G. Cahill and R. Pohl, "Heat flow and lattice vibrations in glasses," *Solid State Communications*, vol. 70, no. 10, pp. 927–930, 1989.

[328] P. Klemens, "Thermal Conductivity and Lattice Vibrational Modes," ser. Solid State Physics, F. Seitz and D. Turnbull, Eds. Academic Press, 1958, vol. 7, pp. 1–98.

[329] Y. Marcus, "The compressibility of molten salts," *The Journal of Chemical Thermodynamics*, vol. 61, pp. 7–10, 2013.

[330] A. Birri, R. Gallagher, C. Agca, J. McMurray, and N. Dianne Bull Ezell, "Application of the Redlich-Kister expansion for estimating the density of molten fluoride psuedo-ternary salt systems of nuclear industry interest," *Chemical Engineering Science*, vol. 260, p. 117954, 2022.

[331] X. Zhou, Y. Zhou, Y. Deng, and Y. Zhang, "Molecular dynamics study on structure, vibrational properties, and transport coefficients of liquid alumina," *Materials*, vol. 15, no. 23, 2022.

[332] C. Landron, L. Hennet, T. E. Jenkins, G. N. Greaves, J. P. Coutures, and A. K. Soper, "Liquid Alumina: Detailed Atomic Coordination Determined from Neutron Diffraction Data Using Empirical Potential Structure Refinement," *Phys. Rev. Lett.*, vol. 86, pp. 4839–4842, May 2001.

[333] K. Machado, D. Zanghi, M. Salanne, V. Stabrowski, and C. Bessada, "Anionic structure in molten cryolite-alumina systems," *The Journal of Physical Chemistry C*, vol. 122, no. 38, pp. 21 807–21 816, 2018.

[334] X. Wang, J. D. Rincon, P. Li, Y. Zhao, and J. Vidal, "Thermophysical properties experimentally tested for NaCl-KCl-$MgCl_2$ eutectic molten salt as a next-generation high-temperature heat transfer fluids in concentrated solar power systems," *Journal of Solar Energy Engineering*, vol. 143, no. 4, 2021.

[335] K. M. Chung, T. Feng, J. Zeng, S. R. Adapa, X. Zhang, A. Z. Zhao, Y. Zhang, P. Li, Y. Zhao, J. E. Garay *et al.*, "Thermal conductivity measurement using modulated photothermal radiometry for nitrate and chloride molten salts," *International Journal of Heat and Mass Transfer*, vol. 217, p. 124652, 2023.

APPENDIX A SUPPORTING INFORMATION FOR ARTICLE 1

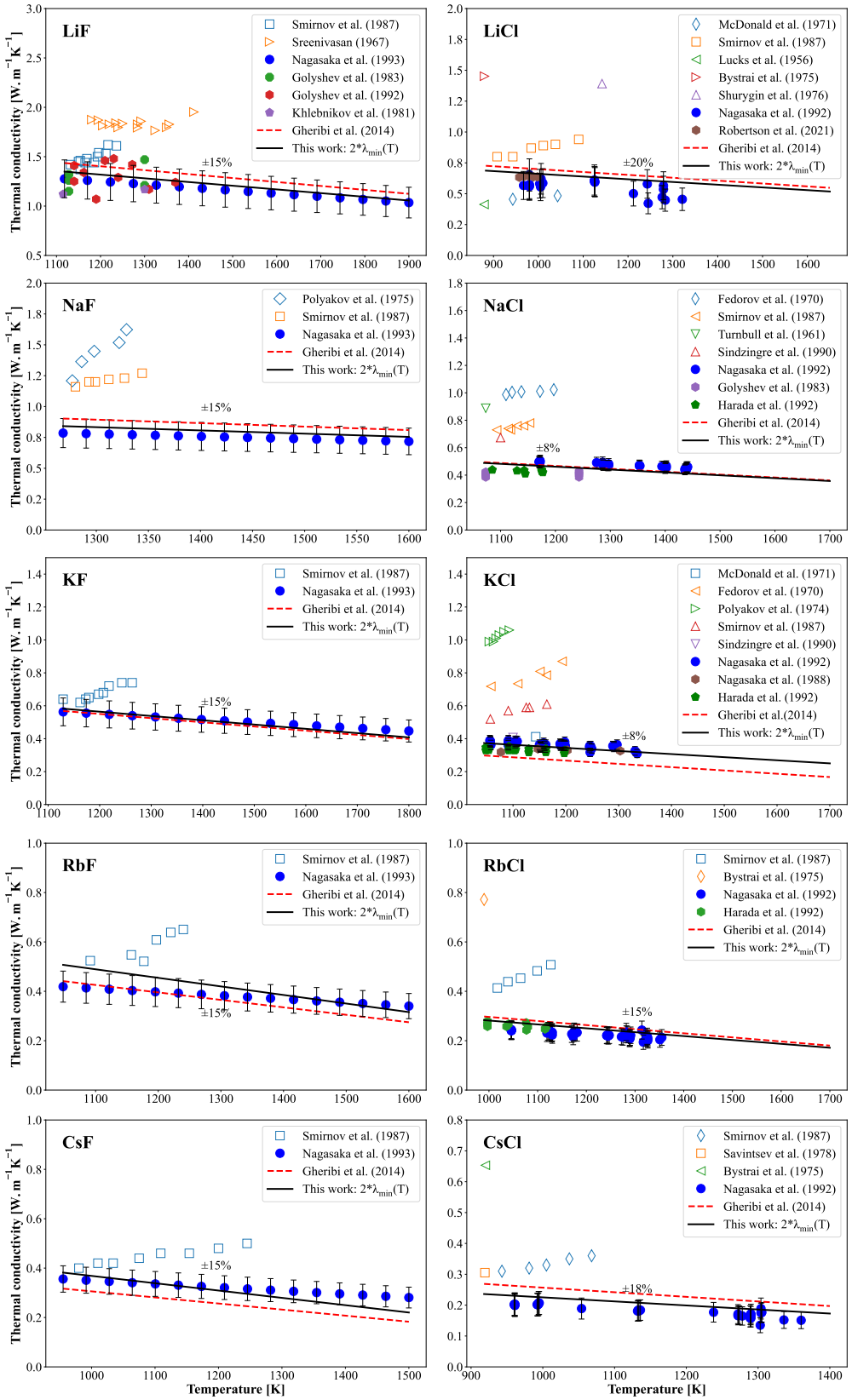

Figure A.1 Predicted (solid line) thermal conductivity has a function of temperature of monovalent fluorides and chlorides in comparison with various reliable (solid symbols), non reliable (open symbols) experimental data sets, and Gheribi et al. semi-empirical model (red dashed line).

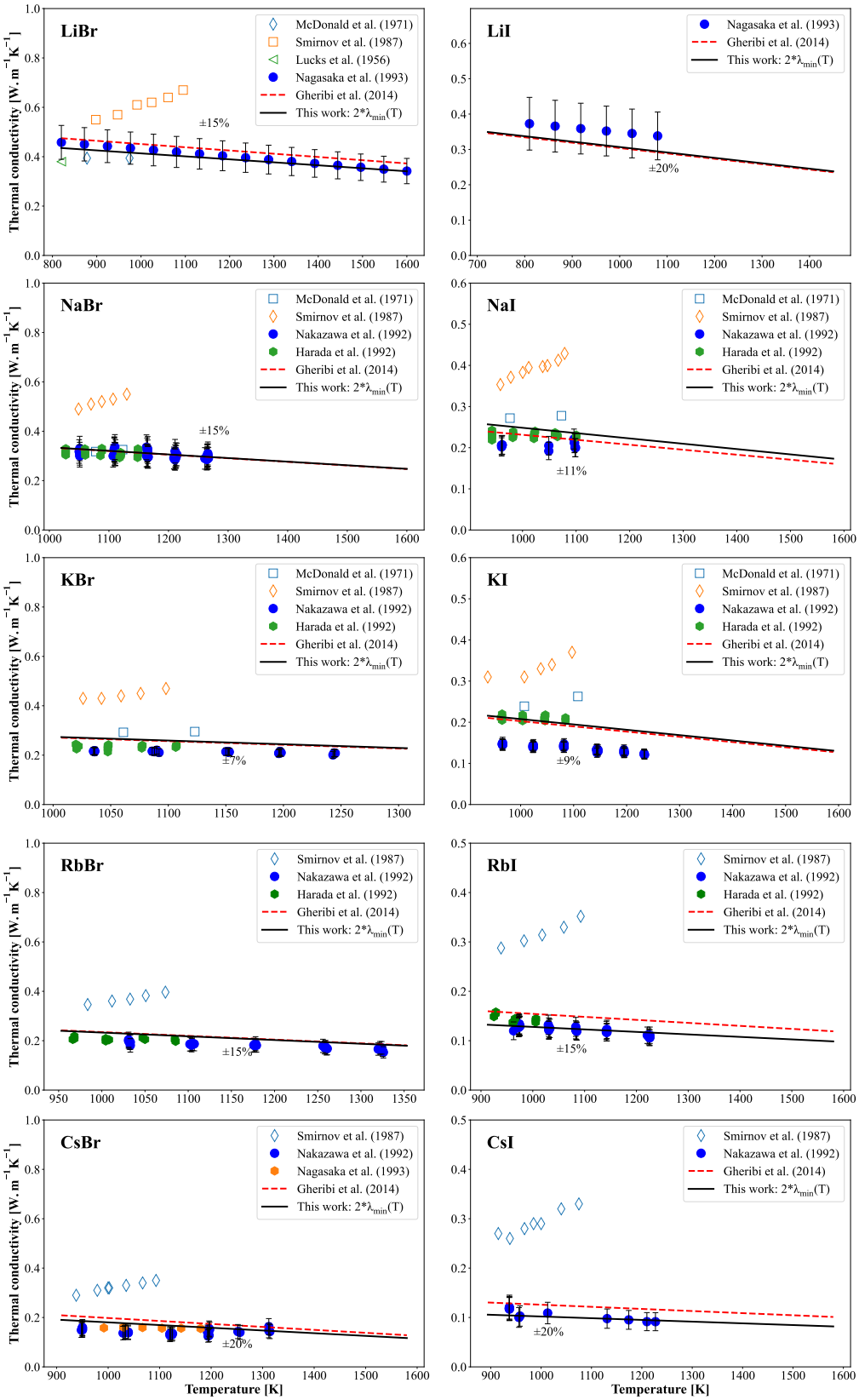

Figure A.2 Predicted (solid line) thermal conductivity has a function of temperature of monovalent bromides and iodides in comparison with various reliable (solid symbols), non reliable (open symbols) experimental data sets, and Gheribi et al. semi-empirical model (red dashed line).

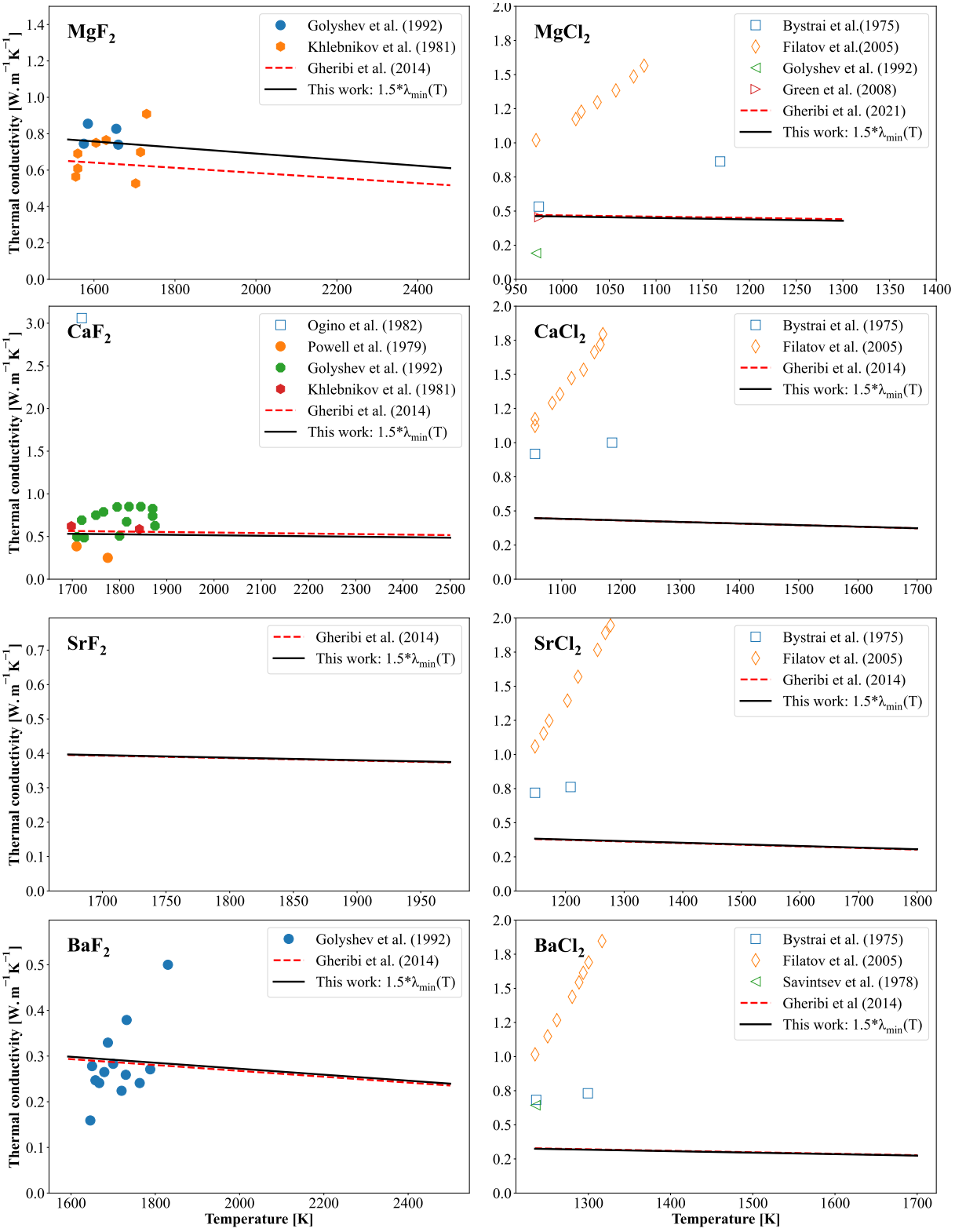

Figure A.3 Predicted (solid line) thermal conductivity has a function of the temperature of divalent fluorides and chlorides in comparison with various reliable (solid symbols), non reliable (open symbols) experimental data sets, and Gheribi et al. semi-empirical model (red dashed line).

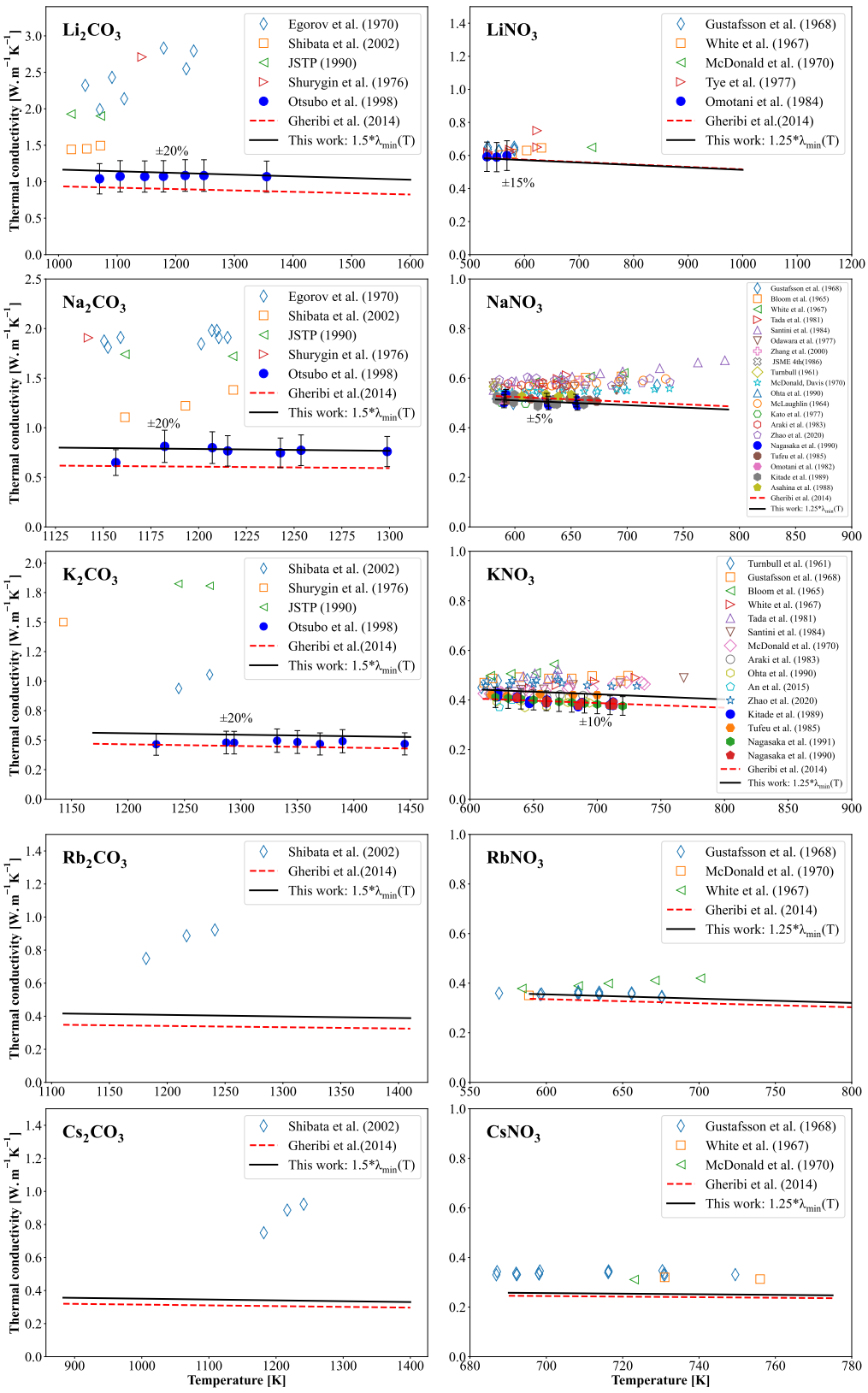

Figure A.4 Predicted (solid line) thermal conductivity has a function of temperature of carbonates and nitrates in comparison with various reliable (solid symbols), non reliable (open symbols) experimental data sets, and Gheribi et al. semi-empirical model (red dashed line).

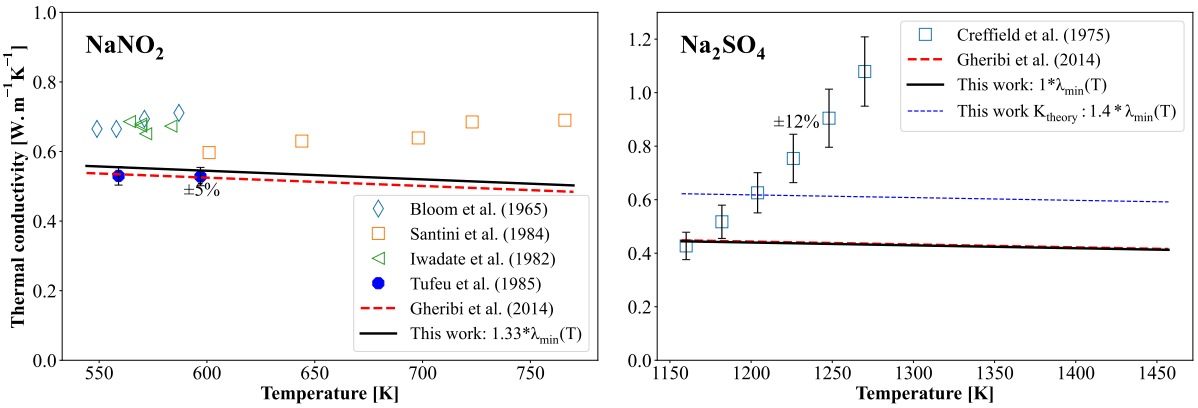

Figure A.5 Predicted (solid line) thermal conductivity has a function of temperature of $NaNO_2$ and Na_2SO_4 in comparison with various reliable (solid symbols), non reliable (open symbols) experimental data sets, and Gheribi et al. semi-empirical model(red dashed line). The sulfate salt family is a polymerizing salt, the constant coefficient $K = 1$ instead of $K_{theory} = 1.4$ (blue dashed line).

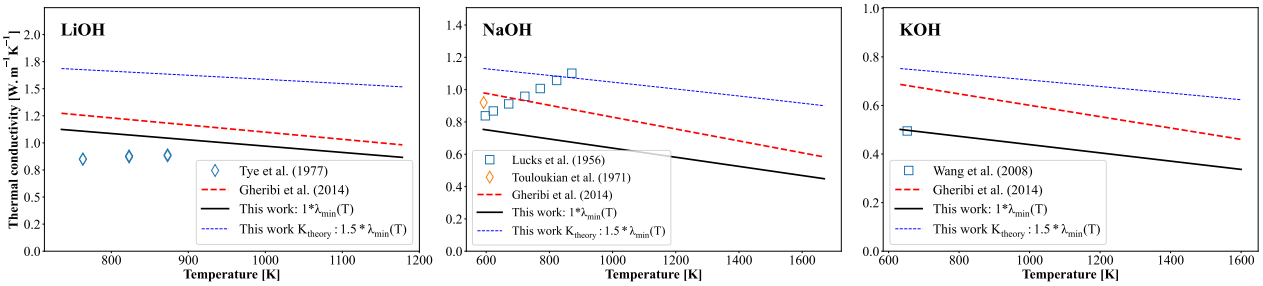

Figure A.6 Predicted (solid line) thermal conductivity has a function of temperature of hydroxides in comparison with various non reliable (open symbols) experimental data sets, and Gheribi et al. semi-empirical model (red dashed line). The hydroxide salt family is a polymerizing salt, the coefficient $K = 1$ instead of $K_{theory} = 1.5$ (blue dashed line)

APPENDIX B SUPPORTING INFORMATION FOR ARTICLE 2

B.1 Numerical simulations

Equilibrium molecular dynamics (EMD) simulations were conducted on simple binary systems within four salt families: fluoride (LiF-NaF, LiF-KF, NaF-KF), chloride (LiCl-NaCl, LiCl-KCl, NaCl-KCl), bromide (LiBr-NaBr, LiBr-KBr, NaBr-KBr, RbBr-CsBr), and iodide (LiI-NaI, LiI-KI, NaI-KI, RbI-CsI). Simulations were performed at a temperature slightly higher than the melting temperature of pure compounds, covering the entire range of compositions in increments of 0.125 mole fraction.

In each simulation, a total of 864 ions (432 cations and 432 anions) were included, with the simulation volume determined by a prior simulation in the isobaric-isothermal statistical ensemble (NPT) at the corresponding temperatures and a pressure of 10^5 Pa. Two sets of NPT simulations were initially performed at the designed simulating temperature. These simulations generated thermally equilibrated configurations. Following this, a new series of EMD simulations were conducted in the canonical statistical ensemble (NVT) to determine the thermal conductivity of the mixtures, using the configurations obtained from the previous NPT simulations. The volume in the NVT simulations remained fixed.

For both NPT and NVT simulations, temperature control was maintained using a Nosé-Hoover thermostat [316], and pressure control was achieved through an extension of the Martyna barostat [297] for NPT simulations. The relaxation times for both the thermostat and barostat were set to 0.5 ps. Equations of motion were integrated using the velocity Verlet algorithm [317], with time steps of 0.5 fs for NPT simulations and 1 fs for NVT simulations. The total simulation time was 0.5 ns for NPT and 5 ns for NVT. All simulations employed periodic boundary conditions and followed the minimum image convention.

The Dipole polarizable Ion model (DPIM) potential was used for describing ionic interactions, which includes charge-charge, charge-dipole, dipole-charge, dipole-dipole, a repulsion contribution, and two dispersion interaction terms [122].

$$\begin{aligned} V_{ij}(r_{ij}) = & \frac{q_i q_j}{r_{ij}} + \frac{q_i \boldsymbol{r}_{ij} \boldsymbol{\mu}_j}{r_{ij}^3} f_4^{ij}(r_{ij}) - \frac{\boldsymbol{\mu}_i \boldsymbol{r}_{ij} q_j}{r_{ij}^3} f_4^{ij}(r_{ij}) \\ & + \frac{\boldsymbol{\mu}_i \boldsymbol{\mu}_j}{r_{ij}^3} - \frac{3(\boldsymbol{r}_{ij}\boldsymbol{\mu}_i)(\boldsymbol{r}_{ij}\boldsymbol{\mu}_j)}{r_{ij}^5} \\ & + B_{ij} e^{-\alpha_{ij} r_{ij}} - \frac{C_6^{ij} f_6^{ij}}{r_{ij}^6} - \frac{C_8^{ij} f_8^{ij}}{r_{ij}^8}. \end{aligned} \tag{B.1}$$

where q_i and μ_i are respectively the charge and the dipole moment of the particle i. The

Born-Mayer-Huggins short range potential term, $B_{ij}e^{-\alpha_i r_i}$, is used to describe the short-distance overlap repulsion of electronic clouds. C_6^{ij} and C_8^{ij} are the dispersion coefficients. The dispersion damping function, f_n^{ij}, for short-range correction of interactions between charge and dipole and dispersion interactions is expressed as follows [126]:

$$f_n^{ij} = 1 - c_n^{ij} e^{-b_n^{ij} r_{ij}} \sum_{i=0}^{n} \frac{(b_n^{ij}\ r^{ij})^k}{k!} \tag{B.2}$$

The long-range electrostatic interactions,$V^{Coul} = \frac{1}{2}\sum_{i\neq j}^{N} \frac{q_i q_j}{r_{ij}}$, are considered by employing a three-dimension Ewald summation method [127]. The DPIM potential of the fluorides, chlorides, bromides and iodides of interests are reported in the literature [128, 138]. The $B_{ij}, \alpha_{ij}, C_6^{ij}, C_8^{ij}, b_n^{ij}, c_n^{ij}$ parameter set of the DPIM formalism is used to describing the total pairwise potentials between ionic pairs. The parameters were calculated by Ishii et al. [128] via a procedure of determining potential parameters of Madden [122] which is based solely on electronic structure calculations, employing Density Functional Theory (DFT). After that, by matching the dipoles and forces on the ions calculated from DFT on condensed phase ionic configurations, the potential parameters are deduced with an objective minimization procedure. As no experimental information has been considered in the parameterization procedure, the generated potentials are *ab initio*.

According to the Green-Kubo (GK) formalism [299], thermal conductivity, a non-equilibrium property, can be calculated from EMD. GK formalism is based on the fluctuation-dissipation theorem reported by Weber [131], therefore, it permits the interpretation of the thermal conductivity from the energy and charge fluctuations obtained from EMD. The entropy of a molten mixture can be calculated by non-convective fluxes of heat, mass, and charge [132]. Similar to our previous work, in the present study, the macroscopic energy flux is calculated as a summation of heat and enthalpic contributions [133], it can be expressed as:

$$\underline{\boldsymbol{J}}_E = \underline{\boldsymbol{J}}_Q + \sum_{i=1}^{N}(h_i + z_i\varphi))\underline{\boldsymbol{J}}_{M,i}, \tag{B.3}$$

where $\underline{\boldsymbol{J}}_E$, $\underline{\boldsymbol{J}}_Q$, and $\underline{\boldsymbol{J}}_{M,i}$ represent the energy, heat and mass fluxes, respectively; h_i and z_i are the partial enthalpy and charge of the component i. Obeying the GK method, the thermal conductivity induced by lattice vibrations for a given molten mixture of a given composition X, at a given temperature T, is evaluated from the simulations as a function of the correlation time, τ:

$$\lambda(T, \tau, \underline{X}) = \frac{1}{T^2}\left(L_{ee} - B^{-1}\sum_{i=0}^{2} L_{ez_i} A_{z_i z_j z_k}\right) \tag{B.4}$$

Where both A and B are the matrix determinants calculated for the MS mixtures as follows:

$$A_{\alpha\beta\gamma} = \begin{vmatrix} L_{e\alpha} & L_{\beta\alpha} & L_{\gamma\alpha} & \cdots \\ L_{e\beta} & L_{\beta\beta} & L_{\gamma\beta} & \cdots \\ L_{e\gamma} & L_{\beta\gamma} & L_{\gamma\gamma} & \cdots \\ \vdots & \vdots & \vdots & \ddots \end{vmatrix}, \quad B = \begin{vmatrix} L_{z_0z_0} & L_{z_1z_0} & L_{z_2z_0} & \cdots \\ L_{z_0z_1} & L_{z_1z_1} & L_{z_2z_1} & \cdots \\ L_{z_0z_2} & L_{z_1z_2} & L_{z_2z_2} & \cdots \\ \vdots & \vdots & \vdots & \ddots \end{vmatrix}. \tag{B.5}$$

Equation B.5 shows the matrix for any compound of MS mixtures. Where $\alpha\,\beta\,and\,\gamma$ is a ternary mixture. It can be reduced to $A_{\alpha\beta} = \begin{vmatrix} L_{e\alpha} & L_{\beta\alpha} \\ L_{e\beta} & L_{\beta\beta} \end{vmatrix}$, $B = \begin{vmatrix} L_{z_0z_0} & L_{z_1z_0} \\ L_{z_0z_1} & L_{z_1z_1} \end{vmatrix}$ for a binary mixture, and $A = L_{ez_0},\ B = L_{z_0z_0}$ for the pure MS.

The transport coefficients L in the above equations are determined through the Green-Kubo formulation [98]:

$$L_{\alpha\beta} = \frac{1}{Vk_B}\int_0^\infty C_{\alpha\beta}(t)dt \tag{B.6}$$

$$C_{\alpha\beta}(t) = \frac{1}{3}\langle \boldsymbol{j}_\alpha(t)\boldsymbol{j}_\beta(0)\rangle \quad (\alpha,\ \beta = e, z) \tag{B.7}$$

Where α and β can be e or z_i; k_B and V are Boltzmann constant and equilibrium volume of the system, respectively; $\boldsymbol{j}_e$ and $\boldsymbol{j}_z$ are correspondingly the energy (e) and charge(z) flux of the i ion. Notice that in Equation B.4, the first term L_{ee}/T^2 is responsible for the thermal conductivity of an electrically neutral fluid. The second term of Equation B.4 describes the thermo-electrical effect on thermal conductivity.

The potential energy for every charged particle must incorporate a self-energy term, which is expressed as [147]:

$$\Phi_i^{self} = -\frac{\alpha}{\sqrt{\pi}}q_i^2 \tag{B.8}$$

where α is the Ewald parameter. And the charge current is defined as:

$$\boldsymbol{j}_{z_1}(t) = \sum_{i\in I}(q_I - q_F)v_i(t) \tag{B.9}$$

In the first cation, where I = 0, and in the second cation, where I = 1 (with $q_F = -1$ representing the formal charge of the anion). The energy current $\boldsymbol{j}_e$ can be derived by considering the self-energy, various forces arising from repulsion, real-space forces, and reciprocal-space energy currents. For more details, please refer to [138, 147].

In practice, the total NVT run was divided into 20 blocks of 0.5ns, and the transport coefficients L were calculated independently in each block. The correlation time, τ, is set to 5ps which is large enough to ensure convergence of the thermal conductivity. Lastly, an average value over all the different blocks is considered as the thermal conductivity of a perfectly

thermally equilibrated system:

$$\lambda(\underline{X}, T) = \lim_{\tau \to \infty} \langle \lambda\ (\tau, T, \underline{X}) \rangle_{all\ blocks} \tag{B.10}$$

B.2 Predicted results of binary systems in comparison to the unreliable experimental dataset

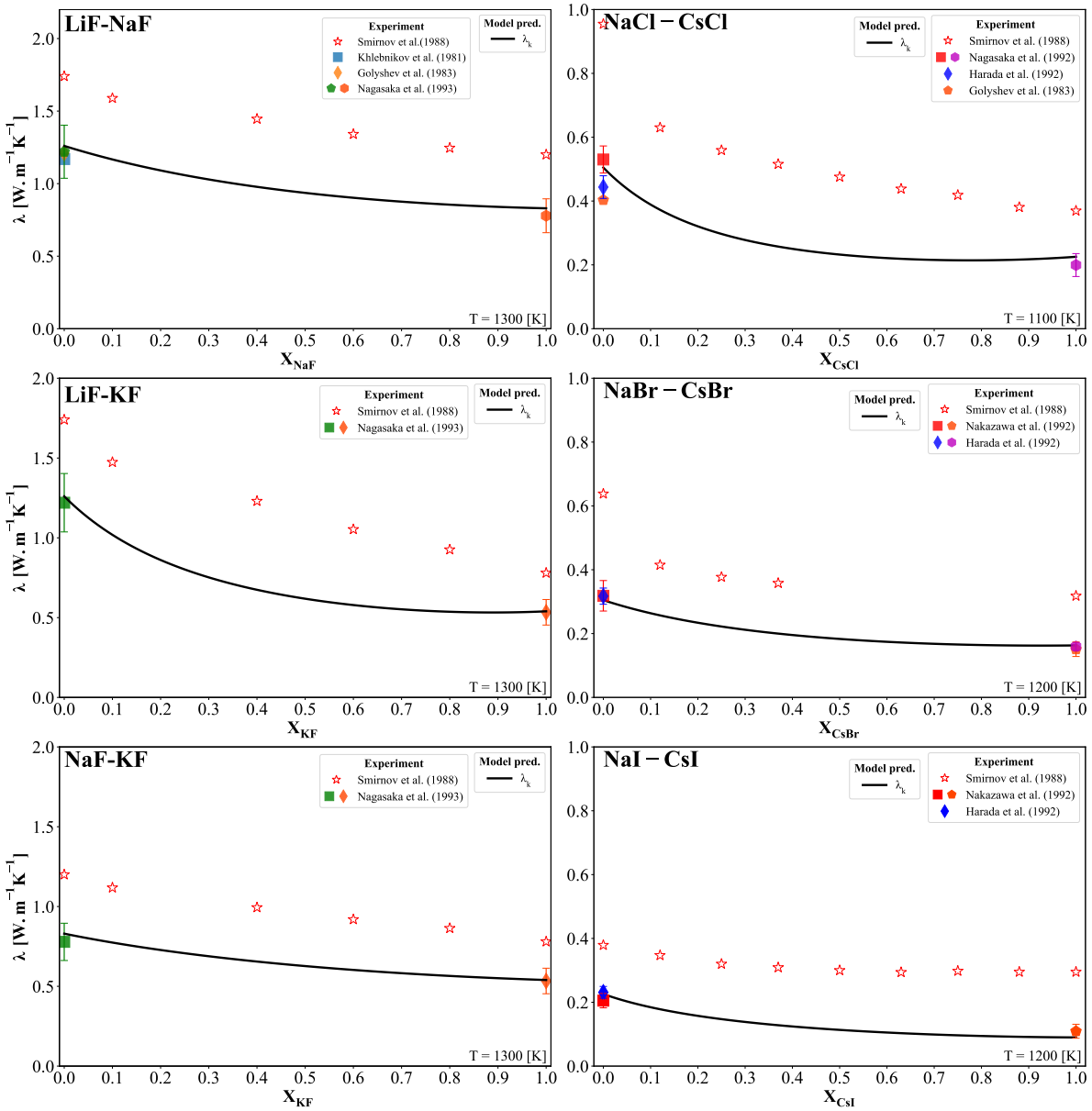

Figure B.1 Predicted (solid line) thermal conductivity of binary fluoride systems as a function of the composition in comparison with the reliable (solid symbol), and unreliable (open symbol) experimental data sets.

B.3 Compositional mapping of ternary systems

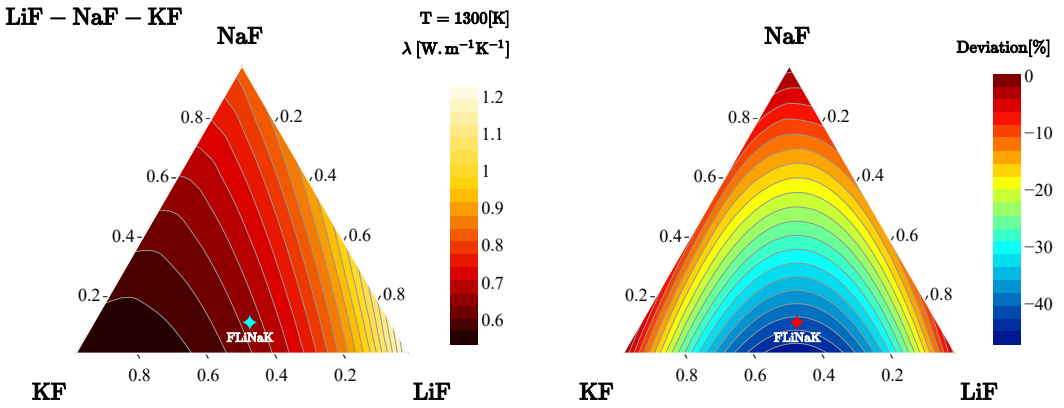

Figure B.2 Predicted thermal conductivity as a function of composition in the LiF-NaF-KF system at 1300 [K] (left), and the corresponding deviation between the theoretical prediction of thermal conductivity from a linear rule behavior (right).

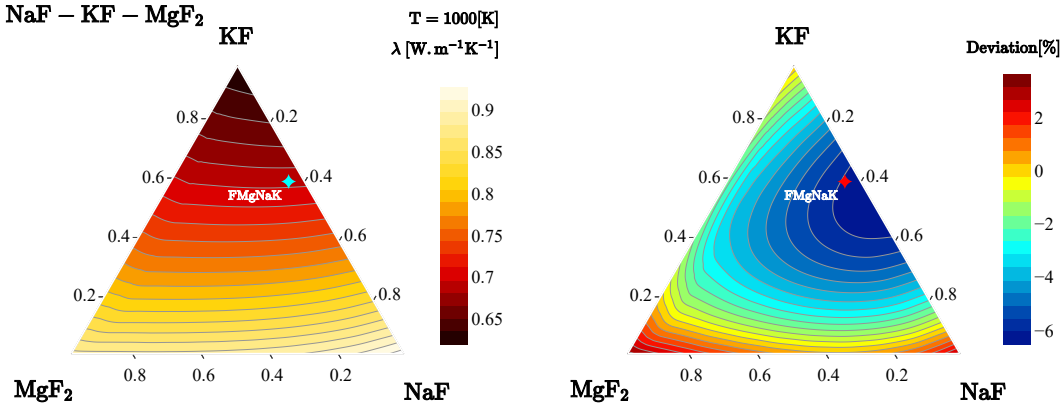

Figure B.3 Predicted thermal conductivity as a function of composition in the NaF-KF-MgF_2 system at 1000 [K] (left), and the corresponding deviation between the theoretical prediction of thermal conductivity from a linear rule behavior (right).

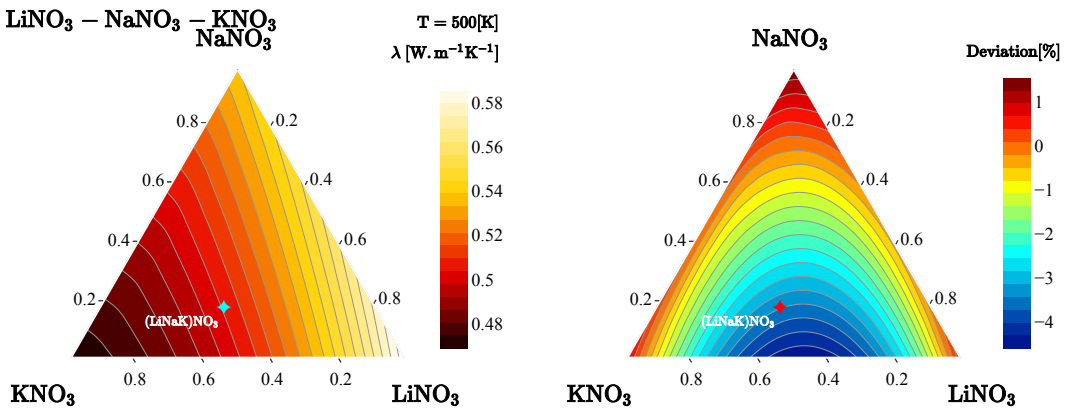

Figure B.4 Predicted thermal conductivity as a function of composition in the $LiNO_3$-$NaNO_3$-KNO_3 system at 500 [K] (left), and the corresponding deviation between the theoretical prediction of thermal conductivity from a linear rule behavior (right).

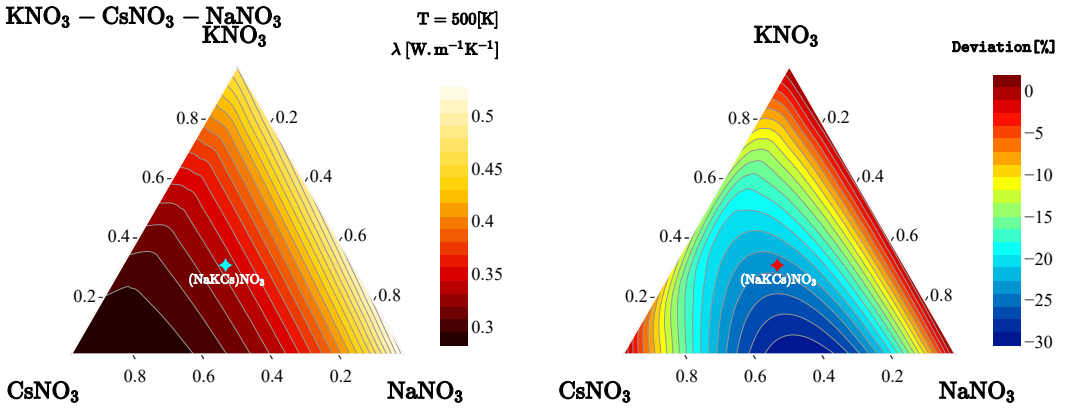

Figure B.5 Predicted thermal conductivity as a function of composition in the $NaNO_3$-KNO_3-$CsNO_3$ system at 500 [K] (left), and the corresponding deviation between the theoretical prediction of thermal conductivity from a linear rule behavior (right).

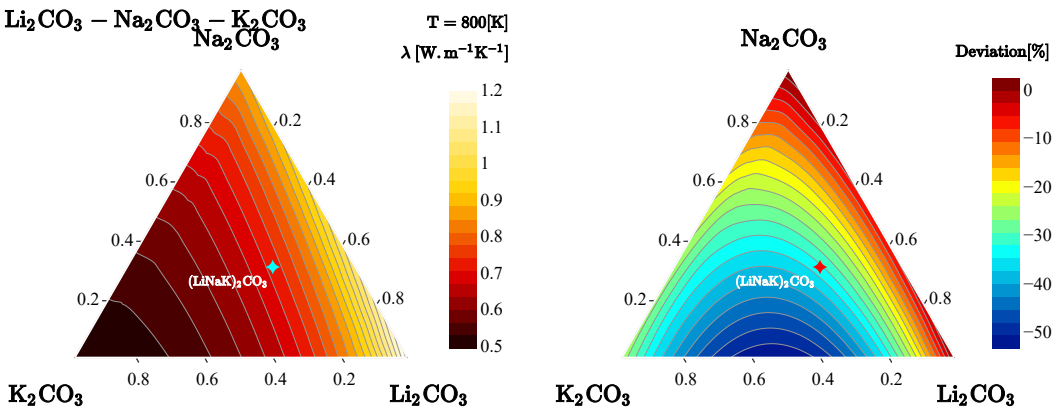

Figure B.6 Predicted thermal conductivity as a function of composition in the Li_2CO_3-Na_2CO_3-K_2CO_3 system at 800 [K] (left), and the corresponding deviation between the theoretical prediction of thermal conductivity from a linear rule behavior (right).

B.4 Energy flux vs thermo-electrical flux for NaCl-KCl binary system

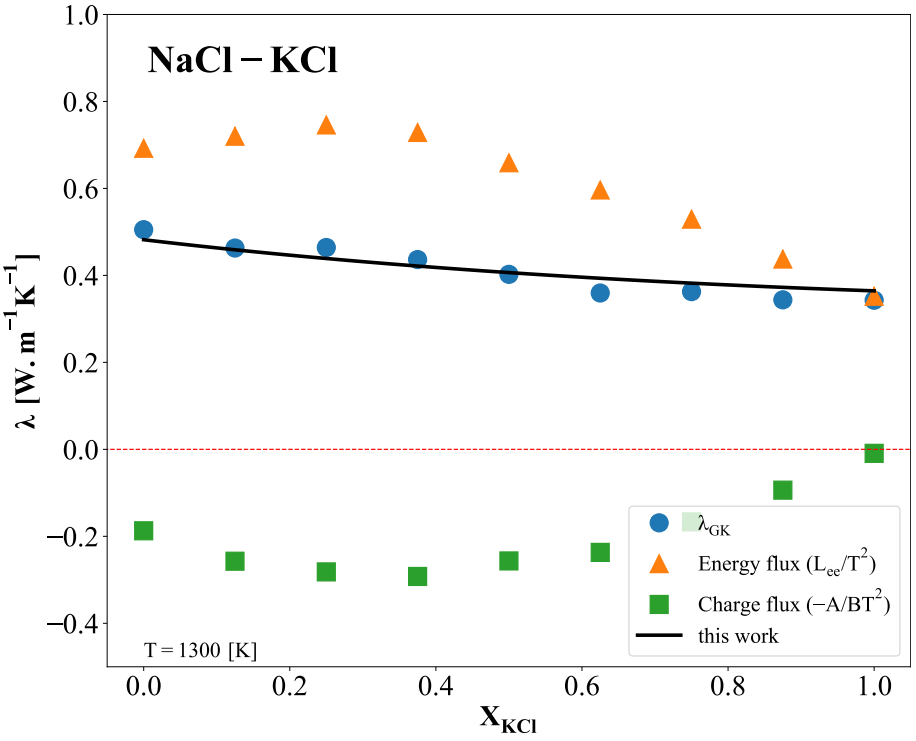

Figure B.7 Comparison of the predicted results with the energy current and charge current obtained from the MD simulation of NaCl-KCl at 1300 [K]

APPENDIX C SUPPORTING INFORMATION FOR ARTICLE 3

Using Equation 6.12, the sound velocity values for the reciprocal molten salt mixture LiCl-KBr were calculated based on the FTsalt Database of FactSage™ 8.4, and compared with the experimental data reported by Prissiajnyi et al. [301] at 1100 [K]. The predictions closely follow the trend of composition variation observed in the experimental work. In particular, at X*nominal* = 0.5, our prediction is nearly identical to the experimental results. However, there is a slight deviation for pure molten LiCl. Additionally, sound velocity calculations for various pure molten salts and mixtures have been compared with available experimental datasets, which are provided in the Supplementary Materials.

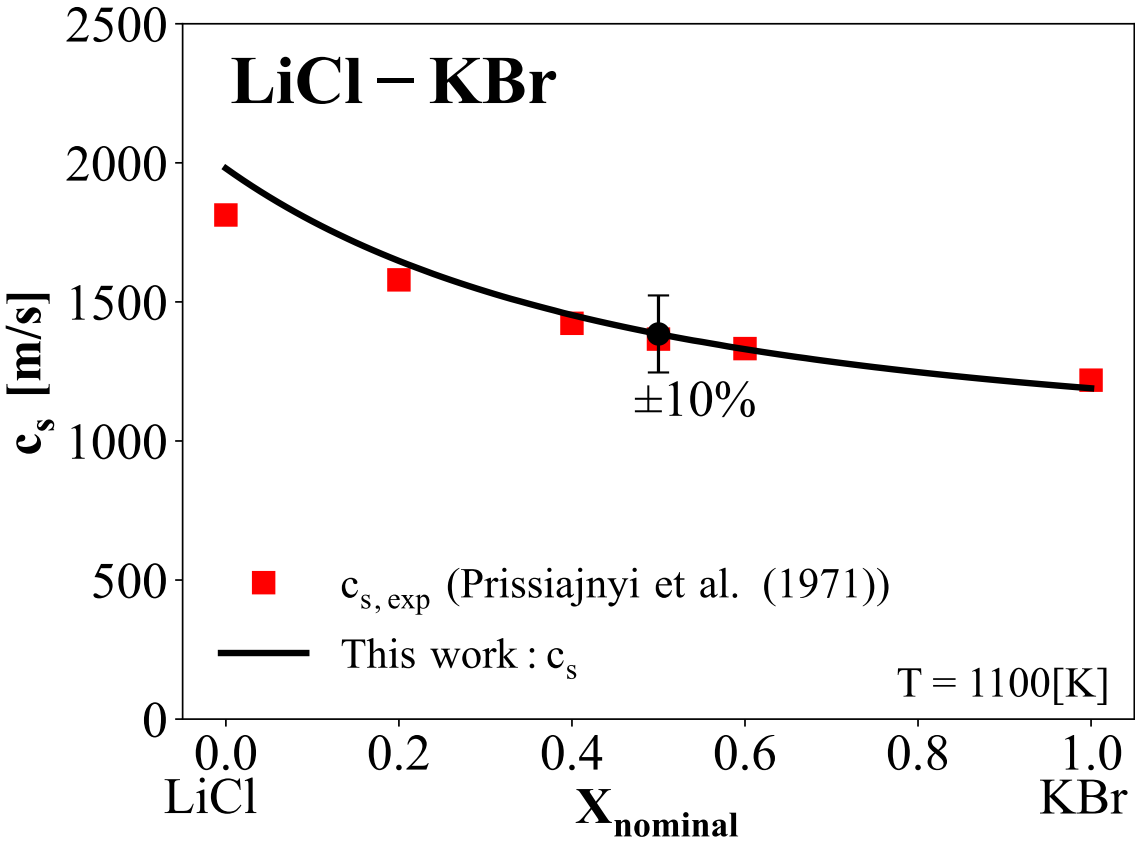

Figure C.1 Calculated sound velocity from the FTsalt Database of FactSage™ 8.4 for LiCl-KBr as a function of composition at 1100 [K], compared to the experimental data of Prissiajnyi et al. [301].

The following figures (Figure C.2, Figure C.3, Figure C.4) offer additional comparisons between EMD results and the predictions of the present model, further demonstrating its predictive capability. In each figure, the end members correspond to common-anion mixtures.

Notably, these figures do not include calibration of the thermal conductivity values for the end members (previously indicated by red dashed lines). Instead, only the predictions from the current model (black solid line) are directly compared with the EMD results, demonstrating a strong agreement in trends between the two datasets. This further reinforces the accuracy and reliability of the present model.

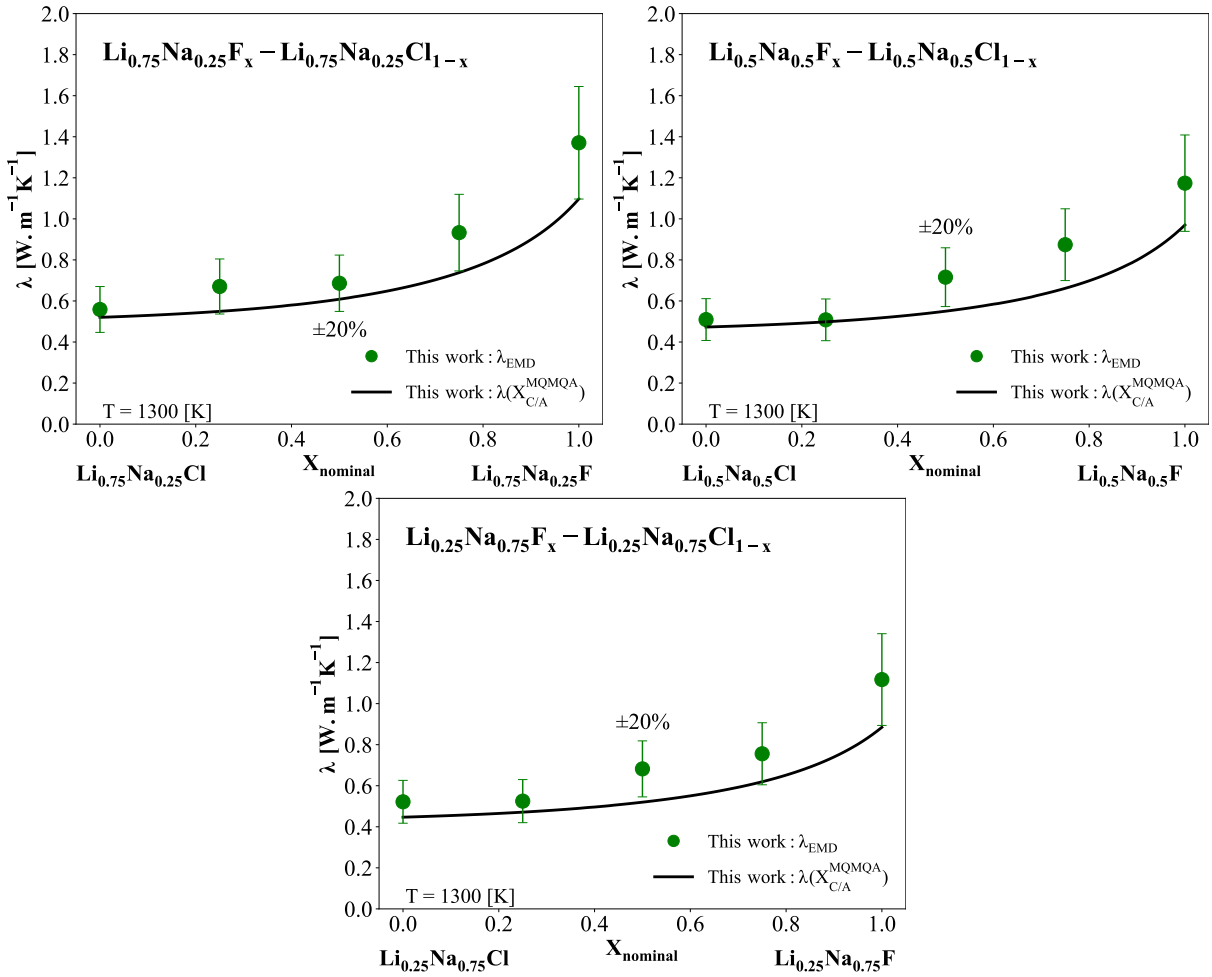

Figure C.2 Predicted thermal conductivity values of reciprocal Li^+, Na^+ / F^-, Cl^- molten mixture in comparison to EMD results by this work at 1300 [K].

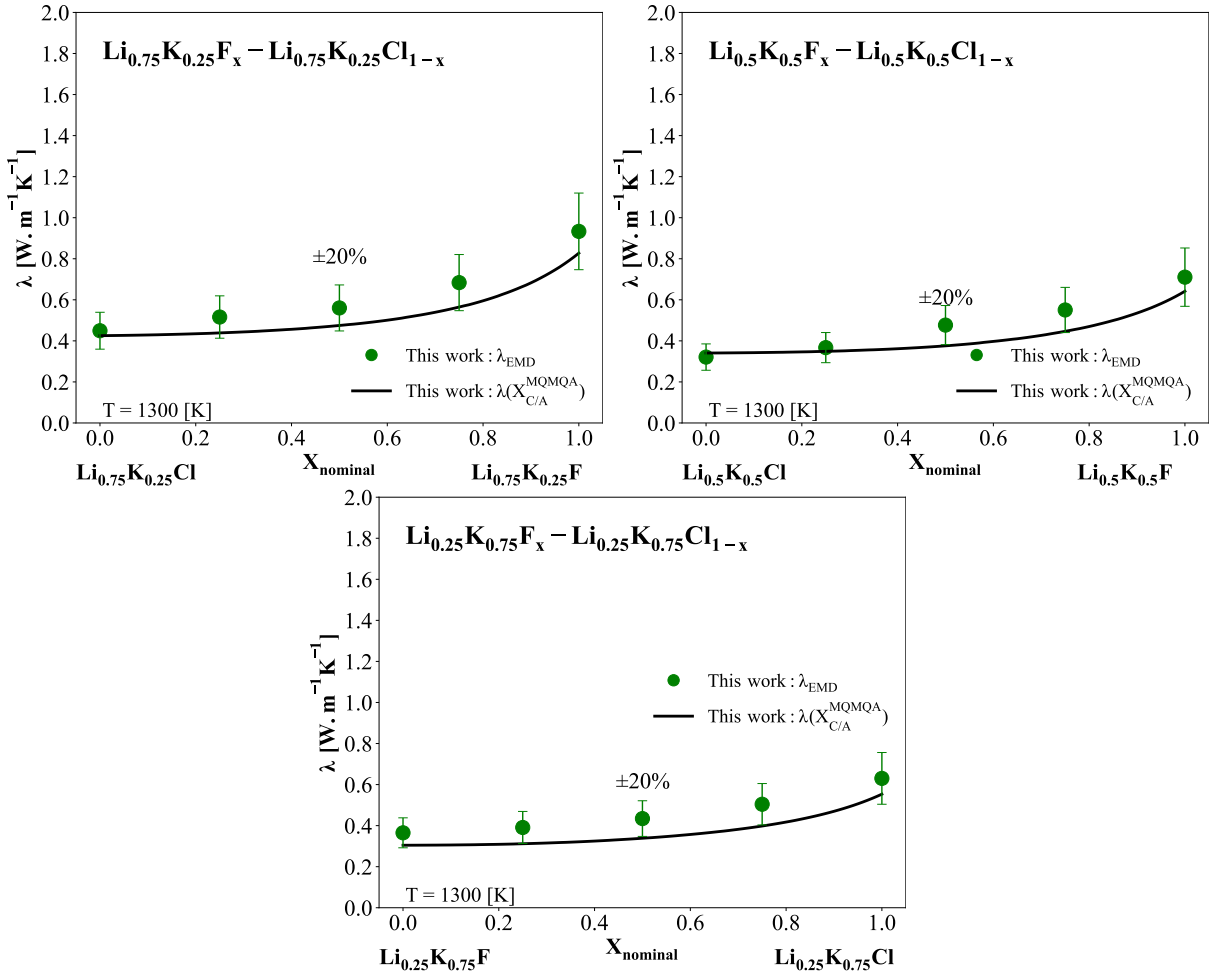

Figure C.3 Predicted thermal conductivity values of reciprocal Li^+, K^+ / F^-, Cl^- molten mixture in comparison to EMD results by this work at 1300 [K].

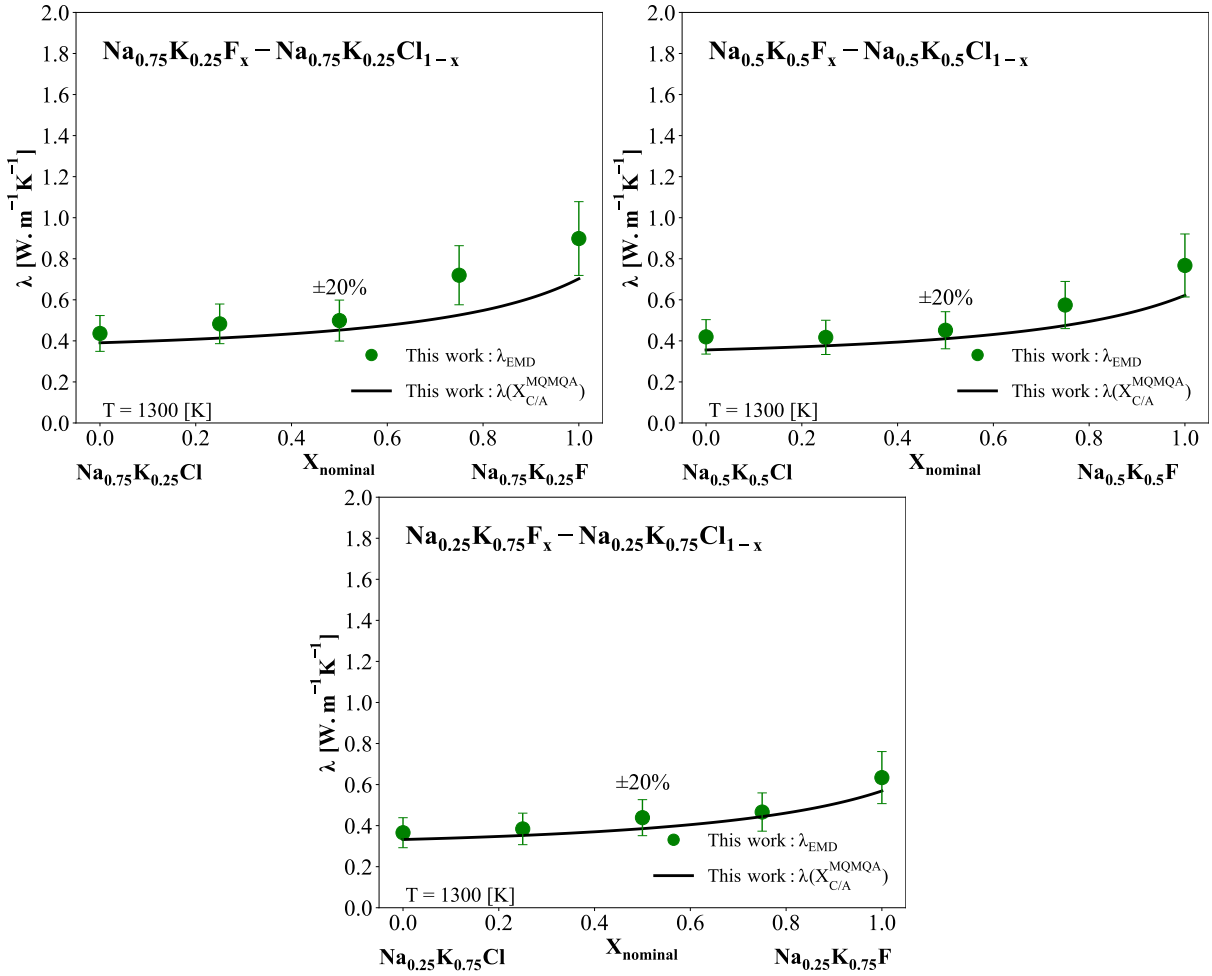

Figure C.4 Predicted thermal conductivity values of reciprocal Na^+, K^+ / F^-, Cl^- molten mixture in comparison to EMD results by this work at 1300 [K].

APPENDIX D SUPPLEMENTARY MATERIALS FOR ARTICLE 3

D.1 Sound velocity

In a previous study [264], the thermal conductivity of pure molten salt was estimated based on sound velocity at its melting temperature. In this work, we modified the sound velocity as a temperature dependent parameter based on the thermal conductivity of each molten salts. The analysis was conducted over a temperature range from 300 [K] below the melting point to 600 [K] above it. The FTsalt Database of Factsage^{TM} 8.4 was used to estimate the temperature-dependent sound velocity. To validate the accuracy of the predicted sound velocity, comparisons were made with available experimental datasets for both pure molten salts and molten salt mixtures (including common-anion mixture and reciprocal mixtures), as shown in the following figures. The predicted sound velocities exhibit excellent agreement with experimental data for most salts, accurately capturing the trends with composition. This is true when compared with the most recent works reported by Stepanov [318, 319]. The only notable discrepancies are a 10% error for CsI and three binary mixtures, LiBr-LiCl, NaF-NaBr and NaF-NaI.

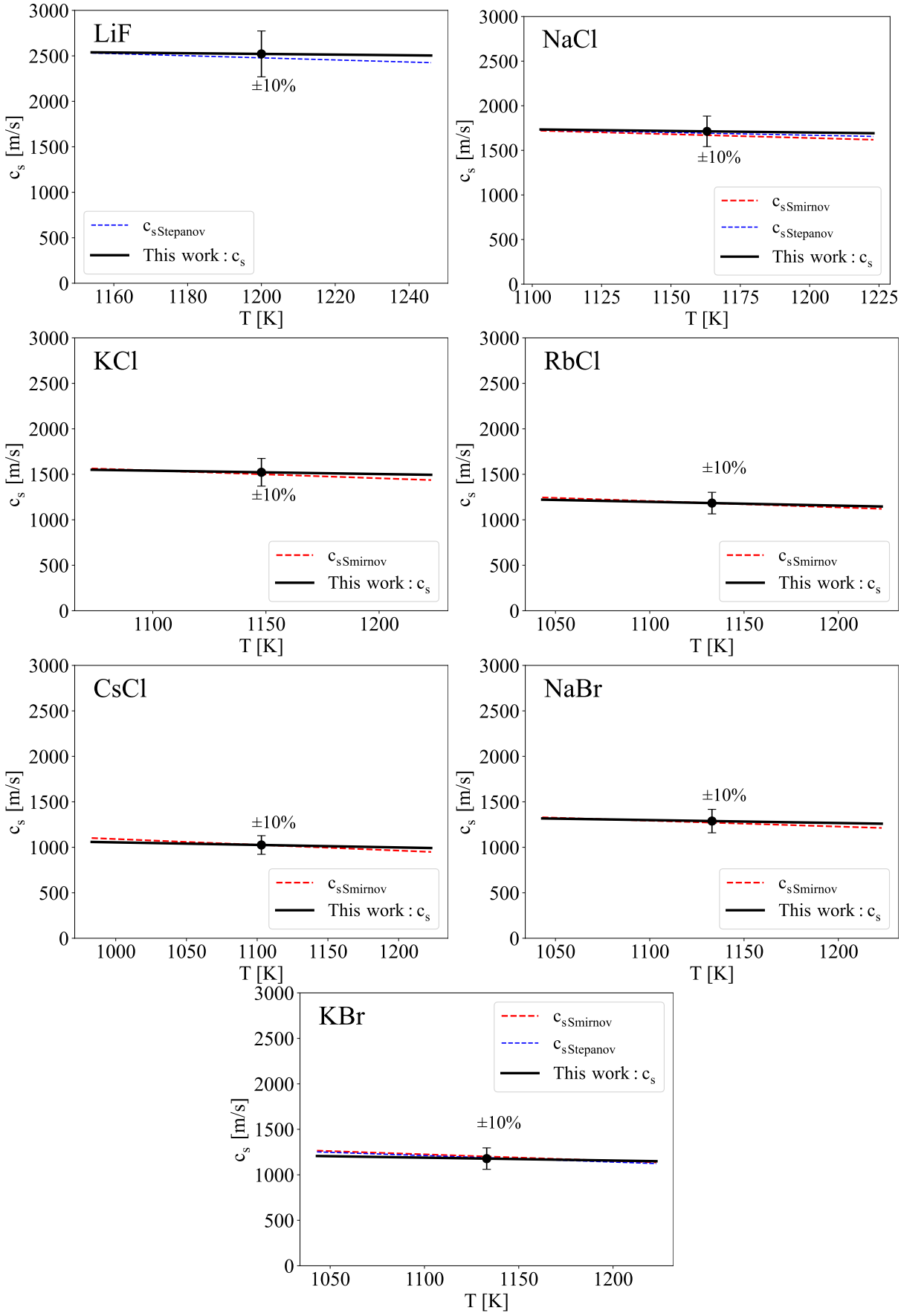

Figure D.1 Comparison of the predicted sound velocities for pure molten salts with available experimental data [318, 320].

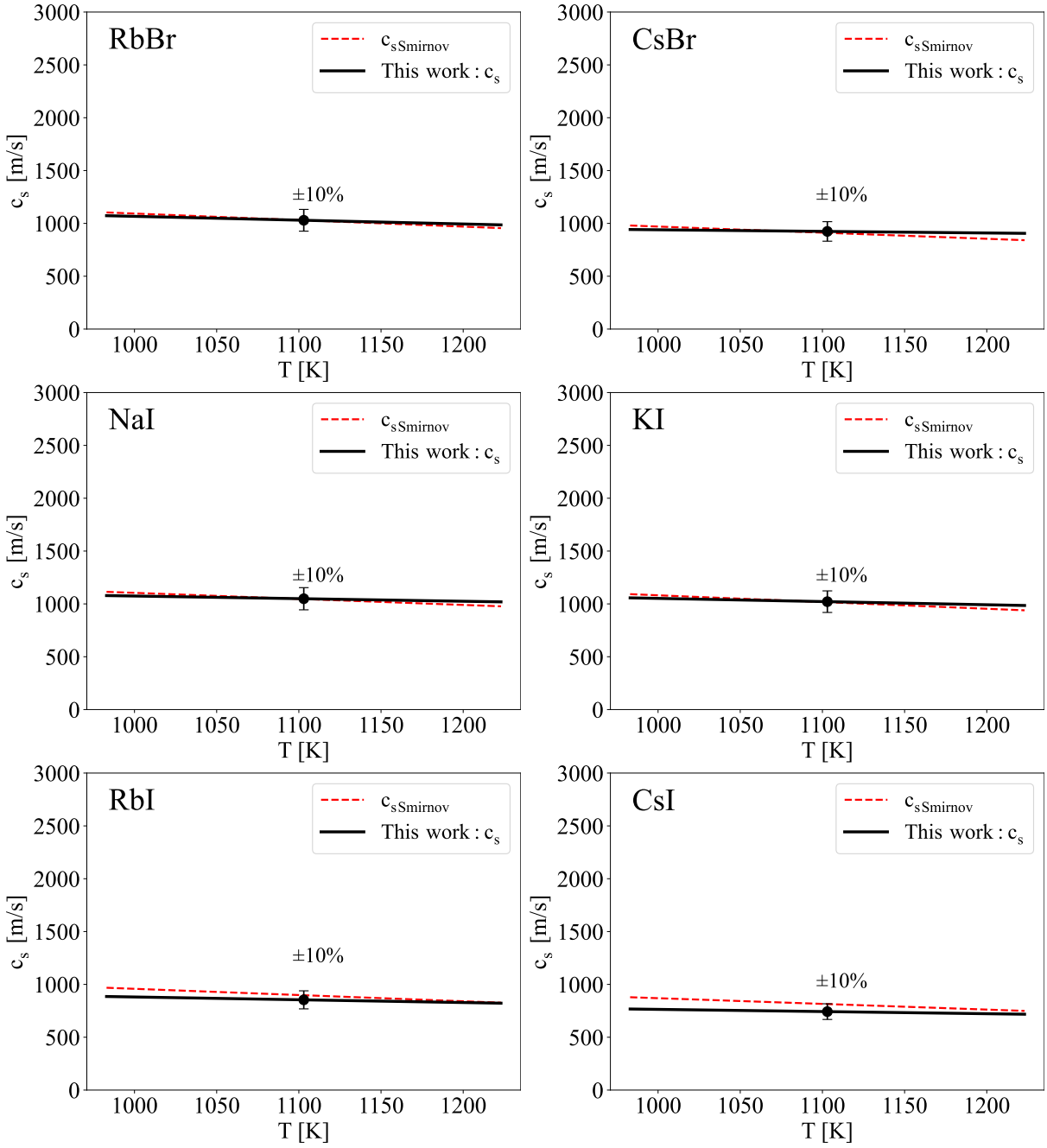

Figure D.2 Comparison of the predicted sound velocities for pure molten salts with available experimental data [318, 320].

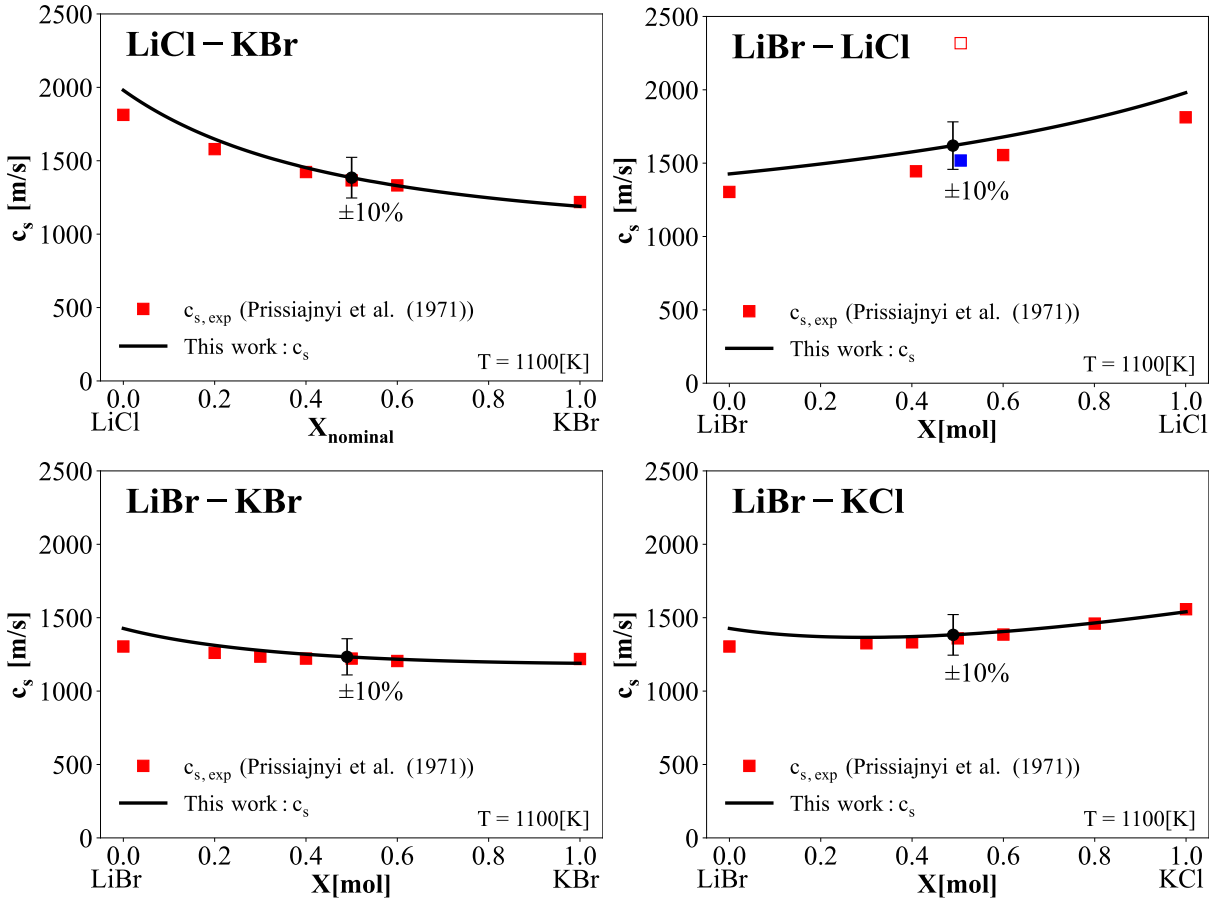

Figure D.3 Comparison of the predicted sound velocities for reciprocal and common-ion molten salt mixtures as a function of composition with the experimental data reported by Prissiajnyi et al. [301] at 1100 [K]. The composition at $(LiBr)_{0.493}$-$(LiCl)_{0.507}$ exhibited a significant deviation from the predicted values, as well as from the trend observed in the experimental data. The reported value of $c_{s0} = 2905[m/s]$ appears to be a manuscript error for this composition, with the likely correct value being $c_{s0} = 2105[m/s]$. Accordingly, the corrected data point is highlighted in blue.

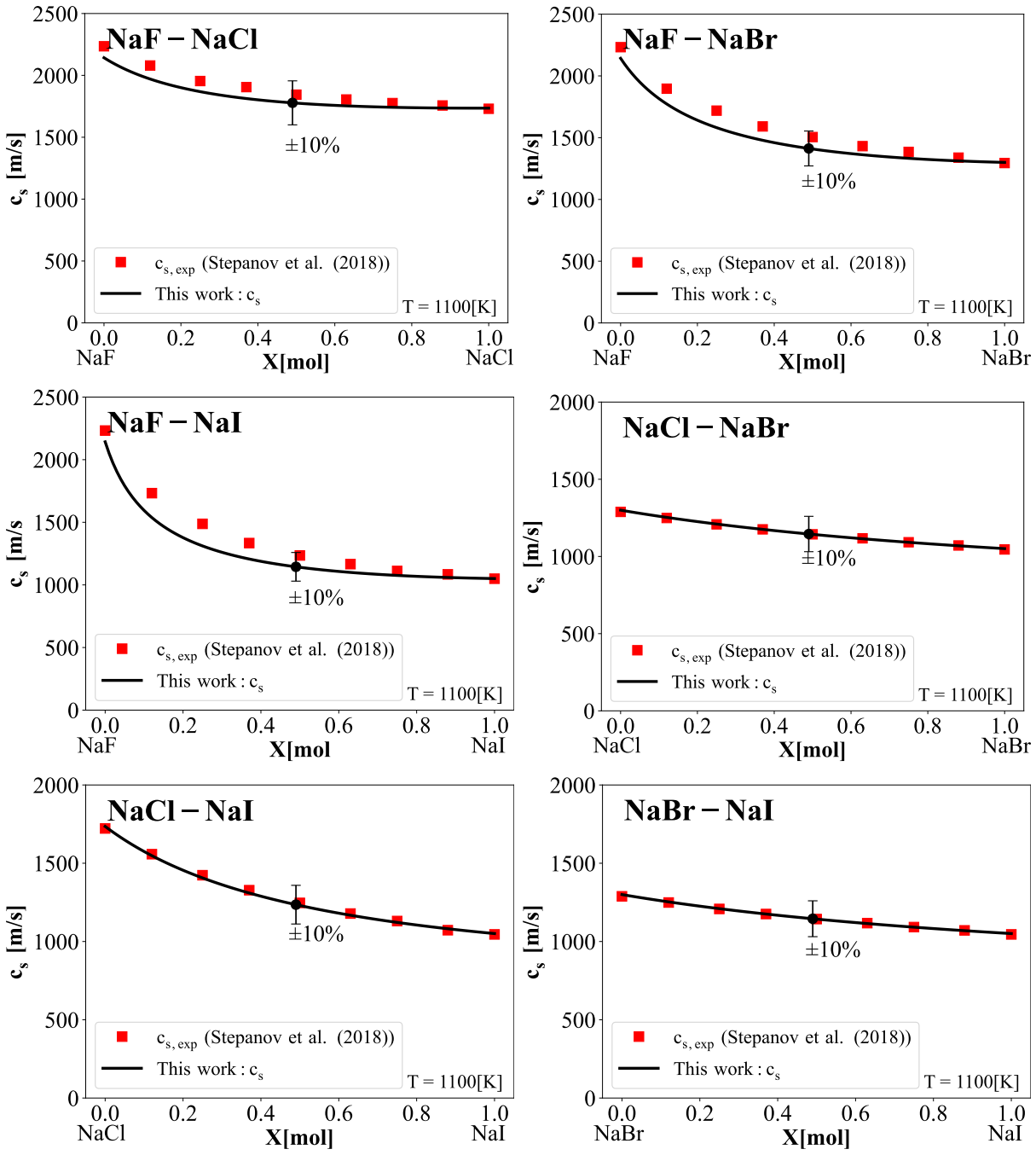

Figure D.4 Comparison of the predicted sound velocities for reciprocal and common-ion molten salt mixtures with the experimental data reported by Stepanov [318] at 1100 [K].

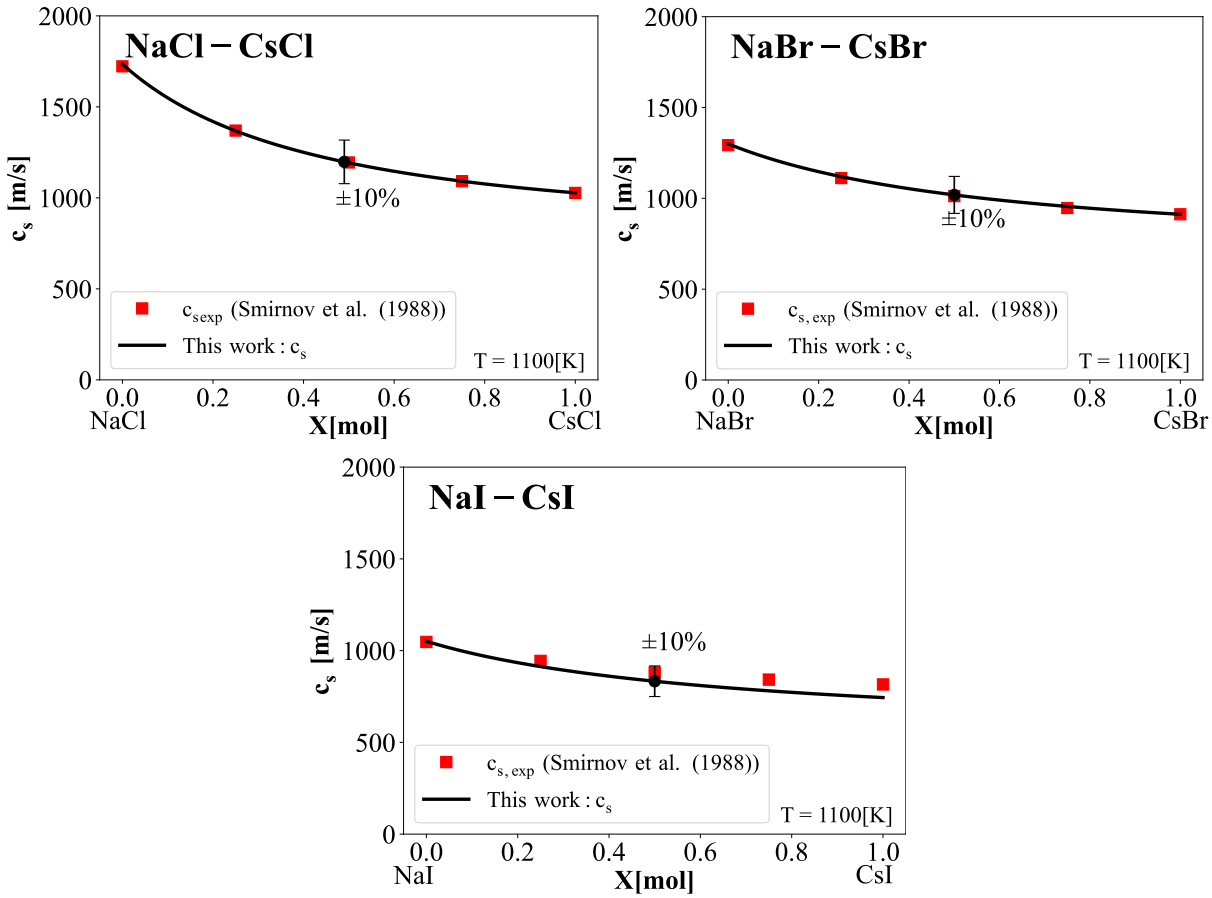

Figure D.5 Comparison of the predicted sound velocities for common-anion molten salt mixtures with the experimental data reported by Smirnov et al. [320] at 1100 [K]

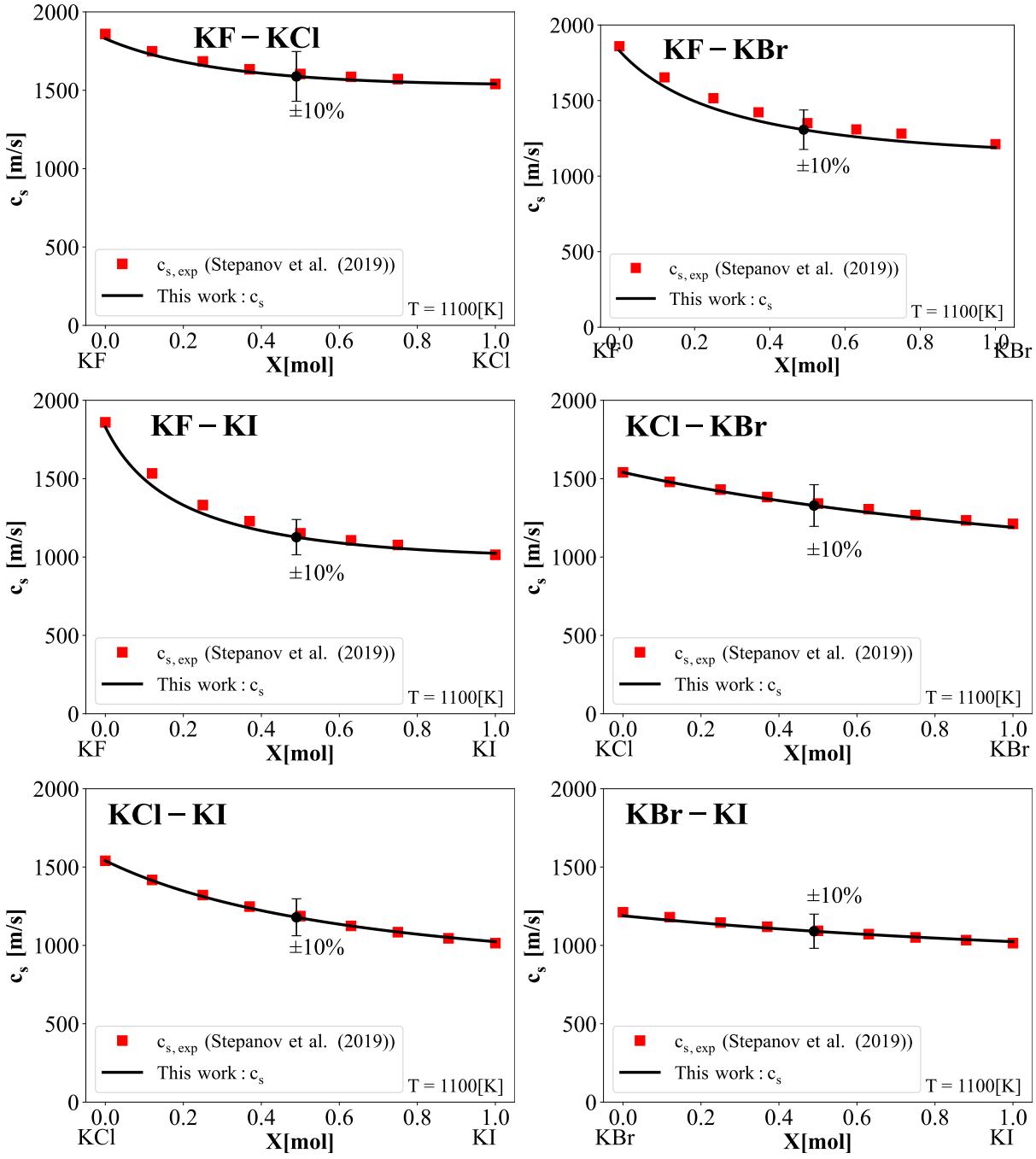

Figure D.6 Comparison of the predicted sound velocities for common-anion molten salt mixtures with the experimental data reported by Stepanov [319] at 1100 [K]

D.2 Modeling the thermal conductivity of common-cation molten salt mixtures

In our previous work [295], we validated a thermal conductivity model only for simple common-anion molten salt mixtures. In this study, we have simulated numerous common-

cation mixtures using equilibrium molecular dynamics (EMD) to verify the predictivity of the present model for common-cation molten salt mixtures, specifically LiF-LiCl, LiF-LiBr, LiF-LiI, LiCl-LiBr, LiCl-LiI, NaF-NaCl, NaF-NaBr, and KF-KCl at 1300 [K]. Unfortunately, no experimental data sets can be found related for the common-cation molten salt mixtures in the literature.

Figure D.7 shows the thermal conductivity predictions (red dashed line) of the common-cation binary mixtures as a function of composition in comparison to the EMD results, which the end members were calibrated to the EMD results. Meanwhile, the predicted values (black solid line) are compared to the experimental datasets. It can be observed that the predictions of the current model are well in agreement with the EMD results for most common-cation mixtures (LiF-LiCl, NaF-NaCl and KF-KCl). However, the heavier anions Br^- and I^- of EMD results displayed less stable and discretely, which could be attributed to the significant mass difference between the ions and the errors in the potentials within the Br^- / I^- solutions. Therefore, the obtained values showed slightly larger, for instance the binary mixture of LiF-LiBr and LiF-LiI. On the other hand, we applied the framework of the polariable ion model (PIM) for the EMD simulation, since LiF is no polarizable, the value obtained of LiF is larger than experimental works, with more scatterings. However, the results of EMD for Na^+ and K^+ binary common-cation mixtures displayed a perfect tendency. The current model predicted in perfect agreement with the EMD results for NaF-NaCl, NaF-NaBr and KF-KCl. Similarly to the common-anion solutions, the reduction of the thermal conductivity regarding to the mass fluctuation played an important role. The larger difference in mass of anions and thermal conductivity of the pure compound, the larger deviation from the linearity presents.

A comparison of the end-member of pure molten salt between reliable experimental works and the current model were shown in the same figure. It can be observed that the predictions of this current model are in good agreement with reliable works. Since the EMD simulation were performed at 1300 [K], the experimental works are mostly done close to the melting points. Thus, some of these works shown slightly difference to the predictions as the values were obtained by the extrapolation to the same temperature.

In summary, these common-cation mixtures demonstrated that the present model is capable of predicting the thermal conductivity of simple monovalent reciprocal molten salt mixtures with reliable accuracy. Furthermore, we are confident that it can also predict the behavior of common-cation with polyatomic anion mixtures, such as nitrates, carbonates, and others.

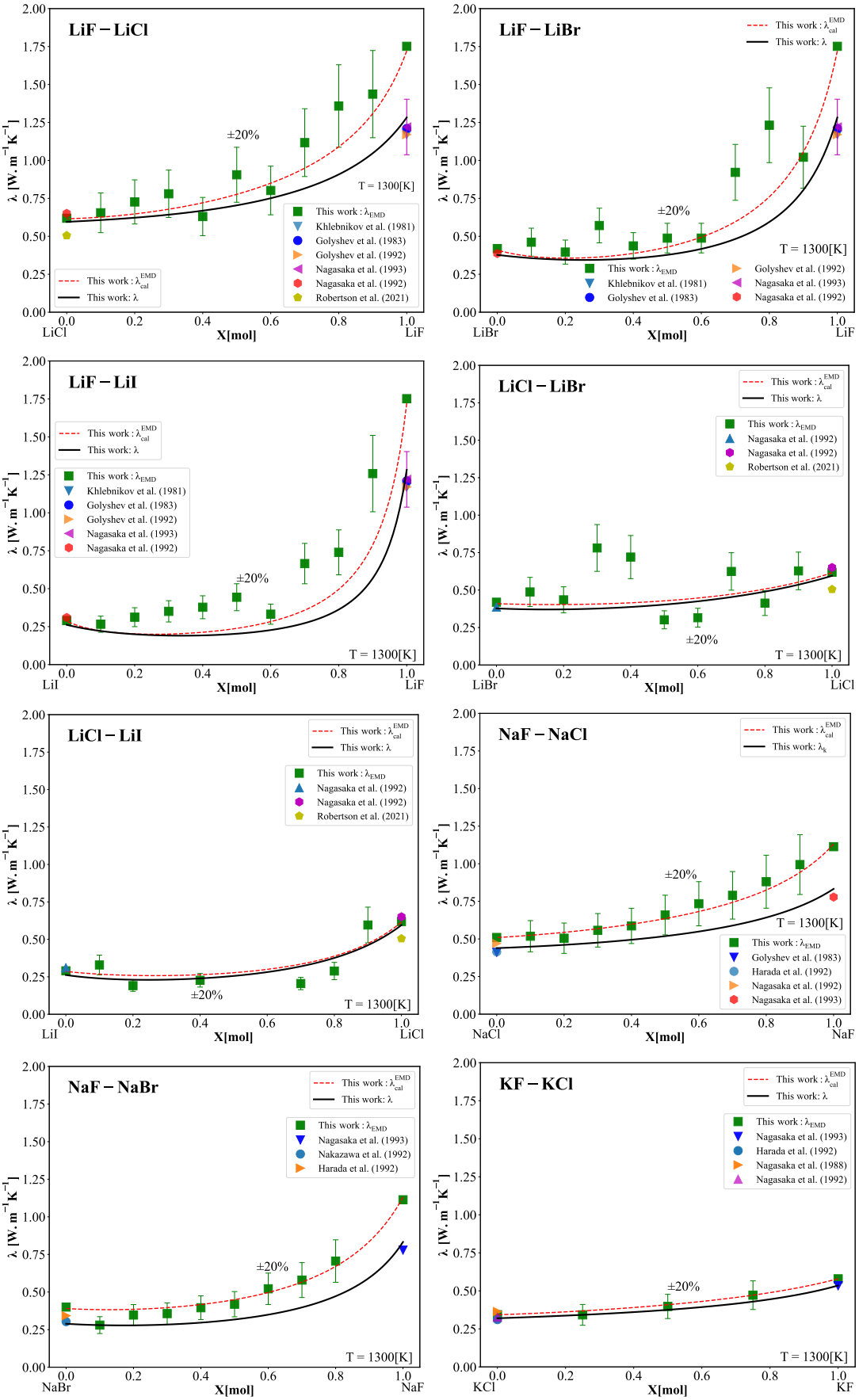

Figure D.7 Predicted thermal conductivity values of common-cation of binary molten salt mixtures in comparison to EMD results of this work and to recommended experimental values at 1300 [K].

APPENDIX E SUPPLEMENTARY WORK: THE ROLE OF THE LOCAL STRUCTURE ON THE THERMAL TRANSPORT WITHIN DISSOCIATED AND COMPLEXED MOLTEN SALT MIXTURES

As part of supplementary work contributing to this thesis, the study by Gheribi et al. [278] investigated the effect of local structures in complex molten salt mixtures on thermal conductivity and has been adapted here to fit the scope of this thesis. This supplementary study extends the work presented in Article 2, focusing on complex molten salt mixtures where strong short–range ordering contributes to the formation of intricate coordination complexes and polymer chains, thereby reducing thermal conductivity within the solutions, for example KCl-$MgCl_2$ and LiF-BeF_2. This behavior can be explained by local perturbations of kinetic energy through mass fluctuations, weighted by a function dependent on the thermal conductivity of an uncorrelated system and the local structure. The local structure is characterized by the concentration of free and complexed ions, determined either experimentally using nuclear magnetic resonance (NMR) or via equilibrium atomistic simulations.
The framework was applied to several complex molten salt mixtures, KCl-$MgCl_2$, NaCl-KCl-$MgCl_2$, and NaF-AlF_3, that demonstrates its capability to predict thermal transport properties across different compositions. Furthermore, the study provides a molecular level perspective of thermal conduction in complex molten salts, highlighting the influence of local ion arrangements and complexation on thermal transport property. These findings offer valuable insights that complement the sub-objectives of this thesis by enhancing the understanding of the mechanisms governing thermal transport in common-ion complex molten salt mixtures, with implications for both fundamental research and industrial applications.

Due to pressing environmental issues, the research on molten salts has drastically increased over the last two decades. Indeed, two of the most promising alternatives to fossil fuels are based on molten salts. Concentrating solar-thermal power (CSP) technology incorporates molten salt thermal energy storage either in the form of sensible or latent heat, mainly using molten salts as fuel, while molten salt fast reactors (MSRs) use molten salts as a coolant and nuclear fuel. CSP technology uses molten salt mixtures at specific eutectic compositions (i.e. where a direct liquid-solid transition is observed), and depending on the technology and working temperature, chlorides, carbonates or nitrates can be used as the working fluid. In their liquid state, these salt mixtures can be considered simple, because they are almost fully dissociated, even if they are formed of heavy anion such as CO_3^{2-}. Thermal spectrum MSRs consider thorium, uranium, and plutonium fluoride salts dissolved

in a LiF-BeF_2 (FLiBe) mixture as both fuel and primary coolant, e.g. LiF-BeF_2-ThF_4-UF_4. Similarly, most fast spectrum reactors consider actinide chloride salts dissolved in chloride molten salts. In general, these mixtures tend to form coordination complexes for which the size increases with the concentration of Be, Th, Pu, or U until polymer chains are formed. Molten salts are also involved in several other important industrial processes. For instance, the Hall-Héroult process for primary aluminium production uses cryolitic melts (NaF-AlF_3-Al_2O_3-CaF_2) to dissolve and electrolyse alumina. Similar to the fuels employed in MSR, cryolitic melts form heavy coordination complexes (fluoroaluminate and oxofluoroaluminate), to the extent that the current within cryolitic melts is carried almost entirely through free Na^+ cations. The design and optimization of industrial or energy related processes require material performance optimization. Maximizing and/or minimizing properties such as heat capacity, thermal expansion, thermal diffusivity, thermal conductivity, diffusion coefficients, electrical conductivity, etc. could influence factors like safety margins, efficiency, and operable conditions.

Among all the molten salts properties, the thermal conductivity (diffusivity) is the least known from both experimental and theoretical perspectives. Yet, this property is critical in characterizing and optimizing industrial processes. In the case of thermal energy storage, maximizing the thermal conductivity is desirable for reducing the heat charging and discharging times, as it is in general very low for molten salts ($\lesssim 1$ W.m^{-1}.K^{-1}). However, from an experimental standpoint, quantifying the thermal transport properties within molten salt mixtures poses significant challenges. All experimental techniques developed to determine the thermal conductivity or diffusivity within liquids suffer from uncertainties and errors associated with the convective, conductive, and radiative thermal losses of the apparatus. These errors generally lead to an overestimation of the thermal diffusivity, particularly at high temperatures. Although the majority of experimental techniques nowadays account for most of the thermal losses, other factors such as chemical reactions between the molten salt and crucible can still significantly bias the measurement of thermal diffusivity, especially with corrosive salts (e.g., fluorides and chlorides) at high temperatures. The presence of bubbles also hinders heat transfer, leading to erroneous measurements. Additionally, due to the electrical conductivity of molten salts, any leakage current from the heating sources into the molten salt will cause an increase in electric power consumption. As demonstrated by DiGuilio and Teja [39], and later by Gheribi et al. [60], these uncontrollable factors often result in an overestimation of the experimental thermal conductivity and a significant increase in the thermal conductivity with temperature.

The most recent experimental studies [40, 47, 70, 100] have demonstrated the decoupling of parasitic contributions from the intrinsic thermal diffusivity. These studies have revealed

that the thermal diffusivity of a wide range of molten salts remains largely unaffected by changes in temperature. In other words, the thermal conductivity of molten salt mixtures decreases with increasing temperature, similarly to thermal expansion. While reliable experimental data can be found for the thermal diffusivity of various pure molten salt compounds, reliable data for mixtures is more scarce. Only a limited amount of reliable experimental data is available for both simple and complex mixtures. Unlike solid-state materials, the understanding of the microscopic mechanisms dictating thermal transport within molten salt mixtures is currently lacking, compounded by the absence of reliable experimental data. This lack of understanding hampers the development of a comprehensive theoretical framework for the field. The intricate nature of molten salts, characterized by their complex composition and dynamic behavior, poses challenges in understanding the intricate processes underlying thermal transport. Consequently, the absence of a clear picture regarding these microscopic mechanisms hinders the ability to accurately predict and model thermal conductivity in molten salt mixtures. Addressing this knowledge gap through further experimental investigations and theoretical advancements is crucial for advancing our understanding of heat transfer in these systems and facilitating their broader applications in various industries.

Equilibrium molecular dynamics (EMD) simulations offer an alternative approach to understanding the local structures of complex and polymer molten salt solutions, providing accurate results of thermal conductivity in our previous studies [133, 151, 152, 321]. Numerous EMD simulations have been conducted for pure KCl and Al_2O_3, binary, and ternary systems comprising fluorides (LiF, NaF, KF, AlF_3) and chlorides (NaCl, KCl, $MgCl_2$) at temperatures slightly higher than their liquidus temperature. The liquidus temperature of the compositions was estimated via Factsage [294]. The simulations were initially performed in the isobaric-isothermal statistical ensemble (NPT) at corresponding temperatures and pressures of 10^5 Pa for two series to generate thermally equilibrated configurations. This was followed by a new series of EMD simulations carried out in the canonical statistical ensemble (NVT), starting from the thermally equilibrated configurations generated by the previous NPT simulations. The relaxation times for both thermostat and barostat were set to 0.5 ps. The equations of motion were integrated using the velocity Verlet algorithm with a time step of 0.5 fs for NPT simulations and 1 fs for NVT simulations. The total simulation time for NPT was 0.5 ns, and for NVT it was 5 ns. Lastly, all simulations were performed using periodic boundary conditions and the minimum image convention.

Numerous models have been attempted to predict the thermal conductivity of molten salt mixtures, and are summarized elsewhere [39]. Early models include those based on the Bridgman model assumes a relationship between sonic velocity and thermal conductance with the liquid structured as a quasi-lattice. This is an assumption still applied in more recent

models [181, 322, 323]. In linear or ideal models, the thermal conductivity is represented as a molar-fraction weighted sum of pure salt's conductivity. However many works have shown that the excess conductivity tends to be negative [50, 55, 182]. Other methods include the rough hard sphere model, the unit cell model, and semi-empirical models [39, 56, 193, 324]. Recently, we presented a model derived from classical kinetic theory and demonstrated its reliability for pure molten salt compounds and mixtures [264, 295]. The current work extends the capability to account for structural influences, such as complexing.

The present study aims at comprehensively explore the underlying microscopic mechanisms responsible for thermal transport in both simple and complex molten salt mixtures. By considering the microscopic origin of heat transfer, we seek to resolve the intricate processes and interactions that govern thermal conductivity in these systems. Through an in-depth investigation of the fundamental factors influencing thermal transport, including molecular structure, interparticle interactions, and energy propagation mechanisms, we wish to shed light on the precise mechanisms influencing the thermal conductivity of molten salts. By bridging the knowledge gap surrounding the microscopic origin of thermal transport, this research contributes to a deeper understanding of heat conduction in molten salt mixtures, with potential implications for a wide range of applications. A series of molecular dynamic simulations using the Polarizable Ion Model (PIM) force field has been conducted to investigate the thermal transport and local structure of complex molten salts. To describe the temperature and composition dependence of thermal conductivity in molten salt mixtures, a theoretical framework based on the kinetic theory has been established. This formalism extends from simple molten salt mixtures, where ions are assumed to be fully dissociated, to complex mixtures involving coordination complexes and polymerization. In order to apply the proposed theoretical model, only a few essential thermophysical data are required, such as the velocity of sound in single molten salt compounds and the mass fraction of ions and complexes present in the mixture. As case studies, the thermal transport in the molten KCl, Al_2O_3, LiF-KF, LiF-NaF-KF (FLiNaK), KCl-$MgCl_2$, NaCl-KCl-$MgCl_2$, and NaF-AlF_3 systems has been thoroughly examined. Some of these systems have been previously evaluated with similar kinetic theory frameworks [238, 264, 295], the present work re-evaluates them with the current improved framework. The model demonstrates a high level of predictive capability, yielding satisfactory results for all studied systems. A direct correlation has been established between the local structure and thermal transport within complex molten salts, elucidated through the analysis of local fluctuations in kinetic energy. Additionally, the proposed model presents the opportunity to develop a reliable large-scale thermal transport database for various industrial and energy applications, which would greatly alleviate the severe lack of experimental data in this field.

The theoretical framework employed in this study is based on the phonon gas model for solids, which draws an analogy to the kinetic theory of gases. In this model, phonons (collective vibrations) in crystals are treated as classical massive particles rather than quasi-particles. The thermal conductivity within a crystal is expressed using the kinetic theory as [325, 326]:

$$\lambda = \frac{1}{3}\sum_{n=1}^{3}\int_{0}^{\infty} C_V(\omega)\,\nu_g(\omega)\,l_{mfp}(\omega)\,d\omega \tag{E.1}$$

Here, C_V, ν_g, and l_{mfp} represent the volumetric heat capacity at constant volume, the phonon group velocity, and the phonon mean free path, respectively. ω is the average frequency over all the vibrational modes within the crystal. However, in amorphous solids, the lack of long-range ordering leads to a different heat transport mechanism. Instead of well-defined phonons, heat is carried through harmonic couplings between non-correlated and delocalized atomic vibrations referred to as "diffusons". To describe the thermal conductivity in amorphous materials, a "random walk" propagation model is employed, where the minimum mean free path is considered to be half the wavelength. Cahill et al. [234, 327] have shown that, within the framework of the Debye approximation, where the velocity of diffusons is identical to the low-frequency speed of sound, the minimum thermal conductivity in the canonical statistical ensemble (NVT) can be expressed as:

$$\lambda_{min}^{NVT}(T) = \left(\frac{\pi}{6}\right)^{1/3} k_B n^{2/3} \sum_{i=1}^{3} c_i \left(\frac{T}{\Theta_D^i}\right)^3 \int_{0}^{\Theta_D^i/T} \frac{x^3 \mathrm{e}^x}{(e-1)} dx \tag{E.2}$$

Here, n and k_B represent the number density per atom and the Boltzmann constant respectively, while Θ_i and c_i denote the velocity of sound and the Debye temperature for the three acoustic modes (two transversals and one longitudinal). It should be noted that Θ_i and c_i are not independent but are related through the equation $\Theta_i = c_i\,(\hbar/k_B)\,(6\pi^2 n)^{1/3}$, where $\hbar$ is Planck's constant. This minimum conductivity model accurately describes the temperature-dependent thermal conductivities of various non-metallic amorphous materials, especially at low temperatures. At high temperatures, beyond the average Debye temperature, the minimum thermal conductivity reaches a plateau, which can be approximated as:

$$\lambda_{min}^{NVT}(T \gtrsim \Theta_D) \backsimeq \left(\frac{9\pi}{16}\right)^{1/3} k_B n^{2/3} \langle c_S \rangle \tag{E.3}$$

where $\langle c_S \rangle$ represents the average sound velocity over the transversal and longitudinal modes. The minimum thermal conductivity has proven to be a reliable description of thermal transport in a wide range of electrically insulating amorphous materials, particularly at low tem-

peratures. According to Equation D3, thermal conductivity remains temperature-independent under constant volume conditions, denoted as $(\partial\lambda/\partial T)_V = 0$. In our previous work [60], we introduced this assumption based on empirical observations derived from both equilibrium and non-equilibrium molecular dynamic simulation results. In the current study, we provide a rigorous theoretical validation for this assumption as a direct consequence of kinetic theory. At high temperatures, the expansion of the lattice can have a pronounced effect on the temperature dependence of thermal conductivity in amorphous solids, i.e., in the NPT (isobaric-isothermal) statistical ensemble $(\partial\lambda/\partial T)_P \neq 0$. The temperature dependence of thermal conductivity in the NPT ensemble can be described by employing a Legendre transformation, leading to the differential equation $(\partial\lambda/\partial T)_V = 0$. This transformation, $\lambda_{min}^{NVT} \rightarrow \lambda_{min}^{NPT}$, was originally introduced by Gheribi et al. [60] and subsequently expanded upon by Robertson et al. [80] to encompass nonlinear temperature effects. However, it has been demonstrated by Robertson et al. that these nonlinear effects on thermal conductivity are insignificant over a broad temperature range, notably when the temperature is only a few hundred degrees Kelvin above the liquidus temperature. From an experimental standpoint, the linear behavior of thermal conductivity with temperature matches the observations from reliable experiments [39, 60, 264]. The linearised solution for the $\lambda_{min}^{NVT} \rightarrow \lambda_{min}^{NPT}$ Legendre transformation can be succinctly expressed in terms of thermodynamic parameters as follows [60, 80]:

$$\lambda_{min}^{NPT}(T) = \lambda_{min}^{NVT} \cdot \left[1 - \alpha_0 \left(\gamma_0 + \frac{1}{3}\right)(T - T_0)\right] \tag{E.4}$$

Here, α_0 and γ_0 represent the thermal expansion coefficient and the Grüneisen parameter, respectively, at a standard temperature T_0. Considering the properties of the most stable phase at standard temperature and pressure, the thermal conductivity of molten salt compounds has been predicted at their melting temperature using Equation E.4 and are presented in Figure E.1 alongside critically assessed experimental values. It is evident that the predicted minimum thermal conductivity for a hypothetical amorphous salt is of the same order as that of molten salts. Although the thermal conductivity of molten salt compounds can be predicted with reasonable accuracy, the approach based on solid phase properties is more qualitative than quantitative. In several compounds, a discrepancy of up to 50% can be observed between the predicted and experimental values. It is also important to note that there are significant deviations between different experimental datasets, often exceeding 20%. The limited accuracy of the minimum thermal conductivity approach is primarily due to the parametrization of the model, which considers the properties of the solid rather than the liquid phase. In a recent study [264], we have extended the minimum thermal conductivity approach for amorphous solids to molten salts by introducing a modification to Equation

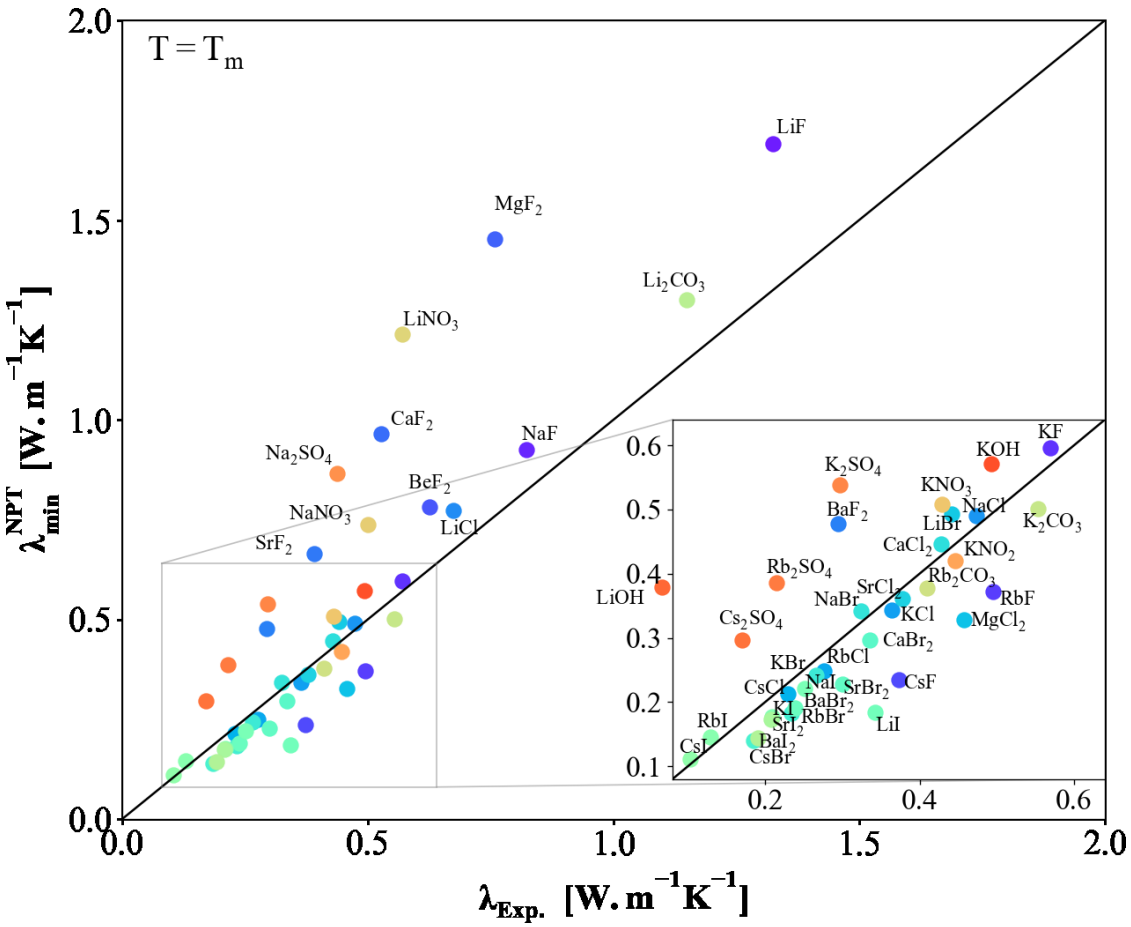

Figure E.1 Experimental vs calculated thermal conductivity of diverse molten salt compounds at their melting temperatures. The thermal conductivity is determined in the NPT statistical ensemble, taking into account the thermophysical properties of the solid compound (thermal expansion, heat capacity, density, bulk modulus, and shear modulus) at a temperature of 298.15 [K], as described by Equation E.4. The experimental thermal conductivity is derived through a rigorous analysis that encompasses a comprehensive evaluation of all available reliable experimental data on thermal diffusivity and thermal conductivity found in the literature [264].

(E.4):

$$\lambda^{msc}(T) = \psi^* k_B n_{liq.}^{2/3} \langle c_S \rangle_{liq.} \left[1 - \alpha_m \left(\gamma_m + \frac{1}{3}\right)(T - T_m)\right] \tag{E.5}$$

Here, ψ^* is a material constant, and T_m represents the melting temperature. The density, velocity of sound, thermal expansion coefficient (α_m), and Grüneisen parameter in Equation E.5 are those of the liquid phase at the melting temperature. The Grüneisen parameter is

dependent on various thermophysical properties that describe λ^{NVT}, namely α_m, $\langle c_S \rangle_{liq.}$, M_w, and C_P. Specifically, it can be expressed as $\gamma_m = \alpha_m \langle c_S \rangle_{liq.}^2 M_w / C_P$. The concept of ψ^* was introduced by analogy to the theoretical description of thermal conductivity in crystals, as proposed by Slack and Klemens [276, 328]. In their theory, they incorporated the number of atoms per primitive crystallographic cell to account for the complex structure of the crystal, which directly affects thermal conductivity. Our previous study [264] focused on exploring the predictive capacity of Equation E.5 by utilizing a specific approximation for ψ^* across a wide variety of molten salt compounds. Through this analysis, we revealed a consistent and robust predictive capability of Equation E.5, regardless of the chemical nature of the molten salts.

Following this, we established that:

$$\boldsymbol{K} = 1 + \frac{n_s^+}{n_s^-} \tag{E.6}$$

Here, n_s^+ and n_s^- respectively represent the number of species involved in cationic and anionic complexes, with $n = 1$ corresponding to free species. NaCl, LiF, and KBr exhibit a value of $\boldsymbol{K}$ equal to 2, whereas alkali carbonates such as Li_2CO_3 and Na_2CO_3 have a value of $\boldsymbol{K}$ equal to 1.5. In the case of $LiNO_3$ or $CaCO_3$, the value of $\boldsymbol{K}$ is 1.25. The extension of the minimum thermal conductivity concept to explain the thermal conductivity of molten salts is based on the assumption that a direct correlation exists between the thermal conductivity of amorphous materials and the liquid phase. This assumption comes from the concept that a direct relationship exists between the thermophysical properties of these two phases, which, at the melting temperature, can be represented as follows:

$$\frac{\langle c_S \rangle_{liq}}{\langle c_S \rangle_{sol.}} = \frac{\epsilon}{\boldsymbol{K}} \frac{n_{sol.}}{n_{liq.}} \tag{E.7}$$

The expression for ϵ is approximately given by $\epsilon \simeq 1.21 \left[1 - \alpha_0 \left(\gamma + 1/3\right) T_m\right]$. In general, ϵ is close to 1 for most salt compounds, indicating a strong correlation between the variation in the velocity of sound and the density at the melting temperature. One theoretical justification of Equation E.7 and, therefore, the transposition of the minimum thermal conductivity concept for amorphous materials to molten salts, can be found in the relationship between the velocity of sound (isothermal compressibility) and the density proposed in the literature. Marcus [329] introduced a semi-empirical approach that establishes a connection between the velocity of sound in molten salts and the ratio between their cohesive energy and density, which demonstrated consistent accuracy across a diverse array of molten salts. This aligns with Equation E.7, as the bulk modulus, and consequently, the velocity of sound of the solid,

is directly correlated to its cohesive energy. Generalizing the model to incorporate complex molten salt compounds, and to some extent, complex ionically bonded molten compounds, requires extending the generalization of $\boldsymbol{K}$ to accurately represent the presence of coordination complexes. Given that a complex molten salt compound is characterized by a local structure comprising a coordination complex where the cations are surrounded by anions, the $\boldsymbol{K}$ term for simple (dissociated) compounds can be extrapolated as follows:

$$\psi^{*}_{comp.} = 1 + \sum_{\substack{i,j \\ i \neq j}} \left(f_{ac_i} \frac{Z^{cat}_{ac_i}}{n^{cat}_{ac_i}} + f_{cc_j} \frac{Z^{an.}_{cc_j}}{n^{an.}_{cc_j}} \right) \tag{E.8}$$

In this context, Z^{cat}_{aci} denotes the coordination number of the cation within the anionic complex ac_i, while $Z^{an.}_{cc_j}$ refers to the coordination number of the anion within the cationic complex cc_j. These coordination numbers represent the average count of anions (or cations) surrounding a given cation (or anion) within their respective coordination complexes. n^{cat}_{aci} and $n^{an.}_{ccj}$ denote the respective numbers of cations and anions involved in the anionic and cationic coordination complexes. Additionally, f_{ac_i} and f_{cc_j} represent the molar fractions of the i$^{\text{th}}$ anionic complex and j$^{\text{th}}$ cationic complex.

We now outline the theoretical framework for describing the compositional dependence of thermal conductivity in molten salt mixtures. In our previous work [277], we introduced a theoretical framework that effectively captures the composition dependence of thermal conductivity in ionically bonded solid solutions. This proposed approach is highly predictive, as it focuses exclusively on a few essential thermo-physical properties of the end-members (unrelated to thermal transport). It is rooted in the simplified solution of the Boltzmann Thermal Equation (BTE) originally presented by Abeles [275] for disordered solid solutions. In the formalism presented by Abeles, the degradation of thermal conductivity induced by the process of dissolution is attributed to two contributing factors: mass fluctuations and elastic strain fluctuations. The contribution of mass fluctuation reflects the localized variation in kinetic energy caused by the difference in mass between the host and solute atoms, while the contribution of elastic fluctuation describes the local variation in elastic potential energy resulting from ion substitution. In the NPT statistical ensemble, a molten mixture can be considered fully relaxed, without inducing significant elastic deformation by the solute atom, as the system reaches a stable, fluid-like state where interatomic forces have equilibrated.

Without compromising generality, the thermal conductivity of a fully relaxed solution, including molten salt mixtures, can be expressed as a function of temperature and composition, as follows [133, 152, 238]:

$$\lambda^{msm}\left(\underline{x}, T\right) = \lambda^{k}\left(\underline{x}, T\right)\left[1 - \delta^{\lambda}_{M}\left(\underline{x}, T\right)\right] \tag{E.9}$$

where $\underline{x} = (x_1, x_2, ...x_n)$ represents the composition vector. The functional δ_M^{λ} describes the local fluctuation of kinetic energy effect upon the thermal transport. The term λ^k, referred to as the "kinetic thermal conductivity", represents the thermal conductivity of the mixture assuming no local fluctuation of kinetic energy induced by the mass difference between the host and solute ions. The calculation of λ^k involves applying the kinetic theory-based approach used for single compounds (Equation E.5), taking into consideration model parameters such as density, velocity of sound, heat capacity, and thermal expansion, which vary with composition. Specifically, at a given temperature T_0, the thermal conductivity derived from kinetic considerations can be expressed as follows:

$$\lambda^k(T) = \psi^*(\underline{x})\, k_B n_{liq.}^{2/3}(\underline{x}, T_0)\, \langle c_S \rangle_{liq.}(\underline{x}, T_0) \left[1 - \alpha(\underline{x}, T_0)\left(\gamma(\underline{x}, T_0) + \frac{1}{3}\right)(T - T_0)\right] \quad \text{(E.10)}$$

In the case of simple molten salt mixtures, the composition-dependent variations in velocity of sound, density, heat capacity, and thermal expansion can be readily obtained from thermophysical property databases, referenced literature sources, or accurately estimated by leveraging the linear relationship between Gibbs energy, its pressure-temperature dependence, and composition (a homogeneous first-degree function of composition). The assumption of an ideal linear behavior of the Gibbs energy and its temperature-pressure derivatives with composition allows for the following approximations: i) a linear variation of the molar volume ($V_m = M/\rho$) with composition, ii) a linear variation of the thermal expansion with volume fraction ($\phi_i = x_i V_i / \sum_i x_i V_i$) and iii) a linear variation of the isothermal compressibility ($\chi = 1/(c_s^2 \rho)$). These approximations have been found to be accurate for simple molten salt mixtures. However, for complex mixtures, significant deviations from the "ideal" behavior of thermophysical properties may be observed [330]. Additionally, it is assumed that the parameter $\boldsymbol{K}$ varies linearly with composition. In our previous research [133,152,238], which also builds upon the kinetic theory, we have formulated the functional δ_M^{λ} specifically for simple molten salt mixtures as:

$$\delta_M^{\lambda}(\underline{x}, T) = h_{diff.}(\underline{x}, T)\ \ g_{mass}(\underline{x}) \quad \text{(E.11)}$$

The function g_{mass} is independent from the temperature and describes the local fluctuation of the kinetic energy with composition through the mass fluctuation only. It is defined in the same way as disordered solid solutions or amorphous mixtures [275]:

$$g_{mass}(\underline{x}) = \sum_{i=1}^{N} x_i \left[1 - \frac{M_{w_i}}{\overline{M}(\underline{x})}\right]^2 \quad \text{(E.12)}$$

where $\overline{M} = \sum x_i M_{w_i}$ is the average molecular weight of the molten salt mixture. The damping factor of diffusons, denoted as $h_{diff.}$, quantifies the attenuation of the local kinetic energy fluctuation effects on the mean free path of diffusons, consequently affecting lattice thermal transport. The amplitude of local kinetic energy fluctuations induced by dissolution decreases with temperature due to the homogenization of thermal excitation. In a prior work [133], also based on kinetic theory, we have derived the following expression for $h_{diff.}$:

$$h_{diff.}\left(\underline{x}, T\right) = \mu \, \frac{\lambda_\sigma\left(\underline{x}, T\right)}{k_B \, \langle c_S \rangle_{liq}\left(\underline{x}, T\right) n_{liq}^{2/3}\left(\underline{x}, T\right)} \tag{E.13}$$

where μ is an adjustable parameter, typically close to 1/2, and λ_σ represents the effective thermal conductivity of the mixtures, where the mean free path of the diffusons is equivalent to the average inter-ionic distance (r_e). In our original formulation [133], we established the relationship that $h_{diff.}$ is proportional to the ratio between the diffuson mean free path and the average interionic distance. However, in order to prevent the diffuson mean free path from being treated as an adjustable parameter, we have expressed $h_{diff.}$ as a ratio of thermal conductivity, as outlined in Equation E.13. This allows us to incorporate $h_{diff.}$ as the description of the degradation of the thermal conductivity with composition, without explicitly considering the diffuson mean free path as a variable that can be adjusted within the model. However, it is crucial to acknowledge that the expression of $h_{diff.}$ mentioned above poses challenges when it comes to its implementation, especially when considering the compositional dependence of the thermophysical properties that must be predicted, particularly in larger systems like ternary and higher-order systems. Furthermore, since h_{diff} is defined as a ratio of thermal conductivities, estimated based on the thermophysical properties of molten salt mixtures, the accuracy of the predicted value of h_{diff} can be limited in various situations. In the case of simple molten salt mixtures such as LiF-KF or NaCl-KCl, where $\boldsymbol{K} = 2$, assuming $\mu = 1/2$ allows us to demonstrate that $h_{diff.}$ closely approximates the ratio $\sum \lambda_i / \lambda^{id}$. Here, λ^{id} represents the ideal thermal conductivity of the mixture defined as the sum of $x_i \lambda_i$ for each component i. Subsequently, by neglecting the quadratic terms ($x_i x_j$), the thermal conductivity of a simple molten salt mixture with N components can be expressed as a function of composition and temperature in the following manner:

$$\lambda\left(\underline{x}, T\right) = \lambda^k\left(\underline{x}, T\right) \left(1 - \sum_{i=1}^{N} \left(\frac{\lambda_i}{\lambda^{id}} \right) x_i \left[1 - \frac{M_{w_i}}{\overline{M}\left(\underline{x}\right)} \right]^2 \right) \tag{E.14}$$

In complex molten salt mixtures, the strong short-range ordering contributes to the formation of intricate coordination complexes and polymer chains accentuating the degradation of the thermal conductivity. The thermal conductivity of a fully polymerized system is assumed

to be close to that of an amorphous solid and like for compounds it should be close to the minimum value predicted by the kinetic theory. If we make the assumption that the increase in $h_{diff.}$ is linearly correlated with the complexion rate (τ), then the thermal conductivity of the molten salt mixture containing complexes can be expressed as follows:

$$\lambda\left(\underline{x},T\right)=\lambda^{k}\left(\underline{x},T\right)\left(1-\tau\left(\underline{x},T\right)\sum_{i=0}^{N}\left(\frac{\lambda_{i}}{\lambda^{id}}\right)x_{i}\left[1-\frac{M_{w_{i}}}{\overline{M}}\right]^{2}\right) \tag{E.15}$$

Here, the term "complexion rate (τ)" represents the measure of complex and polymer formation within a mixture of molten salts. It quantifies the mass-based evolution of these complexes and polymers as they dampen a function describing the local kinetic energy through fluctuations in mass. The total mass coordination complexes and polymers are related to the mass of the system. The expression for the complexion rate can be then written as follows:

$$\tau\left(\underline{x},T\right)=\frac{M_{free}^{*}+M_{comp.}^{*}\left(\underline{x},T\right)}{\overline{M}\left(\underline{x}\right)} \tag{E.16}$$

Where M_{free}^{*} denotes the mass of the free ion species, and $M_{comp.}^{*}$ represents the mass of the complexes formed within the molten salt mixture defined as:

$$M_{comp.}^{*}=\sum_{\substack{i,j\\i\neq j}}\left(f_{ac_{i}}M_{ac_{i}}+f_{cc_{j}}M_{cc_{j}}\right) \tag{E.17}$$

This proposed theoretical formalism builds upon the principles of kinetic theory and extends the understanding of thermal transport from amorphous solids to molten state mixtures, explicitly accounting for local ordering. This new model predictive capabilities eliminates the need for experimental data specifically related to thermal transport for the parameterization. Instead, it relies on a limited set of experimental data on key thermophysical properties (such as density, heat capacity, thermal expansion, and velocity of sound) for pure compounds. The thermal conductivity (or thermal diffusivity) of a mixture is described by the composition dependence through mass fluctuation, which, within the framework of kinetic theory, represents the local kinetic energy fluctuation upon dissolution. The explicit consideration of local ordering is achieved by introducing damping functions that act on the function describing the local fluctuation of kinetic energy. In our model, the local structure is represented by the masses and the molar fraction of coordination complexes and polymers evolving within the molten salt mixtures. For complex molten salt mixtures, accurate knowledge of the amount of complexes/polymers as a function of composition and temperature becomes crucial for parameterizing the model. This information can be obtained from various sources, such as experiments, particularly through Nuclear Magnetic Resonance (NMR)

techniques, estimated through phase equilibria data using a CALPHAD (Calculation of Phase Diagrams) approach, or directly simulated using molecular dynamics simulations. By incorporating these elements, our theoretical formalism provides a comprehensive framework for understanding and predicting thermal transport in complex molten salt mixtures, facilitating advancements in various fields, including materials science and engineering.

The central focus of our current study is to comprehend the role of local structural arrangements in influencing thermal transport within complex molten salt configurations. To address this, we have developed a theoretical framework rooted in kinetic theory. Importantly, this framework explicitly considers the local structural attributes that characterize molten salt mixtures. Our discussion is constructed upon two primary components. Firstly, we present our theoretical approach, which forms the foundation of our investigation. Secondly, we utilize EMD simulations to calculate thermal conductivity and quantify local structural characteristics. This dual approach enables us to provide an analysis of the relationship between local structure and thermal transport in complex molten salt systems.
First, we discuss the case of molten KCl and alumina to explore and validate theoretical models within chemistry. While KCl serves as an illustration of a fully dissociated simple salt, the alumina behavior offers valuable insights, showcasing that the model can be extended to oxides with specific ordering. The thermal conductivity profiles of the KCl and Al_2O_3 compounds have been calculated with respect to temperature using a two-fold methodology. Initially, we employed the fundamental "raw" kinetic model approach, as outlined in Equation D4. Subsequently, we utilized the modified kinetic model provided by Equation D5 to account for the additional effects of local ordering within molten salts. This modified model establishes a bridge between the thermophysical attributes of the molten and crystalline phases, aligning with a corresponding state description. This enhancement improves the model capacity to depict the intricate thermal dynamics of these materials. Figure E.2 presents a comparison of the calculated thermal conductivity with both experimental data and EMD simulations. The kinetic model parameters rely on thermophysical data obtained from the current EMD simulations. The supplementary materials of this paper comprehensively outline how the velocity of sound, density, thermal expansion, and heat capacity are derived from these EMD simulations. In both studied systems, the accuracy of the modified kinetic theory approach is higher than that of the conventional raw kinetic theory approach. This improved predictive capability is true regardless of whether the parameterization is based on solid or liquid thermophysical properties. The predicted thermal conductivity of KCl aligns with various reliable datasets and EMD simulations. This agreement is also observed for the temperature dependence of the thermal conductivity, which further substantiates the initial

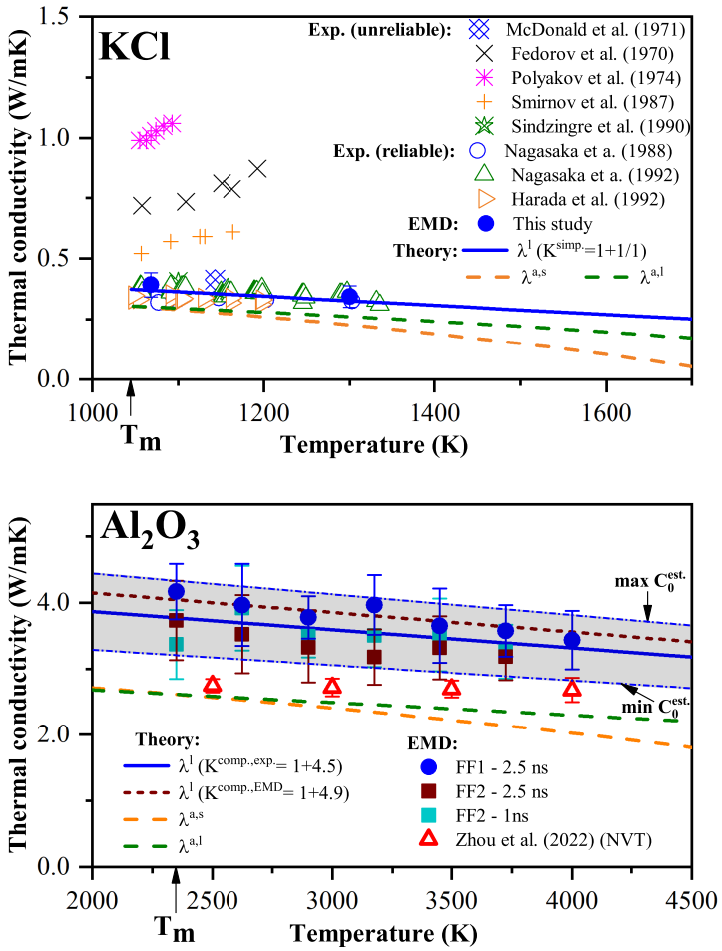

Figure E.2 Comparison of the thermal conductivity of molten KCl and Al_2O_3 with experimental data and EMD Simulation results. The calculated thermal conductivities are plotted as functions of temperature and contrasted with experimental data and EMD simulation outcomes. Here, λ^l represents the thermal conductivity determined using the proposed model (Equation E.5), while $\lambda^{a,s}$ and $\lambda^{a,l}$ denote the thermal conductivities calculated using the 'raw' kinetic model (Equation E.4), considering the thermophysical properties of the solid and liquid phases, respectively. The significant uncertainty in the velocity of sound within molten Al_2O_3 is factored into the thermal conductivity calculation by incorporating upper (max C_0) and lower (min C_0) values of the velocity of sound in the model parameterization. These values correspond to a variation of $\pm 15\%$. T_m indicates the melting temperature. The simulations conducted by Zhou et al. are referenced as: [331].

assumption $(\partial\lambda/\partial T)_V = 0$. The predictive capacity of our proposed model for numerous simple molten salt compounds has already been thoroughly examined and expounded upon in our recent publication [264]. Notably, our prior work details the methodology for identifying

dependable and less reliable experimental datasets. Furthermore, the thermal conductivity predicted by the "raw" kinetic theory model also retains it reasonable accuracy whether the parameterization is based on the thermophysical properties of the solid or the liquid phase. However, the parameterization derived from solid-state properties does exhibit a tendency to overestimate the sensitivity of the thermal conductivity to temperature. This overestimation can be attributed to an amplified thermal expansion effect, which is more evident in the crystalline phase compared to the molten state.

Beyond the comprehension of the thermal transport mechanisms in complex, ionically bonded systems, this study offers a pathway for predicting the thermal conductivity of diverse molten materials with varying chemical compositions and bonding natures. The thermal conductivity of molten oxides, particularly in the context of slags, remains a largely uncharted territory, with almost no reported experimental data in the literature. The kinetic model, detailed in this work, may provide a reliable alternative to address the scarcity of experimental data on the thermal conductivity of molten oxides, a critical factor in numerous industrial and practical applications. In our theoretical predictions, we have incorporated the calculated average coordination number obtained through the current EMD simulations (Z = 4.9) and the experimentally determined value by Landron et al. [332] (Z = 4.5). However, Landron et al.'s reported average coordination number comes with a significant uncertainty of approximately ± 0.3. Similarly to the approach used for molten KCl, we have employed a raw kinetic model, considering both liquid and solid properties for the parametrization, to predict the thermal conductivity within molten Al_2O_3. Lastly, we have examined the influence of the simulation duration by comparing simulations conducted over 1 ns and 2.5 ns. The velocity of sound within molten Al_2O_3, which was utilized to parameterize the theoretical model, is derived from the calculated equation of state, also obtained through EMD simulations. However, it is important to note that this value comes with a significant uncertainty of approximately $\pm 15\%$. This uncertainty is duly considered in the calculations, resulting in a range that represents the upper and lower limits of the theoretical thermal conductivity.

The predicted thermal conductivity with the proposed model aligns with the results from EMD simulations when considering two distinct force fields, FF1 and FF2. In principle, FF2 is anticipated to offer greater precision, as it differs from FF1 by incorporating many-body effects into the short-range repulsion between Al and O ions, as outlined in the 'Numerical Methods' section. Simulations with the FF2 force field lead to thermal conductivity predictions closer to the lower theoretical conductivity limit, while those via the FF1 force field closer to the upper limit. Overall, both force fields lead to predictions within the margin of error of each other force field. The temperature dependence of the thermal conductivity, as simulated through EMD, aligns well with the theoretical model, demonstrating the consis-

tency of the assumption $(\partial\lambda/\partial T)_V = 0$ for molten oxides as well. It is also shown that the kinetic model has improved accuracy over the "raw" model, relative to the EMD predictions, demonstrating that coordination has a significant influence on the thermal conductivity of molten alumina. The thermal conductivity simulations of molten alumina conducted by Zhou et al. [331] reveal a temperature dependence of zero in the NVT ensemble. This further corroborates that $(\partial\lambda/\partial T)_V = 0$ holds true in molten oxides. Furthermore, the thermal conductivity predictions of Zhou et al. are consistent with the theoretical formulation based on the raw kinetic model. However, these predictions still fall within the margin of error when compared to simulations using the FF2 force field, especially at higher temperatures. The disparity of approximately 1 [W.m^{-1}.K^{-1}] between our EMD prediction and that by Zhou et al. primarily comes from a significant contrast in the force fields used to model ion-ion interactions. Notably, Zhou et al. did not consider the polarization of oxygen in the force field. Furthermore, Zhou et al. conducted shorter simulations, lasting less than 1 ns. In our simulations we observed that shorter simulation times can result in an underestimation of the thermal conductivity, particularly near the melting temperature.

The ability of the model to capture microscopic phenomena underlying thermal transport within pure molten salt/oxide compounds is demonstrated through our current theoretical approach. In the case of KCl, the influence of the local structural arrangement on thermal transport appears to be limited. This is expected considering that KCl should behave as a fully dissociated ionic liquid. As such, for other pure simple salt compounds, the kinetic model should accurately predict the temperature-dependent thermal conductivity, consistently with our the kinetic model of our prior work [264], when parameterized using thermophysical properties in the liquid phase. In contrast, accurately predicting the thermal conductivity of alumina, and potentially other oxide melts, also requires considering the average coordination number and, consequently, an assessment of the local ordering. We show that the kinetic model provides reasonable agreement with EMD, proving its capability of handling molten alumina and that the derivation of the model parameters that consider the coordination effect on thermal conductivity is appropriate.

We now move on to discussing the chemical effects on thermal transport within molten salt mixtures. Our recent work evaluated the predictive capacity of the current model on various simple molten salt systems, including fluorides, chlorides, bromides, iodides, carbonates, and nitrates [295]. In Figure E.3 the thermal conductivity of LiF-KF is calculated at 1300 [K] as a function of composition and compared with EMD simulations considering both FF1 and FF2 force fields. A key observation is that the thermal conductivity composition dependence deviates significantly from ideal behavior ($\lambda^{id} = \sum_i X_i\lambda_i$), with discrepancies reaching up to 80% at the equimolar composition. The substantial deviation observed can be attributed

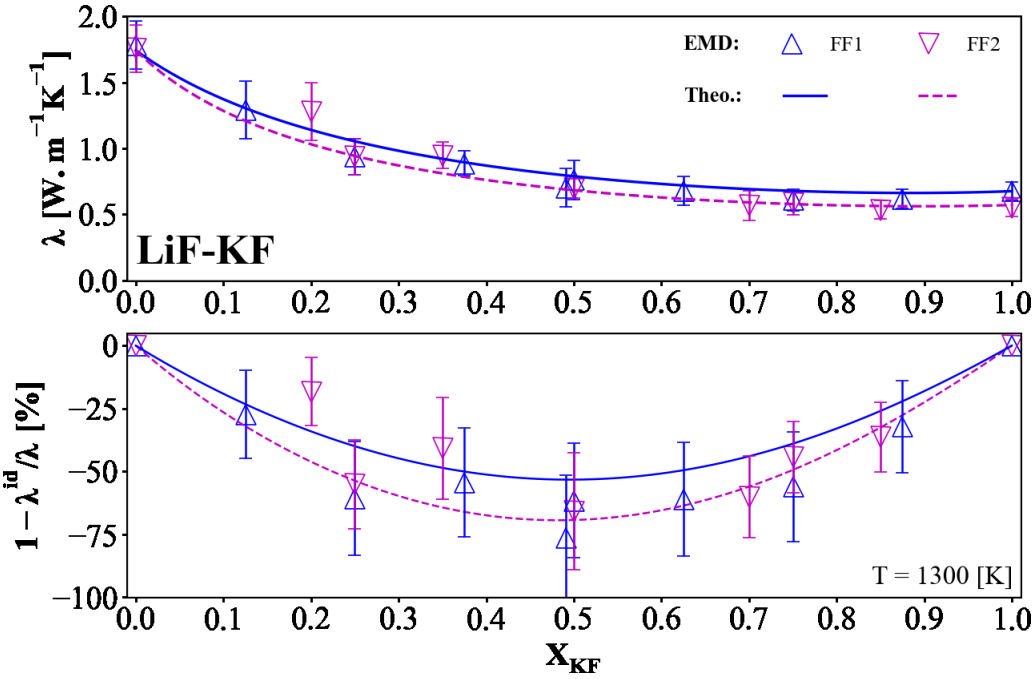

Figure E.3 Comparison of thermal conductivity in the LiF-KF molten system at 1300 K with EMD Simulations using two ionic interaction Force Fields (FF1 and FF2). Theoretical modeling parameterizes the results, incorporating thermal conductivity values obtained via FF1 (solid line) and FF2 (dashed line) for the pure end members. The bottom figure represents the calculated deviation of the thermal conductivity from the linear behavior ($\lambda^{id} = \sum_i X_i \lambda_i$).

to two key factors. First, there exists a relatively significant mass difference between the two cations, with lithium (Li) having a molar mass of 6.94 [g/mol] and potassium (K) a molar mass of 39.1 g/mol. This discrepancy results in substantial fluctuations in kinetic energy when a Li atom replaces a K atom and vice versa. Second, there is a marked contrast in the thermal conductivity between LiF (1.8 [W.m^{-1}.K^{-1}]) and KF (0.45 [W.m^{-1}.K^{-1}]). This divergence increases the influence of kinetic energy fluctuations on the compositional dependence of the mixture thermal conductivity. As it was shown in our prior work, the mass difference and conductivity differences primarily cause deviations from the ideal behavior. In general, the model will be reliable in predicting the thermal conductivity of various simple molten salt mixtures in both composition and temperature, consistently with our prior study. In order to showcase the versatility of our formalism in addressing multicomponent molten salt mixtures, we have calculated the thermal conductivity of FLiNaK, a widely recognized eutectic blend composed of $LiF_{0.465}$-$NaF_{0.115}$-$KF_{0.420}$, across a range of temperatures. Our calculations have been rigorously compared with both credible experimental data and simu-

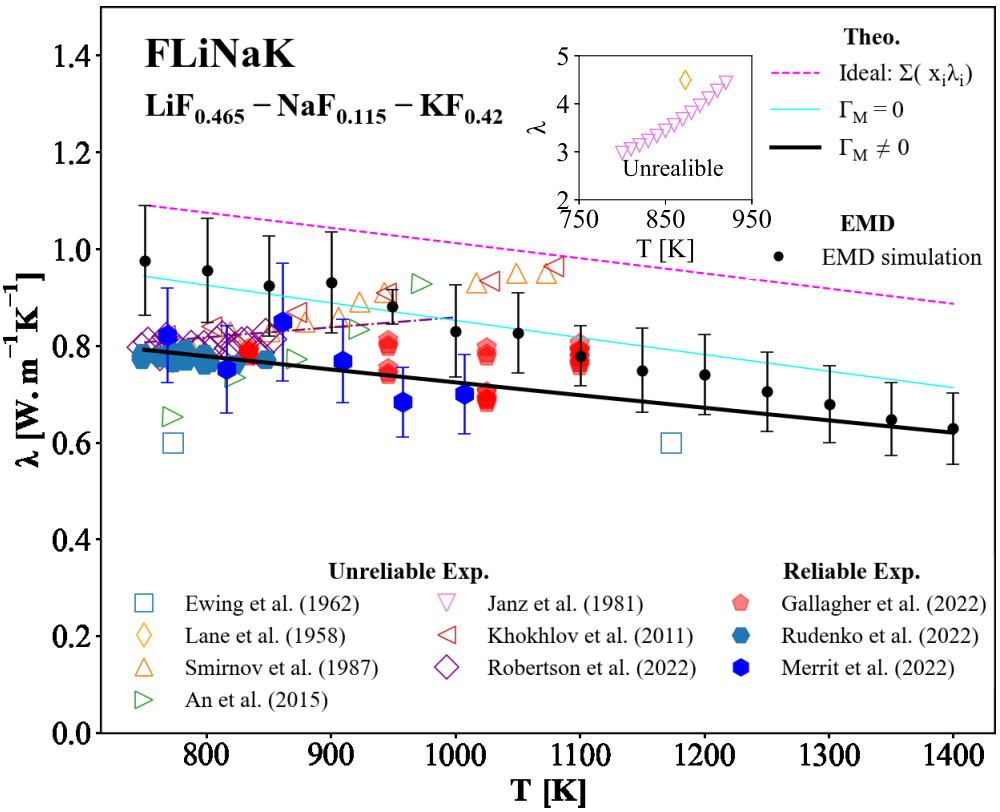

Figure E.4 Calculated thermal conductivity of FLiNaK (LiF-NaF-KF eutectic) as a function of temperature in comparison with reliable data (filled symbols), non-reliable data (open Symbols), and EMD simulations. The thermal conductivity has been calculated under three different conditions: assuming an ideal mixing rule (i.e., $\lambda^{id} = \sum_i x_i \lambda_i$), considering no mass fluctuation (i.e., $\lambda \equiv \lambda^K$), and incorporating the model defined by Equation E14 in this study. Experimental data are referenced as: Ewing et al. [198], Lane et al. [270], Smirnov et al. [56], An et al. [76], Janz et al. [34], Kholkhov et al. [314], Robertson et al. [80], Gallagher et al. [61]and Merrit et al. [68].

lation results obtained through the EMD method, including data of varying reliability. The distinction between reliable and unreliable experimental data has been extensively discussed in prior works [60, 264]. Notably, unreliable experiments often report an increase in thermal conductivity with rising temperature. Experimental data for FLiNaK is frequently deemed unreliable, sometimes even reaching values as high as 5 [$W.m^{-1}.K^{-1}$]. The elevated thermal conductivity reported in these unreliable experiments can be attributed to radiative and convective effects. Overall, in the case of FLiNaK, the predictive capability of EMD is deemed

satisfactory, falling within the margin of error typically associated with reliable experimental datasets reported in the literature. Nevertheless, EMD simulation tends to overestimate the thermal conductivity of FLiNaK, particularly at lower temperatures near its melting point. This overestimation can be attributed to two key factors: the substantial presence of lithium (Li) within the FLiNaK mixture and the inherent limitations of the force field formalism employed to describe the interactions between Li and F ions, as elaborated upon in the Appendix. This challenge arises from the difficulty in accurately predicting thermal transport when lightweight cations such as Li are actively participating in the system, as thoroughly discussed in prior works (Smith et al. [160], Gallagher et al. [61]). Theoretical thermal conductivity calculations were based on the thermophysical properties of single molten compounds such as LiF, NaF, and KF, as previously reported in our study [264]. These calculations have shown a significant concordance with the latest and reliable experimental datasets. The determined thermal conductivity, as well as the experimental counterpart, exhibits a reduction of approximately 35% compared to the ideal thermal conductivity (assuming a linear relationship with composition). Moreover, it is found to be 15% lower than the predicted value represented by λ^k, which assumes zero mass fluctuation and, consequently, zero local kinetic energy fluctuation. In other words, the influence of local kinetic energy on thermal transport in FLiNaK is not as significant as 35%, but rather approximately 15%.

The connection between the local structural features and thermal transport properties in complex molten salts is explored through the examination of two significant examples: the KCl-$MgCl_2$ and NaF-AlF_3 systems. Figure E.5 illustrates the thermal conductivity of KCl-$MgCl_2$ in conjunction with coordination complex parameters and the τ ratio, highlighting the correlation between the local structure and the composition-dependent thermal conductivity. The impact of local ordering on thermal transport in the molten KCl-$MgCl_2$ system is evidenced through the comparison with: (i) excess thermal conductivity, which quantifies deviations from the linear behavior with composition (ideality), ii) the kinetic contribution to the thermal conductivity (λ^k), which explores thermal conductivity under the assumption of no local fluctuations in kinetic energy and (iii) assuming a fully dissociated mixture (i.e., τ=0), which allows us to examine the scenario where the presence of coordination complexes has no effect on thermal transport.

Theoretical predictions and EMD simulations of KCl-$MgCl_2$ thermal conductivity are in reasonable agreement, with a deviation from ideal behavior of approximately 25% at the equimolar composition. Furthermore, both the kinetic thermal conductivity and the calculation assuming $\tau = 0$ show almost negligible excess thermal conductivity. The near agreement between the thermal conductivity of the hypothetically dissociated system and its ideal behavior arises from a compensation between thermal conductivity and mass for the

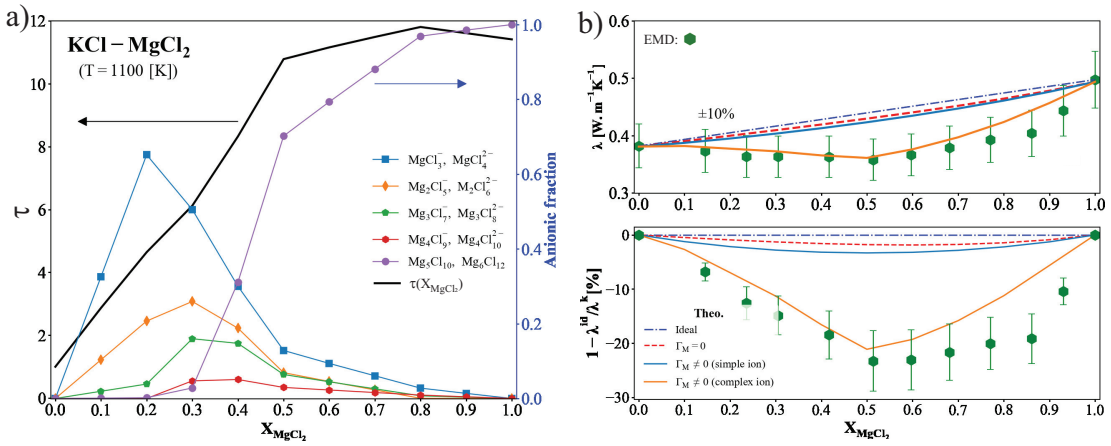

Figure E.5 Correlating calculated local structure with (a) τ, which measures the impact of local kinetic energy fluctuations on thermal transport in the presence of coordination complexes, is reported alongside their quantity and (b) the thermal conductivity and excess thermal conductivity in the Molten $MgCl_2$-KCl system. For comparison, the thermal conductivity was calculated using three different methods: (i) employing an ideal mixing rule ($\sum_i x_i\lambda_i$), (ii) assuming zero local kinetic energy fluctuation ($\Gamma_M = 0$), and (iii) considering a simple mixture with $\tau = 0$.

two end-members of the molten mixture: $\lambda_{MgCl_2}/M_{MgCl_2} \approx \lambda_{KCl}/M_{KCl}$. In summary, the difference in thermal conductivity compensates for the local fluctuations in kinetic energy.

The local structural ordering within the molten KCl-$MgCl_2$ mixture has been calculated using the methodology detailed in [156, 315, 333]. This calculation emphasizes the presence of $Mg_nCl_m^{(m-2)^-}$ complexes (with $m \geq 2n$) and Mg_sCl_{2s} neutral complexes ($s1 = 5$ or 6). The simulation highlights that as $MgCl_2$ content increases, there is a decrease in the amount of $Mg_nCl_m^{(m-2)^-}$ complexes, with Mg_sCl_{2s} complexes becoming more prominent. For values of n up to 3, the abundance of $Mg_nCl_m^{(m-2)^-}$ complexes follows a consistent trend: an increase from the KCl composition to reach a peak around $X_{MgCl_2} = 0.3$, followed by a sharp decrease up to approximately $X_{MgCl_2} = 0.5$. Subsequently, there is a gradual decrease, approaching near-null levels beyond $X_{MgCl_2} = 0.8$. The amount of $Mg_4Cl_9^-$ and $Mg_4Cl_{10}^{2-}$ anions remains significantly low, even though a substantial peak, reaching approximately 5%, is observed within the range of $0.3 \lesssim X_{MgCl2} \lesssim 0.5$. The noticeable increase in neutral complexes, particularly Mg_5Cl_{10} and Mg_6Cl_{12}, at the expense of anionic complexes, is linked with the polymerization process. This phenomenon becomes significant when the predominance of the Mg_sCl_{2s} polymer chain is achieved, typically beyond approximately $X_{MgCl_2} = 0.5$. At this point, it stabilizes at an asymptotic value, and the influence of the local order on thermal transport becomes nearly invariant with changes in composition, as τ exhibits reduced sensitivity to compositional variations.

The theoretical model accurately predicts the thermal conductivity's dependence on composition within the range $X_{MgCl_2} \lesssim 0.5$. However, it tends to slightly overestimate the thermal conductivity beyond this composition range, relative to EMD. The overestimation of thermal conductivity by the theoretical model is evident through the underestimation of excess thermal conductivity. This discrepancy becomes increasingly pronounced as the composition approaches pure $MgCl_2$. The underestimation of the thermal conductivity in our theoretical approach, resulting in an overestimation of the excess thermal conductivity, is directly linked to the underestimated value of the parameter τ. τ that has been calculated assuming that polymer chains contain only Mg_5Cl_{10} and Mg_6Cl_{12}. It is quite likely that longer polymer chains are formed in the $MgCl_2$ rich region, but their identification is challenging due to the limitations of the technique used to accurately characterize these extended polymer structures. Overall, based on this example, it becomes evident that the synergy between EMD simulations using polarizable potentials and the Green-Kubo method consistently emphasizes the importance of local ordering and thermal transport in complex molten salt mixtures. Despite its limitations, the model shows significant improvement over the case where simple dissociation is assumed and EMD results are within 10%.

Extensive research has been conducted in recent years to investigate the thermal conductivity of the NaCl-KCl-$MgCl_2$ eutectic composition, specifically the $(NaCl)_{0.205}$-$(KCl)_{0.413}$-$(MgCl_2)_{0.382}$ mixture [238, 334, 335]. This keen interest is due to its potential use in thermal energy storage within concentrated solar power systems. The NaCl-KCl-$MgCl_2$ system closely resembles the KCl-$MgCl_2$ system, and it is reasonable to assume that KCl and NaCl have a similar impact on local ordering in the presence of $MgCl_2$. Therefore, we can assume that $\tau\left(X_{MgCl_2}\right)$ is the same as for KCl-$MgCl_2$. Based on this assumption, we calculated the thermal conductivity of NaCl-KCl-$MgCl_2$ from 700 [K] (i.e., 40 [K] above the liquidus temperature [294]) up to 1100 [K] and presented it in Figure E.6, comparing it with available experimental data and EMD simulation results. Similarly to the KCl-$MgCl_2$ system, at $X_{MgCl_2} = 0.382$, the calculated thermal conductivity is approximately 15% lower than that of the mixture assumed to consist of dissociated ions, i.e., not complexed. Overall, EMD simulations show good agreement with experimental data, despite both exhibiting some scattering and being reported with a significant experimental error. Because of the significant uncertainties in both experimental data and EMD simulations, reaching a clear conclusion about the temperature-dependent behavior of thermal conductivity in NaCl-KCl-$MgCl_2$ is challenging. However, the experimental data presented by Wang et al. [334] exhibits a temperature dependence that closely aligns with the predictions of the theoretical framework. This suggests that, like molten oxides, the initial idea that $(\partial\lambda/\partial T)_V = 0$ holds true for complex molten salts mixtures. Chung et al. [335] provided two sets of experimental data: one acquired using

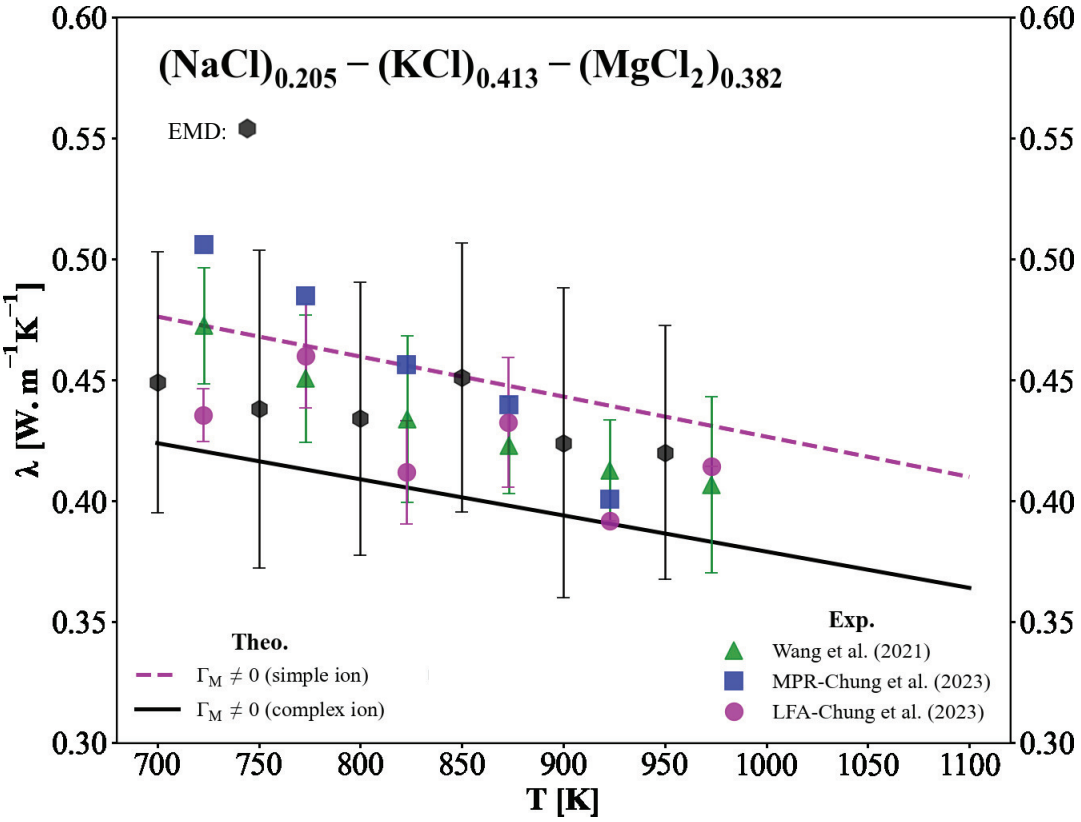

Figure E.6 Calculated thermal conductivity as a function of temperature for the $(NaCl)_{0.205}$-$(KCl)_{0.413}$ - $(MgCl_2)_{0.382}$ eutectic, compared with EMD simulations and recent experimental data reported by Wang et al. [334] and Chung et al. [335].

the modulated photothermal radiometry (MPR) technique and the other employing a laser flash apparatus (LFA). The thermal conductivity data obtained via the MPR technique indicates a $(\partial\lambda/\partial T)_P$ value that is roughly double that of the theoretical predictions, whereas a linear regression applied to the dataset obtained through LFA yields better agreement with the theory.

At first glance, the EMD results suggest a thermal conductivity with a relatively low sensitivity to temperature variations. The substantial uncertainty observed in the EMD results is not attributed to the choice of the force field utilized to describe interionic interactions but rather comes from the application of the Green-Kubo formalism to derive thermal conductivity from the simulated phase trajectories (see Appendix D-1). In the Green-Kubo (GK) expression for the thermal conductivity of a system featuring four different ions, there are

nine evolving Onsager phenomenological coefficients. These coefficients play a pivotal role, particularly in the ratio describing the influence of charge transport on thermal transport. Second-order polynomials involving Onsager's phenomenological coefficients appear in both the numerator and denominator, contributing to significant uncertainties and inherent errors. The combination of EMD with the GK method reveals significant limitations in accurately predicting the thermal conductivity of multicomponent molten salt mixtures. In this context, our theoretical approach emerges as a viable alternative that effectively addresses the challenges associated with the scarcity of experimental data and the inherent constraints of EMD when it comes to accurately predicting temperature-dependent thermal transport properties within complex multicomponent molten salt mixtures.

The NaF-AlF_3 system is of particular interest because it involves the formation of coordination complexes and polymers when AlF_3 starts to dissolve in NaF. The coordination complexes are $AlFn^{(n-3)-}$ fluoroaluminates, and when the concentration of AlF_3 is greater than 0.5, dimers, trimers, and polymers are also formed. The local structural characteristics of NaF-AlF_3 melts were determined through simulations utilizing two distinct force fields: one designed for compositions up to approximately equimolar (FF1), and the other applicable across the entire compositional spectrum (FF2). The discrepancy between these two force fields is discussed in the appendix. Figure E.7 displays the calculated local structure for FF1 and FF2, respectively.

The distinctions in quantified complex anions and higher-order structures (dimers, trimers, and polymers) are visually depicted in Figure E.8, alongside the resultant τ parameters for both FF1 and FF2. We do not intend to assess the accuracy of EMD simulations in predicting local structures within NaF-AlF_3 melts here. Machado et al. [315] have extensively discussed this by comparing simulations based on FF1 with NMR experiments. Compared to FF1, FF2 predicts an exaggerated formation of ${AlF_6}^{3-}$ anionic coordination complexes at the detriment of ${AlF_5}^{2-}$. Additionally, FF1 indicates a negligible presence of dimers above $X_{AlF_3} = 0.3$, while FF2, under the same range of composition, suggests a substantial presence of dimers, trimers, and polymeric chains. The significant disparities between these two parameters result in an inconsistency when considering the parameter τ near $X_{AlF_3} = 0.2$. As the quantity of AlF_3 increases, this deviation becomes more pronounced, and near the equimolar composition, the value of τ predicted by FF1 is half of what is projected by FF2.

The EMD simulations for the thermal conductivity of NaF-AlF_3 systems at 1343 [K], along with their deviations from ideal behavior at the same temperature, are presented in Figure E.9 and E.10, corresponding to the use of FF1 and FF2, respectively. Both sets of simulation data are compared to the singular experimental dataset provided by Khokhlov et al. [314] in the range 1100 - 1373 [K]. Theoretical predictions of the thermal conductivity, considering

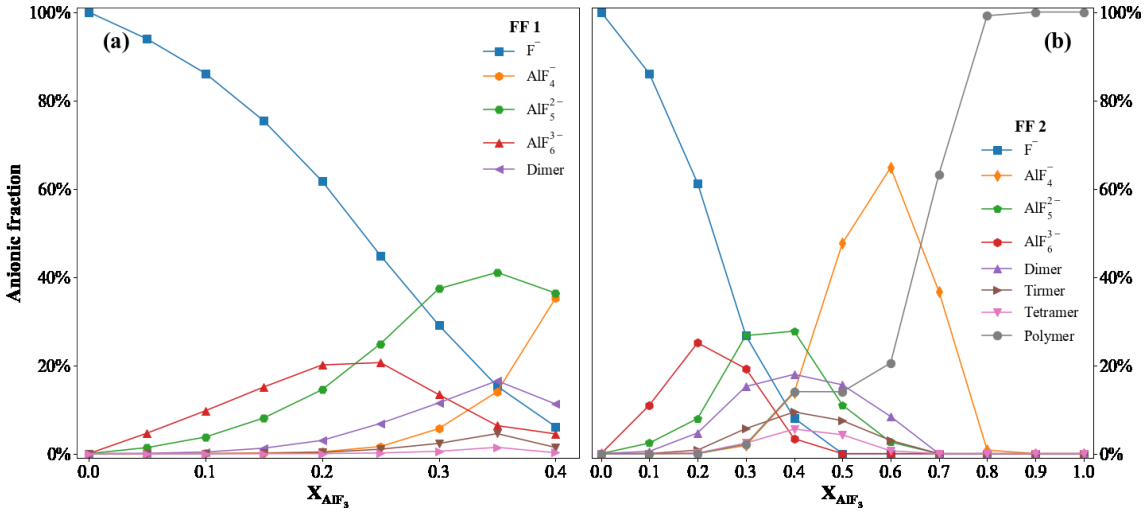

Figure E.7 Calculated local structure of NaF-AlF_3 melts as a function of composition at 1343 K, obtained using two different force fields, FF1 (a) and FF2 (b). Note that FF2 remains valid throughout the entire composition range, whereas FF1 is applicable only up to the equimolar composition.

the influence of the damping factor (τ) induced by local structural effects on kinetic energy fluctuations, are compared to two scenarios: one assuming a dissociated mixture ($\tau = 1$) and the other considering only kinetic contributions (τ). To better represent the impact of local structure on thermal transport, we also assessed deviations from a linear composition-dependent behavior (ideality). This assessment involved EMD simulations, Khokhlov et al.'s experiments, and three theoretical calculations, each with different τ values (τ, $\tau = 1$, and $\tau = 0$). Note that the thermal conductivity of AlF_3 could not be simulated using FF1. Therefore, in our theoretical calculations, we assumed the thermal conductivity of AlF_3 to be identical between FF1 and FF2.

Our EMD simulations closely align with Khokhlov et al.'s experimental data [314], regardless of the force field. However, simulations employing the FF2 force field exhibit a better fit with the data, but both force fields are in good agreement. The apparent underestimation of the thermal conductivity by FF1 can be attributed to a similar underestimation of the thermal conductivity of NaF as a standalone compound when compared to Kolkhov et al.'s experiments and FF2. The discrepancy between the calculated thermal conductivity of NaF using FF1 and the values calculated by FF2 and the experimental data is approximately 0.2 [$W.K^{-1}.m^{-1}$], and this difference remains relatively constant across all compositions. Note that the experimental thermal conductivity of molten NaF is approxi-

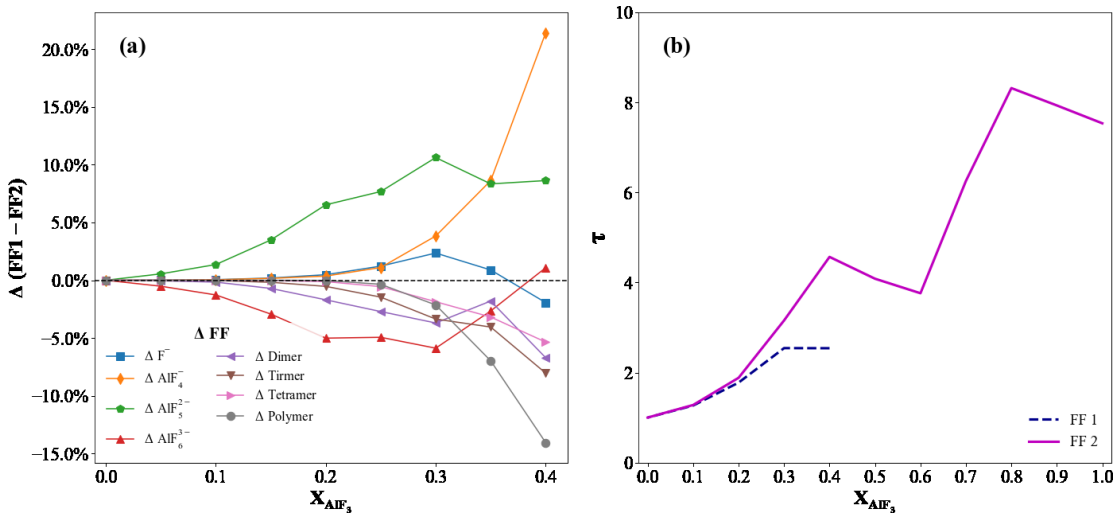

Figure E.8 Differences in terms of complex anions, dimers, trimers, and polymer chains at 1343 [K] (a) and the resulting difference in τ (b) as a function of composition obtained from simulations employing the two different force fields FF1 and FF2.

mately 0.85 [W.K^{-1}.m^{-1}] [264]. Therefore, the predictive capability of FF1, in fact, surpasses that of FF2. The substantial overestimation of the thermal conductivity of molten NaF by Khokhlov et al. is likely caused by neglecting significant radiative and convective effects, as discussed in [39, 60, 264]. Both sets of simulation data are compared to the singular experimental dataset provided by Khokhlov et al. [314] in the range 1100 - 1373 [K]. Note that the data from Khoklov has been reviewed elsewhere and could be biased by parasitic heat losses [39,60,264], but the data may be more reliable at lower temperatures where the magnitude of heat losses are less significant, as illustrated in Figure E4, and could be a reasonable reference for comparison of compositional trends.

The impact of kinetic contributions and mass differences relativity is significant for this mixture, demonstrated by the deviation from linearity for the two cases $\tau = 0$ and $\tau = 1$. When considering the kinetic contribution alone ($\tau = 0$), the results using both force fields show a calculated deviation from linear behavior of approximately 10%. However, this deviation increases to about 25% when we assume a simple dissociated mixture, excluding coordination complexes and polymer chains ($\tau = 1$). Notably, this significant deviation from ideality in NaF-AlF_3 melts at $\tau = 0$ and $\tau = 1$ contrasts with the observations made in the case of the KCl-$MgCl_2$ mixture. This disparity can be attributed to the marked differences in thermal conductivity and molecular mass between the two end members. In the NaF-AlF_3 system, the thermal conductivity difference ($\Delta\lambda$) is approximately 75%, while in the KCl-

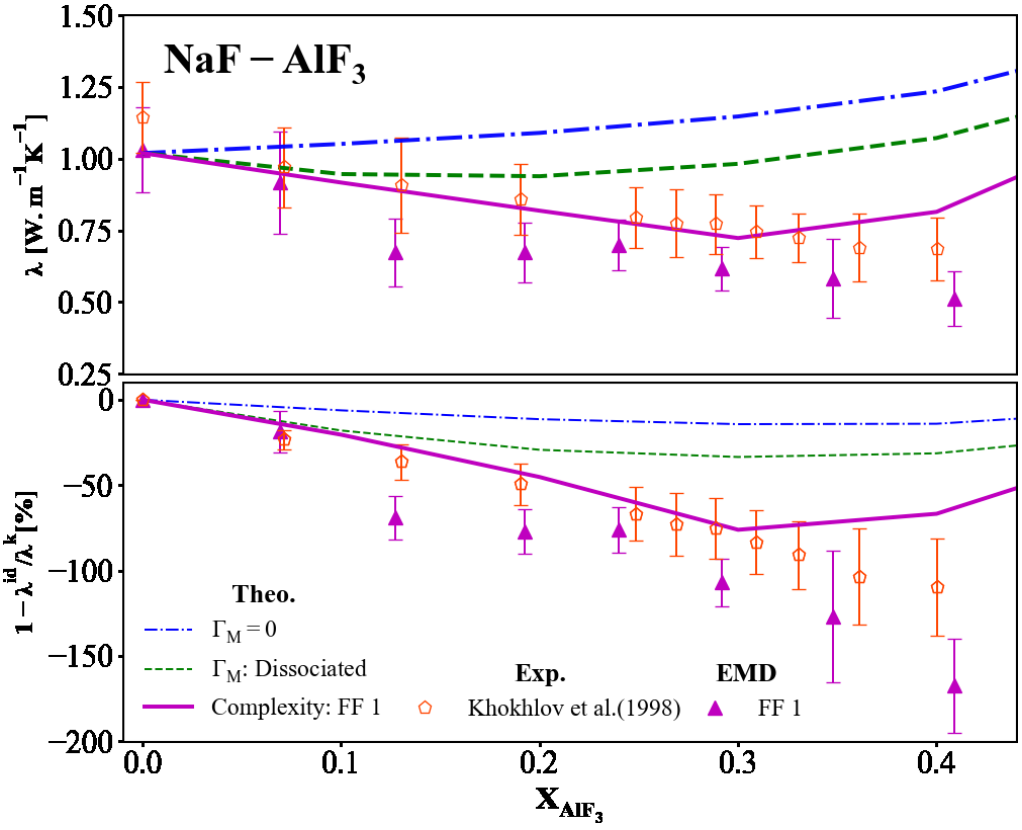

Figure E.9 EMD simulations (filled symbols) of thermal conductivity in NaF-AlF_3 melts at 1343 [K] using the FF1 force field to model interionic interactions, alongside the experimental dataset reported by Khokhlov et al. in the range 1100 - 1373 [K] [314] (open symbols). Theoretical predictions consider τ for damping local fluctuations of kinetic energy f (solid line), a dissociated mixture ($\tau = 1$, dashed line), and the kinetic contribution only ($\tau = 0$, dot-dash line). The bottom figure represents the corresponding deviation from a linear behavior with composition. In the theoretical calculations, the thermal conductivity of AlF_3 which is not accessible in FF1, was assumed based on FF2 calculations.

$MgCl_2$ system, it is only around 20%. Similarly, the molecular mass difference (ΔM) between the two end-members is about 50% for NaF-AlF_3 and approximately 20% for KCl-$MgCl_2$, further influencing the deviation from the ideal conductivity.

The effect of the local structure on thermal transport within NaF-AlF_3 melts can be observed by comparing the results of EMD simulations utilizing FF1 and FF2 with the corresponding theoretical calculations based on the computed local structure parameters derived from these force field models. While the simulation based on FF1 may underestimate the ther-

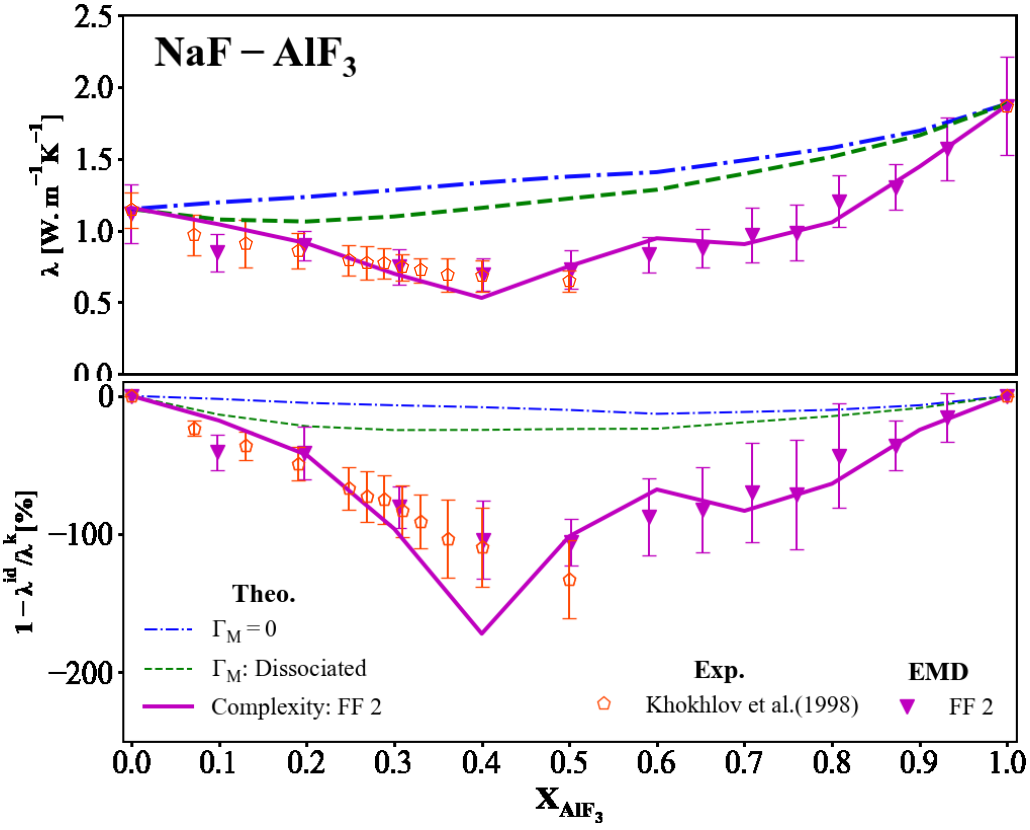

Figure E.10 EMD simulations (filled symbols) of thermal conductivity in NaF-AlF_3 melts at 1343 K using the FF2 force field to model interionic interactions, alongside the experimental dataset reported by Khokhlov et al. in the range 1100 - 1373 [K] [314] (open symbols). Theoretical predictions consider τ for damping local fluctuations of kinetic energy f (solid line), a dissociated mixture ($\tau = 1$, dashed line), and the kinetic contribution only ($\tau = 0$, dot-dash line). The bottom figure represents the corresponding deviation from a linear behavior with composition.

mal conductivity, the corresponding theoretical model provided accurate predictions for the composition-dependent behavior of thermal conductivity. In contrast, the simulation based on FF2 accurately predicts thermal conductivity, while the corresponding theoretical model underestimates it. This discrepancy is evident in the calculated excess thermal conductivity. In the theoretical model using FF1, excess conductivity reaches a minimum of approximately 75% when X_{AlF_3} is around 0.3. On the other hand, raw simulation data show a deviation from ideality as low as 160% near $X_{AlF_3} = 0.4$. The theoretical model using FF2 shows a minimum excess thermal conductivity of around 170% near $X_{AlF_3} = 0.4$, while the minimum

excess thermal conductivity obtained from EMD simulations still occurs near $X_{AlF_3} = 0.4$, but with a deviation around 100%.
The difference between theoretical excess thermal conductivity derived from FF1 and FF2 is directly related to the local structure. FF2 anticipates the formation of heavier complex anions compared to FF1, illustrated by the production of AlF_6 rather than AlF_5 at lower AlF_3 concentrations, $X_{AlF_3} \leq 0.2$, and the generation of dimers, trimers, and polymers as opposed to AlF_4 at higher concentrations, $X_{AlF_3} \geq 0.2$ (see Figure E.7 and E.8). The divergence between the two parameters, τ for FF1 and FF2, becomes pronounced beyond approximately $X_{AlF3} = 0.2$, highlighting the distinction between them in terms of excess thermal conductivity. Considering the insights provided by Machado et al. [315], which underscore the superior accuracy of FF1 over FF2 in predicting the local structure within NaF-AlF_3 melts, we can assume that the excess thermal conductivity estimated through FF1 is the most reliable. However, the substantial peak in the excess thermal conductivity is likely overstated due to inherent limitations of the force field. In this example, it is crucial to emphasize the predictive potential of the proposed formalism, particularly when the local structure is known with a considerable degree of accuracy.

In this present study, we presented and investigated a formalism focused on incorporating the influence of structure on the thermal conductivity of molten salt mixtures, into a kinetic theory-based model. The model was used to predict several molten salt systems, yielding accurate predictive capability on simple and complex ionic-bonded systems, supported by EMD simulations and compared to hypothetical cases of the model isolating the key phenomena contributing to thermal transport (i.e. the raw model, $\tau = 0$ and $\tau = 1$). The proposed model holds substantial potential for streamlining the analysis of temperature and composition-dependent thermal transport in larger-scale ionic-bonded systems. The ability to rapidly and accurately predict simple or complex polymer chains represents a significant advantage from the limitations and inaccuracies in both experimental approaches and atomistic simulation methods. Lastly, this model improves to the fundamental understanding of thermal transport in molten salts and can aid in understanding the interplay between local structural arrangements and thermal transport properties, an area that still requires more development.
Our findings reveal that the thermal conductivity is dependent on local structural attributes which the model accurately captured in several case studies. Notably, the simple salts KCl, LiF-NaF, and LiF-NaF-KF, that had been discussed previously were revisited and compared to a "raw" kinetic model or model with no mass fluctuation, demonstrating that the accuracy of the modified kinetic model still holds and captures key features such as mass and

thermal conductivity differences between mixture constituents. Mixtures with coordination considerations (NaF-AlF_3 and $MgCl_2$ systems) were also demonstrated with the modified kinetic model, factoring in the effects of local ordering, demonstrated superior accuracy over the models without structural components ($\tau = 0$ and $\tau = 1$) when compared to the EMD simulations. The key limitation introduced by the modified model is the need for reliable data on the coordination, which we show can have a substantial effect on the accuracy, for example when different MD force fields were used to estimate the structure of NaF-AlF_3. Lastly, we also demonstrated that the model can provide reasonable predictions on pure melts with local ordering, like Al_2O_3, opening up the possibility of applying it to the largely unstudied oxide melts.

Applying the proposed model offers key advantages over the conventional experimental, theoretical, and atomistic approaches. Experimental methods have high risk for error if not carefully designed and operated. Furthermore, the collection of data is time-consuming as numerous trials are be required to fully characterize a multi-component salt system. To our knowledge, there is no model with theoretical foundations (excluding atomistic simulations) providing comparable predictive capability and scope. As described in our prior works, this model has been widely applied to reliable data for pure compounds and salt mixtures and now has been shown to capture the effects of local structure, suggesting that it can be widely applied to molten salt mixtures. Lastly, this model could offer improvements to prediction, when compared to atomistic simulation methods. For example, in scenarios with a higher number of ions—typically exceeding 4 in ternary systems—conventional methods relying on the Green-Kubo analysis of phase trajectories yield a substantial number of Onsager coefficient components. This, in turn, leads to notable errors in estimating the thermal conductivity. We anticipate that the introduced formalism has the potential to significantly enhance the predictive capabilities of the thermal transport in critical energy systems.

In conclusion, our study not only elucidates the fundamental aspects of thermal transport in molten salts but also provides a reliable predictive framework applicable to a wide range of mixtures. This is particularly pertinent to advanced energy applications like MSRs and CSP systems. Moreover, the proposed model could provide a basis for the development of an engineering database of molten salt thermal conductivity that would support these energy technologies. As demonstrated with molten alumina, the proposed theoretical approach is fundamentally adaptable to molten oxides (slags), representing a significant advancement for various metallurgical applications where slags play a crucial role. Overall, our work provides a robust theoretical foundation to help future explorations into the thermal properties of complex ionic systems, which will have significant implications for both fundamental research and applied industrial research and development.